

STATUS OF THESIS

Title of thesis

SYNTHESIS OF POLYMERIZED IONIC LIQUIDS FOR
CARBON DIOXIDE CAPTURE

I MOHAMED OSMAN HUSSIEN AHMED ALI

hereby allow my thesis to be placed at the Information Resource Center (IRC) of Universiti Teknologi PETRONAS (UTP) with the following conditions:

1. The thesis becomes the property of UTP
2. The IRC of UTP may make copies of the thesis for academic purposes only.
3. This thesis is classified as

Confidential

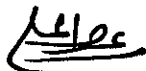
Non-confidential

If the thesis is confidential, please state the reason:

Under patent

The contents of the thesis will remain confidential for 5 years.

Remarks on disclosure:



Signature of Author

Permanent Address:

Faculty of Engineering &
Technology

University of Gezira

P.O. Box. 20, Wad Medani, SUDAN

Endorsed by



Signature of Supervisor

Assoc. Prof. Dr. Mohamed Ibrahim

Abdul Mutalib

Date:

09/12/2011

Date:

09 DEC 2011

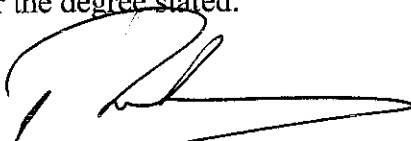
UNIVERSITI TEKNOLOGI PETRONAS

SYNTHESIS OF POLYMERIZED IONIC LIQUIDS FOR CARBON DIOXIDE
CAPTURE

By

MOHAMED OSMAN HUSSIEN AHMED ALI

The undersigned certify that they have read, and recommend to the Postgraduate Studies Programme for acceptance this thesis for the fulfillment of the requirements for the degree stated.



Signature:

Main Supervisor:

Assoc. Prof. Dr. Mohamed Ibrahim Abdul Mutalib

Signature:



Co-Supervisor:

Assoc. Prof. Dr. Cecilia Devi Wilfred

Signature:



Head of Department:

Assoc. Prof. Dr. Shuhaimi Mahadzir

Date:

9/12/2011

Dr. Shuhaimi Mahadzir
Associate Professor & Head
Chemical Engineering Department
Universiti Teknologi PETRONAS

SYNTHESIS OF POLYMERIZED IONIC LIQUIDS FOR CARBON DIOXIDE
CAPTURE

By

MOHAMED OSMAN HUSSIEN AHMED ALI

A Thesis

Submitted to the Postgraduate Studies Programme
as a Requirement for the Degree of

DOCTOR OF PHILOSOPHY

CHEMICAL ENGINEERING DEPARTMENT

UNIVERSITI TEKNOLOGI PETRONAS

BANDAR SRI ISKANDAR

PERAK

DECEMBER 2011

DECLARATION OF THESIS

Title of thesis

SYNTHESIS OF POLYMERIZED IONIC LIQUIDS FOR
CARBON DIOXIDE CAPTURE

I MOHAMED OSMAN HUSSIEN AHMED ALI

hereby declare that the thesis is based on my original work except for quotations and citations which have been duly acknowledged. I also declare that it has not been previously or concurrently submitted for any other degree at UTP or other institutions.



Signature of Author

Permanent Address:

Faculty of Engineering &
Technology
University of Gezira

P.O. Box. 20, Wad Medani, SUDAN

Date: 09/12/2011

Witnessed by



Signature of Supervisor

Assoc. Prof. Dr. Mohamed Ibrahim
Abdul Mutalib

Date: 09 DEC 2011

ABSTRACT

The high level of carbon dioxide (CO₂) content in natural gas reserves discovered lately in Malaysia and some other reservoirs around the globe is one of the major issues that are being faced by the industry nowadays. The existing processes for CO₂ removal suffer from one main setback *i.e.*, the limitation on the maximum content of CO₂ that is allowed in the natural gas feed, at very high purity as required by the industry. It seems that polymerized ionic liquids showed enhanced CO₂ sorption capacities and fast sorption/desorption rates compared with their corresponding ionic liquids.

The main objective of this research is to study the effect of chemical structure of poly ionic liquid (pILs) on their CO₂ sorption rate and capacity.

Thus, a part of our proposed hypothesis, to explain the attraction between CO₂ and pILs, is the dependence of sorption on the ion conductivity of cations and anions of the pILs. This assumption was consistent with Monte Carlo molecular dynamics simulation result which showed a localization of CO₂ molecules around both cation and anion and the dependence of its sorption on the ion conductivity of both cation and anion.

Twelve new pILs are synthesized in a way that makes it possible to study the effect of cation, backbone, substituent alkyl chain length, and anion on CO₂ sorption rate and capacity. The characterization of these polymers includes: structure analysis, topology analysis, chloride content, density, and thermal stability.

Using magnetic suspension balance (MSB) apparatus, the CO₂ sorption results showed that the sorption capacity of pILs is a function of ion conductivity of both cation and anion. The size of the anion also affects CO₂ sorption rate and capacity. The pILs are found to be highly selective towards CO₂ sorption and recyclable

It was found that adding water to pILs leads to a dramatic systematic swelling of pILs depending on the type of gas, the gas flow, the applied gas pressure, and water content of pILs as long as they are exposed to the same conditions. A dramatic enhancement in the CO₂ sorption capacity of pILs was achieved when adding water to them. In addition to the swelling caused by water which offers a larger surface area, water provides cation and anion with really high ion conductivity enhancing CO₂ sorption capacity.

ABSTRAK

Penemuan kuantiti gas karbon dioksida yang tinggi di dalam gas semulajadi di Malaysia dan di telaga gas seluruh dunia merupakan isu utama yang dialami oleh industri sejak kebelakangan ini. Proses yang wujud untuk mengasingkan CO₂ mengalami kelemahan dari segi had kuantiti maksimum CO₂ yang dibenarkan dalam gas asli, memandangkan keaslian tinggi diperlukan oleh industri.

Cecair berion berpolimer menunjukkan kapasiti penjerapan CO₂ yang tinggi dan cepat berbanding dengan cecair berion di suhu bilik.

Objectif utama penyelidikan ini ialah untuk menentukan rekacipta yang optimum bagi cecair berion berpolimer mengasingkan CO₂ dari gas semulajadi.

Sebahagian dari teori yang dikemukakan ialah tarikan antara CO₂ dan cecair berion berpolimer dan kebergantungan penjerapan ke atas konduktiviti ion antara kation dan anion. Teori ini adalah konsisten dengan simulasi molecular dinamik Monte Carlo yang menunjukkan lokalisasi molekul CO₂ sekeliling kation dan anion and kebergantungan penyerapan di atas konduktiviti ion kedua-dua kation dan anion.

Dua belas cecair berion berpolimer telah disintesis untuk menyelidik kesan kation, tulang belakang, panjang rantai alkil, dan anion ke atas penjerapan CO₂ dan kapasitinya. Pengenalpasti struktur polimer termasuk analisa struktur, analisa toplogi, kuantiti klorida, density dan stabiliti thermal.

Hasil penjerapan CO₂ menggunakan pengimbang suspense magnetic menyokong theory bahawa penjerapan ialah factor konduktiviti ion kedua-dua kation dan anion. Saiz anion juga mempengaruhi kadar penjerapan CO₂. Cecair berion berpolimer juga dijumpai sangat peka kepada penjerapan CO₂ dan kitarsemula. Menyerami cecair berion berpolimer dalam pelarut methanol and seterusnya mengeringkannya merendahkan density serta meningkatkan kapasiti penjerapan CO₂

Menambahkan air juga mengaruhi secara dramatik pengembangan cecair berion berpolimer yang bergantung kepada jenis gas, aliran gas dan tekanan yang diaplikasikan, kandungan air dalam cecair berion berpolimer, asalkan ianya didedahkan kepada situasi yang sama. Perubahan dramatic dalam penjerapan CO₂ dicapai apabila air ditambah kepadanya. Tambahan pula pengembangan yang disebabkan oleh air menyediakan permukaan saiz yang lebih besar, di mana air membekalkan cation dan anion dengan konduktiviti ion yang tinggi yang meningkatkan kapasiti kadar penjerapan CO₂.

ACKNOWLEDGEMENTS

First and foremost, I owe an unrepayable debt to Almighty Allah, his blessings have always come upon me boundlessly. Without his blessing and inspiration, this work wouldn't be possible.

This thesis arose from years of research that I have done since I came to Malaysia. During that time, I have worked with a great number of people who has contributed in assorted ways to the research and the making of the thesis deserved special mention. It is a pleasure to convey my gratitude to them all in my humble acknowledge.

I would like to record my gratitude to my supervisor Assoc. Prof. Dr. Mohamed Ibrahim Abdul Mutalib and my co-supervisor Assoc. Prof. Dr. Cecilia Devi Wilfred for their supervision, advice, and guidance from the very early stage of this research as well as giving me extraordinary experiences throughout the work. Above all, they provided me unflinching encouragement and support in various ways. I am indebted to them more than they know.

I gratefully thank Prof. Dr. Yousif Ali Ragab and Assoc. Prof. Dr. Saleh Mohamed Ahmed Abakr (University of Gezira-SUDAN) for their constructive comments on this thesis. I am thankful that in the midst of all their activities, they were willing to correct this thesis.

It is a pleasure to pay tribute also to the sample collaborators. To ionic liquid research group in UTP, I would like to thank for their research-oriented attitude, support, consistent guidance, and encouragement throughout this work. To chemical engineering department staff in UTP, I would like to thank for their kind concern and support during this period. To all technical staff from chemical and mechanical engineering departments from UTP and administrative and technical staff of

PETRONAS Research Center in Kuala Lumpur, I would like to thank for their prolonged assistance for analyzing the samples.

I am very grateful to Dr. Abhijit Chatterjee and Accelry Material Studio Company for their great help in learning and using material studio software.

Where would I be without my family? My parents deserve special mention for their inseparable support and prayers especially during the hard time when I was suffering the Takayasu's arteritis disease. My father, Hussien Ahmed Ali, in the first place is the person who put the fundamentals of my learning character. My mother, Zeinab bt Sheikhna Abdullah, is the one who sincerely raised me with her caring and gentle love. My uncles Fadelallah and Abdulhameed are the people who show me the joy of intellectual pursuit ever since I was a child.

Words fail me to express my appreciation to my wife Nuha Ahmed Ibrahim whose dedication, love and persistent confidence in me, has taken the load off my shoulder. I owe her for being unselfishly letting her intelligence, passions, and ambitions collide with mine. Therefore, I would also thank Nuha's family (Hantabli) for letting me take her hand in marriage, and accepting me as a member of the family, warmly. My son Awaab Mohamed Osman, I would like to thank for his prayers, moral support, great sacrifice, patience, and encouragement for the completion of this work.

I am very grateful to Assoc. Prof. Dr. Mohamed Najeeb Abdella Idris, the Sudanese neurologist who managed to discover the infection caused by Takayasu's arteritis disease before it reached my brain blood vessels.

It is a pleasure to convey my gratitude to those who had been doing every possible effort and prayed for me to recover from my disease, Sheikh Talib Elmokashfi (Elshekeniba), Assoc. Prof. Dr. Mohamed Saeed Dhawelbait, and Prof. Dr. Ali Elameen Eljack (University of Gezira-SUDAN).

I would also like to take this opportunity to express my gratitude to all my friends especially Ms. Fadwa babikr, Mr. Omer Eisa, Dr. Abubakr Khider Ziyada, Mr. Abdelhaffez Omer, and Dr. Abdulbagi Osman for their continuous support.

Finally, I would like to thank everybody who was important to the successful realization of the thesis, as well as expressing my apology that I could not mention everyone who had helped me.

DEDICATION

*To the soul of my grandmother Amna bt, Ali wad Alnaqam
and the soul of my grandfather Sheikhna Abdullah wad
Sheikhna Fadelallah Mohamed Nasr*

To my beloved wife Nuha

& my beloved son Awaab

TABLE OF CONTENTS

ABSTRACT	V
ABSTRAK	VII
ACKNOWLEDGEMENTS.....	IX
DEDICATION	XII
TABLE OF CONTENTS	XIII
LIST OF ABBREVIATIONS.....	XXII
NOMENCLATURE.....	XXVI
CHAPTER 1	1
INTRODUCTION	1
1.1 BACKGROUND OF STUDY	1
1.2 CO ₂ REMOVAL FROM NATURAL GAS.....	3
1.3 CURRENT PROCESSES FOR REMOVAL OF CO ₂ FROM NATURAL GAS	3
1.3.1 CO ₂ REMOVAL WITH AMINES	5
1.3.2 CO ₂ REMOVAL WITH DGA	8
1.3.3 CO ₂ REMOVAL WITH MEMBRANES	10
1.3.4 REMOVAL USING SOLID SORBENTS	13
1.4 IONIC LIQUIDS AND POLYMERIZED IONIC LIQUID	13
1.5 CRITERIA FOR PROCESS SELECTION	14
1.6 CARBON DIOXIDE UTILIZATION	14
1.7 PROBLEM STATEMENT	18
1.8 OBJECTIVE OF THE STUDY.....	19
1.9 SCOPE OF THE STUDY.....	19

1.10 STRUCTURE OF THESIS	20
CHAPTER 2	21
LITERATURE REVIEW.....	21
2.1 IONIC LIQUIDS (ILs)	21
2.1.1 HISTORY	24
2.1.2 STRUCTURE AND PROPERTIES OF IONIC LIQUIDS.....	27
2.1.3 HOW GREEN ARE IONIC LIQUIDS?	29
2.1.4 CO ₂ SOLUBILITY IN IONIC LIQUIDS	30
2.1.4.1 CO ₂ Solubilities in Conventional Ionic Liquids -----	31
2.1.4.2 CO ₂ Solubilities in Task Specific Ionic Liquids-----	33
2.2 POLYMERIZED IONIC LIQUIDS PILS	36
2.2.1 HISTORY	37
2.2.2 CO ₂ SORPTION IN POLY IONIC LIQUIDS PILS.....	40
2.2.2.1 CO ₂ Sorption in pILs's Membrane -----	49
2.2.3 OTHER PROMISING APPLICATIONS OF PILS	51
2.3 SUMMARY	53
CHAPTER 3	55
HYPOTHESIS AND THEORY	55
3.1 CARBON DIOXIDE CHEMISTRY AND PROPERTIES	55
3.2 SORPTION OF CO ₂ IN GLASSY POLYMERS	56
3.3 MOLECULAR DYNAMIC SIMULATION.....	58
3.3.1 SYNTHIA MODULE	58
3.3.2 MONTE CARLO SORPTION SIMULATION	60
3.3.2.1 Energy Components -----	61
3.3.2.2 Monte Carlo Methods -----	63

3.4 SORPTION MEASUREMENT	65
3.4.1 VOLUMETRIC AND PRESSURE-DROP METHODS.....	65
3.4.1.1 Advantages of The Volumetric Method -----	66
3.4.1.2 Disadvantages of Volumetric Methods -----	66
3.4.2 GAS CHROMATOGRAPHY	67
3.4.3 THE GRAVIMETRIC METHOD.....	67
3.4.3.1 Advantages of The Gravimetric Method -----	68
3.4.3.2 Disadvantages of The Gravimetric Method -----	68
3.4.4 MAGNETIC SUSPENSION BALANCE - THE RENAISSANCE OF GRAVIMETRY	69
3.5 SUMMARY	71
CHAPTER 4	73
RESEARCH EXPERIMENTAL AND METHODS	73
4.1 MOLECULAR DYNAMIC SIMULATION.....	73
4.1.1 SIMULATION PROCEDURE	73
4.2 SYNTHESIS OF POLY IONIC LIQUIDS	79
4.2.1 MATERIALS.....	81
4.2.2 SYNTHESIS OF TRIETHYLAMMONIUM BASED POLY IONIC LIQUIDS.....	83
4.2.3 SYNTHESIS OF TRIMETHYLAMMONIUM BASED POLY IONIC LIQUIDS.....	84
4.2.4 SYNTHESIS OF METHACRYLOYLOXY ETHYL TRIMETHYLAMMONIUM BASED PILS	84
4.2.5 SYNTHESIS OF TRIS DIMETHYLAMINO PHOSPHINE BASED POLY IONIC LIQUIDS	85
4.3 CHARACTERIZATION OF POLY IONIC LIQUIDS.....	86
4.3.1 STRUCTURE ANALYSIS.....	86
4.3.2 TOPOLOGY ANALYSIS	87
4.3.3 CHLORIDE CONTENT.....	88

4.3.4 WATER CONTENT	88
4.3.5 DENSITY.....	88
4.3.6 THERMAL STABILITY	88
4.3.7 MOLECULAR WEIGHT ANALYSIS	89
4.4 SORPTION MEASUREMENT	89
4.4.1 EXPERIMENTAL PROCEDURE.....	89
4.5 SUMMARY	96
CHAPTER 5	97
RESULTS AND DISCUSSION.....	97
5.1 MOLECULAR DYNAMICS SIMULATION RESULTS	97
5.1.1 SYNTHIA MODULE	97
5.1.2 SORPTION SIMULATION RESULTS.....	100
5.2 CHARACTERIZATION OF PILS	103
5.2.1 STRUCTURE ANALYSIS.....	103
5.2.1.1 Triethylammonium Based pILs -----	103
5.2.1.2 Trimethylammonium Based pILs -----	104
5.2.1.3 Methacryloyloxy Ethyl Ttrimethylammonium Based pILs -----	104
5.2.1.4 Tris Dimethylamino Phosphine Based pILs -----	105
5.2.2 TOPOLOGY ANALYSIS	105
5.2.3 CHLORIDE CONTENT.....	109
5.2.4 DENSITY.....	110
5.2.5 THERMAL STABILITY	111
5.3 SORPTION OF CARBON DIOXIDE.....	114
5.3.1 EFFECT OF POLYMERIZATION.....	114
5.3.2 EFFECT OF CATION.....	116

5.3.3 EFFECT OF ANION	121
5.3.4 SORPTION ISOTHERMS	124
5.3.5 EFFECT OF TEMPERATURE.....	125
5.3.6 IDEAL SELECTIVITY AND MOLECULAR INTERACTION	126
5.3.7 RECYCLABILITY	128
5.3.8 EFFECT OF WATER	129
5.3.8.1 Swelling Behavior	129
5.3.8.2 Sorption in The Presence of Water	134
5.3.9 EFFECT OF DENSITY REDUCTION	136
5.4 SUMMARY	137
CHAPTER 6	139
CONCLUSIONS AND RECOMMENDATIONS.....	139
6.1 CONCLUSIONS	139
6.2 RECOMMENDATIONS	140
REFERENCES	141
PUBLICATIONS.....	167
APPENDIX A.....	168
NMR SPECTRUM FOR PILS AND THEIR MONOMERS	168
APPENDIX B.....	179
SEM MICROGRAPHS OF PILS	179
APPENDIX C.....	185
DATA FOR SORPTION MEASUREMENT.....	185

LIST OF FIGURES

Fig. 1.1: Natural gas composition.....	2
Fig. 1.2: A simplified flow schematic of a typical a absorption/stripping system for acid gases removal	5
Fig. 1.3: Simple membrane separation operation [14].....	11
Fig. 1.4: CO ₂ as a green carbon resource [19]	15
Fig. 1.5: Organic synthesis using CO ₂ [19].	16
Fig. 1.6: Summarized examples of organic synthesis starting from CO ₂ [21]	17
Fig. 2.1: Scheme of an ionic liquid versus an ionic solution [25]	22
Fig. 2.2: Dialkylimidazolium chloroaluminates ionic liquid	26
Fig. 2.3: Most common reported cations of ionic liquids	27
Fig. 2.4: Task-specific ionic liquid ([pabim]BF ₄) for CO ₂ capture [107].....	34
Fig. 2.5: Some examples of ion exchange resin.....	37
Fig. 2.6: Naflon structure	38
Fig. 2.7: Synthesis of IL monomer BIMT [153].....	41
Fig. 2.8: Synthesis of VIBT and VBIH ionic liquid monomers [149].....	41
Fig. 2.9: Chemical structure of GRTIL cross-likable monomers[163].....	50
Fig. 2.10: Functionalized polymerizable ionic liquid monomers [164]	51
Fig. 3.1: Carbon dioxide resonance structure	55
Fig. 3.2: Carbonate ion resonant structures	56
Fig. 3.3: (a) Conventional apparatus and (b) magnetic suspension balance	71
Fig. 4.1: Computational procedure for Synthia Module	74
Fig. 4.2: Monomer construction and forcefield atoms typing for p[VBTEA][NO ₃] ...	75
Fig. 4.3: Homopolymer construction of p[VBTEA][NO ₃].....	76
Fig. 4.4: Computational procedure for sorption Module	77
Fig. 4.5: CO ₂ construction and its forcefield atoms typing.....	78
Fig. 4.6: Amorphous cell construction of p[VBTEA][NO ₃].....	78
Fig. 4.7: Magnetic suspension balance MSB apparatus located in UTP	90
Fig. 4.8: Julabo, Model F25ME connected to MSB.	90
Fig. 4.9: Dehumidifier (Gas dryer) connected to MSB gas dosing system	91

Fig. 4.10: Example for blank measurement result	92
Fig. 4.11: Example of buoyancy measurement with He	94
Fig. 4.12: Methodology strategy	96
Fig. 5.1: CO ₂ sorption simulation result for selected pILs.	100
Fig. 5.2: Average total energy of CO ₂ sorption for simulated pILs.....	101
Fig. 5.3: Comparison between simulation and experimental results for p[VBTMA][NO ₃] CO ₂ sorption isotherms	101
Fig. 5.4: Simulation results for CO ₂ (red dots) sorption on p[VBTEA][NO ₃] showing the location of CO ₂	102
Fig. 5.5: SEM micrograph for (a) p[VBTEA][Cl], (b) p[VBTEA][NO ₃],	106
Fig. 5.6: XRD patterns of (a) [METMA][Cl], (b) p[METMA][Cl],.....	107
Fig. 5.7: DSC curves for pILs with different anions: (a), p[VBTEA][CH ₃ O ₄ S].....	108
Fig. 5.8: DSC curves for pILs with different substituent length : (a), p[VBTEA][Cl]	109
Fig. 5.9: DSC curves for pILs with different backbones : (a), p[METMA][Cl] (b) p[METMA][NO ₃], (c) p[VBTMA][NO ₃], (d) p[VBTMA][Cl].....	109
Fig. 5.10: Densities of pILs and their corresponding monomers.....	110
Fig. 5.11: Plot of thermal decomposition for pILs with different cations and fixed [Cl] anion.....	112
Fig. 5.12: Plot of thermal decomposition for pILs with different cations and fixed [NO ₃] anion.....	112
Fig. 5.13: Plot of thermal decomposition for pILs with fixed [VBTEA] cation and different anions	113
Fig. 5.14: CO ₂ sorption rate for p[VBTMA][Cl] and its monomer at 10 bar and 25°C	115
Fig. 5.15: Effect of molecular weight on CO ₂ sorption rate and capacity at 10 bar and 25°C.	116
Fig. 5.16: CO ₂ sorption rate for different cations with [Cl] anion at 10 bar and 25°C	117
Fig. 5.17: CO ₂ sorption rate for different cations with [NO ₃] anion at 10 bar and 25°C	118
Fig. 5.18: Effect of backbone on sorption rate and capacity at 10 bar and 25°C	120

Fig. 5.19: CO ₂ sorption rate for p[METMA][Cl] and p[METMA][NO ₃] at 10 bar and 25°C	121
Fig. 5.20: CO ₂ sorption rate for [VBTEA] cation with different anion types at 10 bar and 25°C	122
Fig. 5.21: CO ₂ sorption rate for [VBTMA] cation with different anion types at 10 bar and 25°C	123
Fig. 5.22: Sorption isotherms for p[VBTMA][NO ₃] and p[VBTMA][F ₃ C-SO ₃] at 25°C	124
Fig. 5.23: Sorption isotherms for p[VBTMA][NO ₃] and p[VBTMA][F ₃ C-SO ₃] at different low pressures and 25°C.....	125
Fig. 5.24: CO ₂ sorption isotherms for p[VBTMA][NO ₃] at different temperatures..	126
Fig. 5.25: Sorption rate and capacity for different gases on p[VBTMA][F ₃ C-SO ₃] at 10 bar and 25 °C.	127
Fig. 5.26: Cycles of CO ₂ sorption rate at 1 bar and 25 °C and desorption at 0.02 bar absolute pressure and 25 °C for p[VBTMA][F ₃ C-SO ₃]	128
Fig. 5.27: Sorption rate at 1 bar and 25 °C and desorption by vacuuming p[VBTMA]	129
Fig. 5.28: Effect of pressure on volume of p[VBTMA][Cl] containing 20% wt water.	130
Fig. 5.29: Effect of gas type on volume of p[VBTMA][Cl] containing 20% wt water	131
Fig. 5.30: Elasticity and effect of gas flow-rate on volume of p[VBTMA][Cl] containing 23% wt water.	132
Fig. 5.31: Effect of water content on volume of p[VBTMA][Cl], exposed to a 200ml/min flow rate of argon at 1 bar.	133
Fig. 5.32: Systematic swelling behavior of p[VBTMA][Cl] containing 95.4% wt of water exposed to 200ml/min flow rate of argon at 1 bar.	134
Fig. 5.33: Effect of water on CO ₂ sorption capacity and rate at 1 bar and 25°C.....	135
Fig. 5.34: Effect of water on CO ₂ sorption capacity and rate at 1 bar and 25°C.....	135
Fig. 5.35: Density reduction effect on CO ₂ sorption capacity and rate at 10 bar and 25°C	137

LIST OF TABLES

Table 1.1: Composition of selected natural gases (volume %) [1]	2
Table 1.2: Integral heat of solution for CO ₂ absorption [12].....	8
Table 1.3: General conditions found in natural gas plants [13].....	9
Table 2.1: Anions generally found in ionic liquids [26].....	28
Table 2.2: Butyl imidazolium-based pILs and their sorption capacities	43
Table 2.3: Trimethyl ammonium-based pILs and their sorption capacities	44
Table 2.4: Phosphonium-based pILs and their sorption capacities.....	45
Table 2.5: Methacryloyloxy backbone's pILs with different cations and their sorption capacities.....	45
Table 2.6: pILs with different cations and similar anions and their sorption capacities	46
Table 4.1: Description of atoms types used in the simulation.....	75
Table 4.2: Triethylammonium based poly ionic liquids.	79
Table 4.3: Trimethylammonium based poly ionic liquids.	80
Table 4.4: Methacryloyloxy ethyl trimethylammonium based poly ionic liquids.....	81
Table 4.5: Tris dimethylamino phosphine based poly ionic liquids.	82
Table 5.1: Estimated pILs properties (1) using the Synthia module.....	98
Table 5.2: Estimated pILs properties (2) using the Synthia module.....	98
Table 5.3: Chloride content for non-halogenated pILs.	110
Table 5.4: Densities of synthesized pILs.	111
Table 5.5: Temperature of 10% thermal decomposition for different pILs.....	114
Table 5.6: Ion conductivity for some cations and anions at 25°C [217]	119
Table 5.7: Polarizabilities (α), dipole moments (μ), and quadrapole moments (Q) of some gases [218, 219].....	126
Table 5.8: Pressure Adjustments based on time period	132

LIST OF ABBREVIATIONS

[6-mim][PF ₆]	1-hexyl-3-methyl imidazolium hexafluorophosphate,
AIBN	alpha, alpha'-Azobisisobutyro-bitrile
[am-im][BF ₄]	1-allyl-3-methylimidazolium tetrafluoroborate
[am-im][dca]	1-allyl-3-methylimidazolium dicyanoamide
ATRP	Atom transfer radical polymerization.
BB	Backbone
BIMT	2-(1-butylimidazolium-3-yl)ethylmethacrylate tetrafluoroborate
[bmim][Tf ₂ N]	1-Butyl-3-Methyl-Imidazolium bis(trifluoromethanesulfonyl)imide
COMPASS	Condensed-Phase Optimized Molecular Potentials for Atomistic Simulation Studies
DBMP	2,6-Di-tert-butyl-4-methylphenol
[dca]	dicyanamide
DEA	Diethanolamine
DGA	β,β'-hydroxyaminoethyl ether Diglycolamine
DIPA	diisopropanolamine
DMF	<i>N, N</i> -dimethylformamide
DMSO-d ₆	Deuterated dimethylsulfoxide
DSC	Differential scanning calorimetry
DU	Dow units (for permeability),[(cc.mil)/(day.(100 inches ²).atm)]
[emim]	1-Ethyl-3-Methyl-Imidazolium
Exo	Exothermal
FMO	Frontier Molecular Orbital
fs	Femtosecond , 10 ⁻¹⁵ s
GC	Gas chromatography
GPC	Gel permeation chromatography

GRTILs	Gemini room temperature ionic liquids
HOMO	Highest Occupied Molecular orbital
IC	Ion chromatography
ILM	Immobilized liquid membranes
ILs	Ionic liquids
LUMO	Lowest Unoccupied Molecular orbital
[Mac(PEO) ₇ Elm][TFSI]	Hepta(ethyleneoxide)methacrylate-3-ethylimidazolium (trifluoromethane-sulfonyl)imide
MDEA	Methyldiethanolamine
MEA	Monoethanolamine
MSB	Magnetic suspension balance
NMR	Nuclear magnetic resonance
NPT	Thermodynamics ensemble for Constant- pressure/constant-temperature dynamics
NVE	Thermodynamics ensemble for Constant-volume/constant- energy dynamics
NVT	Thermodynamics ensemble for Constant-volume/constant- temperature dynamics
[omim]	1-Octyl-3-Methyl-Imidazolium
[pabim][BF ₄]	1-n-propylamine-3-butylimidazolium tetrafluoroborate
p[bDMADMVBP][Cl]	poly-bis(dimethylamino)-N,N-dimethyl-N-(4-vinylbenzyl Phosphinaminium chloride
p[bDMADMVBP][NO ₃]	poly-bis(dimethylamino)-N,N-dimethyl-N-(4-vinylbenzyl Phosphinaminium nitrate
[P(C ₄) ₄]AA	Tetrabutylphosphonium amino acids
PEG	Polyethylene glycol
PEO	Poly(ethylene oxide)
pILs	Poly ionic liquids
p[MABI][BF ₄]	Poly[1-(2-Methacryloyloxy)ethyl-3-butylimidazolium tetrafluoroborate
p[MATMA][BF ₄]	Poly[2-(Methacryloyloxy)ethyltrimethylammonium tetrafluoroborate

p[METMA][Cl]	poly- Methacryloyloxy ethyl trimethylammonium chloride
p[METMA][NO ₃]	poly- Methacryloyloxy ethyl trimethylammonium nitrate
ppmv	ppm per volume (<i>i.e.</i> , volume of gaseous pollutant per 10 ⁶ volumes of ambient air)
ps	picosecond , 10 ⁻¹² s
PSA	Pressure swing absorption
psig	pound-force per square inch gauge
p[tDMAVBP][Cl]	poly- tris(dimethylamino)(4-vinylbenzyl)phosphonium chloride
p[VBBI][BF ₄]	Poly[1-(p-vinylbenzyl)-3-butylimidazolium tetrafluoroborate
p[VBTEA][CH ₃ COO]	poly-Vinylbenzyl triethylammonium acetate
p[VBTEA][CH ₃ SO ₄]	poly-Vinylbenzyl triethylammonium methylsulfate
p[VBTEA][Cl]	poly-Vinylbenzyl triethylammonium chloride
p[VBTEA][NO ₃]	poly-Vinylbenzyl triethylammonium nitrate
p[VBTMA][Cl]	poly-Vinylbenzyl trimethylammonium chloride
p[VBTMA][NO ₃]	poly-Vinylbenzyl trimethylammonium nitrate
p[VBTMA][TFMS]	poly-Vinylbenzyl trimethylammonium trifluoromethanesulfonate
p[VBTPA][NO ₃]	poly-Vinylbenzyl tripropylammonium nitrate
p[VdF][HFP]	poly(vinylidene fluoride)-hexafluoropropylene copolymer
Pz	Piperazine
RAM	Random-access memory
RTILs	Room-temperature ionic liquids
SCF	Standard cubic foot
SEM	Scanning electron microscopy
SG	Side group
SILMs	Supported ionic liquid membranes
TEA	Triethanolamine
TGA	Thermogravimetric analyzer
TMGL	1,1,3,3-tetramethylguanidium lactate.
TSILs	Task-specific ionic liquids

VDW	Van der Waals
[VBIH][PF ₆]	1-(4-vinylbenzyl)-3-butylimidazolium hexafluorophosphate
[VBIT][BF ₄]	1-(4-vinylbenzyl)-3-butyl imidazolium tetrafluoroborate
VOCs	Volatile organic compounds
XRD	X-ray diffraction

NOMENCLATURE

B	Buoyancy
b	Hole affinity constant
C	Gas solubility (concentration) in mL(STP)/mL
C_D	Concentration by normal dissolution
C_H	Concentration by hole filling
\hat{C}_H	Hole saturation capacity
C_P^S	Heat capacity of solid polymer
E_{coh1}	Fedors cohesive energy per mole
E_m	Total energy of a configuration m
E_m^{SS}	Intermolecular energy between the sorbate molecules
E_m^{SF}	interaction energy between the sorbate molecules and the framework
H_i	Henry's constant
h^S	Partial molar enthalpy of the sorbate component in the reservoir
h^F	partial molar enthalpy of the sorbate component in the framework
M	Molecular weight per repeat unit
m_{ADS}	Specific uptake
m_{BAL}	Balance reading
$m_{BAL,CORR}$	Corrected mass of sample container and sample after sorption
m_S	Mass of the sample
m_{SC}	Mass of empty sample container
m_{SC+S}	Mass of sample container and sample
N	Number of non-hydrogen atoms in the system
N_1	Number of perhalogenated carbon atoms
N_2	Number of BB aromatic imide group
N_3	Number of BB hetrocyclic fused aromatic rings except imides
N_4	Number of oxygen atoms in aromatic BB rings
N_5	Number of side group correction
N_6	Number of Br attached to SG atoms or to non-aromatic BB atoms

N_7	Number of Br attached to aromatic BB atoms
N_8	Number of single, unsubstituted meta aromatic BB rings
N_9	Number of single, unsubstituted ortho aromatic BB rings
N_{10}	Number of hydrogen-containing substituent, attached to single aromatic BB rings
N_{11}	Number of substituents not containing hydrogen, attached to single aromatic BB rings
N_{12}	Number of resonance around six-membered single unsubstituted aromatic BB rings
N_{13}	Number of BB ester with aliphatic group on both sides
N_{14}	Number of acetone type ester
$N_{(backbone\ ester)}$	Number of ester (-COO-) group in the backbone of the polymeric repeat unit
N_{Br}	Number of bromine atoms in the polymeric repeat unit
$N_{carbonate}$	Number of carbonate (-OCOO-) groups in the polymeric repeat unit
$N_{C=C}$	Number of carbon-carbon double bonds in the polymeric repeat unit
N_{Cl}	Number of chlorine atoms in the polymeric repeat unit
N_{cyc}	Number of non-aromatic rings with no double bonds along any of the edges of the ring in the polymeric repeat unit
N_{ether}	Number of ether (-O-) linkages in the polymeric repeat unit
N_{fused}	Number of rings in fused ring structures in the polymeric repeat unit
N_H	Number of hydrogen atoms
N_m	The set of sorbate loadings of all components in configuration m
N_{MV}	Number of atoms and or groups for molar volume calculation in the polymeric repeat unit
N_{per}	Correction term for permeability calculation
N_{rot}	Total number of rotational degrees of freedom in a repeat unit
$N_{(-S-)}$	Number of divalent sulfur atoms located anywhere in the repeat unit
N_{Si}	Number of silicon atoms in the polymeric repeat unit
$N_{sulfone}$	Number of sulfur atoms in the highest oxidation state in the polymeric repeat unit

N_{Yd}	Correction term for temperature of half decomposition
p	Gas pressure in bar
P_{CO_2}	Permeability of carbon dioxide
p_i	CO ₂ pressure
P_{N_2}	Permeability of nitrogen
P_{O_2}	Permeability of oxygen
Q	Quadrupole moment
s^S	Partial molar entropy of the sorbate component in the reservoir
s^F	partial molar entropy of the sorbate component in the framework
T	Absolute temperature
$T_{d, \frac{1}{2}}$	Temperature of half decomposition
T_g	Glass transition temperature
U_m^S	Total intramolecular energy of the sorbate molecules
V	Volume of the body
V_S	Volume of the sample
V_{SC}	Volume of empty sample container
V_{SC+S}	Volume of sample container and sample
$V(T)$	Coefficient of volumetric thermal expansion
V_w	Van der Waals volume
V	Molar volume
$V_{(298K)}$	Molar volume at room temperature [cm ³ /mole]
v	newchor
$.0_\chi$	Zeroth-order atomic connectivity indices
$.0_\chi^V$	Zeroth-order valence connectivity indices
$.1_\chi$	First-order atomic connectivity indices
$.1_\chi^V$	First-order valence connectivity indices
x_{1-13}	Structural parameters
x_i	Mole fraction of sorbed gas in term of monomer unit
$Y_{d, \frac{1}{2}}$	Molar thermal decomposition function
α	Polarizability

α_r	Volumetric thermal expansion coefficient [ppm/K]
μ	Dipole moment
δ	Solubility parameter
β	Reciprocal temperature
K_B	Boltzmann constant

CHAPTER 1

INTRODUCTION

1.1 Background of Study

Natural gas is of great importance, not only as a source of energy, but also as a raw material for the petrochemical industry. Schemes are being developed in order to utilize natural gas. From a recent finding, oil is still considered to be the major source of energy, contributing some 40% of the total energy consumption, while coal and natural gas account for 26% and 21% respectively. However, it is a known fact that natural gas reserves have exceeded oil reserves significantly [1].

Natural gas is a cleaner fuel compared to other fossil fuels because when it is burned it emits lower quantities of greenhouse gases [2]. It is a mixture of hydrocarbons, mainly methane as a dominant component besides ethane, propane, butane, and higher hydrocarbons. Beside hydrocarbons, natural gas also contains small or large amounts of non-hydrocarbon gases such as carbon dioxide, nitrogen, and hydrogen sulfide (see Fig. 1.1)

The composition of natural gas varies from one location to another; Table 1.1 shows the composition of a wide variety of natural gas from different fields. The impurities in the natural gas streams include carbon dioxide, water vapor, hydrogen sulfide and nitrogen. These components are corrosive, and hydrogen sulfide is also toxic; hence, removal of the contaminants is necessary to meet pipeline requirements.

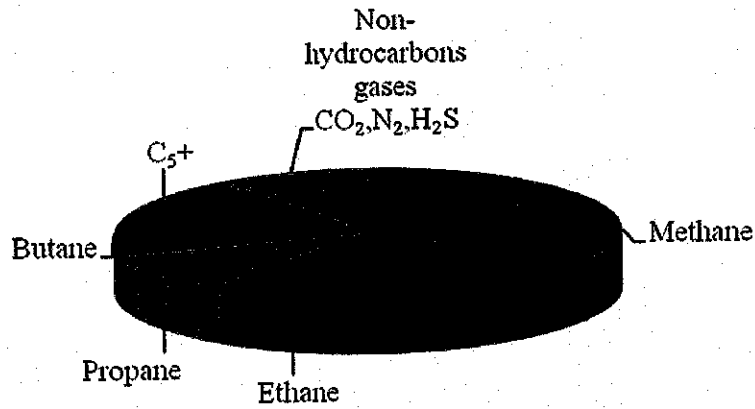


Fig. 1.1: Natural gas composition

The pipeline specifications for these components are: <2% for CO₂, <4 ppm for H₂S, and <0.1 g/m³ for H₂O [3-6].

Table 1.1: Composition of selected natural gases (volume %) [1]

Area	France	New Zealand	Texas	Texas
Field	Lacq	Kapuni	Terrell	Cliffside
CH ₄	69.3	46.2	45.7	65.8
C ₂ H ₆	3.1	5.2	0.2	3.8
C ₃ H ₈	1.1	2.0	-	1.7
C ₄ H ₁₀	0.6	0.6	-	0.8
C ₅ ⁺	0.7	0.1	-	0.5
N ₂	0.4	1.0	0.2	26.4
CO ₂	9.6	44.9	53.9	-
H ₂ S	15.2	-	-	-

Natural gas is used for the purpose of domestic heating, powering electricity production, air conditioning, fueling transportation vehicles, and fulfilling industrial heating.

The increasing utilization of natural gas as one of the means to provide energy from clean fuel has led to the increase in its exploration and production. One of the major issues facing the industry nowadays, particularly in Malaysia, is the high carbon dioxide (CO₂) content in the natural gas reserves discovered lately. The CO₂ has to be removed as it has the effect of lowering the heat value per unit volume from the natural gas. In addition, it could also poison catalysts used for gas processing involving natural gas as feed, thus severely retarding the process reaction.

1.2 CO₂ Removal from Natural Gas

CO₂ has no heating value and its removal is required in many cases particularly to increase the energy content of the natural gas per unit volume. CO₂ removal is also required as a result of it forming a CO₂CO₂ complex which is corrosive in the presence of water. For natural gas fed to cryogenic plants, removal of CO₂ is imperative to prevent possible solidification of the CO₂, which could cause pipeline blockage in the plant. Also it promotes hydrate formation, which is another potential source for pipeline blockage. In addition to the above, CO₂ has to be removed from natural gas prior to it being sent to downstream processes producing petrochemical products as it could poison the reactor catalyst such as in ammonia production.

1.3 Current Processes for Removal of CO₂ from Natural Gas

Processes for the removal of CO₂ could be divided into two main types, namely adsorption onto a solid surface (dry process), and absorption into liquid solvent (wet process). There are few other minor processes such as membrane separation that rely upon different diffusion rates for hydrocarbons and CO₂ through a membrane layer, and cryogenic distillation which exploits the relative volatility differences between

hydrocarbons and CO₂. These last two methods require large amount of energy due to the compression power needed for separation, and the amount of cooling required in order to operate under cryogenic temperature. In addition, for membrane separation, often pretreatment is required to avoid fouling and blockage of the membrane as a result of particle contaminants carried by the gas mixture flow. Thus, the application of these methods has been quite limited [7].

On the other hand, the adsorption and absorption processes find wider application as their energy requirement is much lower. These two processes can also be divided into the following categories:

- 1) Non-regenerative, where the materials used in treating the gas are not recovered in these processes.
- 2) Regenerative processes with recovery. These include physical absorption processes (water wash, Selexol, Fluor solvent, etc.), the amine processes (MEA, DEA, DGA, etc.), hot carbonate processes (Benfield, Catacarb), Alkacid processes, molecular sieves, etc.

The Adsorption process has a disadvantage in the sense that the solid absorber bed used for adsorbing the CO₂ becomes quickly saturated when high CO₂ concentration is present in the gas mixture flow. The bed has to undergo quick regeneration to avoid using extremely large bed.

The absorption process using amines as a solvent shows good potential for CO₂ absorption. However the regeneration of the solvent could be energy intensive depending on the solvent used. In addition, some of the amines form corrosive substances upon decomposition thus having to limit their concentration to a relatively low value *i.e.* about 15-20 wt %. This in turn affects the absorption capability of the solvent. Many developments have been made on improving the amine solvents lately such as the diglycolamine process (DGA) patented by Fluor Corporation [8].

1.3.1 CO₂ Removal with Amines

This is the most widely used process for acid gases treatment in natural gas and petroleum processing industries. The application of alkanolamines for acid gas treatment refers to Bottoms' patent in 1930 [9, 10]. In his patent, Bottoms discloses the use of triethanolamine (TEA) in an aqueous solution as an acid gas (H₂S and CO₂) absorbent for natural gas treatment plant.

A simplified schematic flow diagram of a typical gas treatment operation using amine solvents is shown in Fig. 1.2. A sour gas containing H₂S and/or CO₂ is introduced at the bottom of a high-pressure absorber where it rises and the counter currently contacts the descending aqueous alkanolamine solution that is introduced at the top of the absorber. The CO₂-rich amine solution that is produced is then pumped through heat exchangers where its temperature is raised. It is then introduced at the top of a stripper where it countercurrently contacts the stripping steam at an elevated temperature and reduced pressure. The steam strips the CO₂ and H₂S from the solution and the lean alkanolamine solution is pumped through the heat exchanger, where it is cooled, and reintroduced at the top of the absorber [11].

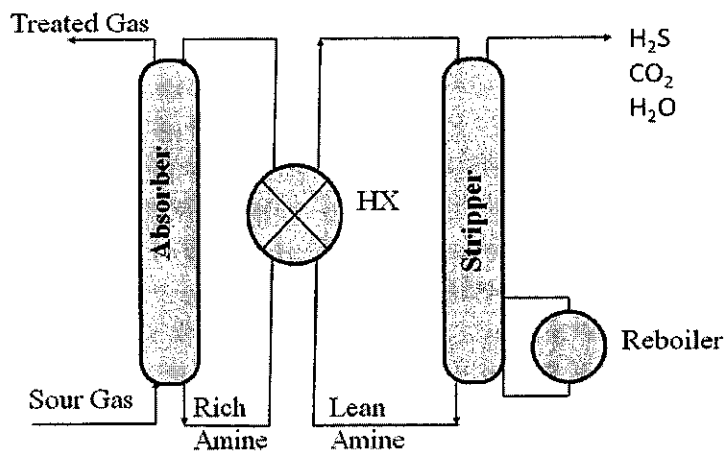


Fig. 1.2: A simplified flow schematic of a typical a absorption/stripping system for acid gases removal

Although the pioneering efforts using amines started with TEA, current advances have provided newer formulations emphasizing primary and secondary amine functionality. TEA has been displaced largely due to its low acid gas affinity (since it is a tertiary amine), and low capacity because of its high equivalent weight [12].

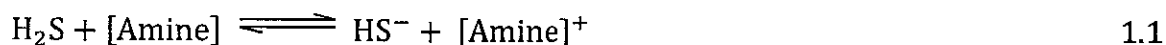
The most common used alkanolamines in industries for gas purification are monoethanolamine (MEA), diethanolamine (DEA), methyldiethanolamine (MDEA), diisopropanolamine (DIPA), and diglycolamine (DGA).

According to the degree of substitution on the central nitrogen, the alkanolamines are being classified; a single substitution denoting a primary amine, a double substitution, a secondary amine, and a triple substitution, a tertiary amine. Each of the alkanolamines has at least one hydroxyl group and one amino group. In general, the hydroxyl group reduces the vapor pressure and increases water solubility, while the amino group provides the necessary alkalinity in water solutions to remove acid gases.

The lone pair electrons on the nitrogen atom of amine functional group dominate the chemistry of amines. This lone pair electron makes the amines basic and nucleophilic. Due to these features amines readily react with acids to form acid-base salts [13]. This structural characteristic plays the major role in the acid gas removal capabilities of the various amine solvents. Primary amine (*e.g.* MEA) which has two hydrogen atoms attached to the nitrogen atom has the highest alkalinity level, compared to secondary amines which contain a single hydrogen atom attached to the nitrogen (*e.g.* DEA) thus having an intermediate level of alkalinity. The tertiary amines (*e.g.* TEA) with no hydrogen atom attached to the nitrogen atom have the lowest alkalinity level [12].

H₂S and CO₂ are acid gases because they dissociate to form a weak acidic solution when they come into contact with water or an aqueous medium, while amines are weak organic bases. The acid gases and the amine base will combine chemically to form an acid base complex in the solvent. In the absorber column the acid gas absorption of H₂S is based only on acid–base reaction.

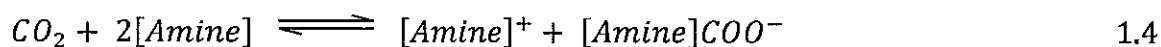
Regardless of the structure of the amine, H₂S reacts instantaneously with the primary, secondary, or tertiary amine through a direct proton transfer reaction as shown in Equation.1.1 below to form the hydrosulfide:



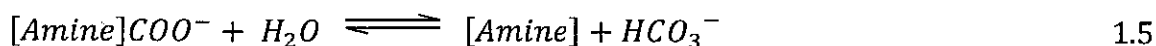
For CO₂ removal the basis of chemistry is a combination of indirect “acid-base reaction” and direct “carbamate-reaction”. The acid base reaction as shown in equations 1.2 to 1.3 may take place with any of the alkanolamines, regardless of the amine structure but is kinetically slow due to the slow carbonic acid dissociation step to bicarbonate;



Only with the primary and secondary amines the second reaction for CO₂ “carbamate reaction” may occur as shown in equation 1.4 below:



The rate of CO₂ absorption through the carbamate reaction is much more rapid than the CO₂ hydrolysis reaction, but to some extent slower than the H₂S absorption reaction. The stoichiometry of the carbamate reaction indicates that the capacity of the amine solution for CO₂ is limited to 0.5 mole of CO₂ per mole of amine if the only reaction product is the amine carbamate. However, the carbamate can undergo partial hydrolysis, as shown below in Equation 1.5, to form bicarbonate, regenerating free amine. Thus, CO₂ loading greater than 0.5 moles is possible through the hydrolysis of the carbamate intermediate to bicarbonate.



Studies have shown that the heat of solution for CO₂ absorption decreases from primary to secondary to tertiary amines as shown in Table 1.2. As primary amines

have a great affinity for CO₂, they require more energy for regeneration of the absorbent. Due to this high energy requirements, many primary amines are no longer used as a regenerative sorbent in pressure swing absorption (PSA) processes. On the other hand, tertiary amines do not exhibit sufficient affinity for CO₂ [12].

Table 1.2: Integral heat of solution for CO₂ absorption [12]

Amine	Type	Integral heat of Solution, [Cal/g. CO ₂]
MEA	Primary	1485
DEA	Secondary	1260
DGA	Primary	1476
MDEA	Tertiary	1035
TEA	Tertiary	837
DIPA	Secondary	1296

1.3.2 CO₂ Removal with DGA

Diglycolamine process using DGA® as the solvent was patented by The Fluor Corporation and was commercialized in the late sixties by Fluor and Jefferson Chemical Company, a predecessor to Texaco Chemical Company and Huntsman Corporation. DGA is a primary amine having a low vapor pressure which permits its use in higher concentrations, typically 50 to 60 weight percent, resulting in significant lower circulation rates and energy requirements. The advantages of DGA agent include [11]:

- Low capital and operating cost due to lower circulation requirements.
- High reactivity.
- Better mercaptan removal compared to other alkanolamines.

- Low freezing point; 50 wt% solution freezes at $-30\text{ }^{\circ}\text{F}$, while 15 wt% MEA and 25wt% DEA solutions freeze at $25\text{ }^{\circ}\text{F}$ and $21\text{ }^{\circ}\text{F}$, respectively.

Some of the disadvantages of DGA are:

- Nonselective removal in mixed acid gas systems.
- Absorbs aromatic compounds from inlet gas which complicates the sulfur recovery unit design
- Higher solvent cost relative to MEA and DEA.

Plants for treating natural gas have DGA concentration ranging from 40 to 70 wt%. All of the natural gas sweetening plants using DGA are capable of reducing H_2S concentration to less than 0.25 grains of $\text{H}_2\text{S}/100\text{ SCF}$. CO_2 concentration can also be reduced to less than 100 ppmv in most medium and high-pressure applications. Typical conditions found in natural gas plants are shown in Table 1.3.

Table 1.3: General conditions found in natural gas plants [13]

Range of Feed Gas Composition		0.5–25 Mole % CO_2 0-33 Mole% H_2S			
Range of Treating Pressures		60-1150 psig			
Range of Feed Gas Temperatures		65-120 $^{\circ}\text{F}$			
Typical Treated Gas Quality					
Low pressure		Medium Pressure		High pressure	
$\text{H}_2\text{S},[\text{ppmv}]$	$\text{CO}_2,[\text{ppmv}]$	$\text{H}_2\text{S},[\text{ppmv}]$	$\text{CO}_2,[\text{ppmv}]$	$\text{H}_2\text{S},[\text{ppmv}]$	$\text{CO}_2,[\text{ppmv}]$
<4	>100	<4	<100	<4	<100

The acid gas loading of the rich DGA solution depends on three key factors; the DGA concentration, $\text{CO}_2/\text{H}_2\text{S}$ percentage, and the material of construction. Plants which process natural gas with high $\text{CO}_2/\text{H}_2\text{S}$ ratio generally operate with rich DGA acid gas loading of 0.35 to 0.40 moles of total acid gas/ mole DGA. Lean DGA loadings in these plants will normally be approximately 0.1 mole of acid gas/ mole DGA. Plants with low $\text{CO}_2/\text{H}_2\text{S}$ ratios generally have loadings of 0.03 to 0.07 moles acid gas/mole DGA.

Natural gas containing low $\text{CO}_2/\text{H}_2\text{S}$ ratio is considered to be less corrosive to process in amine sweetening systems. DGA plants, treating this type of gas, typically use higher acid gas loadings in the rich DGA which, in conjunction with lower lean solution loadings, results in a considerable increase in the net acid gas pickup per mole of DGA.

The same as in the case with loadings, the energy requirement to regenerate the DGA solution is also affected by the $\text{CO}_2/\text{H}_2\text{S}$ ratio in the natural gas feeds. Plants operate with high $\text{CO}_2/\text{H}_2\text{S}$ feed require less energy compared to feed with low $\text{CO}_2/\text{H}_2\text{S}$ ratio. Plants operating with high $\text{CO}_2/\text{H}_2\text{S}$ ratio possibly will require 1.0 to 1.5 moles of water vapor per mole of acid gas in the regenerator overhead. Low $\text{CO}_2/\text{H}_2\text{S}$ ratio of 0.2/1 may require 2.5 to 3.5 moles of water vapor per mole of total acid gas in the regenerator overhead. A reflux ratio of this magnitude is common for low pressure treating plants which are required to produce natural gas with less than 0.25 grains of $\text{H}_2\text{S}/100$ SCF [13].

1.3.3 *CO₂ Removal with Membranes*

Membranes, thin barriers that allow passage of certain substances, are currently available for CO_2 removal from natural gas streams. On the other hand, membranes that have immobilized amine or alkali carbonate solutions or have been treated to attach amine functionality to its surfaces can be classified as a chemical absorption process. Fig. 1.3 shows the simplest membrane operation. The idea of using

polymeric membrane for separating gases is nearly a century old, but it has been commercially widely used only in the last 20 years. Their uses rely on both porous and non-porous membranes. Porous membranes rely on either pore size exclusion or Knudsen diffusion differences between molecules to achieve the required separation. While non-porous membranes rely on solution-diffusion differences between gases dissolving within the membrane material to achieve the desired separation. Both of these types of membranes rely on gas partial pressure gradients across the wall of the device to drive the gas molecules across.

Membrane materials that are currently available for natural gas treatment are polymer based, *i.e.*, cellulose acetate, polyimides, polyamides, polysulfone, polycarbonates, and poly-etherimide. Cellulose acetate membrane is contained in spiral wound configuration that compromise between high surface achievable in hollow fiber membranes and low-cost fabrication of flat sheet cross-flow membranes. The diffusion of water vapor through the membranes matrix reduces the diffusion of CO₂ molecules.

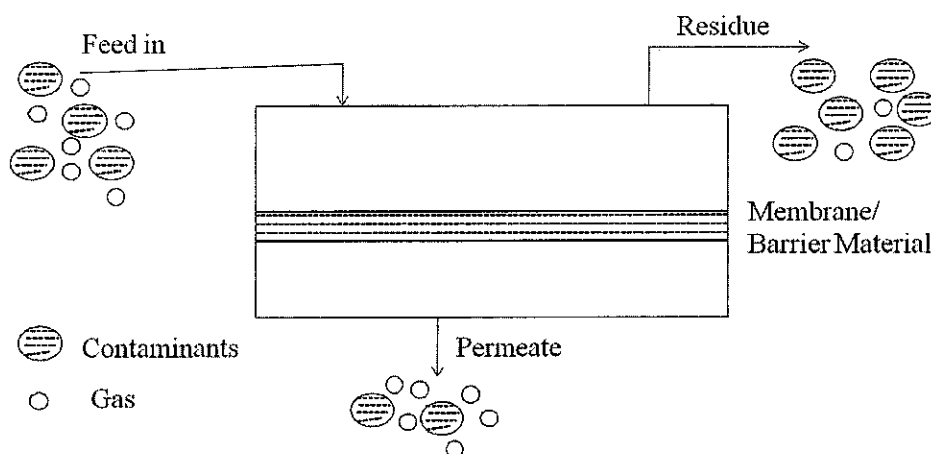


Fig. 1.3: Simple membrane separation operation [14].

Silicon rubber and polyethersulfone membranes have shown the ability to enhance CO₂ flux through the membrane walls. The plasma polymerized membranes and thin film composite membranes are introduced for the purpose of increasing the CO₂ flux

[15, 16]. To have a feasible solution, all of the attempts to increase the CO₂ flux must not produce an equivalent increase in CH₄ diffusivity.

To increase the CO₂ flux through the membrane, researchers have attempted to use facilitated transport via Immobilized Liquid Membranes (ILM). Immobilized Liquid Membranes, which are porous membranes, rely on a liquid trapped inside the membrane pores to provide a transport increase for CO₂ across the membrane walls. By using a selective solution with a high affinity for CO₂, researchers are able to achieve a facilitated transport of CO₂ through the solution. The challenges in using Immobilized Liquid Membrane come from finding a solution which combines the ability to mix with CO₂ along with very low vapor pressure to keep its presence within the pores of membranes. The solution within the membrane pores should be compatible with the membrane materials itself and maintain enough viscosity to enhance CO₂ transport all the way through the membrane.

The uses of membranes in the past have demonstrated the need for pretreatment of the feed stream when processing natural gas. Membrane life was found to be too short as well. Natural gas can contain a wide variety of contaminants that quickly reduce membrane effectiveness and force premature replacement of the elements. Substances usually found in natural gas streams which lower the performance of CO₂ removal membranes include:

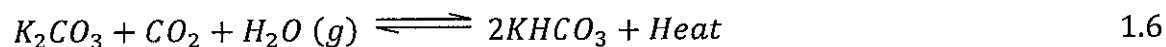
- Liquids: Liquids cause swelling of the membranes and can destroy the membrane.
- Heavy hydrocarbons, approximately > C15: Significant levels of these compounds slowly coat the membrane surface, thus decreasing permeation rate.
- Particulate material: Particles can block the membrane flow area.
- Certain corrosion inhibitors and additives: some corrosion inhibitors and additives are destructive to the membrane systems.

1.3.4 Removal Using Solid Sorbents

Solid-based CO₂ capture processes operate in a cyclic mode of alternating reaction-regeneration cycles. Sorbent is consumed and CO₂ captured during reaction; and CO₂ is liberated as the sorbent is regenerated. Operation may occur in circulating fluidized-bed or transport reactors for steady state operation, or using multiple fixed-bed reactors with reaction and regeneration gas flow alternating between the suitable reactors.

Solid processes possess many potential advantages compared to gas absorption. Solids may be used over a wide range of temperature ranging from near ambient to 700°C. No liquid wastes are generated, and spent solids may often be disposed without too much environmental precautions.

The Benfield Process [17, 18]; an example of the alkali metal carbonate process, is dependent on the chemical reaction between hot potassium carbonate and acid gases for removal of CO₂. Equation 1.6 shows this reaction:



This is a reversible reaction with a heat of reaction about half that is found in similar amine based reactions systems. This means that the energy required for regeneration can be much less than that found in amine processes.

The key factors in the further development of solid processes are the cost and durability of the reactive solids, along with the development of technology to manage the large solid circulation rates.

1.4 Ionic Liquids and Polymerized Ionic liquid

Ionic liquids are organic salts with melting points usually below 100°C. Exploring and understanding the solubility of various gases in ionic liquids have gained a great interest in the last few years. Due to their attractive properties i.e. extremely low

vapor pressures, wide liquid ranges, non-flammability, thermal stability, tunable polarity, good electrolytic properties and easy recycling, Ionic liquids becomes attractive candidate sorbents for CO₂ capture and separation. However, desorption of CO₂ in ionic liquid media and regeneration of the sorbent require significant amount of thermal energy. Moreover, the viscosity of ionic liquids is relatively high, about 5-fold higher than that of a traditional aqueous solution of MEA leading to an additional energy penalty in pumping the sorbent. By polymerizing the ionic liquids, the CO₂ absorption and desorption rates becomes much faster than those in ionic liquids and the absorption/desorption is completely reversible. The chemical and molecular structure of the ionic liquids in monomeric and polymeric form affects the gas absorption capacity.

1.5 Criteria for Process Selection

There are many variables involved in a gas separation process, which make the selection of the most suitable process for a particular application, very difficult. The most important factors that have to be normally considered are [7]:

1. The types and concentration of impurities in the gas, and the degree of separation desired.
2. The selectivity of the acid gas removal required, if any.
3. Temperature and pressure at which the feed gas is available and the product gas to be produced.
4. The volume of the gas to be processed, and its hydrocarbon composition.
5. The CO₂ to H₂S ratio in the gas.
6. The economics of the process.

1.6 Carbon Dioxide Utilization

CO₂ has many commercial uses with new applications continually being created. CO₂ may be used in either a vapor, liquid, solid or supercritical state in a particular

application. It is converted into liquid forms at approximately 250 – 300 psig for economical storage and transportation. CO₂ vaporizers can convert bulk CO₂ liquid into vapor which can be utilized in applications such as the carbonation of beverages, increasing the hardness of desalinated water, or the process of pH adjustment.

Bulk CO₂ liquid may possibly be utilized as a low temperature heat transfer fluid or as a cascade mechanical refrigeration system. Solid CO₂ is produced by expanding bulk liquid CO₂ to near atmospheric pressure prior to compacting them to form solid in a dry ice press. It is often used for food freezing. Supercritical CO₂ is produced by increasing the temperature and pressure of bulk liquid CO₂ above their critical values. Many separation and cleaning applications can make use of the advantages of the solubility and / or low surface tension properties of supercritical carbon dioxide.

Carbon dioxide is an easily available renewable carbon source, which has the advantages of being non-toxic, abundant, and economical (Fig. 1.4) [19]

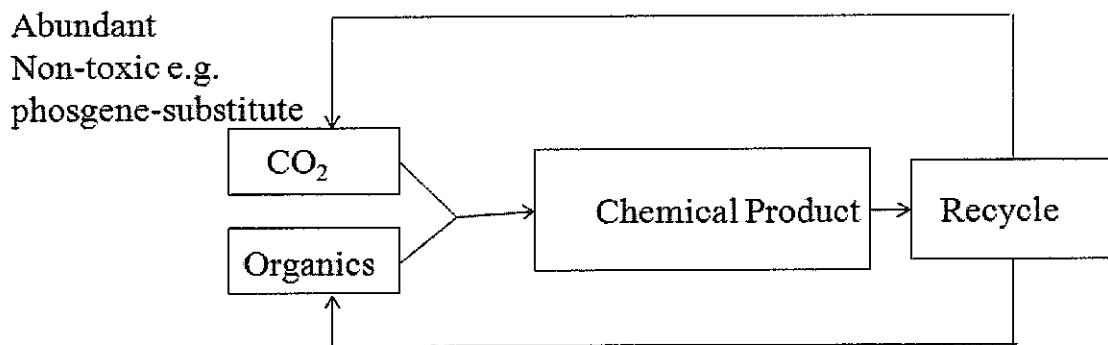


Fig. 1.4: CO₂ as a green carbon resource [19]

Few industrial processes have been utilizing CO₂ as a raw material. As it is the most oxidized state of carbon, the biggest challenge for establishing industrial processes based on CO₂ as a raw material is its low energy level. This means a large energy input is required for CO₂ transformation.

There are four main methodologies for transforming CO₂ into useful chemicals:

- Using high-energy starting materials such as hydrogen, unsaturated compounds, small – member ring compounds and organometallics compounds.
- Choosing oxidized low-energy synthetic targets such as organic carbonate.
- Shifting the equilibrium towards the product side by removing a particular compound.
- Supplying physical energy such as light or electricity.

Selecting appropriate reactions can lead to a negative Gibbs free energy (Fig. 1.5).

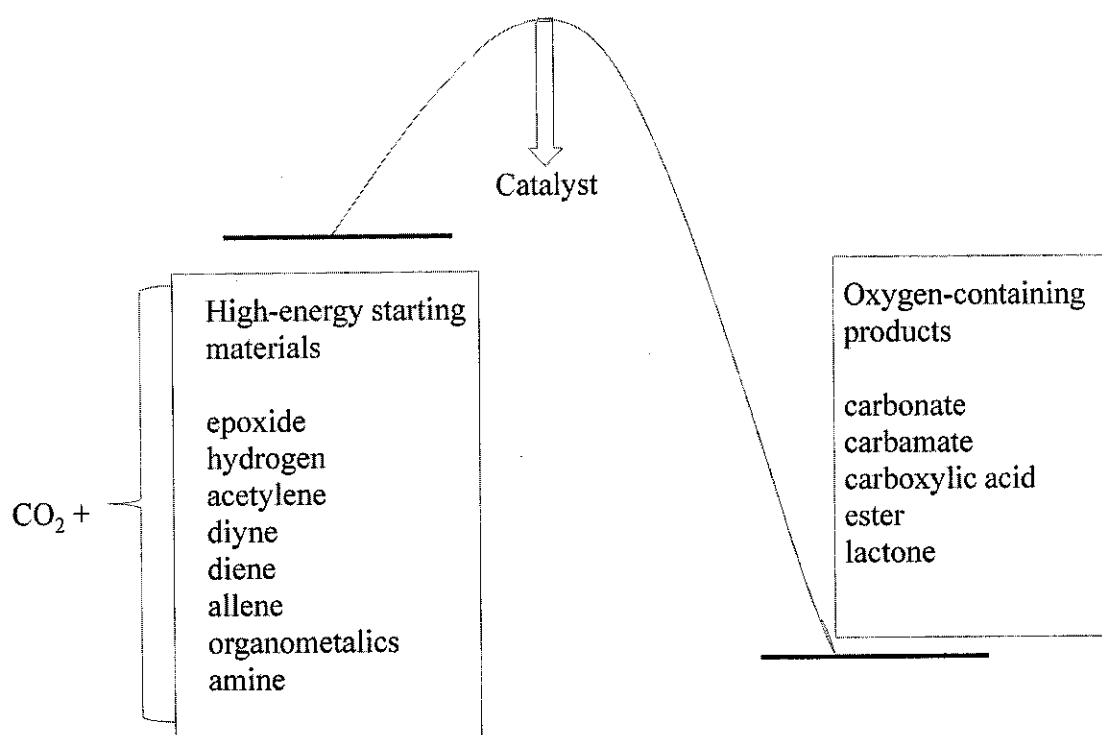


Fig. 1.5: Organic synthesis using CO₂ [19].

A lot of research have been conducted on reactions using CO₂ as a raw material *e.g.* reduction of CO₂ under photo-irradiation, or under electrolytic conditions, or

production of synthesis gas through reforming of natural gas with CO₂. Many of these reactions produce rather small molecules such as carbon monoxide and formic acid.

Carbon dioxide is an anhydrous acid that rapidly reacts with basics. An example of this reaction is the CO₂ reaction with organometallic reagents such as Grignard reagents even at low temperatures. Water, alkoxides, and amines also react with CO₂ in the same way to produce compounds with carboxyl or carboxylate groups. These reactions expediently produce carbonic and carbamic acids. Further reactions of these compounds with electrophiles lead to the formation of organic carbonates and carbamates. On the other hand, reactions of CO₂ with low valent metal complexes such as nickel (0) and palladium (0) and unsaturated compounds lead to the formation of five-member metallalactones (see Fig. 1.6) [20]. As the valence of the metal increases by two, this type of reaction is called an oxidative cycloaddition.

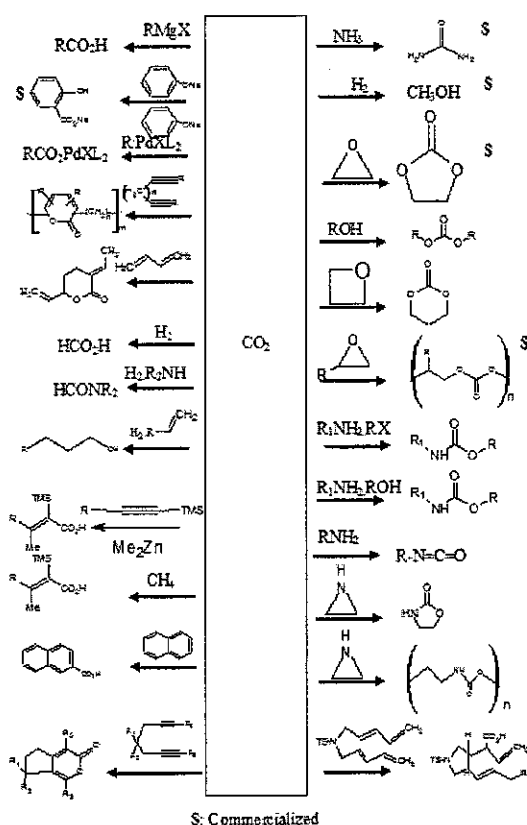


Fig. 1.6: Summarized examples of organic synthesis starting from CO₂ [21]

1.7 Problem Statement

One of the major issues facing by the industry nowadays, particularly in Malaysia, is the high carbon dioxide (CO₂) contents in the natural gas reserves discovered lately. The existing processes for CO₂ removal suffer from one main setback *i.e.*, the limitation on the maximum content of CO₂ that is allowed in the natural gas feed, prior to its separation to produce natural gas at high purity as required by the industry. This has led to researchers working on alternative solvents or technology to overcome the problem. The use of ionic liquids in place of conventional solvents has received considerable attention lately. Firstly, they are known to be much safer and cleaner by not releasing any volatile toxic organic materials due to their extremely low vapor pressure and high thermal stability which can be as high as 300°C. Such high temperature leads to better reaction kinetics for the absorption process as well as smaller absorber sizes. Secondly, easy and straight-forward separation from the component absorbed using conventional distillation causing little losses of the ionic solvents. However, the ionic liquids suffer the problem of having high viscosity which makes them hard to be handled in the industry. This high viscosity which is about 5-fold higher than that of a traditional aqueous solution of MEA will lead to an additional energy penalty when pumping the sorbent. Besides these, desorption of CO₂ in ionic liquid media and regeneration of the sorbent requires significant amount of thermal energy.

RTILs are also lack of mechanical stability and may not be suitable for certain applications where a solid material is necessary. Polymerized ionic liquids (pILs), which could be formed by polymerizing the ionic liquid monomer, will incorporate macromolecular structure with ionic liquid. Polymerized ionic liquids showed enhanced CO₂ sorption capacities and fast sorption/desorption rates compared with room temperature ionic liquids. Studies, conducted on pILs for CO₂ capture, where looking at the effect of changing the chemical structure of pILs. These studies fail to find guidelines and factors that will enhance the sorption capacity of CO₂ by changing the chemical structure of pILs. The studies also report the effect of cation and anion on CO₂ sorption capacity without conducting a molecular dynamics simulation to

study the location of adsorbed CO₂ on pILs. It is also worth to mention that the available data on sorption of carbon dioxide on polymerized ionic liquids are basically on [PF₆] and [BF₄] based anion polymers which make it difficult to apply in the industry as they may form explosive HF gas.

1.8 Objective of the Study

The objectives of this project are to:

- I. Develop novel polymerized ionic liquids that could be potentially exploited for CO₂ sorption.
- II. Determine the CO₂ sorption kinetics for the synthesized polymerized ionic liquid.
- III. Study the effect of polymerized ionic liquids structures on CO₂ sorption by measuring the CO₂ sorption capacity and rate for pILs with different cation, backbone, alkyl length, central atom, and anion.
- IV. Study the effect of water presence in polymerized ionic liquids on CO₂ sorption.

1.9 Scope of the Study

The scope of this study is to:

- I. Synthesize pILs with different chemical structures. The synthesis will be directed by Monte Carlo molecular dynamic simulation results by checking the location of CO₂ and ion conductivity effect.
- II. Using magnetic suspension balance, the CO₂ sorption rate and capacity on pILs at fixed pressure and temperature is studied to enable finding guidelines and factors that affect the sorption capacity.

- III. Water with different ratios is added to pIL of high CO₂ sorption capacity and the sorption of CO₂ will be measured using MSB to study the effect of water on sorption rate and capacity

1.10 Structure of Thesis

In Chapter Two, literature review on the main topic of this thesis will be covered in details. This review includes the history of ionic liquids, their structure and properties, the carbon dioxide solubility in conventional and task specific-ionic liquids. This chapter also details the history of poly ionic liquids, their carbon dioxide sorption, and other promising applications of poly ionic liquids.

Chapter Three, details the theory. A hypothesis explaining the sorption of CO₂ on poly ionic liquids will be introduced. It also covers the molecular dynamic simulation methods theory including the Synthia module and Monte Carlo sorption module. A description of the various techniques typically used in measuring gas sorption will be covered focusing on the technique used in this work.

Chapter Four, details the experimental methods of the research. Computational procedure for Molecular Dynamics simulation is given in details. A detailed description of synthesis of poly ionic liquid will be given followed by details of the experimental procedure and apparatus used for characterization of these poly ionic liquids. The procedure of sorption measurement is also explained.

Chapter Five presents the results from molecular dynamic simulation. It also covers the characterization results for the new synthesized polymerized ionic liquids. The sorption measurement results studying the effect of poly ionic structure, effect of temperature, effect of pressure, ideal selectivity and molecular interactions, recyclability, and effect of water are presented and analyzed.

Finally, the conclusions followed by recommendations for future work are summarized in Chapter Six.

CHAPTER 2

LITERATURE REVIEW

2.1 Ionic liquids (ILs)

The use of ionic liquids (ILs), which are special salts with melting temperature below 100°C, have recently attracted considerable attention as potential alternatives to conventional organic solvents in a variety of synthetic, catalytic, and electrochemical applications. These salts typically consist of bulky organic cations and in/organic anions; demonstrate distinct selectivity and reactivity when compared to conventional solvents. The ionic solvents are composed entirely of ions, and strongly resemble ionic melts that may be produced by heating metallic salts. The constituents of ionic liquids are constrained by high columbic forces, exhibiting practically no vapor pressure. This unique property gives them the capability to expand traditional laws of chemistry. They can be made immiscible with water and/or a number of organic solvents, allowing for more efficient reactions and separations to take place [22].

There are large variations of ionic liquids that can be made from these salts by varying the ions used. According to Seddon [23], new ionic solvents could be made by coupling different positive and negative ions for countless reactions. This led to the possibility of customizing the design of ionic solvents for a specific application. Chemists are constantly creating new ionic liquids by trying different ion mixes and discovering just how smoothly and efficiently their reaction could proceed. To a certain extent they are close to producing an ionic liquid for almost any reaction that would normally use toxic organic solvents. [24]. A part from the above, physical and chemical properties such as density, conductivity, viscosity, Lewis acidity, hydrophobicity, and hydrogen-bonding capability, of the ionic solvents can be

changed by varying the structure of the component ions to obtain the desired solvent properties.

Room temperature ionic liquids consist solely of ions. However, unlike conventional molten salts (for example, molten sodium chloride), these materials often melt below 100°C. This is achieved by incorporating a bulky asymmetric cation into the molecular structure thus stopping the ions from packing easily. Since the melting temperature is low, ionic liquids can act as solvents in which reactions can be performed, and because the liquid is made of ions rather than molecules, such reactions often give distinct selectivities and reactivities when compared with conventional organic solvents.

In term of associated ions, these compounds look like classical molten salts. For instance, when sodium chloride is heated above 800 °C, it produces a molten salt that is a liquid ionic material. While sodium chloride at normal temperature dissolves in water to form an ionic solution as in Fig. 2.1 unlike molten salts, ionic liquids exhibit lower viscosity, are not corrosive, and are liquids below 100 °C.

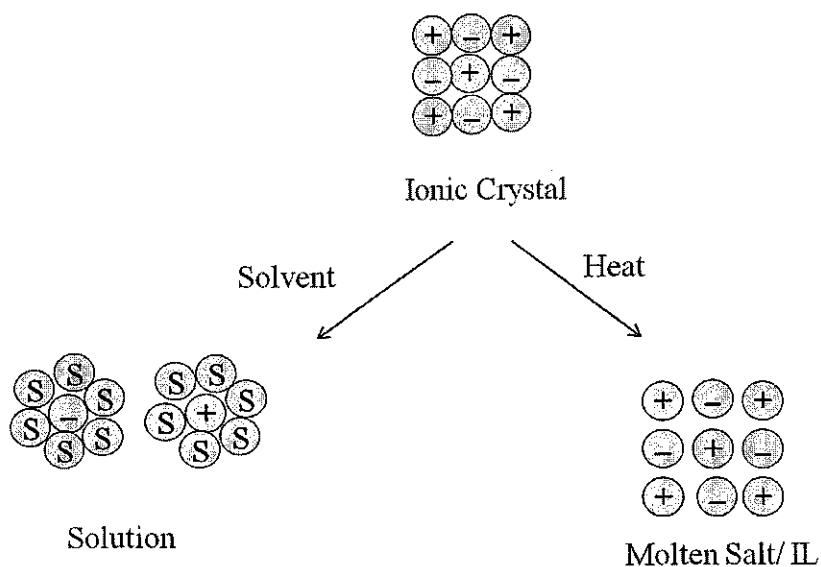


Fig. 2.1: Scheme of an ionic liquid versus an ionic solution [25]

Prior to 1979 the two terms “Ionic Liquids” and “molten Salts” were commonly used in a similar way. But now the term ionic liquids is used almost exclusively for room temperature ionic liquids (RTILs), while the term molten salts denotes salts with melting points above 100°C. According to Wasserscheid and Keim, this illogical line drawn between molten salts and ionic liquids at melting temperature of 100°C can be justified by the abrupt improvement in the range of applications for liquid salts below this temperature [26].

It seems illogical to limit the definition of ionic liquids to 100°C melting point. This is because for certain processes, the operating temperature could be well above the melting point of the ionic liquids which could be solid at 100°C, which means that we can still utilize the properties of the ionic liquid in liquid form. So a more logical definition for ionic liquids is ILs are organic salts that composed of organic cation and organic or inorganic anion which are liquid at an operating temperature that is below their decomposition temperature.

The liquid nature or low melting point of these salts depends on some factors as discussed by Holbery *et al.* [27]. The major factors influencing the melting point are charge size, charge distribution on the respective ions, and the asymmetric extent of the cation. Generally, larger ions result in a decrease in melting point due to the delocalization of charge, less charge density and therefore reduced Columbic attraction between the ions. The failure of the ions to fit into crystal lattice owing to the sizes of the ions involved, described as “packing inefficiency” has been anticipated as a key factor in rationalizing the low melting points of some ionic liquids [28]. Large anions with many degrees of freedom reduce crystallization until lower melting points are obtained [29].

Room-temperature ionic liquids have been utilized as clean solvents and catalysts in green chemistry, as electrolytes for batteries, and in photochemistry and electrosynthesis. They remained to be non-volatile even at elevated temperatures providing flexibility for a number of reaction and separation schemes. Salts based upon poor nucleophilic anion such as $[\text{BF}_4]^-$, $[\text{PF}_6]^-$, $[\text{CF}_3\text{CO}_2]^-$, $[\text{CF}_3\text{SO}_3]^-$, etc, are

water and air insensitive and possess remarkably high thermal stability. Many of these materials are based around the imidazolium cation such as 1-alkyl-3-methylimidazolium. By changing the anion or the alkyl chain on the cation, a wide variation in properties such as hydrophobicity, viscosity, density and solvation can be obtained [30].

Significant research progress has been made in the use of ionic liquids in chemical processes. However, they have not yet been commercially significant for industrial exploitation, mainly due to the high cost of producing them [22].

2.1.1 *History*

The beginning of ionic liquids is difficult to identify. In the past if a chemist discovered oil instead of a crystalline product, the undesired oil was regarded as a vain synthetic attempt. The chemist performing AlCl_3 catalyzed Friedel-Craft alkylation in the middle of the nineteenth century may possibly have accidentally developed the first ionic liquid. The red oil they often discarded as an unsuccessful synthetic attempt today would indeed be considered as an ionic liquid.

The first ambient temperature ionic liquid reported back in 1914 was ethylammonium nitrate discovered by Walden [31]. This salt has a melting point of 12°C but usually contains 200-600 ppm of water.

Even though the first synthesis of ionic liquids was described at an early date, only within the last ten years the ionic liquids have become widely popular. The reason behind that is the fact that the field of low temperature ionic liquids was dominated by the chloroaluminate containing ionic liquids. These compounds are air sensitive and possess high melting points. In 1948 Hurley and Weir developed the first ionic liquid with chloroaluminate ions (N-alkylpyridinium chloroaluminates) at Rice Institute in Texas as electrolytes for electroplating aluminum [32]. However till the mid to late 1970's there was no report on the chloroaluminate systems.

U.S Air Force Academy began the first major research in the ionic liquid field in the late 1970's. Wilkes and Osteryoung groups reported then on their discovery of the first room temperature chloroaluminate ionic liquids [33, 34]. These ionic liquids are N-alkylpyridinium halide mixtures with aluminum chloride. These liquids are used as a media for electrochemical applications [35-43]. These ionic liquids are developed by these researchers at the U.S Air force in an effort to replace the LiCl/KCl molten salt electrolyte used in thermal batteries. The reason behind this replacement is the high operating temperatures (375-550⁰C) of thermal batteries which caused material problems inside the battery and incompatibilities with close-by materials [29].

Some of the physical properties of alkylpyridinium chloroaluminate liquids were reported by Hussey *et al.* in 1979. The problem of these liquids is that they are very much subjected to both chemical and electrochemical reduction fairly easily [33].

In the midst of 1960's and early 1970's, the synthesis and application of monocationic quaternary ammonium salts with melting points below 100⁰C as new types of solvent systems was reported. The anions reported are [I]⁻, [Br]⁻, [SCN]⁻, [ClO₄]⁻, [NO₃]⁻, picrate and tetraalkylboride. However, these ionic liquids haven't been studied comprehensively as the chloroaluminates [44-49].

Wilkes and co-workers reported in 1982 the preparation and physical properties of the first example of ionic liquids based on dialkylimidazolium chloroaluminates (Fig. 2.2). These ionic liquids show interesting chemical properties, such as superacidity. They are also excellent non-volatile catalysts for Friedel-Crafts alkylation and acylation reactions as catalyst and solvent [50, 51].

Hussey *et al.* [52] reported on synthesis and properties of (aluminum bromide-1-methyl-3-ethylimidazolium bromide) ionic liquid in 1986. This system was investigated further by Osteryoung group as a media for electrochemical and spectroscopic studies [52-54].

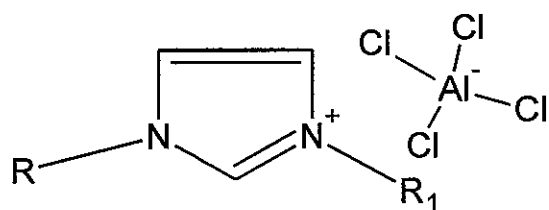


Fig. 2.2: Dialkylimidazolium chloroaluminates ionic liquid

Osteryoung and his group also reported on NMR investigation for the N-butylpyridinium-aluminum chloride system. Compared to the alkylpyridinium chloroaluminates which are discovered since the 1940's, the ethylmethylimidazolium chloroaluminate compound showed a wider liquid range and electrochemical window (electrochemical window is the electrochemical potential range over which, the liquid is not oxidized or reduced at the electrode) of greater than 3.0 V which resulted in a tremendous increase in research activities in this field [55, 56].

Unfortunately, these ionic liquids are unstable in water and air due to their high reactivity towards water. This oriented the search for water-stable anions, resulting in the findings of tetrafluoroborate, hexafluorophosphate, nitrate, sulfate, and acetate ionic liquids in 1992 as a major breakthrough by Wilkes and Zaworotho [56]. Since their discovery, water-stable ionic liquids have been at the center of interest as novel environmentally friendly solvents for different applications. This led to a dramatic increase in the number of applications investigated for ionic liquids. The range of possible anion and cation has extended vastly and new ionic liquids are found constantly.

The possibilities of choosing different anions enable the researchers to vary the ionic liquids properties. An example for that is the hydrophobic or hydrophilic properties that can be provided through customized ILs to fit specific application. Ionic liquids have been described as designer solvents [57-59]. It is estimated by Holbery and Seddon that there are around one trillion (10^{18}) available room temperature ionic liquids [60]. This changeability allows for almost unlimited potential in terms of applications. According to Dr. Wilkes, "the applications will be limited only by our imagination" [27].

2.1.2 Structure and properties of ionic liquids

Ionic liquids are in general composed of relatively large organic cations associated with small organic or inorganic polyatomic anions. The difference between low melting points ionic liquids and their crystalline solid relatives is because of the presence of the organic cation. The most commonly reported monocationic species include imidazolium, ammonium, pyrrolidinium, pyridinium, phosphonium, guanidinium, and sulfonium are shown in Fig. 2.3.

The associated anions as shown in Table 1.1 are relatively small compared to the cation size. This range of anions and cations make it possible to synthesize a wide range of ionic liquids.

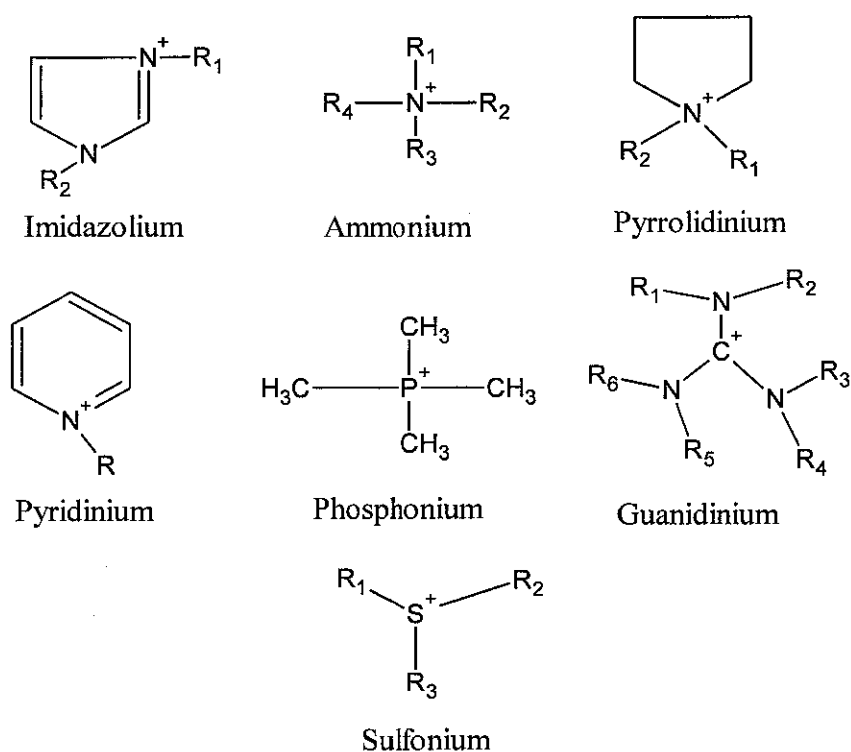


Fig. 2.3: Most common reported cations of ionic liquids

It is feasible to tune the physical and chemical properties of ionic liquids by varying the nature of cations and anions. In a way, ionic liquids can be made task-specific.

Generally, ionic liquids have many properties similar to conventional organic solvents such as good solvation qualities. In addition, they also have a wide liquid temperature range which may allow for tremendous kinetic control in reactions.

The most important physical property of ionic liquids is their negligible vapor pressure [52, 61, 62]. This negligible volatility decreases the risk of worker exposure and the loss of solvent to the atmosphere. As a result, ionic liquids can be described as odorless. They don't evaporate at normal conditions, and most of them do not combust, even when exposed to direct flame. This may lead to suggest that ionic liquids can be basically safer and more environmentally benign than traditional volatile organic solvents.

Table 2.1: Anions generally found in ionic liquids [26]

AlCl_4^-	Al_2Cl_7^-	PF_6^-	BF_4^-
NO_3^-	CF_3SO_3^-	$(\text{CF}_3\text{SO}_2)_2\text{N}^-$	SbF_6^-
ArSO_3^-	CF_3CO_2^-	CH_3CO_2^-	HSO_4^-
NO_2^-	HexBEt_3	OTS^-	AuCl_4^-
Carborane	Cl^-	AlCl_{10}^-	AlEtCl_3^-
BCl_4^-	AlBr_3^-	PO_4^{3-}	$\text{C}_{10}\text{H}_{21}\text{COO}^-$

Other properties of ionic liquids are their good thermal stability, high ionic conductivity, and the wide electrochemical window leading to high electrochemical stability of ionic liquids against oxidation or reduction reactions [63]. Moreover, ionic liquids have a good solvency power for organic and inorganic materials, polar and non-polar; this makes them suitable for catalysis [64, 65]. These properties depend on the type of cation, anion, and substituents. This makes it possible to tailor an ionic liquid for a particular application. Adjusting the structure of either cation or anion can have a large impact on many properties such as melting point, viscosity, density, and gas and liquid solubility [66-70].

2.1.3 *How green are ionic liquids?*

Anastas and Warner have outlined the basic principles of green chemistry as a basis for judgments on sustainability as follows [71]:

1. Prevention (prevention of waste production rather than remediation of waste once formed).
2. Atom economy.
3. Less hazardous chemicals.
4. Design safer chemical products.
5. Safer solvents and auxiliaries (with lower environmental impact).
6. Energy-efficient by design (energy consumption close to necessary thermodynamically energy).
7. Use of renewable feedstocks.
8. Shorter synthesis (avoid derivatization).
9. Catalysis selectivity (more selective, less by-products).
10. Design for degradation.
11. Real-time analysis for pollution prevention.
12. Inherently safer chemistry for accident prevention.

Due to their negligible vapor pressure, which prevents evaporation into the air and allow simple recycling, ionic liquids are regarded as environmentally benign replacement for volatile organic solvents. But is this sufficient for the safe chemical industry of the future? According to Prof. Robin Roger “Before we can say that ionic liquids are green, we have to look at their entire life cycle. People are calling ionic liquids green because they are not volatile, but we have to look at how they are made all the way through to recycling and disposal”. Therefore environmental issues have to be tackled before ionic liquids can be used in an industrial scale [72].

In a lot of ionic liquids synthesis pathways, halogen atoms are involved. Halogen atoms in ionic liquids are undesirable, due to their low hydrolysis stability, high toxicity, low biodegradability and high disposal cost. For instance, fluorinated anions

such as $[\text{BF}_4]^-$ and $[\text{PF}_6]^-$ are very sensitive to water which may lead to formation and release of the corrosive and toxic hydrogen fluoride. Likewise, the alkyl halides used in synthesis of many ionic liquids are considered as greenhouse gases and ozone-depleting materials. Consequently, halogen-free ionic liquid have been developed to overcome this problems *i.e.* ionic liquids with alkyl sulfate, alkyl carbonate and alkyl sulfonate anions [27, 73, 74].

Volatile organic compounds (VOCs) are used in manufacturing ionic liquids. Moreover, ionic liquids themselves are of VOCs. However, in 2002 there had been real advances in synthesis of solventless ionic liquids by Rajender Varma and Vasudevan Namboodiri at EPA's National Risk Laboratory in Cincinnati, OH USA. They managed to prepare the 1-alkyl-3-methylimidazolium halides in open containers in microwave oven without the need of any solvent [75, 76].

Recycling the ionic liquids is one of the challenges that researchers are facing; because many processes may involve water or VOCs for cleaning up ionic liquids. In 2001 Joan Brennecke successfully used the supercritical CO_2 to remove dissolved organic compounds in ionic liquids. On the other hand, Roger and Davis managed to clean the ionic liquids in their contaminated metal process by heating under vacuum [72].

Over the last few years, the engineering data for ionic liquids has been extended tremendously. Unfortunately, only scarce data on toxicity are available till now.

2.1.4 CO_2 Solubility in Ionic Liquids

Due to their negligible vapor pressure, which is caused by columbic attraction between the ions; ionic liquids has become an attractive material for gas processing [77]. A number of investigations have shown that CO_2 is highly soluble in ionic liquids. Depending on their structure and sorption mechanisms, ionic liquids can be classified into two categories: conventional ionic liquids and task-specific ionic liquids. The conventional ionic liquid can take up less amount of CO_2 due to the

physical interaction between CO₂ and the ionic liquids, whereas, the task-specific ones with alkaline groups could take up larger amount of CO₂ than conventional ionic liquids due the reactivity between the alkaline group of ionic liquids and CO₂ [78].

2.1.4.1 CO₂ Solubilities in Conventional Ionic Liquids

Blanchard *et al.* had shown that CO₂ is highly soluble in imidazolium-based ionic liquids and supercritical CO₂ can be utilized to extract solute from ionic liquids [79-82]. Reporting the solubilities of different gases in several ionic liquids, Anthony found water and benzene to be most soluble, followed by nitrous oxide, carbon dioxide, ethylene, ethane, methane, oxygen, and argon. Gases with large dipole moments (*e.g.* water) or quadrupole moments (*e.g.* CO₂ and N₂O) showed the highest solubilities in ionic liquids, while the solubilities of non-polar gases well agreed with their polarizability. Nevertheless, CO and N₂ solubilities do not follow these trends showing that the dipole and quadrupole moments and polarizability cannot fully describe the behavior of gases in ionic liquids [83].

In comparison between the [bmim][Tf₂N], [bmim][BF₄], and [bmim][PF₆], Anthony [83] reported a considerably higher affinity for CO₂ with the anion [Tf₂N]. This shows that the anion plays a major role in determining the gas solubilities in ionic liquids. The nature of cation has lesser influences on CO₂ solubility. By changing the cation from imidazolium to quaternary ammonium to pyrrolidinium, all with [Tf₂N] anion, only little difference in CO₂ solubility occurred. By replacing the hydrogen at position 2 on the imidazolium ring with a methyl group, the solubility of CO₂ will only slightly decrease. In their study of high-pressure solubility of CO₂ in imidazolium-based ionic liquids with anions [PF₆] and [BF₄], Lim *et al.* [84] concluded that an ionic liquid with longer alkyl-chain cation [omim] showed a 10% improvement in solubility of CO₂ compared with shorter alkyl-chain cation [bmim] due to the favorable interaction between CO₂ and the alkyl side chain. Moreover, they realize that the water content has a minor effect on gas solubility depending on the nature of cation and anion. When changing the anion from [BF₄] to [PF₆], the solubility will increase by a factor

of 10%. By increasing the water content by 4 to 10 times, the solubility of CO₂ at 313.15 °K decreases by 7 to 8% at 8 to 10 MPa and 2 to 3% at higher pressures around 20 to 30 MPa respectively.

A number of factors (*i.e.* free volume, size of the counter ions, and strength of cation-anion interactions) seem to rule CO₂ solubility in room temperature ionic liquids (RTILs) [85]. The higher solubility shown by longer alkyl-side chain may be due to the increased free volume available for CO₂ with corresponding decrease in cation-anion interaction [86, 87]. Molecular simulation carried out by Cadena et.al [88] showed that the CO₂ organized strongly about the [PF₆] anion in a “tangent-like” configuration that maximizes favorable interactions but is more diffusely distributed around the imidazolium ring.

Other researchers [79, 89] reported that CO₂ solubility in ionic liquids approaches a maximum between 70 mol % and 90 mole %, and the system can still maintain two phases even up to 3100 bar. This behavior is unusual compared to an organic liquid-CO₂ mixture, which reaches its critical point at a certain pressure and thus formed a single phase. Generally, the absorption of CO₂ in conventional ionic liquids is very limited due to its physical interaction, although it is higher than the solubility of CO₂ in conventional organic solvents (*i.e.* heptanes, ethanol, benzene, etc.). At room temperature and atmospheric pressure the equilibrium of these ionic liquids will reach around 0.10-0.15 wt% which is obviously too low for industrial utilization.

Scovazzo *et al.* [90] studied gas separation using non-[PF₆] anion [emim] based ionic liquids supported membrane. The studied RTIL-membranes are made from the following water stable anions: bis(trifluoromethanesulfonyl)amide [Tf₂N], trifluoromethanesulfone [CF₃SO₃], chloride [Cl], and dicyanamide [dca]. They reported CO₂ permeabilities of 350 barrers (for [Cl]) to 1000 barrers (for [Tf₂N]) combined with CO₂/N₂ ideal selectivities of 15 (for [Cl]) to 61 (for [dca]). These permeability/selectivities place RTIL-membranes above the upper-bound in a CO₂/N₂ Robeson plot of selected polymers. The CO₂/CH₄ ideal selectivities range from 4 (for [Cl]) to 20 (for [dca]), thus placing the [dca]-membrane above the upper-bound for

the CO₂/CH₄ Robeson plot [90]. Camper and co-worker [91] reported the performance of room-temperature ionic liquids (RTILs)-based traditional membranes, concluding the performance of RTIL-based membranes on Robeson plots. It was found to be more applicable for RTIL-based membranes in CO₂/N₂ separation rather than CO₂/CH₄.

Concerning natural gas purification, some hygroscopic imidazolium-based ILs (*i.e.* [bmim][PF₆], [C₈mim][BF₄], and [C₈mim][PF₆]) have the ability to dehydrate [92-94]. The presence of water along with acetate anion in some ILs like [hmim][acetate] and [bmim][acetate] may enhance the sorption through weak bonding with CO₂ [95].

Ignoring corrosion of the equipment, one-third the heat capacity of imidazolium-based ILs in comparison with aqueous systems may have deep effect in the high price of ILs [96-100]. Regeneration process to recover the RTILs can be easily done either by pressure swing process coupled with vacuum treatment or by heating or bubbling nitrogen through the absorbent [96, 101, 102]. Also, when mixing RTILs or task-specific ionic liquids (TSILs) with amines, the regeneration will require temperature swing involving vacuum heating [103].

2.1.4.2 CO₂ Solubilities in Task Specific Ionic Liquids

Visser *et al.* suggested that it is possible to synthesize a wide range of ionic liquids incorporating “task-specific” functional groups. These new TSILs have been proven to be useful in both synthetic and separation applications [104-106].

Bates and co-worker [107] reported their first designed TSIL for CO₂ capture by introducing a NH₂ functional group, 1-n-propylamine-3-butyylimidazolium tetrafluoroborate ([pabim][BF₄]) (see Fig. 2.4). This functional group has shown an obvious superiority of their “task-specific” ionic liquid compared to “conventional” ionic liquid 1-hexyl-3-methyl imidazolium hexafluorophosphate, [6-mim][PF₆] reported by Brennecke group [79, 80]. The equilibrium solubility of CO₂ for this task-

specific ionic liquid reaches a level of 7.4 wt% at atmospheric pressure and room temperature.

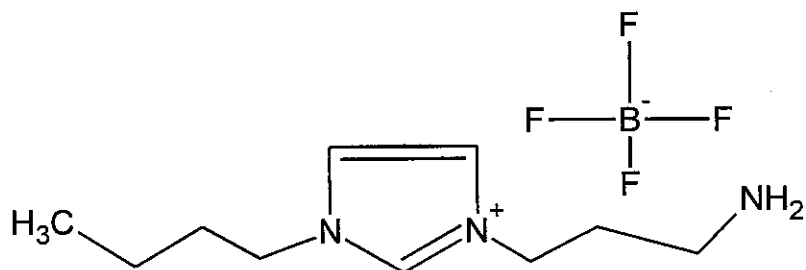


Fig. 2.4: Task-specific ionic liquid ([pabim]BF₄) for CO₂ capture [107].

Zhang *et al.* [108] reported a new kind of task-specific ionic liquid, tetrabutylphosphonium amino acids ([P(C₄)₄]AA). In order to increase the absorption rate of CO₂ in these highly viscous ionic liquids, the [P(C₄)₄]AA ionic liquids are coated on a porous silica gel to structure a thin film. At room temperature and atmospheric pressure the equilibrium molar ratio between CO₂ and [P(C₄)₄]AA reached a level of 1:2. Interestingly, in the presence of small amount of water, the [P(C₄)₄]AA ionic liquids could increase its uptake of CO₂ to be at an equal molar amount.

An imidazolium cation with a perfluoroalkyl chain was reported to have enhanced solubility of CO₂ relative to its corresponding RTILs. However this will result in formation of a carbamate salt, which requires additional energy to decomplex the chemically bound CO₂. Adding a fluorinated group was reported to increase the viscosity of RTILs significantly [103, 107].

Bara *et al.* [109] studied the solubility and ideal selectivity of imidazolium-based RTILs with oligo(ethylene glycol) substituents. The solubility of CO₂, N₂, and CH₄ in these [Pnmim][Tf₂N] are reported to be similar to its corresponding RTILs [Cnmim][Tf₂N] analogues, while the solubilities of N₂ and CH₄ are lower in oligo(ethylene glycol)-based RTILs. As a result, CO₂/N₂ and CO₂/CH₄ ideal solubility selectivities are reported to be 30-75% higher in the oligo(ethylene glycol)-based RTILs than their corresponding RTILs [109].

TSILs have a CO₂ absorption ability to reach up to three times of corresponding RTILs. It was found that there was a steady increase in CO₂ sorption uptake with a rise in pressure, which shows an evidence for both chemical and physical sorption. This effect is not noticeable in the case of aqueous amine solutions which have stoichiometric limitations [101]. TSILs, 1-allyl-3-methylimidazolium tetrafluoroborate [am-im][BF₄] and 1-allyl-3-methylimidazolium dicyanoamide [am-im][dca], perform like chemical solvents at pressures of ≤1 bar. However, at higher pressures they follow the performance of RTIL [bmim][BF₄]. Conversely, amine solutions accomplished their maximum capacities at about 2 bar and no further increase is observed as the pressure increases. Whereas, TSILs continue to have steady increases in CO₂ absorption with ascending pressure. This behavior shows that TSILs possess both chemical and physical sorption [101,110]. Reversible sequestration of CO₂ can be achieved by attaching primary amine moiety to imidazolium cation without affecting the ionic-liquid stability [85]. The addition of water to TSILs is found to increase CO₂ uptake capacity which might be due to the formation of bicarbonate [107, 111].

It is meaningful to observe that not all the ionic liquids containing –NH₂ group can absorb CO₂ efficiently. Zhang *et al.* [112] reported the sorption of CO₂ on guanidine based ionic liquids, *e.g.*, 1,1,3,3-tetramethylguanidium lactate (TMGL). They reported that it can only absorb 0.25 wt% CO₂, which is lower than the expected amount calculated based on the absorption molar ratio of 1:2 between CO₂ and –NH₂ group if it follows the same mechanism as [pabim][BF₄] and [P(C₄)₄]AA. The fundamental reason is that the large Frontier Molecular Orbital (FMO) energy gap (9.53 eV) between Highest Occupied Molecular orbital (HOMO-5) of TMGL and Lowest Unoccupied Molecular orbital (LUMO) of CO₂, is much larger than the energy gap (6.07 eV) between HOMO of [pabim][BF₄] and LUMO of CO₂. It is the carbocation that lowers the HOMO-5 energy of TMGL and weakens its nucleophilicity. As a consequence, TMGL could not interact efficiently with CO₂.

A molecular orbital study on the design of task-specific ionic liquids for capturing CO₂ performed by Yu *et al.* [113], showed that the electron-donating groups

attaching -NH_2 coupled with the intra-molecular hydrogen bonds associated with the H atom on -NH_2 in ionic liquids may possibly raise the FMO energy on -NH_2 and consequently enhance the interactions between -NH_2 and CO_2 . Based on this theoretical understandings and systematic calculations, Yu et.al designed two new task-specific ionic liquids which are tetrabutylphosphonium alanine $[\text{P}(\text{C}_4)_4][\text{Ala}]$ and tetrabutylphosphonium glycine $[\text{P}(\text{C}_4)_4][\text{Gly}]$. These two task-specific ionic liquids are experimentally proven to be effective for capturing CO_2 [113].

Despite their tunable property, TSILs suffer higher viscosities compared to their corresponding RTILs or other commercially available CO_2 scrubbing solutions, thus leading to a serious limitation for their application in industry. CO_2 capture will result in a sharp increase in viscosity of TSILs forming a gel-like material [114]. This disadvantage can be avoided by utilizing mixtures of TSILs and RTILs or by coating TSILs onto porous membranes [85].

2.2 Polymerized Ionic Liquids pILs

Due to their liquid nature, RTILs lack mechanical stability and may not be suitable for certain application where a solid material is required. Polymerized ionic liquids (pILs), which could be formed by polymerizing the ionic liquid monomer, will integrate macromolecular structure with ionic liquid. The properties of pILs are strongly related to both polymer backbone and ionic liquid structure. The structure of the cation and anion (*i.e.* ion type and substitute groups on cation) determine the physicochemical properties of ionic liquids. The effect of ionic liquid moiety on polymer properties such as ionic conductivity, microwave absorption and CO_2 sorption is still under investigation and much more remains to be learned. Unlike the ionic liquids or ionic liquid/polymer mixture, where both cation and anion are mobile, pILs are restricted in mobility compared to their counter ions [115].

2.2.1 History

It is very important to draw attention to the well known polymers to which ionic liquids may look similar. Past studies on long-established examples (*i.e.* ion exchange resins (see Fig. 2.5) and sulfonic acids membrane materials (see Fig. 2.6) could give important insight into the nature, molecular forces, and properties of recent developed pILs [116-118].

Driven by the need to develop polymer electrolytes that combine compositional stability to avoid evaporation of the liquid component, have high ion conductivity, high selectivity, and low glass transition temperature, has somewhat directed researchers to begin synthesizing polymers derived from polymerizable monomeric ionic liquids [116].

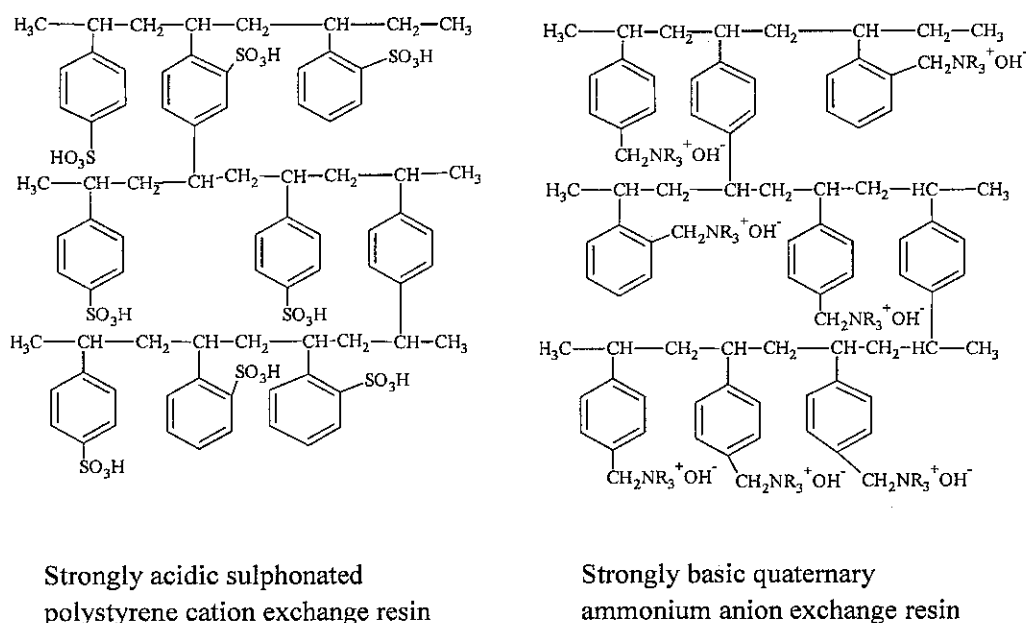


Fig. 2.5: Some examples of ion exchange resin

In order to translate the benefits of ILs to polymer electrolytes, scientists have been following two main strategies namely:

- I. Mixing conventional polymer matrices with ionic liquids to design a polymer electrolyte.
- II. Designing functional polymers having some of the ILs characteristics [119].

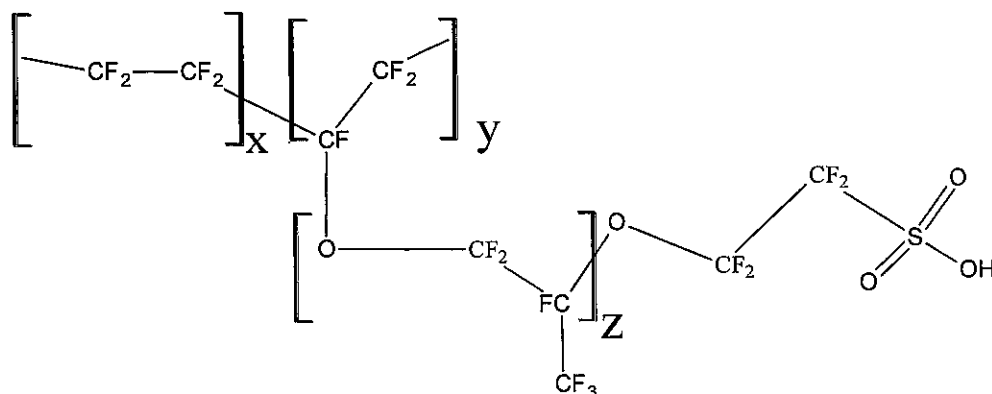


Fig. 2.6: Naflon structure

Watanabe *et al.* reported the synthesis of haloaluminate derivatives of poly (4-vinylpyridinium chloride and bromide) noting two approaches namely:

- I. Direct reaction of the polymer with aluminium chloride
- II. By dissolution in 1-alkylpyridinium chloroaluminate melts [120-122].

Using the first approach, the synthesis of gel electrolytes from ILs and poly(vinylidene fluoride)-hexafluoropropylene copolymer [PVdF(HFP)] is reported by Fuller *et al.* [123, 124]. Also high-temperature proton conducting membranes based on perfluorinated membrane-ionic liquid composites have been reported by groups of researchers [125, 126]. A free radical cross-linked of certain vinyl monomers in ILs is reported to have strong mechanical properties and highly conductive electrolyte films [127-129]. Flexible solid polymer electrolytes based upon ternary mixtures of ionic liquid and classical PEO/lithium salt is reported by Shin *et al.* [130, 131]. Introducing ILs into polymer structure to design polymer electrolyte for actuator has also been reported [132, 133].

The same approach has been used by Marcilla *et al.* by dissolving poly(1-vinyl-3-ethylimidazolium)[Tf₂N], [BF₄], [Br] in the corresponding ionic liquids [bmim][Tf₂N], [BF₄], [Br]. The mixtures show no phase separation over period of weeks [119].

The dissolution of a series of polycations into [NMe₃Et][AlCl₄] prepared by reacting bis(N-heterocycles) with α,ω -dihaloalkanes, is reported by Ogata *et al.* [120]. Motivated by the necessity to produce ionic polymer electrolytes for quasi-solid-state dye sensitized solar cells, Suzuki and co-worker, following the same strategy, have prepared an imidazolium polymer in which the polymer chains, consisting of alkyl-imidazolium units, formed by reacting alkyl-bis(imidazole)s and diiodoalkyls [134, 135].

Using the second synthetic approach, Ohno *et al.* reported a pioneering work in synthesizing different types of pILs to develop high performance electrolytes. They proposed a direct polymerization of ionic liquids by introducing a vinyl group covalently attached onto the imidazolium cation ring. 1-Vinylimidazole is quaternized with a series of alkyl halides. These halides can be replaced with certain anions, to prepare ionic liquid monomer [136-141]. By introducing a polymerization group such as the vinyl group, onto an imidazolium cation the physicochemical properties of ILs will be improved due to the more widely space π -conjugated orbitals [142].

Marcilla *et al.* reported a simple route for synthesis of pILs. Halide exchange of polycations with anion can be carried out to produce hydrophobic ionic liquids, (e.g. [Tf₂N]) [143, 144]. Tang *et al.* reported the synthesis and characterization and application of imidazolium and ammonium-based pILs for CO₂ sorption [145-149]. Snedden and coworkers and Watantabe *et al.* have reported the synthesis of an ion gel by in situ radical crosslinking of vinyl monomers in ionic liquid and their applications as membrane and gel electrolyte [128, 150]. Muldoon and Gordon reported the first synthesis of polymer microparticles made from an IL monomer through suspension polymerization of 1-vinyl-3-butyl-imidazolium bis(trifluoromethylsulfonyl)imide.

They concluded that the resins made of pILs could offer great promise for catalysis applications [151].

2.2.2 CO₂ Sorption in poly Ionic Liquids pILs

The use of pILs as sorbents comes as a second major area of research interest after solid polymer electrolytes [152]. Due to their ionic structure, high thermal stability, processability, and durability, polymerized ionic liquids (pILs) may have many potential applications, among which is gas separation. Polymerized ionic liquids (pILs) are generally polymerized by conventional free radical polymerization. Shen *et al.* reported a living/controlled free radical polymerization of ionic liquid monomer, 2-(1-butylimidazolium-3-yl)ethylmethacrylate tetrafluoroborate (BIMT) [153] via atom transfer radical polymerization (ATRP) (refer to Fig. 2.7).

It is found that the catalyst, initiator, and monomer concentration strongly affected the polymerization rate and control over the polymerization. The CuBr complexes polymerized BIMT rapidly without any control, while CuCl catalyst polymerized BIMT yielding a high conversion with good control. Low monomer concentration will lead to an incomplete polymerization of BIMT [153].

Ionic liquid monomers 1-(4-vinylbenzyl)-3-butyl imidazolium tetrafluoroborate (VBIT) and 1-(4-vinylbenzyl)-3-butyl imidazolium hexafluorophosphate (VBIH), are synthesized by quaternization of *N*-butylimidazole with 4-vinylbenzylchloride and a subsequent anion exchange reaction with sodium tetrafluoroborate or potassium hexafluorophosphate as shown in Fig. 2.8. These ionic liquid monomers are further polymerized by copper-mediated ATRP. Polymerized ionic liquid pVBIT showed 0.305% (w/w) CO₂ sorption capacity (2.22 mole% VBIT units) at a pressure of 592.3 mmHg and at room temperature. Under the same conditions the CO₂ absorption capacity of [bmim][BF₄] is reported to be 0.256 w% (1.30 mole%). Characterization of pVBIT showed an amorphous structure and a good thermal stability with a T_g of 84°C [149, 154]. Shen's research group reported synthesis and CO₂ sorption of

polymerized ionic liquids with different cations, anions and backbones. A summary of these pILs and their sorption equilibrium capacity at 22°C and 0.78 atm is summarized in Table 2.2 until Table 2.6.

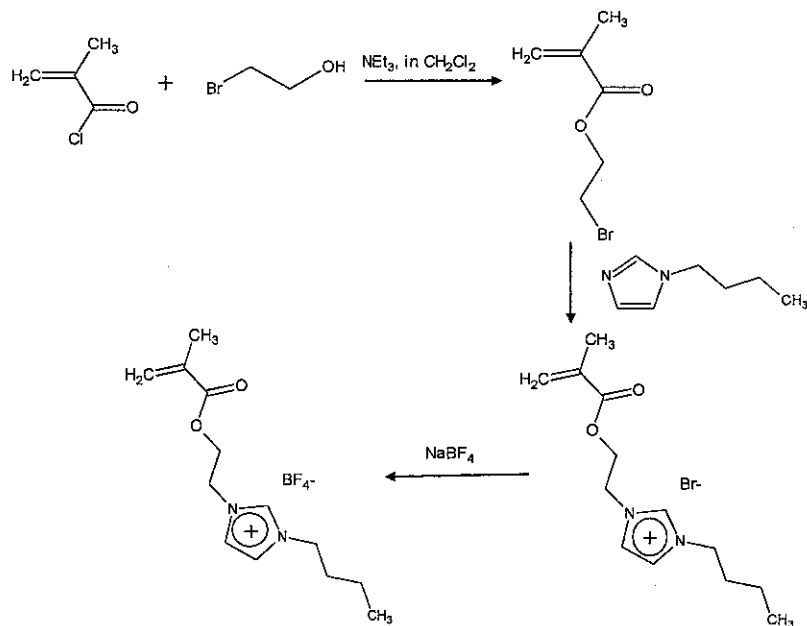


Fig. 2.7: Synthesis of IL monomer BIMT [153]

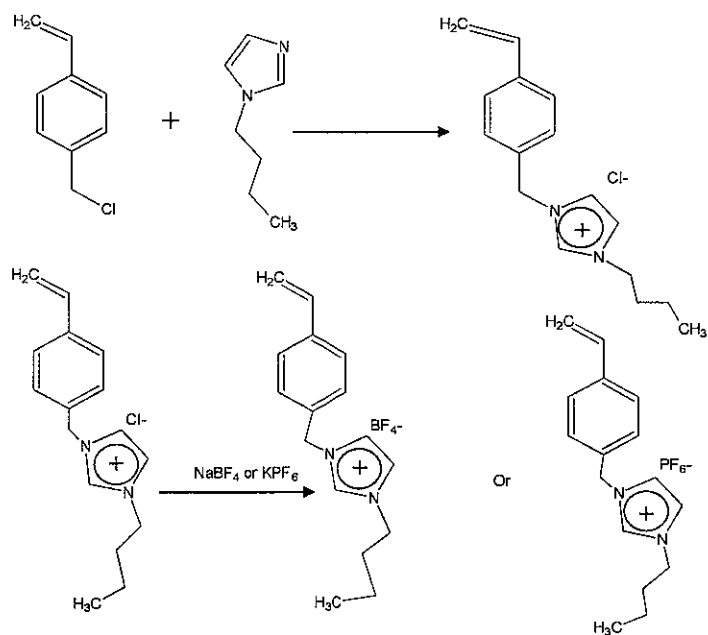


Fig. 2.8: Synthesis of VIBT and VBIH ionic liquid monomers [149]

Under a pressure of 592.3 mmHg and at room temperature, the sorption of these polymers and their corresponding monomer are measured as follows: 10.22 mole% for (p[VBtMA][BF₄]), 7.99 mole% (p[MATMA][BF₄]), 2.22 mole% (p[VbBI][BF₄]), 2.27 mole% (p[VbBI][Tf₂N]), and 1.80 mole% ([MABI][BF₄]) of CO₂ related to their monomer units. Under the same conditions, the monomers [VBtMA][BF₄], [MATMA][BF₄], and [VbBI][BF₄] did not report any CO₂ take up due to their crystalline structures. [MABI][BF₄] monomer which is a liquid shows a sorption capacity similar to the capacity of [bmim][BF₄] ionic liquid which is reported to be 1.34 mole%.

Based on this, Shen research group [146] concluded that the CO₂ sorption capacity of ionic liquid can be significantly increased by polymerizing them [145, 146, 148]. The CO₂ sorption capacities for these pILs are also radically higher than other neutral polymer solids *i.e.* polymethacrylates, polystyrene and polycarbonates [155-157].

The cation, anion, and polymer backbone have an effect on CO₂ sorption capacity; among them cations play a key role. Tetraalkylammonium-based ILs for example, showed much higher CO₂ sorption capacity compared to the imidazolium-based ILs. This may be explained by the fact that the tetraalkylammonium cation is having a higher positive charge density which may lead to stronger interaction with CO₂ compared to that of the delocalized positive charge of imidazolium [145, 146, 148]. To judge on whether the cation or anion plays the major role on CO₂ sorption capacity, a molecular dynamic simulation should be carried out to determine the locations of CO₂ on pILs. This was not done by Tang *et.al.*.

Substituents on the ammonium cation also showed an effect on sorption capacity. By decreasing the length of the substituent, the sorption rate is forced to increase. According to Shen's research group, this indicates that a large substituent group on the cation blocks CO₂ sorption [147]. This is a good explanation for the substituents effect on CO₂ sorption capacity but it ignores another very important factor which is the effect of substituents lengths on the central charged atom of the cation.

Table 2.2: Butyl imidazolium-based pILs and their sorption capacities

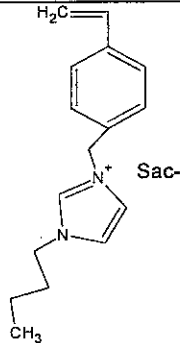
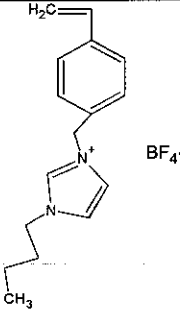
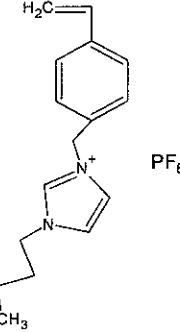
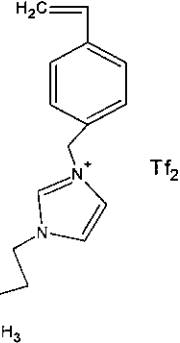
Polymer name	Polymer Abbreviation	monomer structure	CO ₂ sorption equilibrium capacity at 0.78atm CO ₂ , 22°C of pIL
p-Vinylbenzyl-3-butylimidazolium o-benzoic sulphimide	p[VBBI][Sac]		1.55 mole%
p-Vinylbenzyl-3-butylimidazolium tetrafluoroborate	p[VBBI][BF ₄] Or pVBIT		2.22 mole%
p-Vinylbenzyl-3-butylimidazolium hexafluorophosphate	p[VBBI][PF ₆] Or pVBIH		2.75mole%
p-Vinylbenzyl-3-butylimidazolium bis(trifluoromethylsulfonyl)imide	p[VBBI] [Tf ₂ N]		2.27 mole%

Table 2.3: Trimethyl ammonium-based pILs and their sorption capacities

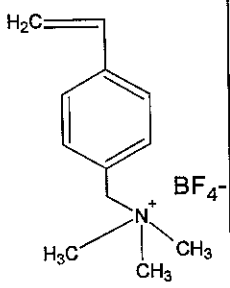
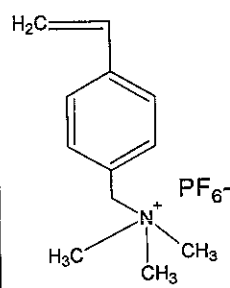
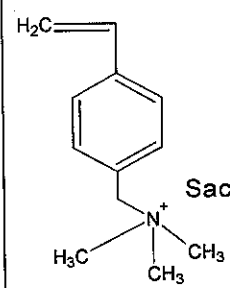
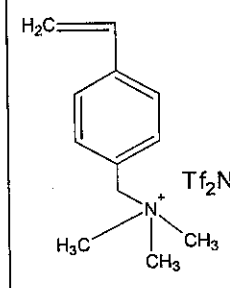
Polymer name	Polymer Abbreviation	monomer structure	CO ₂ sorption equilibrium capacity at 0.78atm CO ₂ ,22°C of pIL
p-Vinylbenzyltrimethyl ammonium tetrafluoroborate	p[VBTMA][BF ₄]		10.22 mole%
p-Vinylbenzyltrimethyl ammonium hexafluorophosphate	p[VBTMA][PF ₆]		10.2 mole%
p-Vinylbenzyltrimethyl ammonium benzoic sulphimide	p[VBTMA][Sac]		2.8 mole%
p-Vinylbenzyltrimethyl ammonium bis(trifluoromethylsulfonyl)imide	p[VBTMA][Tf ₂ N]		2.7 mole%

Table 2.4: Phosphonium-based pILs and their sorption capacities

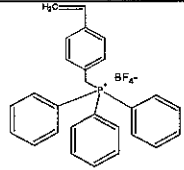
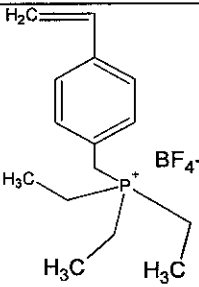
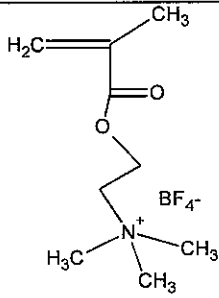
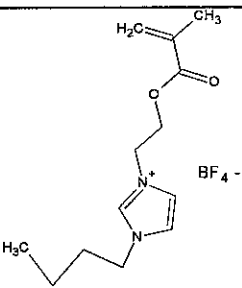
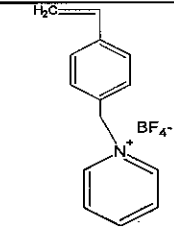
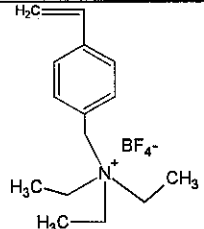
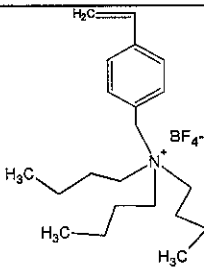
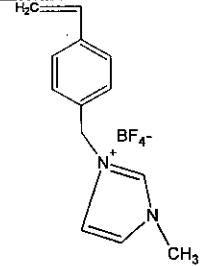
Polymer name	Polymer Abbreviation	monomer structure	CO ₂ sorption equilibrium capacity at 0.78atm CO ₂ ,22°C of pIL
p-Vinylbenzyl-triphenyl phosphium tetrafluoroborate	p[VBTPP][BF ₄]		7.8 mole%
p-Vinylbenzyltriethyl phosphonium tetrafluoroborate	p[VBTEP][BF ₄]		3.9 c[mL(STP)/mL]

Table 2.5: Methacryloyloxy backbone's pILs with different cations and their sorption capacities

Polymer name	Polymer Abbreviation	monomer structure	CO ₂ sorption equilibrium capacity at 0.78atm CO ₂ ,22°C of pIL
p[2-Methacryloyloxy) ethyltrimethylam monium tetrafluoroborate	p[MATMA][BF ₄]		7.99 mole%
p-[1-(2-Methacryloyloxy) ethyl-3-butylimidazolium tetrafluoroborate	p[MABI][BF ₄] Or pBIMT		1.77 mole%

On the other hand, the anions showed little effect on CO₂ sorption capacity [145, 146]. For instance p[VBBI][BF₄] and p[VBBI][Tf₂N] reported the same CO₂ sorption capacity, which is in contradiction to the findings from the room temperature ionic liquids. In ionic liquids, anions play a major role in the CO₂ solubility; and the Tf₂N anion is reported to enhance CO₂ solubility [88, 148]. This leads Shen's research group to conclude that for pILs, fluorine atoms are not a key factor for CO₂ as in ILs and an inorganic anion will have a higher capacity [147].

Table 2.6: pILs with different cations and similar anions and their sorption capacities

Polymer name	Polymer Abbreviation	monomer structure	CO ₂ sorption equilibrium capacity at 0.78atm CO ₂ ,22°C of pIL
p-Vinylbenzyl- pyridinium tetrafluoroborate	p[VBP][BF ₄]		3.6 mole%
p-Vinylbenzyltriethyl ammonium tetrafluoroborate	p[VBTEA][BF ₄]		4.85 mole%
p-Vinylbenzyltributyl ammonium tetrafluoroborate	p[VBTBA][BF ₄]		3.1 mole%
p-Vinylbenzyl-3-methyl imidazolium tetrafluoroborate	p[VBMI][BF ₄]		3.0 mole%

A polystyrene backbone has higher CO₂ sorption capacity compared to polymethylmethacrylate and polyethylene glycol backbones. It is found that the polyethylene glycol backbone has the lowest sorption capacity [146, 148].

It can be realized that, Tang *et.al.* did not give an explanation how the sorption capacity of CO₂ will be affected by the anion type and the criteria that enable pILs with polystyrene to give a higher CO₂ sorption capacity compared to polymethylmethacrylate and polyethylene glycol backbones .

Studying the effect of cross-linking on sorption capacity of pILs, Shen's research group found that the cross-linking decreases the sorption capacity due to reduction in the polymer void due to the cross-linking of polymer [147]. But if the case is a void volume, then the pILs with polymethylmethacrylate backbone is expected to have a better CO₂ sorption capacity due to their porous structure compared to polystyrene backbone pILs.

Wet p[VBTMA][BF₄] with 13.8 mole% water showed a CO₂ sorption capacity of 7.9 mole%, lower than that reported for dry P[VBTMA][BF₄] (10.22 mole%). This indicates that moisture will slightly decrease the sorption capacity [146]. As the pILs swelled when adding water to them and this was not noticed by Tang *et.al.*, this conclusion is not correct because the new volume should be taken into account when calculating sorption capacity.

Sorption rate for these pILs is really fast compared to ILs. It took only several minutes for them to reach the 95% of their equilibrium, whereas the ILs [MABI][BF₄] and [bmim][BF₄] took 400 min to reach the equilibrium. The fast sorption of pILs is affected neither by particle size nor by surface area. When replacing the [BF₄] in p[VBBI][BF₄] with Cl anion, p[VBBI][Cl] showed slower sorption rate even with the same magnitude of particle size, this suggests that the fast CO₂ sorption is one characteristic of the pILs [145, 146]. In contradiction with what is mentioned above, Shen's group reported later that the particle size and surface area really affect the sorption rate of CO₂ due to the process of CO₂ diffusion from the surface into the

polymer bulk [147, 148]. Suggesting Barrer's theory, Shen *et al.* proposed the mechanism for CO₂ diffusion into pILs. It involves two mechanisms, ordinary dissolution and hole-filling. The proposal suggested that the sorption of CO₂ into pILs involves absorption and adsorption [147, 148].

Desorption rate of pILs is also found to be fast. It took only 15 minutes under vacuum to complete desorption, whereas in ILs desorption is known to be relatively slow. After four cycles of sorption/desorption the kinetics and sorption capacity remained the same, proving that the sorption/desorption in pILs is completely reversible [145, 146].

At 12 bar pressure, p[VBtMA][BF₄] absorbed 44.8 mole% of CO₂ which is much higher than that reported by RTILs [88]. Shen *et al.* calculated the adsorption capacity of p[VBtMA][BF₄] assuming a mono layer of CO₂ to be 0.02 w%, which is much less than the reported 1.70 w%. This leads them to suggest that the CO₂ sorption of pILs involves more absorption (the bulk) and less adsorption (the surface). Regarding the ideal selectivity, pILs showed no sorption capacity for both N₂ and O₂ under the same conditions [146]. Up to 180 bar and 75°C, p[VBtMA][BF₄] and p[BVMI][BF₄] are found to be still glassy polymer and their CO₂ uptake decreases with increasing temperature and increases with ascending pressure till it reaches a point beyond which it becomes insensitive to pressure [158].

The isothermal process of CO₂ sorption in pILs is correlated by Shen's research group and found to be well fitting into dual-mode sorption model, which describe the gas solubility in glassy polymer. This suggest that the CO₂ sorption into pILs had two parts, one dissolved into matrix, and the second adsorbed into microvoids following Langmuir hole-filling process [159]. With the same backbone and similar anion the sorption capacity of CO₂ is found to decrease in the order of ammonium > pyridinium > phosphonium > imidazolium cations. By comparing the computed values of Henry's law constant (k_D) and the affinity constant for Langmuir mode (b), it is found to be in the same order of magnitude. This showed that the ammonium cation has the strongest interaction with CO₂ whereas the imidazolium has the weakest. Ammonium

based pILs has a high saturation capacity c_H for Langmuir mode, suggesting a high fraction of microvoids compared to imidazolium-based ones [159].

In contradiction with what is reported before by Shen's research group [148] they stated that the anion is an important factor that affects the sorption capacity [159]. The BF_4 polymers are found to have higher values of k_D , b , and c_H which show stronger interaction with CO_2 and higher microvoids volume fraction, in contradiction with the Tf_2N which shows lower values of k_D , b , and c_H resulting in a lower value for CO_2 sorption capacity. The low value of microvoid volume of Tf_2N polymer may be due to the plasticization caused by the anion Tf_2N which is shown by its low value of glass transition temperature T_g . The polystyrene backbone polymers are more rigid than the polymethylmethacrylate ones resulting in a higher sorption capacity of CO_2 for polystyrene backbone polymers. The long alkyl substituents on cation may hinder the interaction between CO_2 and the cation due to the steric effects and plasticizing of the polymer resulting in a low microvoids volume. This will result in a reduction in CO_2 sorption capacity. Cross-linking the polymer will hinder the interaction with CO_2 but will increase the microvoid volume due to the rigidity. These two contradicting factors will lead to a reduction in CO_2 sorption capacity for cross-linked pILs [159].

Green *et al.* reported that the fundamental mechanism of gas adsorption in pILs is still unclear [152].

2.2.2.1 CO_2 Sorption in pILs's Membrane

Different methods and materials have been carried out in the industry and research for purification of exhaust gas streams and sweetening of natural gas. Ionic liquids could be used as neat fluids or processed into supported ionic liquids membranes for gas separation.

One of the disadvantages of supported ionic liquid membranes (SILMs) is the leaching of the liquids through the membrane pores when the pressure drop exceeds

the liquid stabilizing forces in the matrix [85]. Making up membranes of pILs may be a good option for CO₂ capture [160].

Membranes made by grafting polyethylene glycol (PEG) onto p[VBtMA][BF₄] and p[MATMA][BF₄] are reported by Shen's research group to be CO₂ selective for CO₂/CH₄ and CO₂/N₂ separation, and more mechanically stable than those made of pure p[VBtMA][BF₄] and p[MATMA][BF₄] pILs. Within the same permeability, the p[VBtMA][BF₄]-grafted-PEG and p[MATMA][BF₄]-grafted-PEG showed high CO₂ selectivity due to solubility differences not diffusivity differences [161].

Bara *et al.* reported the permeability of CO₂, CH₄, N₂, into membranes made of different pure pILs. The permeability increases in a non-linear manner as the n-alkyl substituent in cation is lengthened. Plotting the performance of these pILs membranes on the Robeson plot for CO₂/N₂ showed that they perform as good as or even better than many other polymers. Whereas the CO₂/CH₄ system is found to be less impressive on the Robeson plot compared to other polymeric membrane [162].

Bara and coworkers synthesize cross-linkable gemini room temperature ionic liquids (GRTILs) (see Fig. 2.9) and photo-cross-linked them into thin film. Permeability of CO₂, CH₄, and N₂ into the resultant membrane is found to be much lower than that for pure pILs membranes due to the highly restricted diffusion. On the other hand the separation factors are found to be similar to pure pILs membranes. The fluxes of CH₄ and N₂ are small enough not to be transported through the film [163].

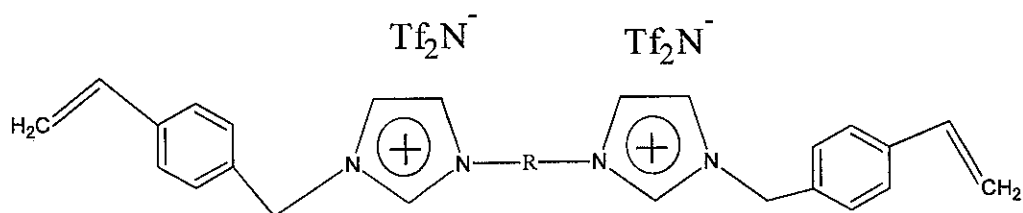


Fig. 2.9: Chemical structure of GRTIL cross-likable monomers[163]

Functionalized pILs membranes are synthesized by Bara *et al.* by introducing oligo(ethylene glycol) or nitrile-terminated alkyl substituents into the imidazolium

cation as shown in Fig. 2.10. These functionalized membranes are tested for CO₂/N₂ and CO₂/CH₄ systems and found to have a greater separation factors than those with comparable length n- alkyl substituents having the same level of CO₂ permeability [164]. Studying the effect of anion on gas separation performance of pILs membranes in the presence of 20 mole % of nonpolymerizable ionic liquid, Bara and co-workers found that the permeability of CO₂, CH₄, and N₂ increased by 2 to 5 times relative to those in pure pILs membranes.

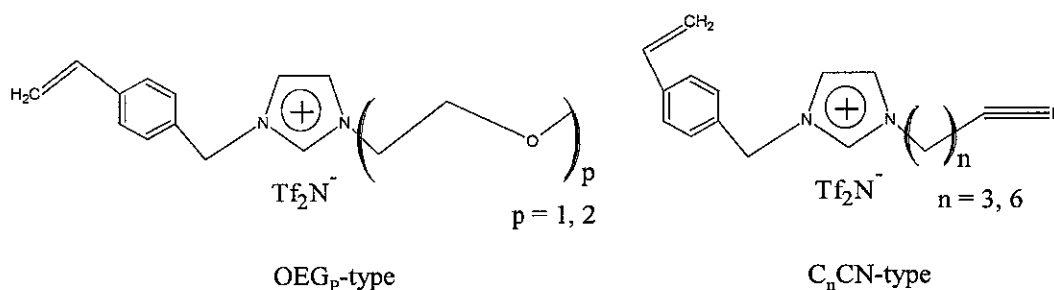


Fig. 2.10: Functionalized polymerizable ionic liquid monomers [164]

This large increment in permeability results in slightly diminished ideal selectivities for CO₂/CH₄ and CO₂/N₂ compared to the free RTIL pILs membranes. These pILs-RTIL composite membranes are more favorable for CO₂/N₂ separation than CO₂/CH₄ separation [165]. Different pILs-RTIL composite membranes with various types of functional groups attached to the imidazolium cation (alkyl, ether, nitrile, fluoroalkyl, and siloxane) are tested for permeability of CO₂, CH₄, and N₂. In the presence of 20% free RTIL, the permeability increased by 100% to 250% compared to pILs membrane without free RTIL addition. The functional group in RTIL cation affects both permeability and selectivity for CO₂/N₂ and CO₂/CH₄ separation [160, 166].

2.2.3 Other Promising Applications of pILs

Eliminating the known disadvantages of liquid electrolytes such as leakage, flammability, toxicity, and instability, is the main driving force for synthesizing

polymerized ionic liquids. This is first done by Yoshizawa and Ohno[137, 167]. Since then polymerized ionic liquids have gained a lot of research interests as a promising area for electrolytes and become the major area of research for poly ionic liquids promising applications [115, 119, 124, 129, 141, 142, 152, 168-187].

Study carried out by Ohno *et al.* on anion effects on polymer conductivity and glass transition (T_g) of cryloyl-containing pILs hepta(ethyleneoxide)methacrylate-3-ethylimidazolium (trifluoromethane-sulfonyl)imide ($[\text{Mac}(\text{PEO})_7\text{Em}^+][\text{TFSI}^-]$), showed that the larger the anion, the larger the ion conductivity and the lower the T_g . It is realized that the chain flexibility by means of larger space between the ethylene oxide backbone and the ionic liquid moiety will result in a larger ion conductivity value[139, 167]. Imidazolium based pILs with different substituents (methyl, ethyl, benzyl, etc) did not show a significant change in ion conductivity of polymers. Again altering the cation type (*i.e.* pyrrolidinium, piperidinium etc.) did not show a significant change in T_g and ion conductivity as chain flexibility and anion size did [175]. Polymerization through the anion is believed to increase ion conductivity and reduce the T_g value by offering a better mobility and flexibility for the cation [141]. By introducing vinyl groups into cation and anion, co-polymerizing a vinyl imidazolium cation with a vinyl sulfonate, results in a poor ion conductivity due to lack of mobility for both cation and anion [136]. Increasing the time of polymerization, which will result in a higher molecular weight will lead to a lower ion conductivity value showing that the increased molecular weight of the crosslinked polymer is behind its low value of ion conductivity. All reported pILs have shown a lower value of ion conductivity compared to their ionic liquid monomers, but still there is a real potential for solving the problem of electrolyte leakage by exploring the factors that control the ion conductivity of pILs for optimum pILs that can replace the liquid electrolytes. Research will continue in the coming years to tune the architecture and chemical structure of pILs to reduce the T_g and increase ion conductivity [152].

Other possible promising applications of pILs including desulfurization [188], dye-sensitized solar cells [189], sensors, biosensor and actuator [190-193], radio

frequency absorbers [194], chiral separation [195, 196], and hydrorepellent [197] are still under investigation by different research groups around the world.

2.3 Summary

Ionic liquids are organic salts that are composed of an organic cation and an organic or inorganic anion which are liquids at operating temperature below their decomposition temperature.

Ionic liquids lack mechanical stability and may not be suitable for certain applications where a solid material is required. Polymerizing the ionic liquid monomer will integrate the macromolecular structure with ionic liquid properties.

Because of their ionic structure, high thermal stability, processability, and durability, polymerized Ionic liquids (pILs) may have many potential applications, among which is gas separation.

Polymerizing the ionic liquid can significantly increase the CO₂ sorption capacity. Sorption rate for these pILs is relatively much faster compared to ILs. The cation, anion, and polymer backbone influence the CO₂ sorption capacity; among them the cation plays the major role. Polystyrene backbone showed higher CO₂ sorption capacity compared to polymethylmethacrylate and polyethylene glycol backbones.

Shen's research group stated that cross-linking decreases the sorption capacity due to decrement in polymer void as a result of the cross-linking. But if the case is a void volume, then the pILs with polymethylmethacrylate backbone should always have a better CO₂ sorption capacity compared to polystyrene backbone pILs due to the porous structure of polymethylmethacrylate pILs. In contradiction with what is reported before by Shen's research group they stated that the anion is having an influence on the sorption capacity.

Shen's research group did not give a clear reason behind the effect of chemical structure of pILs on their sorption rate and capacity. In order to determine the effect of

cation and anion on CO₂ sorption rate and capacity, molecular dynamic simulation should be carried out to check the location of adsorbed CO₂ molecules on pILs. Beside this, the research group concentrates on synthesizing pILs with PF₆ and BF₄ anions which are not applicable in the industry due to the risk of forming explosive and corrosive HF gas.

Obviously, the fundamental mechanism of gas adsorption in pILs is still unclear and a further study is required to understand the mechanism to enable a better design of pIL structure for CO₂ separation. This study will be covered by this work.

CHAPTER 3

HYPOTHESIS AND THEORY

3.1 Carbon Dioxide Chemistry and Properties

Carbon dioxide CO_2 is a non-polar linear molecule with a $\text{C}=\text{O}$ bonds which has a length of 1.15 \AA . A typical $\text{C}=\text{O}$ bond length is 1.22 \AA . The reduction in the length of this bound is due to the three resonances structure of CO_2 as shown below in Fig. 3.1 [198].

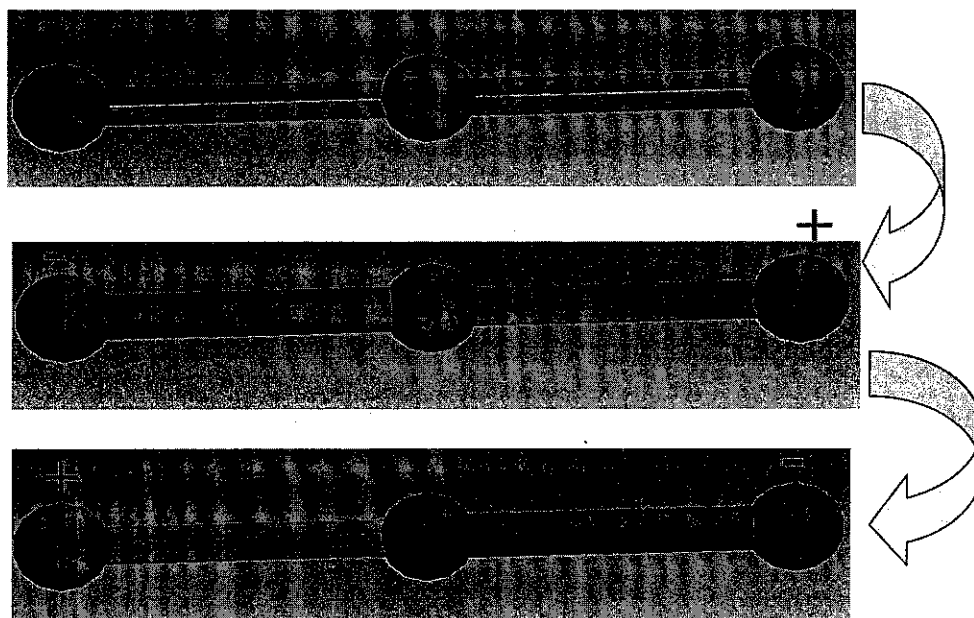


Fig. 3.1: Carbon dioxide resonance structure

Normally CO_2 does not react directly with absorbents; instead it forms intermediate compounds *i.e.* carbonate ion and carbonic acid. The carbonate ion CO_3^{2-} is coplanar having bond angles of 120° and consists of three $\text{C}-\text{O}$ bonds each with a bond length of 1.31 \AA . This length is approximately midway between the single bond length (1.43 \AA)

and double bond length (1.22Å). This may be due to resonance among three possible structures as shown in Fig. 3.2 [199].

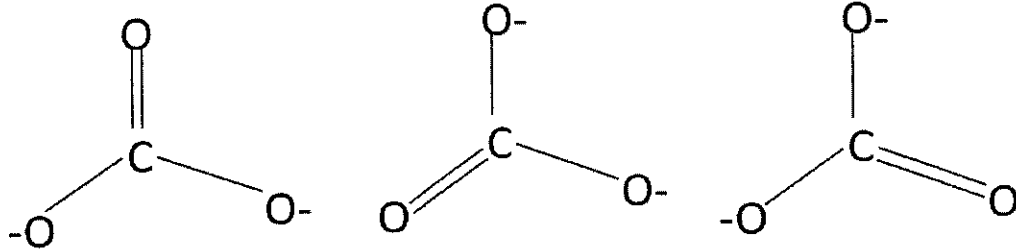


Fig. 3.2: Carbonate ion resonant structures

For carbonic acid, H_2CO_3 the same planar resonance structures as the carbonate are believed to apply [199].

3.2 Sorption of CO_2 in Glassy Polymers

The dual-mode model can be used to describe the gas solubility in glassy polymer. The dual sorption mechanism divides the sorption of the gas into two idealized parts as shown in eq. 3.1

$$C = C_D + C_H = Hp + \frac{\hat{C}_H bp}{1 + bp} \quad 3.1$$

The first part covers the Henry dissolution (C_D) where the gas is dissolved in the polymer matrix according to Henry's law eq. 3.2

$$C_D = Hp \quad 3.2$$

The second part covers the Langmuir sorption (C_H) where the gas molecules is absorbed in the microvoids holes by the hole-filling process according to eq. 3.3

$$C_H = \frac{\hat{C}_H bp}{1 + bp} \quad 3.3$$

According to Tang *et al.* [159] the dual-mode model can describe the CO₂ sorption in pILs very well and C_D is mainly determined by the interaction between the CO₂ and the polymer.

To explain the interaction between the pILs and CO₂ the following hypothesis is proposed for this work;

- I. As shown earlier from the resonance structure of carbon dioxide, charge interaction between the pILs and CO₂ are suggested. This charge interaction will enhance the selectivity of sorption towards CO₂.
- II. As the polymer is a rigid system we can take the cation and anion as standalone parts.
- III. As the cation include the backbone of the polymer and the substituent, the overall ion conductivity will affect the sorption capacity. Higher anion ion conductivity will result in higher sorption capacity and quicker sorption rate. To ensure an easy accessibility of the gas to the charged sites in pILs, a small size of the anion will be favorable.
- IV. By polymerizing the polymerizable ionic liquids, more surface area to host the CO₂ will be provided as the structure changes from crystalline to amorphous form.

In order to prove this mechanism, a molecular dynamic simulation is performed so as to check the CO₂ sorption of pILs with different ion conductivity values and identify the locations of adsorbed CO₂. Identification of CO₂ location will show if the cation and anion are behaving as standalone parts or not. Based on this molecular dynamics simulation results, the synthesis of poly ionic liquids (pILs) will be directed by changing their structure in terms of backbone, anion and cation and central atom. This structure change will result in ion conductivity change. The sorption results will show if the sorption capacity will follow the change in ion conductivity or not.

3.3 Molecular Dynamic Simulation

Synthia module of Accelrys Material Studio software is used to predict the polymer properties. This is followed by sorption simulation using the Monte Carlo method.

3.3.1 Synthia Module

Synthia module is a model that allows a rapid estimate to be made on polymer properties using empirical and semiempirical methods. With the aid of Synthia module a wide range of thermodynamic, mechanical, and transport properties can be predicted for bulk amorphous homopolymers and random copolymers. The key advantage of Synthia is that no database such as those used in group contribution method is required, and properties can be predicted for any polymer which composed of any arrangement containing the following nine elements: carbon, hydrogen, nitrogen, oxygen, silicon, sulfur, fluorine, chlorine, and bromine. The methodology for Synthia module is based on correlations developed by Dr. Josef Bicerano [200]. Basically, Synthia module uses a number of correlations to determine the properties of polymers. For molar volume and density at room temperature calculation, eq.3.4 and eq.3.5 are used

$$V_{(298K)} = 3.64277 \cdot \chi + 9.798697 \cdot \chi^V - 8.542819 \cdot \chi + 21.693912 \cdot \chi^V + 0.978655 N_{MV} \quad 3.4$$

$$N_{MV} = 24N_{Si} - 18N_{(-S-)} - 5N_{sulfone} - 7N_{Cl} - 16N_{Br} + 2N_{(backbone\ ester)} + 3N_{ether} + 5N_{carbonate} + 5N_{C=C} - 11N_{cyc} - 7(N_{fused} - 1) \quad 3.5$$

The last term will only be used when $N_{fused} \geq 2$

The Coefficient of volumetric thermal expansion at 298 K [ppm/K] is predicted by using eq. 3.6 when $T < T_g < 298K$.

$$V(T) = 0.15V(298K) \frac{(T - T_g)}{(1.42T_g + 44.7)} + V(298K)[1 + \alpha_r(298K) \cdot (T_g - 298)] \quad 3.6$$

In order to estimate the molar heat capacity of solid at 298 K in [J(g K)] eq. 3.7 is used

$$C_p^S(298K) = 8.985304 \cdot \chi^0 + 20.920971 \cdot \chi^V + 7.304602(N_{rot} + 5N_{Si}) \quad 3.7$$

For glass transition temperature T_g eq. 3.8 and eq.3.9 are to be used

$$T_g = 351.00 + 5.63\delta + 31.68 \frac{N_{Tg}}{N} - 23.94x_{13} \quad 3.8$$

$$N_{Tg} \equiv 15x_1 - 4x_2 + 23x_3 + 12x_4 - 8x_5 - 4x_6 - 8x_7 + 5x_8 + 11x_9 + 8x_{10} - 11x_{11} - 4x_{12} \quad 3.9$$

To estimate the temperature of half decomposition, which is the temperature at which the loss of weight during pyrolysis at a constant rate of temperature rise reaches 50% of its final value, Synthia module takes eq.3.10 to eq.3.12

$$T_{d, \frac{1}{2}} = \frac{Y_{d, \frac{1}{2}}}{M} \quad 3.10$$

$$Y_{d, 1/2} = 7.17N - 2.3N_H + 12.52 \cdot \chi^V \quad 3.11$$

$$N_{Yd} \equiv 14N_{(-S-)} + 21N_{(BB \text{ sulfone})} + 5N_{(BB \text{ amide})} + 4N_{(BB \text{ Si-O bonds})} + 12N_1 + 41N_2 + 17N_3 + 9N_4 - 7N_5 + 20N_6 + 25N_7 - 10N_8 - 30N_9 + 5N_{10} + 10N_{11} + 8N_{12} - 5N_{13} - 5N_{14} \quad 3.12$$

Eqs.3.13 to 3.16 are used by Synthia module to calculate the permeability [DU] of oxygen, nitrogen, and carbon dioxide.

$$v \equiv \frac{E_{coh1}}{V} - 196 \frac{V}{V_w} + 110 \frac{N_{rot}}{N} - 57 \frac{N_{per}}{N} \quad 3.13$$

$$P_{O_2} = 4991.6 \exp(-0.017622v) \quad 3.14$$

$$P_{N_2} = 1692.1 \exp(-0.019038v) \quad 3.15$$

$$P_{CO_2} = 31077.9 \exp(-0.019195v) \quad 3.16$$

3.3.2 Monte Carlo Sorption Simulation

Accelrys Material Studio sorption module allows the simulation of a pure sorbate (or mixture of sorbate components) which is absorbed in a sorbent framework. To simulate the sorption equilibrium, Material Studio software provides three ways: fixed loading (canonical ensemble), fixed pressure (grand canonical ensemble), and Henry constant (uniform ensemble). Additionally, the adsorption isotherm task enables the running of a series of fixed pressure simulations over a specified fugacity range in a single step. The sorbate location task enables the finding of the global minimum energy sites for sorbates in the framework by running cycles of fixed loading simulation series where the temperature is steadily reduced over the series.

The Sorption module supported two Monte Carlo simulation methods: the Metropolis Monte Carlo Method [201] and the configurational bias Monte Carlo method [202]. The Metropolis Monte Carlo method can be used to study the adsorption of sorbate molecules without internal degrees of freedom in porous frameworks. This method is the method of choice for sorbate molecules which are small compared to the size of the pores and do not have a high degree of torsional flexibility. In the Metropolis conventional method, trial configurations are generated without any bias. The sorbate structure will be treated as a rigid body where translations and reorientations are incorporated.

Additional torsional degree of freedom is included in the configurational bias method. In this method, the translations, reorientation, and torsion, will be selected with a bias

towards low energies. This bias method is useful for large flexible sorbate, where the Metropolis method becomes inefficient.

3.3.2.1 Energy Components

The energy components of sorption is described by the following set of equations

$$\beta = \frac{1}{K_B T} \quad 3.17$$

The total energy of configuration m is given by eq. 3.18

$$E_m = E_m^{SS} + E_m^{SF} + U_m^S \quad 3.18$$

As the framework is fixed throughout the simulation, the intramolecular energy of the framework is not included; its energy contribution is fixed and vanishes, as the only energy differences that play a role in the sorption. This is also true for the intramolecular energy of the sorbate molecules when only translational and rotational degrees of freedom are present. Though, for consistency with the Sorption methods which have sample intramolecular degrees of freedom, the intramolecular energy is always included in the total energy.

The total intramolecular energy U^S which is the sum of the intramolecular energy of all sorbates of all components is given by eq.3.19

$$U^S = \sum_{\{N\}_m} u_{intra} \quad 3.19$$

For efficiency reasons, Sorption internally adds a hard core to every atom in the system. . This means that when two atoms in a configuration are so close resulting in an overlap of their hard cores, the energy of the pair is infinite. Since this implies an infinite energy for the configuration, no energy estimation is required. The hard-core radius is chosen in a way that the effect on the calculated properties is negligible. For typical systems and temperatures below 1000°K, energy and density are not

considerably affected by using hard cores; though, the computation time can decrease by several orders of magnitude.

The Ewald & group summation method in Sorption calculates the electrostatic energy contribution to both E^{SS} and E^{SF} using different methods, in order to improve the computational efficiency. The electrostatic interaction between the sorbate molecules is evaluated using charge groups. A charge group is a small group of atoms that are close to each other and which have a net charge of zero or almost zero. An electrostatic energy is calculated for each pair of charge groups whose centers are within the cutoff distance that is specified when the calculation is set up. As charge groups are charge neutral, the main error introduced by using a cutoff distance is due to dipole-dipole interactions. But, such interactions are generally of low energy and act over short distances. Ewald & group summation method evaluates the electrostatic interaction between sorbate molecules and the framework using the Ewald summation method. In this method, each partial charge on the sorbate molecule interacts with the entire periodic framework. In order to estimate the infinite sum, each partial charge is screened by a charge distribution of opposite strength. The interaction between the two screened charges can be evaluated directly; Fourier transformation is used to evaluate the electrostatic energy contained in the periodic lattice of charge distributions. The accuracy of the Ewald method mainly depends on the width of the screening charge distribution. In the case of sorption, the accuracy of the Ewald method is set as an energy tolerance, from which the width of the screening charge distribution, as well as the cutoff distance in real and reciprocal space, are derived.

Sorption enables the option to return the energy and density fields associated with each sorbate component. Fields are three-dimensional distributions of the property value over the entire framework volume and are estimated on a regular grid. The field data are also used to calculate the isosteric heat introduced below. The isosteric heat, Q , of a component is defined in eq. 3.20

$$Q^{SF} = h^S - h^F \quad 3.20$$

As the framework is typically favored over the gaseous reservoir, the value of the isosteric heat is usually positive. At equilibrium:

$$h^S - h^F = T(S^S - S^F) \quad 3.21$$

So, using the Clapeyron equation, the following expression is obtained:

$$Q^{SF} = (v^S - v^F) \left[\frac{dp}{d(\ln T)} \right] = RT \left[\frac{d(\ln p)}{d(\ln T)} \right] \quad 3.22$$

In the second expression, the partial molar volume in the framework can be neglected with respect to that in the reservoir and the reservoir is assumed to be ideal. The remained partial derivative can be evaluated in the grand canonical ensemble, resulting in

$$Q^{SF} = RT - G \quad 3.23$$

Where G is defined as:

$$G = \langle E \rangle - \mu_{intra} \langle N \rangle \quad 3.24$$

In Sorption, G is referred to as the "grand potential". If the lowest energy configurations are returned, they will be ordered by the value of the grand potential.

3.3.2.2 Monte Carlo Methods

Experimentally, a molecular system can be described by a small number of parameters, such as volume and temperature. The collection of molecular configurations that satisfy this partial knowledge is called an ensemble of configurations. An ensemble is described by a distribution function, ρ_m , which represents the probability of each configuration, m, in the ensemble.

The Monte Carlo methods used in sorption, sample the configurations in an ensemble by generating a chain of configurations, m, n, ..., where the probability of transition

from m to n is π_{mn} . Thus, if configuration m is sampled with a frequency ρ_m , then, on average, $\rho_m\pi_{mn}$ of them are transformed to n. Similarly, $\rho_n\pi_{nm}$ of configurations n are transformed to m. Obviously, these fluxes must be the same to conserve the density, ρ , otherwise, there would be a net flow from m to n (or vice versa) and this will increase ρ_n (or ρ_m) leading to a different ensemble. Therefore, the detailed balance condition for equilibrium can be obtained from eq.3.25.

$$\rho_m\pi_{mn} = \rho_n\pi_{nm} \quad 3.25$$

In the Monte Carlo sorption methods, the step to transform configuration m to n is a two-stage process. First, a trial configuration is generated with probability α_{mn} . Secondly, either the proposed configuration, n, is accepted with a probability of P_{mn} or the original configuration, m, is retained with a probability of $1 - P_{mn}$. The overall transition probability, π_{mn} , is thus can be obtained from eq.3.26

$$\pi_{mn} = \alpha_{mn}P_{mn} \quad 3.26$$

It is easy to confirm by substitution that the following choice for the acceptance probability:

$$P_{mn} = \min \left[1, \frac{\alpha_{nm} P_n}{\alpha_{nm} P_m} \right] \quad 3.27$$

satisfies eq. 3.26. Depending on the ensemble being simulated and the selected Monte Carlo method, this expression can be simplified even further.

In the Metropolis Monte Carlo Method, trial configurations are generated without bias, provided that $\alpha_{mn} = \alpha_{nm}$. For instance, the probability of displacing a molecule from 5 to 5.5 Å in the x direction is the same as the probability of displacing a molecule from 5.5 to 5 Å. Obviously, the probability of displacing a molecule from 5 to 5.5 Å in the x direction could equally be halved, provided twice as many of these attempts are accepted, precisely as calculated by eq. 3.26.

In the Configurational bias Monte Carlo Method, trial configurations are generated in a biased way. A bias is introduced towards high density ρ to avoid having to attempt configurations with low density ρ , which are most likely to be rejected by the acceptance test. By calculating the bias factor, α_{mn} , of each attempt, and applying eq. 3.26, the biased Monte Carlo method is guaranteed to sample the same ensemble as the Metropolis Monte Carlo method.

3.4 Sorption Measurement

Many factors can influence the accuracy when measuring CO₂ solubilities in liquids or sorption of CO₂ in solids or polymers. The purification of the gas and liquid is extremely important because the impurities will affect the results; completely degassing the solvent prior to the measurements is the most important step to ensure that the absorbed gas as measured during the experiment is the true gas solubility. Precise measurement of the related parameters such as temperature, pressure, volume, and/or mass is extremely important, as a precise control of any adjusted parameters (*e.g.* temperature and pressure control). Precise gas solubility measurements depend on attaining the true equilibrium value of absorbed gas. Lastly, an accurate method to determine the true amount of dissolved gas must be developed for the particular system used. In the following survey the researchers will concentrate on various experimental methods for measuring gas solubilities and how these factors are addressed [83], [203], and [204].

3.4.1 Volumetric and Pressure-Drop Methods

The majority of methods for measuring gas solubilities in liquids are modifications on one of two techniques occurring at constant temperature. In the first technique which is called the pressure-drop method, the volume is kept constant whereas the pressure drop is measured during the gas absorbed into the liquid. In the second technique, which is often referred to as the volumetric method, the pressure is held constant,

while the volume change which needed to maintain the pressure while the gas is absorbed by the liquid is measured. In both cases the pressure, temperature, and volume before and after absorption are known. As a result, the amount of absorbed gas can easily be calculated by using an equation of state converting pressure, volume, and temperature to moles.

The first volumetric gas solubility apparatus is designed by Ostwald before 1900 [205]. It consists of three parts: a system for measuring the gas volume of one or more burets to measure either dry or wet (gas saturated to the vapor pressure of the solvent) gas, a stirred and thermostated cell where the contact between the degassed solvent and gas takes place under known temperature and total pressure, and a system for measuring the pressure consisting of one or more manometers. The volumetric apparatus has the choice of measuring the gas absorption either in the pure dry state or in the solvent saturated state.

Several groups have reported gas solubility measurements in ionic liquids using variations of these techniques [79], [206], and [207].

3.4.1.1 *Advantages of The Volumetric Method*

- The advantages of the volumetric method are as listed below:
- Simple setup and easy operation.
- Only pressure and temperature measurements are required; and it can be designed to be corrosion resistant.
- Direct temperature measurement of the sample can be made.

3.4.1.2 *Disadvantages of Volumetric Methods*

The disadvantages of the volumetric method are as listed below:

- Poor vacuum at sample.
- Thermal gradient.

- Requires relatively high sample amount.
- Accumulation of error (dead volume).
- Sample re-activation cannot be measured.
- Indirect measurement where a calculation using equation of state is required.

3.4.2 *Gas Chromatography*

One of the methods to measure the gas solubilities in liquids is the gas chromatography method in two different techniques [204]. The first technique is the extractive technique, where the gas of interest will be passed through the solvent till it saturated and then coated on a column. To extract the gas of interest, a non-absorbing gas is passed through the column. Using the gas chromatography (GC), the carrier gas will be analyzed to determine the amount of removed solute gas. In this technique, and in order to avoid removing the solvent in the column by the carrier gas, it is important to saturate the carrier gas with the solvent prior to passing it through the column.

In the second techniques, the gas solubilities in the solvent are measured at infinite dilution. First the pure solvent is coated on a column and then flowing a carrier gas containing the solute of interest. The absorbed gas can be calculated from the retention time of the solute in the column. This technique is used by several researchers to measure the infinite dilution activity coefficients of organic compounds in a variety of ionic liquids [208-213].

3.4.3 *The Gravimetric Method*

This techniques is commonly used for adsorption of gases onto solids but is rarely used for absorption of gases into liquids because any loss of the liquid due to evaporation affects the final weight of the sample. However, due to the non-volatile nature of the ionic liquids, the gravimetric technique works well for these systems. In this technique, the gas solubility is determined by measuring the change in the weight

of sample upon absorption. An important factor to account for when measuring gas solubilities by the gravimetric technique is the effect of buoyancy on the measurements. In some apparatus like IGA from Hiden Analytical, a counterweight side symmetric to the sample side is used to minimize these effects, but they still need to be taken into consideration.

3.4.3.1 *Advantages of The Gravimetric Method*

There are several advantages of using a gravimetric microbalance to measure gas solubilities. Ensuring that equilibrium has been reached is an important issue when measuring gas solubilities. The gravimetric balance allows the user to monitor the mass change as time progress; as equilibrium is reached, the mass change will approach zero. Once there are no longer changes in mass, the sample is at equilibrium. Ensuring that the initial liquid or solid has been fully degassed prior to the measurement is also an important factor in order to determine how much gas is dissolved in the sample. Again, the ability to monitor the mass change as time progresses allows the user to ensure that the mass has stopped decreasing during the degassing step before proceeding to the solubility measurement.

The gravimetric method has greater flexibility as being able to perform in-situ studies, thus avoiding re-exposure of the sample to atmospheric conditions. By using the gravimetric method, the correction factor (buoyancy) can be calculated or measured. Also a small sample amount is possible to be handled, beside that the kinetics of sorption process can be recorded.

3.4.3.2 *Disadvantages of The Gravimetric Method*

The disadvantages of the gravimetric method are listed below:

- Limited temperature and pressure range.

- Corrosion problem.
- Direct temperature measurement of the sample cannot be made.
- Buoyancy effect acting on sample.

3.4.4 *Magnetic Suspension Balance - the Renaissance of Gravimetry*

In the 1980's Ruhr-Universität Bochum developed a new method whereby samples could be weighed in closed vessels without any contact. The principle is as follows: a sample is weighed by means of a new kind of magnetic suspension balance (which has been patented worldwide) from the outside and the suspension force is contactlessly transmitted from the pressurized measuring cell to a microbalance at ambient atmosphere. This means that mass changes of a sample can be recorded even under extreme conditions with the utmost accuracy. Since the mid 80's these magnetic suspension balances have been applied to fundamental research work with enormous success.

Far up until at least the middle of the last century gravimetry played a predominant role in the investigation of physical and chemical processes. The decline of gravimetric measuring technology which has taken place since then results from two circumstances. The first one is due to modern spectroscopy. These instruments with their extremely high resolution have more or less taken the place of gravimetry for qualitative analysis. The second one is due the fact that none of the gravimetric instruments developed up to the 1980's are really suitable for general use under controlled environments. Only the development of new and reliable magnetic suspension balances in the late 80's with an extremely wide application range changed this situation. Now, mass changes can be recorded under nearly all conditions with utmost precision. As a result, all restrictions which prevented broad application of gravimetry in the past have been eliminated. This is all the more important as none of the modern spectroscopic methods can achieve anywhere near the accuracy of gravimetry in the case of quantitative measurement.

Magnetic suspension balances allow the changes in force and mass which act on samples under controlled environments (pressure, temperature, corrosive gases or fluids), to be measured with high accuracy. By means of these measurements it is possible to determine transport quantities and state quantities very easily and accurately (sorption, diffusion, surface tension, density), chemical reactions can be investigated (corrosion, decomposition, combustion etc.) or production processes can be simulated (polymerization, coating, drying etc.)

The main difficulty when using conventional gravimetric instruments is the direct contact between the measuring cell (sample atmosphere) and the weighing instrument. The balance can be damaged or disturbed by the measuring atmosphere and the measuring atmosphere can be adversely affected by flushing gases and pollution. These limitations considerably reduce the field of application of conventional measuring devices (See Fig. 3.3).

The new, reliable suspension balance makes it possible to weigh samples contactlessly under nearly all environments. Instead of hanging directly at the balance the sample to be investigated is linked to a so-called suspension magnet which consists of a permanent magnet, a sensor core and a device for decoupling the measuring load (sample). An electromagnet, which is attached to the underfloor weighing hook of a balance, maintains a freely suspended state of the suspension magnet via an electronic control unit. Using this magnetic suspension coupling the measuring force is transmitted contactlessly from the measuring chamber to the microbalance, which is located outside the chamber under ambient atmospheric conditions. Consequently, this arrangement eliminates almost all restrictions which are inherent to conventional gravimetric measuring instruments [214].

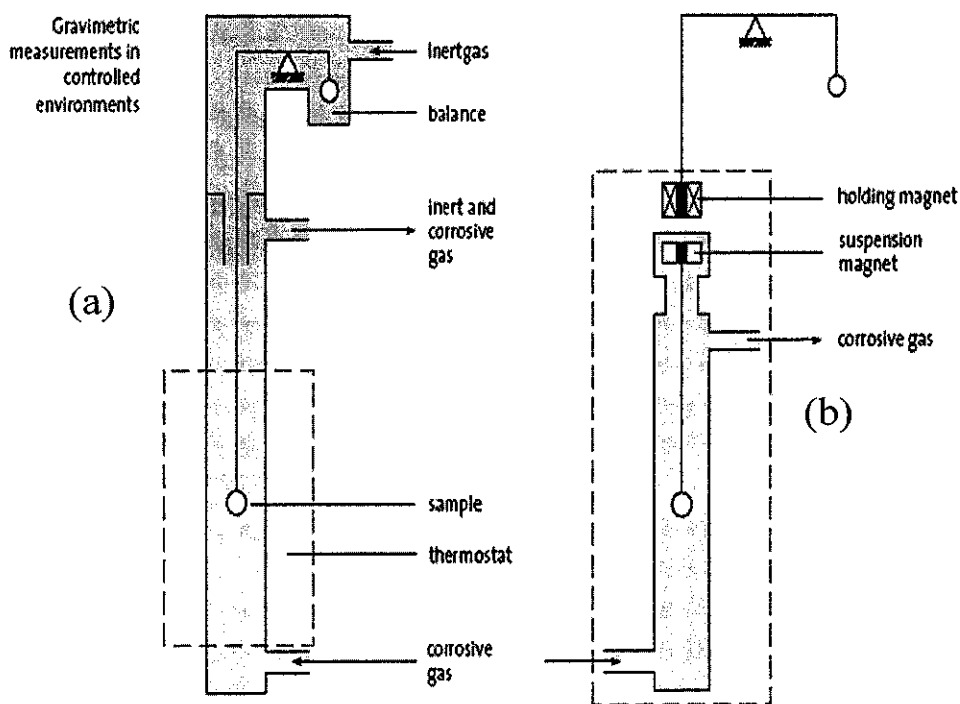


Fig. 3.3: (a) Conventional apparatus and (b) magnetic suspension balance

For all of the above mentioned advantages of the gravimetric method with magnetic suspension balance, a magnetic suspension balance (MSB) is to be used for measuring the sorption of carbon dioxide on pILs.

3.5 Summary

A hypothesis is introduced to explain the CO₂ sorption to pILs.

The theory behind the Synthia module and Monte Carlo molecular dynamic simulation, which will be implemented to predict the synthesized pILs properties and their CO₂ sorption, is addressed.

The theory of different methods for sorption measurement are elaborated with its advantages and disadvantages including justification for choosing the appropriate method used in this work.

CHAPTER 4

RESEARCH EXPERIMENTAL AND METHODS

4.1 Molecular Dynamic Simulation

Synthia module of Accelrys Material Studio version 4.1 software is used to predict the polymer properties. This is followed by sorption simulation using the Monte Carlo method. Three types of pILs are chosen for this simulation. These polymers which differ in their ion conductivity are p[VBTPA][NO₃], p[VBTEA][NO₃], and p[VBTMA][NO₃].

4.1.1 Simulation Procedure

Synthia module and Monte Carlo sorption module simulations run on HPxw8400 workstation 8.00 GB of RAM.

The computational procedure for Synthia module is shown in Fig. 4.1. The monomer is constructed and all its forcefield atoms types are assigned as shown in Fig. 4.2 and Table 4.1.

The Discover Material Studio simulation engine is used. This simulation engine incorporates a broad spectrum of molecular mechanics and dynamics methodologies that have demonstrated applicability to molecular design. The Condensed-Phase Optimized Molecular Potentials for Atomistic Simulation Studies (COMASS) forcefield is assigned for the Discover energy type. For the Non-bond setting which allows applying cutoffs or other methods of controlling non-bond, the Van der Waals (VDW) and Columb, with Atom based summation method is selected.

For Discover minimizer, which allows optimization of molecular structure with its energy at a minimum, smart ultra-fine minimization is assigned. In Discover dynamic that allows the selection of thermodynamic ensemble and choosing temperature and pressure control methods for the simulation, thermodynamics ensemble constant-volume/constant-temperature dynamics (NVT) is used.

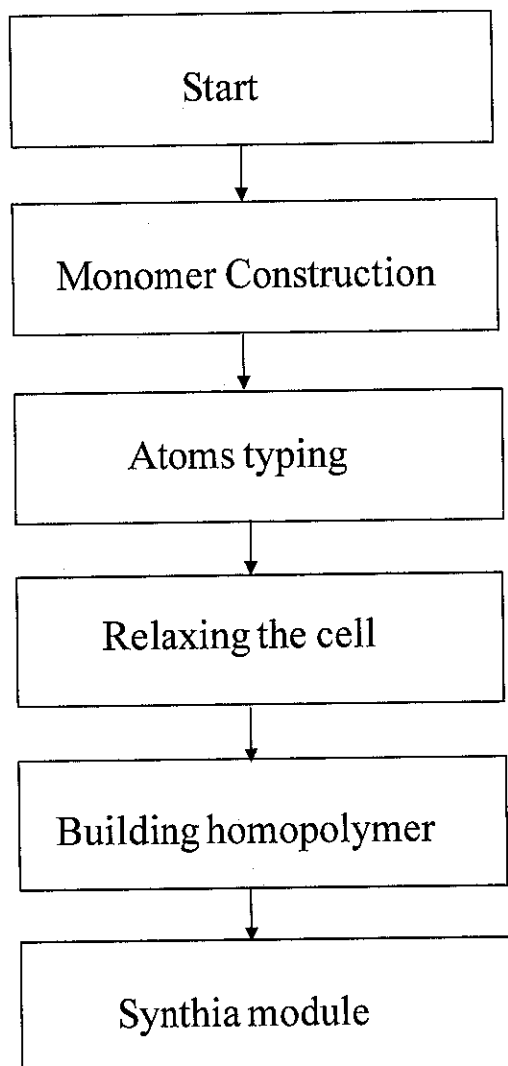


Fig. 4.1: Computational procedure for Synthia Module

In this ensemble, the dynamics are modified to allow the system to exchange heat with the environment at a controlled temperature. The temperature is set at 298 K, number of steps at 5000, time step 1.0 femtosecond (fs), and dynamic time 5.0 picoseconds (ps).

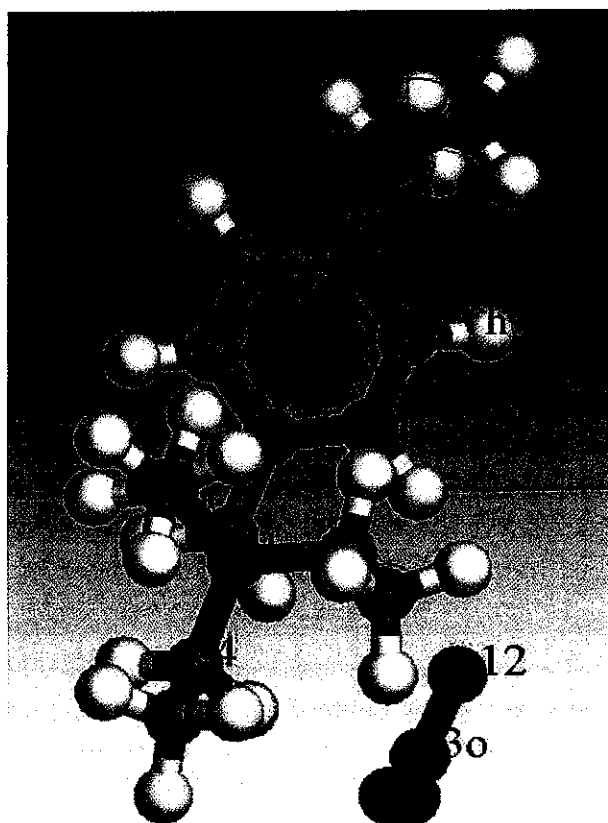


Fig. 4.2: Monomer construction and forcefield atoms typing for p[VBTEA][NO₃]

Table 4.1: Description of atoms types used in the simulation

Atom type	Description	Atom type	Description
c3a	carbon SP2 aromatic	n3o	nitrogen, SP2 in nitro group
c4	carbon SP3, generic 4 bonds	o12	oxygen, SP2 in nitro group [-NO ₂]
h1	hydrogen, non-polar	o1=*	oxygen in CO ₂
n4+	nitrogen, SP3 in protonated amine	c2	carbon, sp in O=C=O, S=C=S

After minimizing the constructed monomer, the homopolymer of the monomer is built as shown in Fig. 4.3 and Synthia module is run.

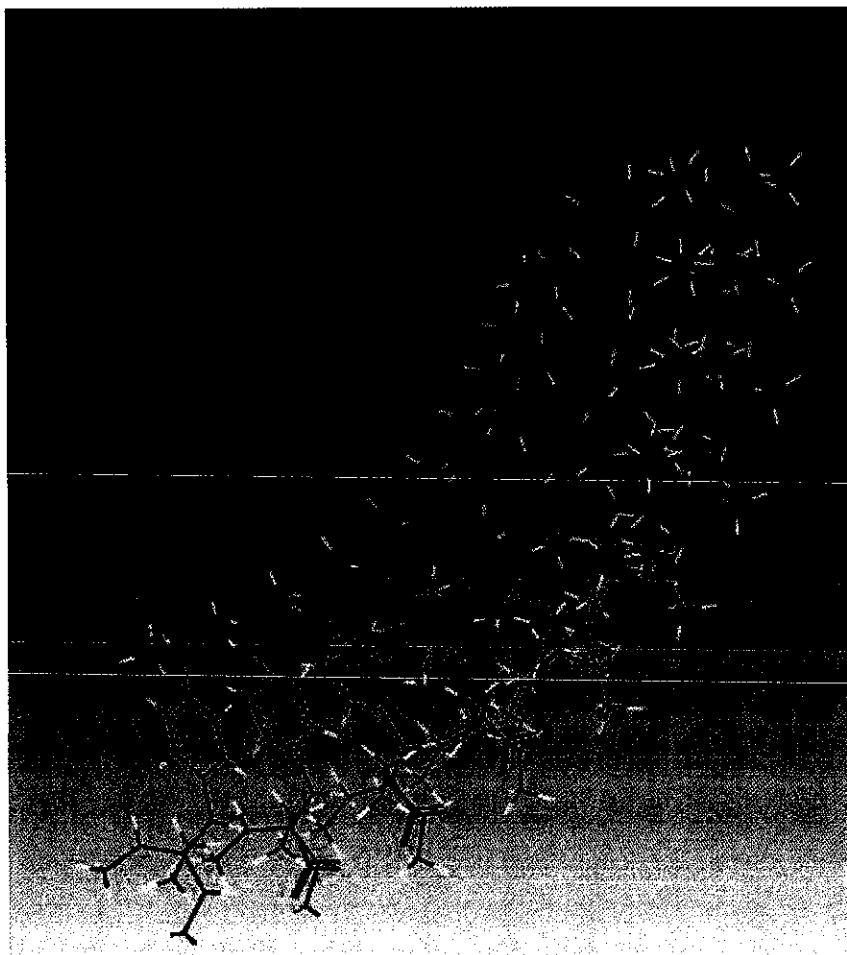


Fig. 4.3: Homopolymer construction of p[VBTEA][NO₃]

The computational procedure for Monte Carlo sorption simulation is as shown in Fig. 4.4. The CO₂ is constructed and all its forcefield atoms types are assigned as shown in Fig. 4.5 and Table 4.1. The Discover Material Studio simulation engine for CO₂ is set as the setting of the monomer.

After building the homopolymer in the Synthia module, the amorphous cell is constructed as shown in Fig. 4.6. The Amorphous Cell module provides a comprehensive set of tools to perform atomistic simulations on complex systems containing dense amorphous polymers, liquids and other non-crystalline materials. The Discover Material Studio simulation engine is used. For Discover energy,

COMASS forcefield is assigned. For the Non-bond, the Van der Waals (VDW) and Columb, with atom based summation method is selected.

For Discover minimizer, smart ultra-fine minimization is assigned. In Discover dynamic, thermodynamics ensemble constant- volume/constant-energy dynamics (NVE) is used. In NVE the Newtonian equations of motion, which conserve the total energy, are used. The temperature is allowed to vary, but the energy is not allowed to vary beyond a set value between dynamics steps. The NVE ensemble is followed by thermodynamics ensemble constant- pressure/constant-temperature dynamics (NPT). NPT is used for periodic systems. The size and possibly the shape of the unit cell are allowed to vary, while the temperature is controlled. In these ensembles, the temperature is set at 298 K, number of steps at 50000, time step 1.0 fs, and dynamic time 50.0 ps.

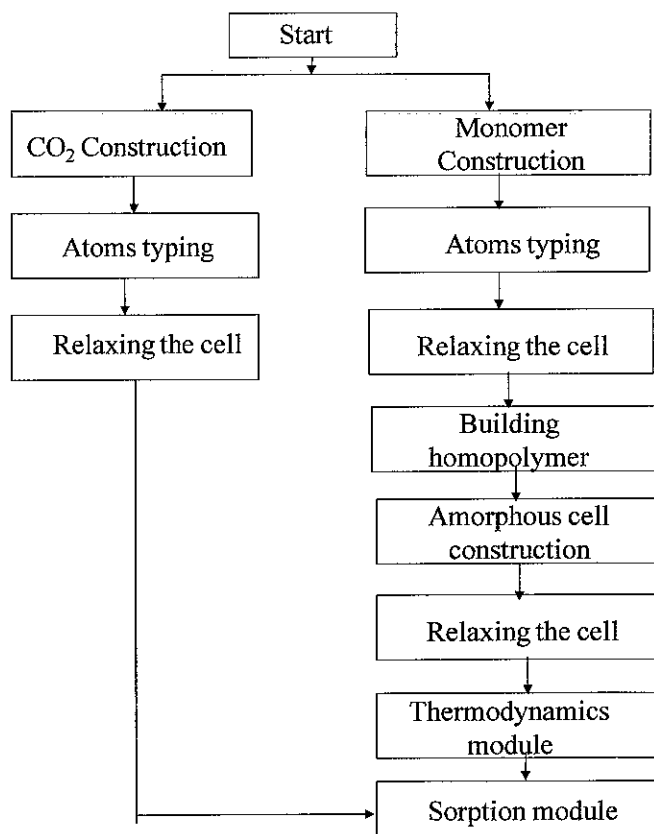


Fig. 4.4: Computational procedure for sorption Module

After minimizing and dynamic optimizing the amorphous cell, the sorption module is run. The task for sorption is specified as adsorption isotherm with Metropolis method at ultra-fine quality with minimized CO₂ structure as sorbate. COMPASS is assigned as the energy forcefield with ultra-fine quality. Ewald & group summation electrostatic method is used with atomic based Van der Waals method.

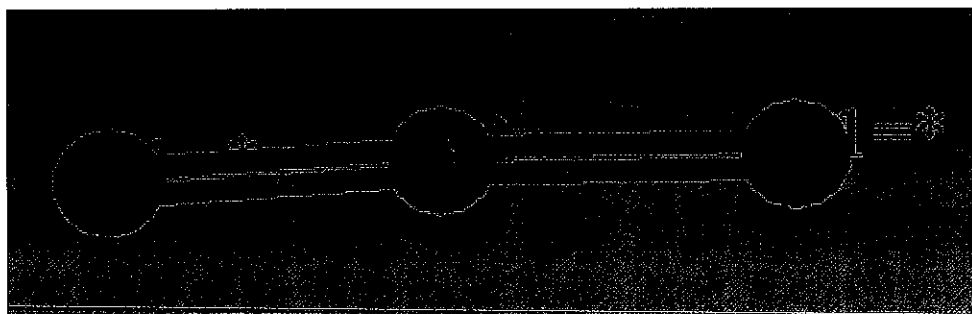


Fig. 4.5: CO₂ construction and its forcefield atoms typing

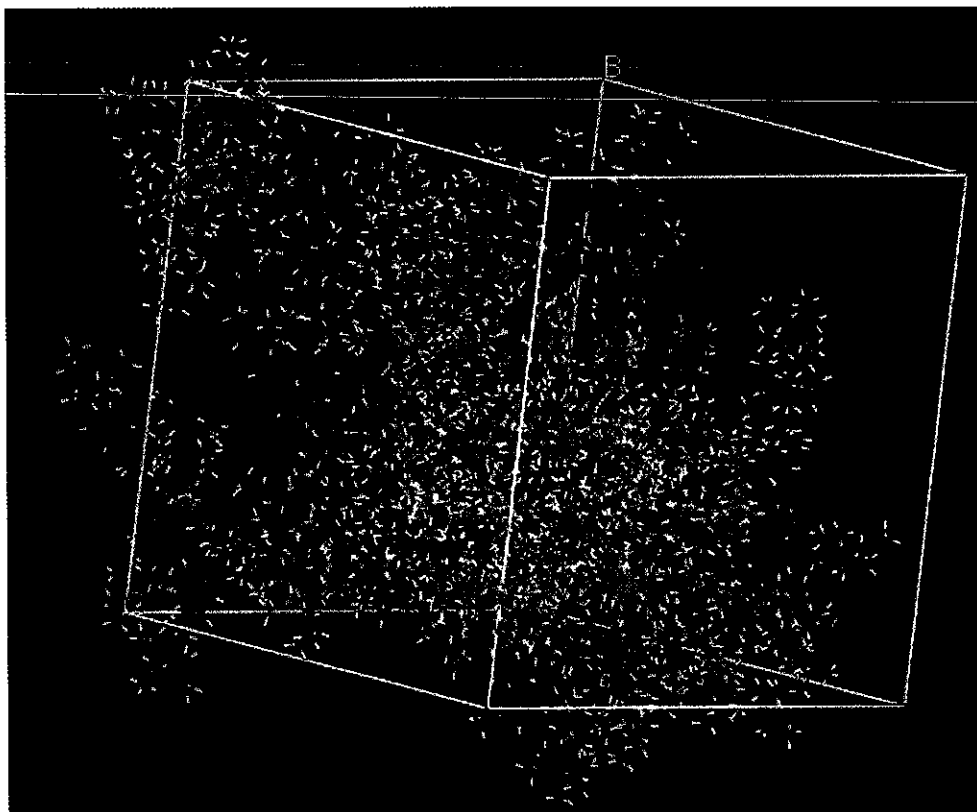


Fig. 4.6: Amorphous cell construction of p[VBTEA][NO₃]

4.2 Synthesis of Poly Ionic Liquids

Twelve poly ionic liquids are synthesized and characterized to measure their CO₂ sorption. These polymerized ionic liquids are listed in Table 4.2 to Table 4.5.

Table 4.2: Triethylammonium based poly ionic liquids.

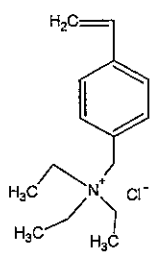
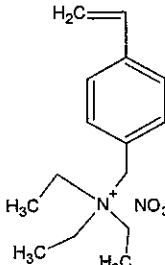
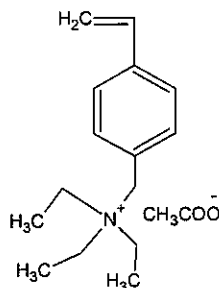
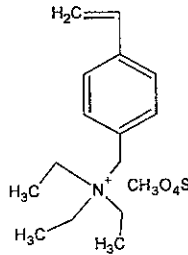
Polymer name	Polymer Abbreviation	monomer structure
poly-Vinylbenzyl triethylammonium chloride	p[VBTEA][Cl]	
poly-Vinylbenzyl triethylammonium nitrate	p[VBTEA][NO ₃]	
poly-Vinylbenzyl triethylammonium acetate	p[VBTEA][CH ₃ COO]	
poly-Vinylbenzyl triethylammonium methylsulfate	p[VBTEA][CH ₃ O ₄ S]	

Table 4.3: Trimethylammonium based poly ionic liquids.

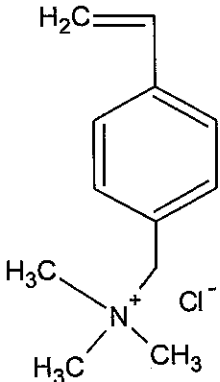
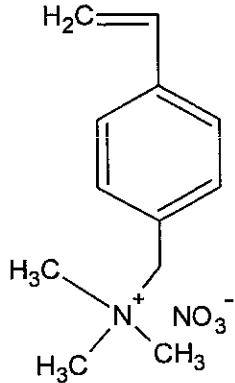
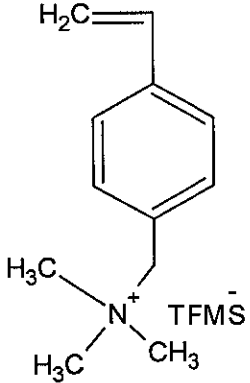
Polymer name	Polymer Abbreviation	monomer structure
poly-Vinylbenzyl trimethylammonium chloride	p[VBTMA][Cl]	
poly-Vinylbenzyl trimethylammonium nitrate	p[VBTMA][NO ₃]	
poly-Vinylbenzyl trimethylammonium trifluoromethanesulfonate	p[VBTMA][TFMS]	

Table 4.4: Methacryloyloxy ethyl trimethylammonium based poly ionic liquids.

Polymer name	Polymer Abbreviation	monomer structure
poly- Methacryloyloxy ethyl trimethylammonium chloride	p[METMA][Cl]	
poly- Methacryloyloxy ethyl trimethylammonium nitrate	p[METMA][NO ₃]	

4.2.1 Materials

The chemicals used in the synthesis of the pILs are: (ar- (vinylbenzyl) trimethylammonium) chloride 99%, Methanol anhydrous 99.8%, anhydrous *N, N*-dimethylformamide (DMF) 99.89%, anhydrous acetonitrile 99.8%, sodium trifluoromethanesulfonate 98%, triethylamine 99.5% , [2-(Methacryloyloxy) ethyl]trimethylammonium chloride 75 wt. % in H₂O, and sodium methyl sulfate 98% are purchased from Aldrich. Anhydrous diethyl ether \geq 99.97%, sodium nitrate \geq 99.0%, anhydrous sodium acetate \geq 99.0%, and Diethylamine \geq 99.5% are purchased from Sigma-Aldrich. α, α' -Azobisisobutyro-nitrile (AIBN) \geq 98% is purchased from R&M. 2,6-Di-tert-butyl-4-methylphenol (DBMP) \geq 99.0%, 4-vinylbenzyl chloride \geq

90%, and tris(dimethylamino)phosphine $\geq 97.0\%$ are purchased from Fluka. All chemicals used in synthesis and purification are used without any further purifications.

Table 4.5: Tris dimethylamino phosphine based poly ionic liquids.

Polymer name	Polymer Abbreviation	monomer structure
poly-bis(dimethylamino)-N,N-dimethyl-N-(4-vinylbenzyl) Phosphinaminium chloride	p[bDMADMVBP][Cl]	
poly-bis(dimethylamino)-N,N-dimethyl-N-(4-vinylbenzyl) Phosphinaminium nitrate	p[bDMADMVBP][NO ₃]	
poly-tris(dimethylamino)(4-vinylbenzyl)phosphonium chloride	p[tDMAVBP][Cl]	

Gases N₂ 99.9999%; Ar 99.999%; He 99.999%; CO 99.97%; CH₄ 99.995%; CO₂ 99.9% are purchased from MOX-Linde gases Sdn Bhd Malaysia.

The synthesis methods are developed based on method described by Tang *et al.* [146].

4.2.2 Synthesis of Triethylammonium Based Poly Ionic Liquids

To a dried 250 ml flask; 0.16 mole of 4-vinylbenzyl chloride, 0.168 mole of triethylamine, and 0.4 gm of DBMP are added. The reaction mixture is stirred under nitrogen at 50°C for two days. The formed solid vinylbenzyl triethylammonium chloride [VBTEA][Cl] is washed with diethylether and filtered and further dried under vacuum.

5 gm of [VBTEA][Cl], 50 mg of AIBN, and 10 ml of DMF are charged into a reaction flask under nitrogen atmosphere, the flask is immersed in an oil bath at 60° C for 6 hours. A white solid is formed. This formed polymer p[VBTEA][Cl] is poured in methanol, filtered and dried under vacuum at 100°C. Further drying is done in a vacuum oven at 100°C for three days.

[VBTEA][Cl], is mixed with 0.002 excess moles of sodium nitrate or sodium acetate or sodium methyl sulfate separately in 50 ml of acetonitrile and stirred at room temperature for two days. The salt precipitates are removed by filtration. The filtrates are concentrated under vacuum and then poured in to 100 ml of diethyl ether to precipitate out the products [VBTEA][NO₃], [VBTEA][CH₃COO], and [VBTEA][CH₃O₄S]. These products are collected by filtration and dried under vacuum. 5 gm of [VBTEA][NO₃] or [VBTEA][CH₃COO] or [VBTEA][CH₃O₄S], 50 mg of AIBN, and 10 ml of DMF are charged separately into a reaction flasks under a nitrogen atmosphere, the flasks are immersed in an oil bath at 60° C for 6 hours. These formed polymers p[VBTEA][NO₃], p[VBTEA][CH₃COO], and p[VBTEA][CH₃O₄S] are poured into methanol, filtered and dried under vacuum at 100°C. Further drying is done in a vacuum oven at 100°C for three days.

4.2.3 *Synthesis of Trimethylammonium Based Poly Ionic Liquids*

10 gm of (ar- (vinylbenzyl) trimethylammonium) chloride, [VBTMA][Cl], 100 mg of AIBN, and 20 ml of DMF are charged into a reaction flask under nitrogen atmosphere, the flask is immersed in an oil bath at 60° C for 6 hours. A white solid is formed. This formed polymer (p[VBTMA][Cl] is poured into methanol, filtered and dried under vacuum at 100°C. Further drying is done using a vacuum oven at 100°C for three days.

[VBTMA][Cl] is mixed with 0.002 excess moles sodium nitrate or sodium trifluoromethanesulfonate separately in 50 ml of acetonitrile and stirred at room temperature for two days. The salt precipitates are removed by filtration. The filtrates are concentrated under vacuum and then poured into 100 ml of diethyl ether to precipitate out the products [VBTMA][NO₃] and [VBTMA][TFMS]. These products are collected by filtration and dried under vacuum. 5 gm of [VBTMA][NO₃] or [VBTMA][TFMS], 50 mg of AIBN, and 10 ml of DMF are charged separately into a reaction flasks under a nitrogen atmosphere, the flasks are immersed in an oil bath at 60° C for 6 hours. The formed polymers p[VBTMA][NO₃] and p[VBTMA][TFMS] are poured into methanol, filtered and dried under vacuum at 100°C. Further drying is done using vacuum oven at 100°C for three days.

4.2.4 *Synthesis of Methacryloyloxy Ethyl Trimethylammonium Based pILs*

Water from [2-(Methacryloyloxy) ethyl] trimethylammonium chloride 75 wt. % in H₂O is removed under vacuum. 10 gm of 2-(Methacryloyloxy) ethyl] trimethylammonium chloride, [METMA][Cl], 100 mg of AIBN, and 20 ml of DMF are charged into a reaction flask under a nitrogen atmosphere, the flask is immersed in an oil bath at 60° C for 6 hours. A white solid is formed. This formed polymer (p[METMA][Cl] is poured in methanol, filtered and dried under vacuum at 100°C. Further drying is done using vacuum oven at 100°C for three days.

[METMA][Cl], is mixed with 0.002 excess moles of sodium nitrate in 50 ml of acetonitrile and stirred at room temperature for two days. The salt precipitate is removed by filtration, the filtrate is concentrated under vacuum precipitating out the product [METMA][NO₃]. The product is collected by filtration and dried under vacuum. 5 gm of [METMA][NO₃], 50 mg of AIBN, and 10 ml of DMF are charged separately into a reaction flask under a nitrogen atmosphere, the flask is immersed in an oil bath at 60° C for 6 hours. The formed polymer p[METMA][NO₃] is poured into methanol, filtered and dried under vacuum at 100°C. Further drying is done using vacuum oven at 100°C for three days.

4.2.5 Synthesis of Tris Dimethylamino Phosphine Based Poly Ionic Liquids

i. To a dried 250 ml flask, 0.16 mole of 4-vinylbenzyl chloride, 0.168 mole of tris(dimethylamino)phosphine, and 0.4 gm of DBMP are added. The reaction mixture is stirred at 40°C for two days in a closed system equipped with condenser after purging the air from the flask using nitrogen. The formed solid is washed with diethylether and filtered and further dried under vacuum producing bis(dimethylamino)-N,N-dimethyl-N-(4-vinylbenzyl Phosphinaminium chloride [bDMADMVBP][Cl]. 5 gm of [bDMADMVBP][Cl], 50 mg of AIBN, and 10 ml of DMF are charged into a reaction flask under nitrogen atmosphere, the flask is immersed in an oil bath of 60° C for 6 hours. The formed polymer p[bDMADMVBP][Cl] is poured in methanol, filtered and dried under vacuum at 100°C. Further drying is done using vacuum oven at 100°C for three days.

[bDMADMVBP][Cl], is mixed with 0.002 excess moles of sodium nitrate in 50 ml of acetonitrile and stirred at room temperature for two days. The salt precipitate is removed by filtration, the filtrate is concentrated under vacuum precipitating out the product [bDMADMVBP][NO₃]. The product is collected by filtration and dried under vacuum. 5 gm of [bDMADMVBP][NO₃], 50 mg of AIBN, and 10 ml of DMF are charged into a reaction flask under a nitrogen atmosphere, the flask is immersed

in an oil bath at 60° C for 6 hours. The formed polymer p[bDMADMVBP][NO₃] is poured into methanol, filtered and dried under vacuum at 100°C. Further drying is done using vacuum oven at 100°C for three days.

ii. To a dried 250 ml flask, 0.16 mole of 4-vinylbenzyl chloride, 0.168 mole of tris(dimethylamino)phosphine, and 1.66 gm of DBMP are added. The reaction mixture is stirred at 40°C for two days in a closed system equipped with a condenser after purging the air from the flask using nitrogen. The formed solid is washed with diethylether, filtered and further dried under vacuum producing tris(dimethylamino)(4-vinylbenzyl)phosphonium chloride [tDMAVBP][Cl]. 5 gm of [tDMAVBP] [Cl], 50 mg of AIBN, and 10 ml of DMF are charged into a reaction flask under a nitrogen atmosphere, the flask is immersed in an oil bath at 60° C for 6 hours.. The formed polymer p[tDMAVBP][Cl] is poured in methanol, filtered and dried under vacuum at 100°C. Further drying is done using vacuum oven at 100°C for three days.

4.3 Characterization of Poly Ionic Liquids

The characterization of pILs includes: structure analysis, topology analysis, chloride content, water content, density, thermal stability, and molecular weight analysis.

4.3.1 Structure Analysis

In order to check the structure and the purification of the synthesized pILs, two different techniques are used; namely nuclear magnetic resonance (NMR) spectroscopy and elemental analysis [215]. ¹H NMR spectra are recorded on a Bruker advance DRX-400 spectrometer operating at 400 MHz, with deuterated DMSO-d₆ as the solvent. The chemical shifts (δ) are reported in ppm and are referenced to tetramethylsilane as an internal standard (δ = 0 ppm). Multiplicities are abbreviated as follow, *s*, single; *d*, doublet; *t*, triplet; *m*, multiplet; *q*, quarted; and *br*, broad.

The elemental analysis to determine the percentage of elements for synthesized pILs is done using LECO CHNS-932 element analyzer. As the pILs are highly hydrophilic, a simultaneous water content measurement is performed to correct the weight of the sample. The average of at least three measurements is reported.

4.3.2 Topology Analysis

To study the topology and morphology of the synthesized pILs, two different techniques are used.

The X-ray diffraction (XRD) is a technique used to characterize the crystallographic structure. The analysis is recorded on a Bruker D8 advance automated powder diffraction system operating in the normal transmission mode with Ni-filtered Cu K α radiation.

The glass transition temperature (T_g) is defined as the temperature at which the forces holding together the distinct components of an amorphous solid are overcome by thermally-induced motions within the time scale of the experiment, so that these components are able to undergo large-scale molecular motions on this time scale, and is limited mainly by the inherent resistance of each component to such flow[200]. The common method used to determine the T_g is differential scanning calorimetry (DSC).

The DSC experiments are carried out on Perkin Elmer Pyris 1 DSC. Each synthesized pIL (5-10 mg) is first heated to 200 °C under protection of nitrogen at a flow rate of 20 ml/min, then immediately cooled with liquid nitrogen to -50 °C. The sample is then scanned at heating rate of 10 °C/min. the results are recorded from -50 °C to 300 °C.

4.3.3 Chloride content

To determine the chloride content, an ion chromatograph (IC) Metrohm Model 761 Compact is used. The equipment used equipped with Metrosep A Supp 5-150 (6.1006.520) (4.0 mm × 150 mm) analytical column and a Metrosep A Supp 4/5 guard column (4.0 mm × 5 mm). The eluent used is a mixture of 3.2 mM Na₂CO₃ and 1.0 mM NaHCO₃. The data are analyzed with the aid of Metrodata IC Net 2.3 software [215]. The average of three readings is recorded.

4.3.4 Water content

To determine the water content of the pILs for CHNS calculations, coulometric Karl Fischer autotitrator, Mettlor Toledo DL39 with CombiCoulomat fritless Karl Fischer reagent from Merck is used. The average value of three measurements is considered for further analysis and calculations [215].

4.3.5 Density

To measure the density of the synthesized pILs, an Ultrapycnometer 1000 Version 2.2 instrument is used. This instrument is design for measuring the true volume and density of powders, foams and bulk solids. The samples are run for ten times and the average of the last three readings is recorded.

4.3.6 Thermal Stability

Thermal stability is the stability against degradation upon exposure to elevated temperatures in an inert environment. The Dynamic Thermogravimetric analyzer (TGA) Perkin Elmer Pyris 1 TGA is used to study the thermal stability. The heating rate is 10 °C/min a under nitrogen atmosphere with a flow rate of 20 ml/min.

4.3.7 Molecular Weight Analysis

The molecular weight is determined using gel permeation chromatography (GPC) system consisting of a Waters size exclusion chromatograph, equipped with two 300 mm Waters Styragel solvent-saving columns (molecular weight $5 \times 10^2 - 3 \times 10^4$ and $5 \times 10^3 - 6 \times 10^5$). The detector is Waters 2414 refractive-index detector. The used eluent is DMF containing 0.05 M LiBr at a flow rate of 0.3 mL/min. The temperature of the column is adjusted to 70 °C. The standards used to generate the calibration curve are a series of poly(ethylene glycol) having a molecular weight range of 970-270000 [149]. This test is performed by the equipment supplier.

4.4 Sorption Measurement

4.4.1 Experimental Procedure

Sorption measurements are performed using the magnetic suspension balance (MSB) from Rubotherm GmbH (Germany) rated at 500 bar and 500 °C, as seen in Fig. 4.7.

The MSB consists of a sorption chamber where the sample is exposed to a gas at the desired temperature and pressure, and a microbalance with accuracy up to five decimals of a gram. This balance is isolated from the sample and exists at ambient conditions as shown in Fig. 3.3. An electromagnet is connected to the microbalance and adjusted to keep the permanent magnet in suspension. The permanent magnet is connected to a rod-rod-basket assembly and located in the sorption chamber. Hence, the microbalance measures a weight which is proportional to the electromagnetic force that keeps the rod-rod-basket assembly in suspension. A heating circulator (Julabo, Model F25ME) is used to control the temperature of the sorption chamber with an accuracy of ± 0.5 °C (see Fig. 4.8). The apparatus is also equipped with an electrical heater for heating above 150 °C up to 500 °C. The apparatus is equipped with a dehumidifier to dry the gas. This gas dryer consists mainly of a high pressure

(200 bar at room temperature) resistant stainless steel column filled with zeolite 4A as a drying agent. Zeolite 4A will adsorb the water presence in the gas flowing through the column (inner diameter 3 cm, length 35 cm).

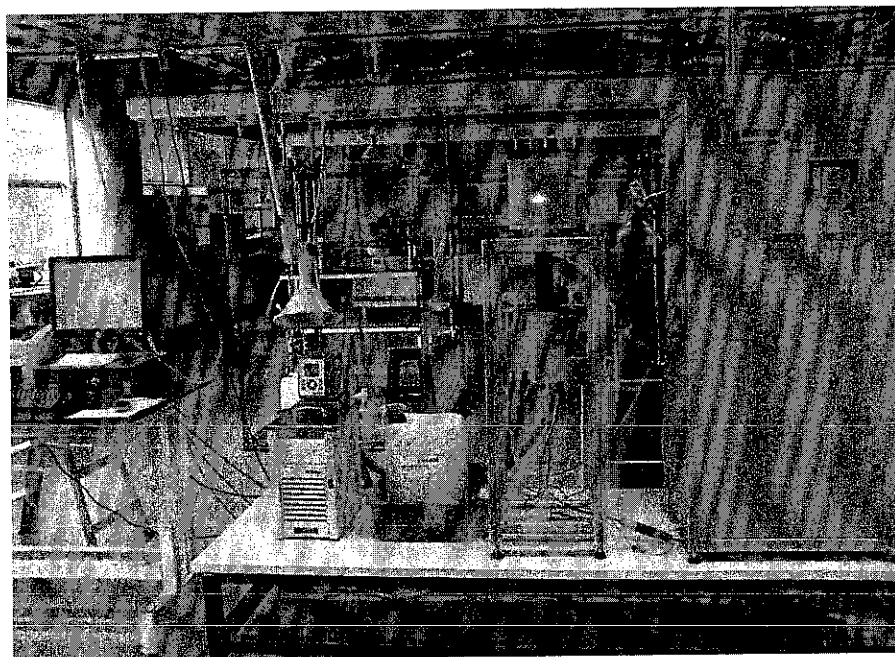


Fig. 4.7: Magnetic suspension balance MSB apparatus located in UTP



Fig. 4.8: Julabo, Model F25ME connected to MSB.

An electrical heater is located outside the column for heating the drying agent up to 300 °C for reactivation. A thermal isolation material covers the column in order to reduce heat loss to the environment. The column and all other parts of the dryer are located in an aluminum rack as seen in Fig. 4.9.

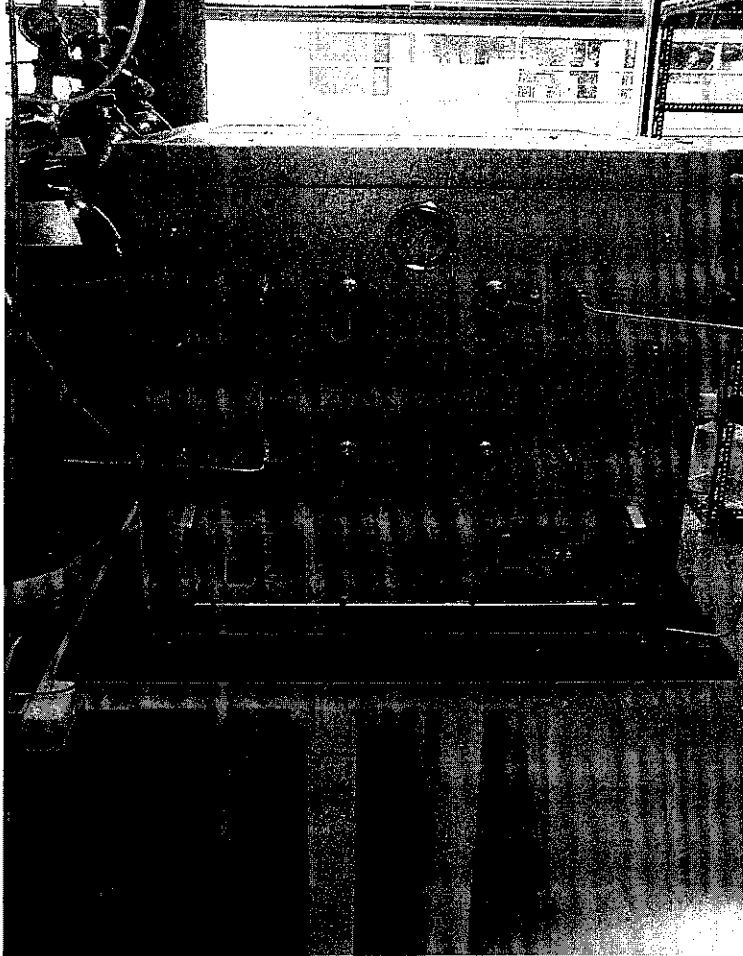


Fig. 4.9: Dehumidifier (Gas dryer) connected to MSB gas dosing system

In order to overcome the condensation problem of CO_2 at elevated pressure, the gas dosing inlet line is equipped with a controlled external electrical heater.

In a typical experiment, initially a blank measurement is performed to measure the weight m_{SC} and volume V_{SC} of the empty sample container. A blank measurement is basically measuring an adsorption isotherm without a sample in the sample container.

Starting from vacuum, the pressure is increased stepwise with nitrogen. The experimental data, balance reading (m_{BAL}), temperature (T), and pressure (p) are recorded. Using the temperature and the pressure data, the density of the gas in the MSB sorption chamber can be calculated using Peng-Robinson equation of state. The balance reading (m_{BAL}) is plotted as a function of density of the gas (ρ), resulting in a straight line with a negative slope as shown in Fig. 4.10.

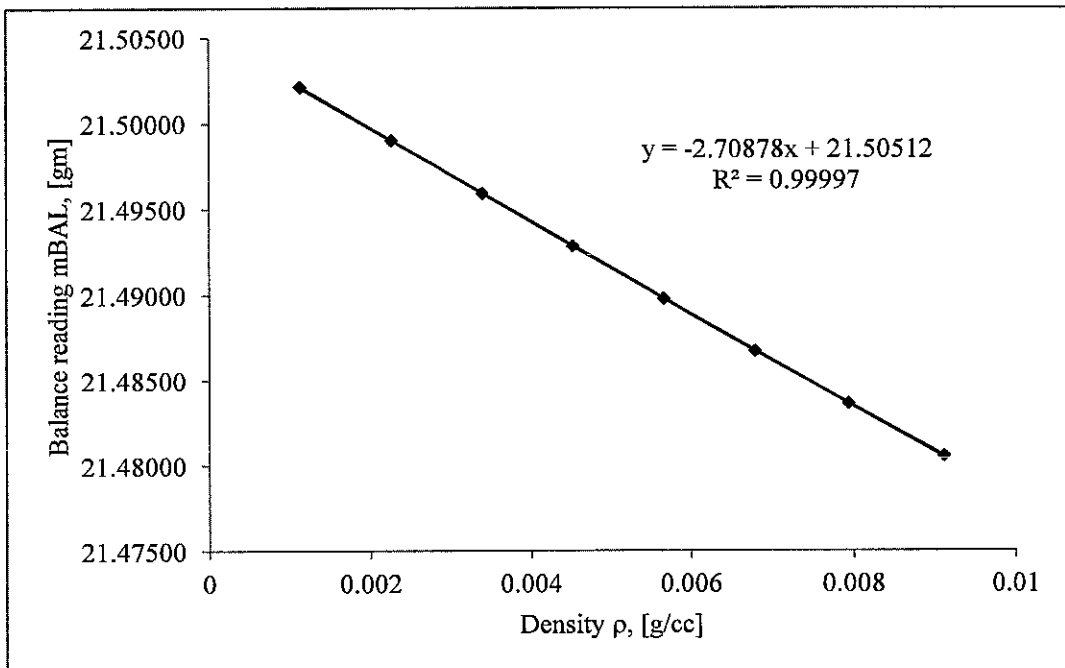


Fig. 4.10: Example for blank measurement result

The negative slope of the measured masses of the empty sample container with increasing pressure (density) of the gas is due to the buoyancy acting on the sample container. The buoyancy (B) effect is proportional to the density as shown in eq. 4.1.

$$B = \rho V \quad 4.1$$

A linear regression method is applied on the measurement data i.e. density of the gas versus the measured masses shown in Fig. 4.10, and the eq. is rewritten as eq. 4.2

$$m_{BAL} = m_{SC} - \rho V_{SC} \quad 4.2$$

The values of the parameters of this linear function are determined by a regression using spreadsheet (MS EXCEL). The mass of the sample container in the vacuum is the balance reading at the vacuum as eq. 4.3.

$$m_{SC} = m_{BAL}(p = 0, \rho = 0) \quad 4.3$$

Resulting from this regression, the weight of the empty sample container (m_{SC}) and the volume of the sample container (V_{SC}) are calculated.

Secondly, the sample is loaded in the MSB by filling the sample container with the sample. After closing the sorption chamber, the sample is degassed by evacuating and heating the chamber at 120 °C until the reading of the microbalance remains unchanged over one hour. Then the sorption chamber is cooled. This reactivation step is to ensure that the sample is free of moisture or any adsorbed gas or solvent.

Thirdly, in order to determine the volume of the sample (V_S) and the mass of the sample (m_S) located in the sample container, a buoyancy measurement has to be carried out. The measurement is performed as measuring an adsorption isotherm of the sample in the MSB by stepwise, increasing the pressure at constant temperature. Helium gas is chosen because it is not adsorbed by the sample and as a result, the mass and volume of the sample will not be changed.

By plotting the m_{BAL} during the buoyancy measurement with helium versus the density of the gas, again straight line with negative slop is the result as shown in Fig. 4.11.

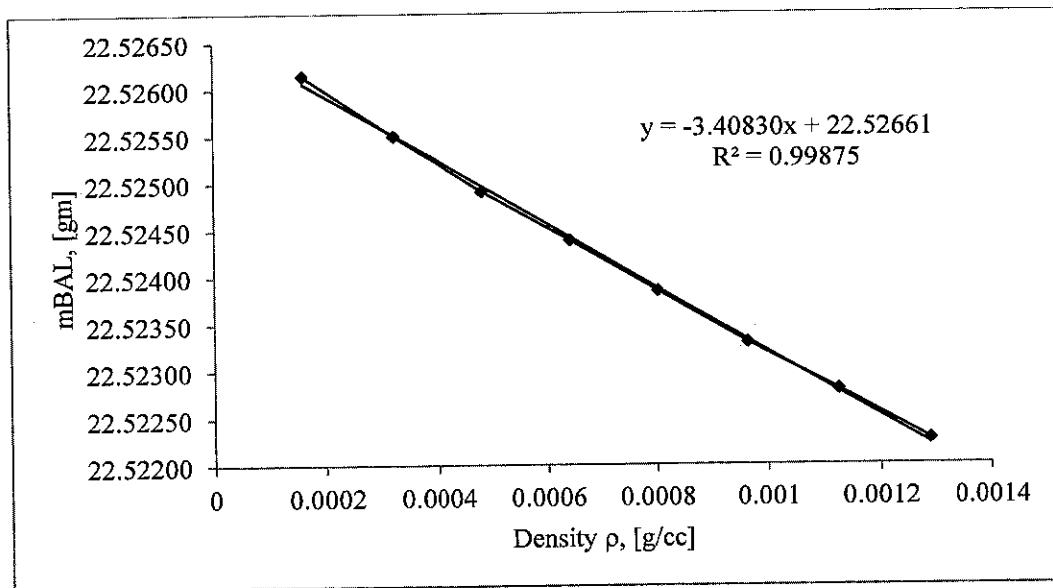


Fig. 4.11: Example of buoyancy measurement with He

The linear regression of the measured masses versus the density of the helium gives results to eq. 4.4

$$m_{BAL} = m_{SC+S} - \rho V_{SC+S} \quad 4.4$$

To calculate m_S and V_S eq. 4.5 and 4.6 are to be used

$$V_S = V_{SC+S} - V_{SC} \quad 4.5$$

$$m_S = m_{SC+S} - m_{SC} \quad 4.6$$

Finally after performing the buoyancy measurement, the sorption measurement can be performed. Usually for the sorption measurement, the pressure of the gas in the MSB is increased stepwise at constant temperature. The recorded balance reading needs to be corrected for the buoyancy effect acting on the sample and sample container according to eq. 4.7.

$$m_{BAL,CORR} = m_{BAL} + \rho V_{SC+S} \quad 4.7$$

By subtracting the mass of the empty sample container (eq. 4.8), the mass of the sample with adsorbed gas (m) is calculated.

$$m = m_{BAL,CORR} - m_{SC} \quad 4.8$$

The mass change of the sample due to adsorption (Δm) is determined by subtracting the mass of reactivated sample (m_S) from the mass of sample (m) following eq. 4.9.

$$\Delta m = m - m_S \quad 4.9$$

By dividing this mass change of the sample due to the sorption by the mass of reactivated sample, the specific uptake (m_{ADS}) in [gm] gas adsorbed per [gm] adsorbent material is determined as in eq. 4.10.

$$m_{ADS} = \frac{\Delta m}{m_S} \quad 4.10$$

The specific uptake in [g/g] can be recalculated in a specific amount of gas adsorbed by dividing it by the molar mass of the gas to be expressed in [mole] gas adsorbed per [gm] of adsorbent material.

It is very essential to mention the importance of ensuring equilibrium during measurement for each specific measurement at constant pressure and temperature. Monitoring the weight change over time makes it easy to determine the time necessary for equilibrium to be reached by noting how long it is needed before the mass stops rising significantly.

Fig. 4.12 explains the methodology strategy being followed in this research.

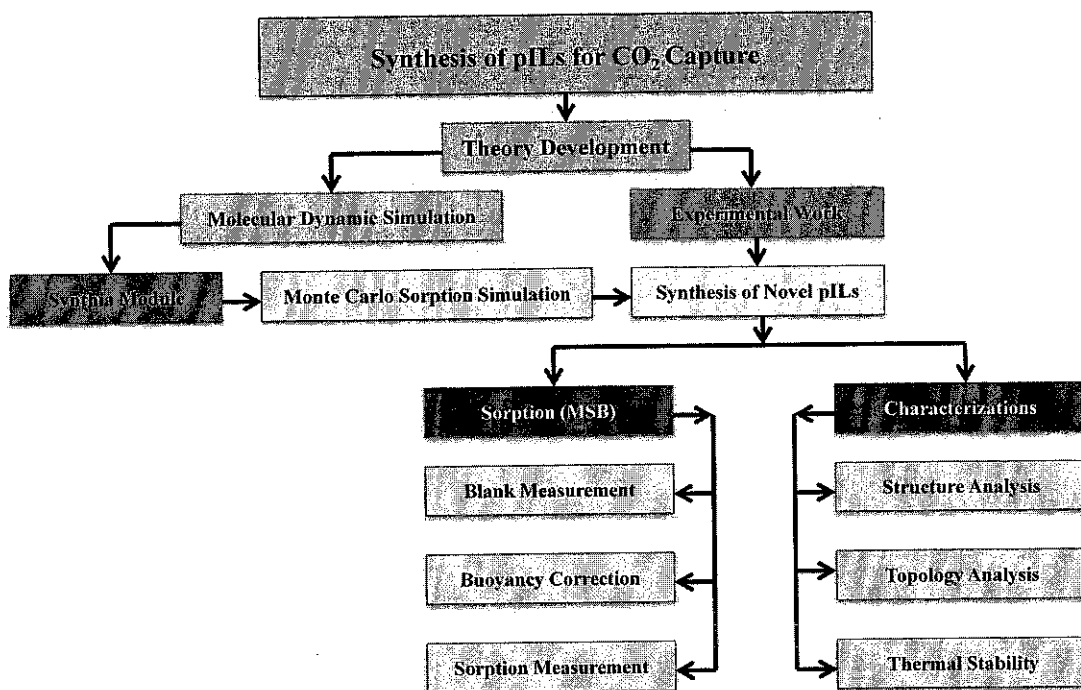


Fig. 4.12: Methodology strategy

4.5 Summary

Different types of techniques and methods that are utilized for the simulation and analysis have been elaborated.

Synthia module and Monte Carlo molecular dynamic simulation computational procedures are explained in details to predict the synthesized pILs properties and their CO₂ sorption.

Detailed methods of synthesizing different groups of pILs are explained. The characterization of these pILs involved different types of techniques including structure analysis (NMR and CHNS), topology analysis (XRD, and DSC), chloride content, water content, thermal stability, and molecular weight determination.

A comprehensive description of the MSB and its sorption measurement methods and calculations are elaborated to generate the rate of sorption and sorption isotherm.

CHAPTER 5

RESULTS AND DISCUSSION

5.1 Molecular Dynamics Simulation Results

Three different pILs having different ion conductivity are selected for molecular dynamics simulation to predict their properties and simulate their CO₂ sorption. These polymers are poly-Vinylbenzyl tripropylammonium nitrate p[VBTPA][NO₃], poly-Vinylbenzyl triethylammonium nitrate p[VBTEA][NO₃], and poly-Vinylbenzyl trimethylammonium nitrate p[VBTMA][NO₃]. As proposed previously, in a theory to explain the mechanism of CO₂ sorption on pILs, sorption depends on ion conductivity. By varying the substituent around the cation from methyl to ethyl to propyl groups, the positive charge density of cation will be weakened leading to lower ion conductivity. Simulating the CO₂ sorption of these polymers will direct our synthesis.

5.1.1 *Synthia Module*

The Synthia module is known to predict reliable polymer properties [200]. For the above mentioned three pILs the reliability of predicting the pILs properties utilizing the Synthia module is checked. Some chosen properties resulting from using the Synthia module, are tabulated in Table 5.1 and Table 5.2.

From the simulation results it appears that the molar volume $V_{(298K)}$ and coefficient of volumetric thermal expansion $V(T)$ increase with the increasing length of substituent attached to cation from methyl to ethyl to propyl. The density (ρ) of the polymer decreases with increasing length of n-alkyl substituent attached to cation and this is understandable due to the increment in polymer volume.

Table 5.1: Estimated pILs properties (1) using the Synthia module

polymer	$V_{(298K)}$ [cm ³ /mole]	$V(T)$, [ppm/K]	ρ , [g/cm ³]	$C_p^S(298K)$, [J/(g K)]	T_g , [K]
p[VBTPA] [NO ₃]	302.1	306.66	1.06735	439.96	312.87
p[VBTEA] [NO ₃]	253.86	287.46	1.10442	367.61	335.86
p[VBTMA] [NO ₃]	202.22	265.05	1.17835	290.47	366.92

Table 5.2: Estimated pILs properties (2) using the Synthia module

polymer	$T_{d, \frac{1}{2}}$, [K]	P_{O_2} , [DU]	P_{N_2} , [DU]	P_{CO_2} , [DU]
p[VBTPA] [NO ₃]	617.5	616.50	176.66	3184.73
p[VBTEA] [NO ₃]	608.9	576.9	164.4	2962.7
p[VBTMA] [NO ₃]	587.7	580.25	165.46	2981.27

The molar heat capacity $C_p^S(298K)$ also follows the increment trend with the substituent. The glass transition temperature (T_g) decreased with the increment in the length of the substituent. The temperature of half decomposition ($T_{d, \frac{1}{2}}$) follows the rise in substituent length. The permeability of oxygen (P_{O_2}), nitrogen (P_{N_2}), and CO₂ (P_{CO_2}) is following the order of p[VBTPA][NO₃] > p[VBTEA][NO₃] > p[VBTMA][NO₃]. If the permeability and topology of the polymer is the major factor

that influences the sorption of CO₂ in pILs, then it is expected p[VBTPA][NO₃] to provide the highest CO₂ sorption followed by p[VBTMA][NO₃] and p[VBTEA][NO₃] but this is not the case as proposed in the earlier theory providing the following order p[VBTMA][NO₃] > p[VBTEA][NO₃] > p[VBTPA][NO₃].

To validate the simulation results, a comparison is made between some experimental results and the simulation result. The measured density (see section 5.2.4) for p[VBTEA][NO₃] is 1.1170 [gm/cm³], while for p[VBTMA][NO₃] is 1.1805 [gm/cm³]. The deviations of density simulation results from the measured ones for p[VBTEA][NO₃] and p[VBTMA][NO₃] are 1.12% and 0.18% respectively which leads to a conclusion that the prediction of Synthia module fitted the actual density of pILs obeying the n-alkyl length trend.

Considering the glass transition temperature (T_g) experimental results (see section 4.2.2), for p[VBTEA][NO₃] is 382.02 °K, while for p[VBTMA][NO₃] is 440.34 °K. The deviations of T_g simulation results from the measured ones for p[VBTEA][NO₃] and p[VBTMA][NO₃] are 12.08% and 16.67% respectively. The reported value for standard deviation for Synthia T_g correlation is 6.7% [200]. Obviously, the Synthia correlation does not fit for estimating the glass temperatures for pILs but obeys the n-alkyl length trend.

The values of measured temperature of half decomposition (see section 5.2.5) for p[VBTEA][NO₃] and p[VBTMA] [NO₃] are 683 °K and 578 °K. The estimated values (see Table 5.2) report a deviation of 10.8% and 1.7% respectively. The reported value for standard deviation for Synthia T_{d,1/2} correlation is 7% [200]. The estimated values follow the n-alkyl length trend. It can be concluded that not all Synthia module correlations are fit for predicting pILs properties, a need for additional term describing ion conductivity of the polymer may be required for more accurate predictions.

5.1.2 Sorption Simulation Results

Monte Carlo molecular dynamic simulation for poly-Vinylbenzyl tripropylammonium nitrate p[VBTPA][NO₃], poly-Vinylbenzyl triethylammonium nitrate p[VBTEA][NO₃], and poly-Vinylbenzyl trimethylammonium nitrate p[VBTMA][NO₃] is performed to predict their CO₂ sorption isotherm at 25 °C up to 10 bar. The simulation result is shown in Fig. 5.1

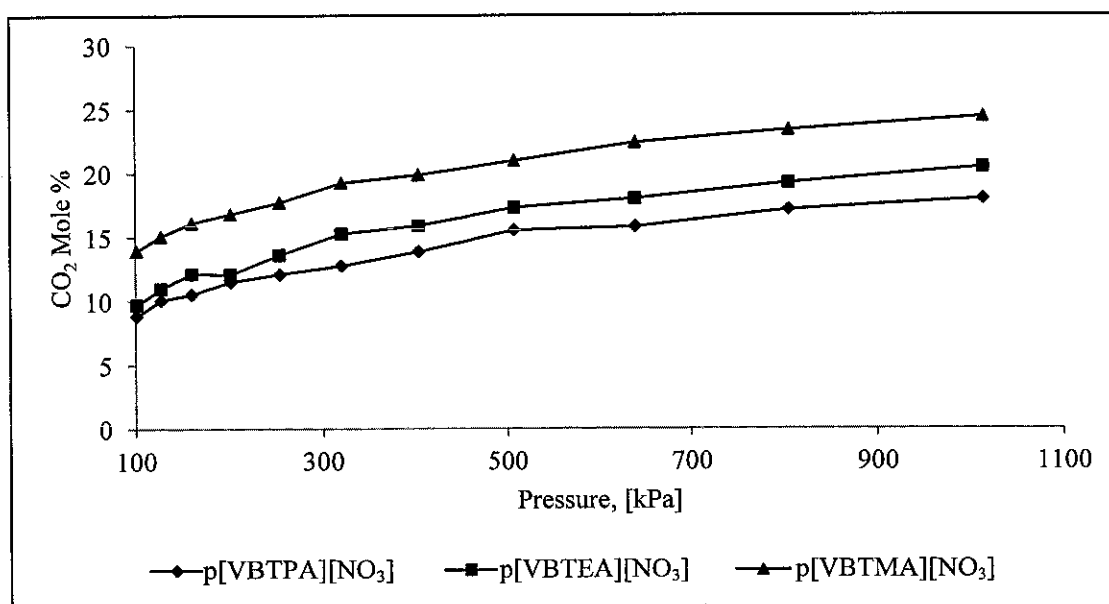


Fig. 5.1: CO₂ sorption simulation result for selected pILs.

Increasing the n-alkyl length of the substituent from methyl to ethyl to propyl leads to a reduction in the positive charge of the cation, resulting in ion conductivity reduction due to the electron donating characteristic of these groups (propyl > ethyl > methyl). The n-alkyl length will also affect the steric effect, a longer alkyl chain lead to more steric effect.

As seen from the simulation results, the CO₂ sorption capacity is in accordance with the ion conductivity of the cation as the anion is fixed for the three types of pILs.

The average total energy of sorption is shown in Fig. 5.2. (Note: the values of energy are negative). The values of total energy of sorption are in agreement with the sorption capacity of the pILs.

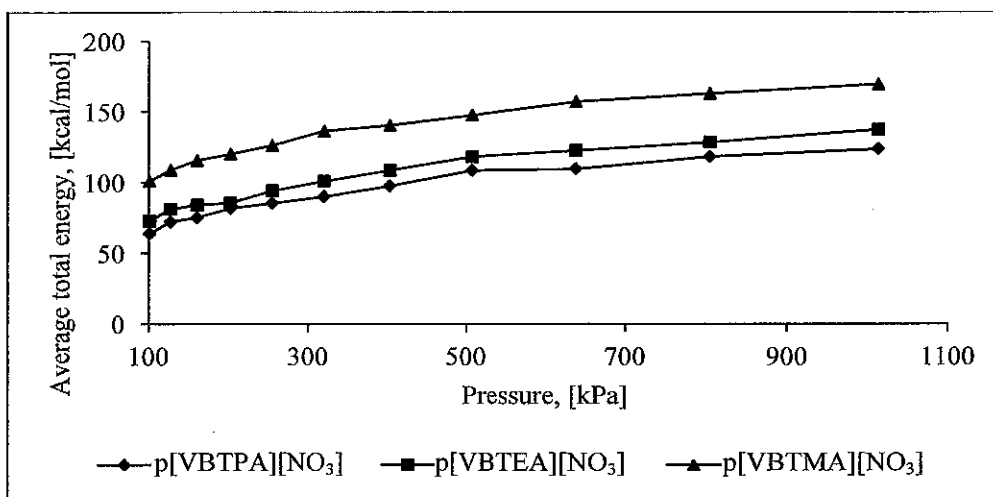


Fig. 5.2: Average total energy of CO₂ sorption for simulated pILs.

To validate the simulation results, the p[VBTMA] [NO₃] experimental results (see section 5.3), are compared with the simulated ones as shown in Fig. 5.3 showing an average deviation of 7.2% which is acceptable.

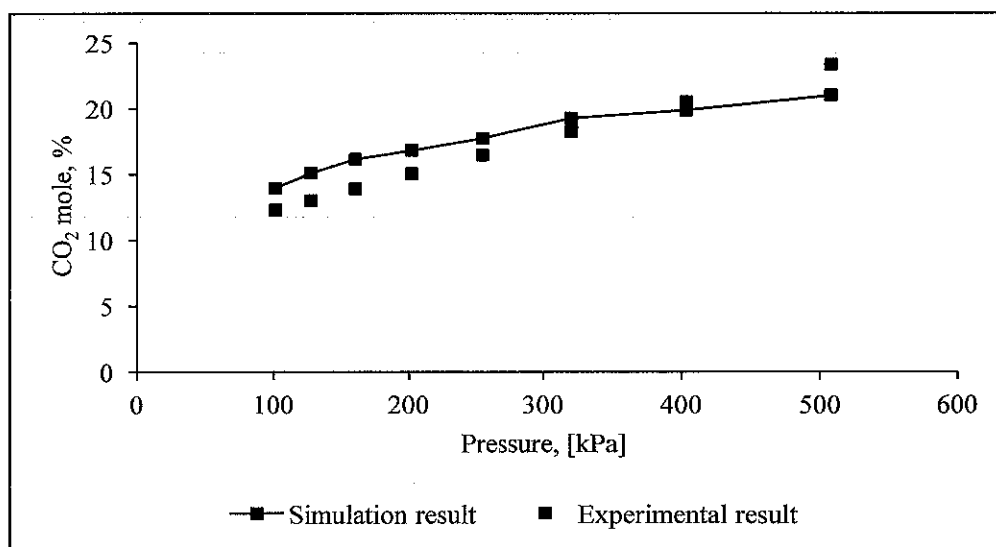


Fig. 5.3: Comparison between simulation and experimental results for p[VBTMA][NO₃] CO₂ sorption isotherms

From Fig. 5.4 we can visualize that the CO₂ molecules are located around both cation and anion, indicating that both cation and anion have an influence on CO₂ sorption capacity.

Based on these results, pILs with different cations (*i.e.* different substituent length, backbone) and different anions (see Table 4.2-Table 4.5) will be synthesized and their sorption capacity will be measured.

Varying the backbone and the substituent length will result in different ion conductivity of the cation. The selected anions are having different ion conductivity values, and these include organic and inorganic anions.

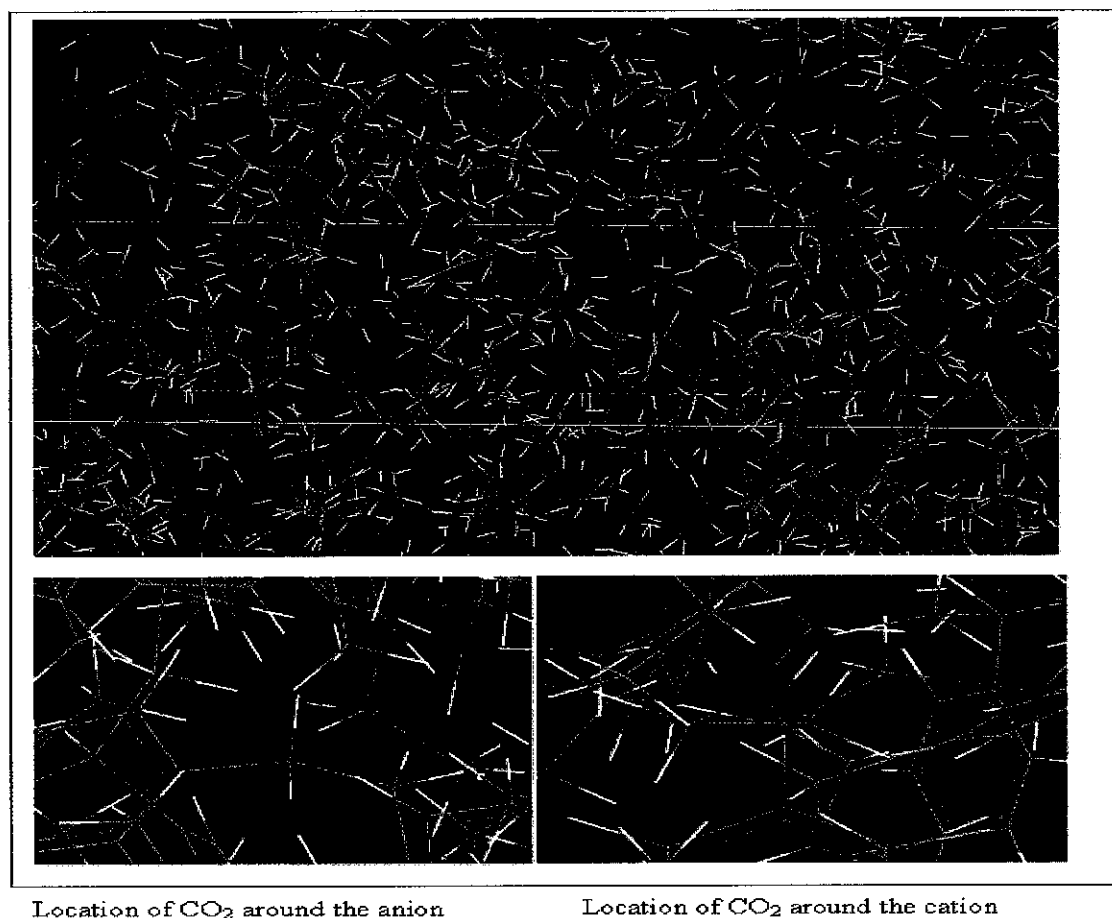


Fig. 5.4: Simulation results for CO₂ (red dots) sorption on p[VBTEA][NO₃] showing the location of CO₂

5.2 Characterization of pILs

The characterization of the twelve synthesized new pILs includes structure analysis and chloride content to ensure the purity of the synthesized pILs, topology analysis to study the surface morphology and structure (*i.e.* crystallinity) of the synthesized pILs, density, and thermal stability to specify the decomposition temperature of the pILs.

5.2.1 Structure Analysis

To check the structure of the synthesized polymers ^1H NMR and CHNS are used. The NMR and CHNS results are as follows:

5.2.1.1 Triethylammonium Based pILs

p[VBTEA][Cl]: ^1H NMR (DMSO- d_6 , 400MHz, ppm) 9.05 (br, 2H), 8.25 (br, 2H), 7.12 (br, 2H), 3.09 (br, 6H), 2.33 (br, 1H), 2.08 (br, 2H), 1.20 (br, 9H). Calculated elemental analysis for $(\text{C}_{15}\text{H}_{24}\text{Cl N})_n$: C, 70.92; H, 9.46; N, 5.52; S, 0. Found: : C, 70.85; H, 10.18; N, 4.72; S, 0.04 .

p[VBTEA][NO₃]: ^1H NMR (DMSO- d_6 , 400MHz, ppm) 8.99 (br, 2H), 7.58 (br, 2H), 6.51-6.99 (br, 2H), 4.46-5.85 (br, 6H), 2.93 (br, 1H), 0.99- 2.46 (br, 11H). Calculated elemental analysis for $(\text{C}_{15}\text{H}_{24}\text{N}_2\text{O}_3)_n$: C, 63.74; H, 8.5; N, 9.92; S, 0. Found: C, 63.21; H, 9.19; N, 9.98; S, 0.06.

p[VBTEA][CH₃COO]: ^1H NMR (DMSO- d_6 , 400MHz, ppm) 9.51 (br, 2H), 7.77 (br, 2H), 6.13 (br, 2H), 3.44 (br, 6H), 1.25 (br, 15H). Calculated elemental analysis for $(\text{C}_{17}\text{H}_{27}\text{NO}_2)_n$: C, 73.54; H, 9.73; N, 5.05; S, 0. Found: C, 72.65; H10.76; N, 5.86; S, 0.02.

p[VBTEA][CH₃O₄S]: ^1H NMR (DMSO- d_6 , 400MHz, ppm) 7.28 (br, 2H), 6.54(br, 2H), 4.81 (br, 1H), 4.42 (br, 3H), 3.21 (br, 6H), 1.56- 2.42 (br, 2H), 1.23 (br, 9H).).

Calculated elemental analysis for $(C_{16}H_{27}NO_4S)_n$: C 58.28; H, 8.20; N, 4.25; S, 9.71.
Found: C, 57.83; H, 9.16; N, 4.60; S, 9.58.

5.2.1.2 *Trimethylammonium Based pILs*

p[VBTMA][Cl]: $^1\text{HNMR}$ (DMSO- d_6 , 400MHz, ppm) 7.37 (br, 2H), 6.56 (br, 2H), 4.93 (br, 2H), 3.20 (t, 9H), 3.09 (s, 1H), 1.60 (br, 2H). Calculated elemental analysis for $(C_{12}H_{18}ClN)_n$: C 68.01; H, 8.50; N, 6.61; S, 0. Found: C, 67.41; H, 8.99; N, 6.06; S, 0.04.

p[VBTMA][NO₃]: $^1\text{HNMR}$ (DMSO- d_6 , 400MHz, ppm) 7.20 (br, 2H), 6.53 (br, 2H), 4.55 (br, 2H), 3.05 (br, 9H), 2.81 (br, 1H), 1.54 (br, 2H). Calculated elemental analysis for $(C_{12}H_{18}N_2O_3)_n$: C 60.43; H, 7.55; N, 11.75; S, 0. Found: C, 60.07; H, 7.96; N, 12.39; S, 0.02.

p[VBTMA][TFMS]: $^1\text{HNMR}$ (DMSO- d_6 , 400MHz, ppm) 7.13 (br, 2H), 6.54 (br, 2H), 4.37 (br, 2H), 3.04 (br, 9H), 2.94 (br, 1H), 1.47 (br, 2H). Calculated elemental analysis for $(C_{13}H_{18}F_3NO_3S)_n$: C 47.94; H, 5.53; N, 4.30; S, 9.83. Found: C, 47.45; H, 5.92; N, 4.70; S, 10.45.

5.2.1.3 *Methacryloyloxy Ethyl Trimethylammonium Based pILs*

p[METMA][Cl]: $^1\text{HNMR}$ (DMSO- d_6 , 400MHz, ppm) 4.44 (br, 2H), 3.92(br, 2H), 3.38-3.61 (br, 9H), 3.28 (br, 1H), 0.86-2.13 (br, 2H). Calculated elemental analysis for $(C_9H_{18}ClNO_2)_n$: C 51.75; H, 8.62; N, 6.71; S, 0. Found: C, 51.15; H, 9.87; N, 6.96; S, 0.01.

p[METMA][NO₃]: $^1\text{HNMR}$ (DMSO- d_6 , 400MHz, ppm) 4.45 (br, 2H), 3.98(br, 2H), 3.36 (br, 9H), 3.14 (br, 1H), 0.88-1.21 (br, 2H).). Calculated elemental analysis for $(C_9H_{18}N_2O_5)_n$: C 46.09; H, 7.68; N, 11.95; S, 0. Found: C, 47.11; H, 8.55; N, 11.23; S,0.06.

5.2.1.4 Tris Dimethylamino Phosphine Based pILs

p[bDMADMVBP][Cl]: ^1H NMR (DMSO- d_6 , 400MHz, ppm) 7.99 - 8.64 (br, 4H), 7.51(br, 2H), 5.94 (br, 2H), 4.82-5.3 (br, 6H), 4.19-4.80 (br, 12H), 2.77 (br, 1H). Calculated elemental analysis for $(\text{C}_{15}\text{H}_{27}\text{ClN}_3\text{P})_n$: C, 57.00; H, 8.55; N, 13.30; S 0. Found: C, 55.92; H, 9.41; N, 11.95; S, 0.05.

p[bDMADMVBP][NO $_3$]: ^1H NMR (DMSO- d_6 , 400MHz, ppm) 7.8 - 9.6 (br, 2H), 7.25-7.8 (br, 2H), 6.4-7.2(br, 2H), 5.2-6.2 (br, 2H), 3.6-5.8 (br, 6H), 3.0-3.65 (br, 12H), 2.59 (br, 1H). Calculated elemental analysis for $(\text{C}_{15}\text{H}_{27}\text{N}_4\text{O}_3\text{P})_n$: C 52.57; H, 7.89; N, 16.36; S, 0. Found: C, 52.50; H, 8.58; N, 15.95; S, 0.01.

p[tDMAVBP][Cl]: ^1H NMR (DMSO- d_6 , 400MHz, ppm) 7.54 - 8.59 (br, 2H), 6.21-7.35(br, 2H), 5.19-5.94 (br, 2H), 3.28-4.75 (br, 18H), 2.77 (br, 1H) , 1.05-2.21 (br, 2H). Calculated elemental analysis for $(\text{C}_{15}\text{H}_{27}\text{ClN}_3\text{P})_n$: C 57.00; H, 8.55; N, 13.30; S, 0. Found: C, 55.71; H, 9.48; N, 12.98; S, 0.01.

For NMR spectrum of these polymers and their monomers refer to appendix A.

5.2.2 Topology Analysis

The SEM micrographs for the pILs (see Fig. 5.5 and appendix B) showed a non-porous structures for all synthesized pILs except for p[METMA][Cl], p[METMA][NO $_3$], and p[tDMAVBP][Cl]. If the topology structure by means of surface area of pILs plays the major role in CO $_2$ sorption capacity, then these three pILs will give the highest CO $_2$ sorption rate and capacity as their surface area to host the CO $_2$ is higher compared to others.

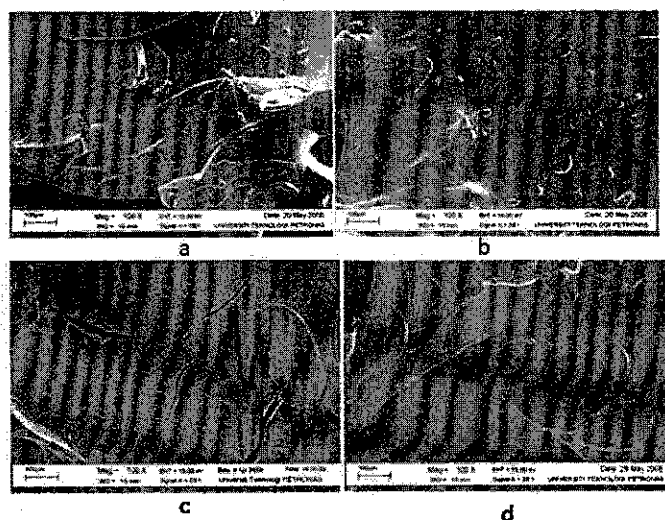


Fig. 5.5: SEM micrograph for (a) p[VBTEA][Cl], (b) p[VBTEA][NO₃], (c) p[METMA][Cl], and (d) p[METMA][NO₃]

The XRD patterns for pILs and their correspondent's monomers (see Fig. 5.6) showed crystalline peaks for the monomers while there are no crystalline peaks in polymers spectrums. This indicates that by polymerization, an amorphous structure can be achieved.

The DSC curves for pILs with different anions types are shown in Fig. 5.7. The anion type strongly affected the glass transition temperature T_g of the polymer. It can be realized that the polymers with inorganic anion [NO₃] has a higher T_g than those of organic and [Cl] anions.

The glass transition temperatures for the polymers with a fixed cation and backbone p[VBTEA] but different anions are as follows: p[VBTEA][CH₃O₄S] (-36 °C) < p[VBTEA][Cl] (13 °C) < p[VBTEA][CH₃COO] (44 °C) < p[VBTEA][NO₃] (105 °C). The organic anions [CH₃O₄S] and [CH₃COO] and anion [Cl] can tremendously reduce the T_g value due to plasticization effect by the anions [147, 148]. Plasticizers increase the amorphous nature of the polymers and reduce the crystallinity of the polymer. This reduction in T_g value helps in increasing the chain flexibility of the polymer. The increment in chain flexibility is a measure of the chain ability to rotate around the chain bond [216].

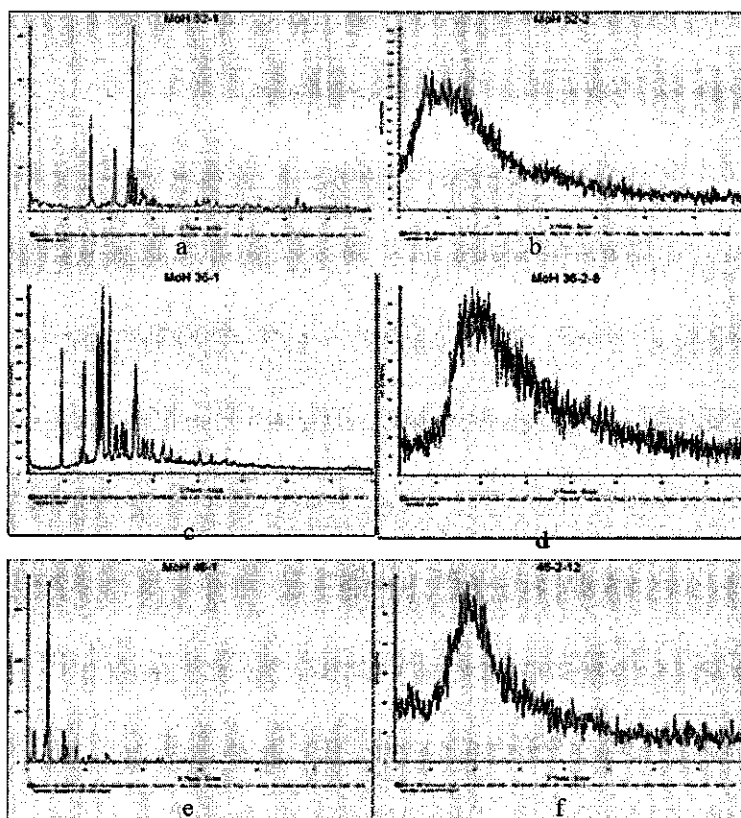


Fig. 5.6: XRD patterns of (a) [METMA][Cl], (b) p[METMA][Cl], (c) [VBTEA][NO₃], (d) p[VBTEA][NO₃], (e) p[VBTMA][NO₃], (f) p[VBTMA][NO₃],

Studying the effect of length of the substituent alkyl group chain on the T_g of the polymers showed the T_g of the polymer decreases with increasing length of the alkyl chain attached to cation as shown in Fig. 5.8. The order of the T_g for these polymers are as follows: p[VBTEA][Cl] (13 °C) < p[VBTMA][Cl] (150 °C) and p[VBTEA][NO₃] (105 °C) < p[VBTMA][NO₃] (167 °C). Fig. 5.9 shows also the DSC curves for pILs with different backbones (polystyrene and methacryloyloxy ethyl backbones). The order of the T_g are as follow: p[METMA][Cl] (80 °C) < p[VBTMA][Cl] (150 °C) and p[METMA][NO₃] (115 °C) < p[VBTMA][NO₃] (167 °C). Poly ionic liquids with polystyrene backbones have higher T_g compare to those with methacryloyloxy ethyl backbones.

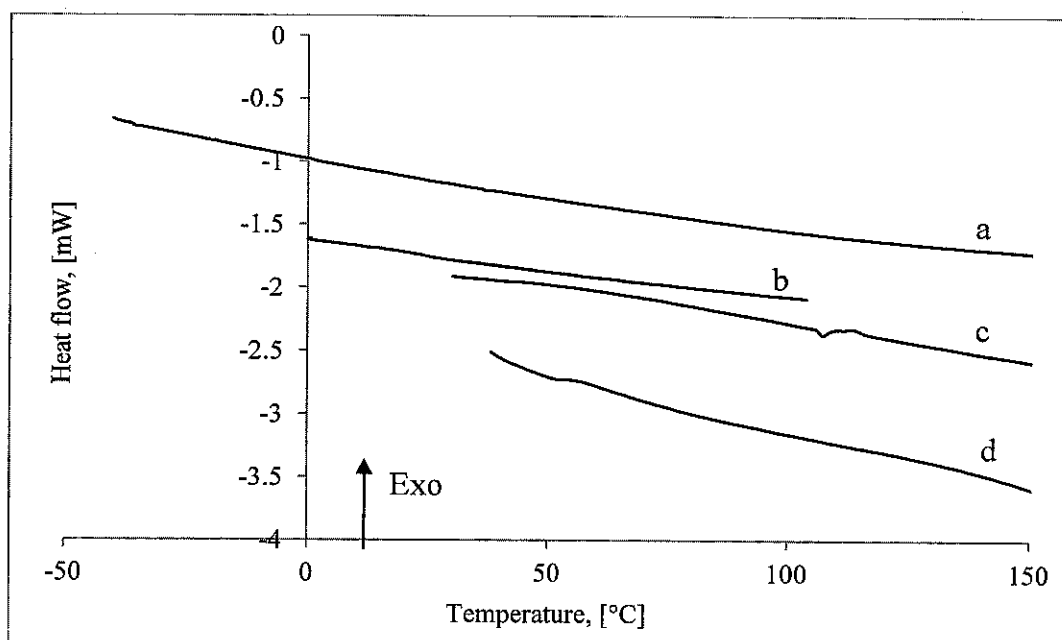


Fig. 5.7: DSC curves for pILs with different anions: (a), p[VBTEA][CH₃O₄S] (b) p[VBTEA][Cl], (c) p[VBTEA][NO₃], (d) p[VBTEA][CH₃COO]

We can conclude that both the cation (substituent and backbone) and the anion of pILs affect their glass transition temperature T_g . These T_g results give a good indication of the degree of amorphous nature of the polymer and further the surface area of the polymer. Overall, it can be concluded that the lower the T_g value the higher surface area of the polymer due to amorphous structure increasing. These DSC results are also another indication that pILs are amorphous as there is no melting or crystalline peak appearing in the plot.

In their suggestion for the mechanism of CO₂ sorption on pILs, Tang *et al.* [159] reported that the plasticization which reduces the T_g leads to decrement in microvoid fraction of the pILs resulting in a very low CO₂ sorption capacity. If this is the case then the pILs with [Cl] anion should give lower sorption capacity than those with [NO₃] anions as we have seen from the T_g results but this is not the cause (see section 5.3.3).

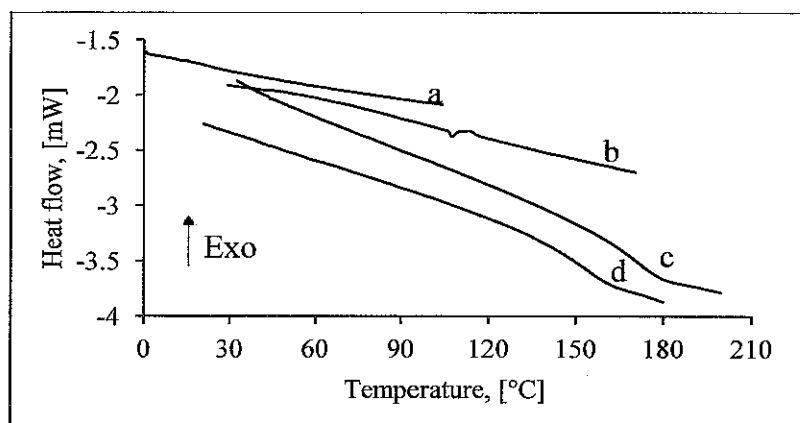


Fig. 5.8: DSC curves for pILs with different substituent length : (a), p[VBTEA][Cl] (b) p[VBTEA][NO₃], (c) p[VBTMA][NO₃], (d) p[VBTMA][Cl]

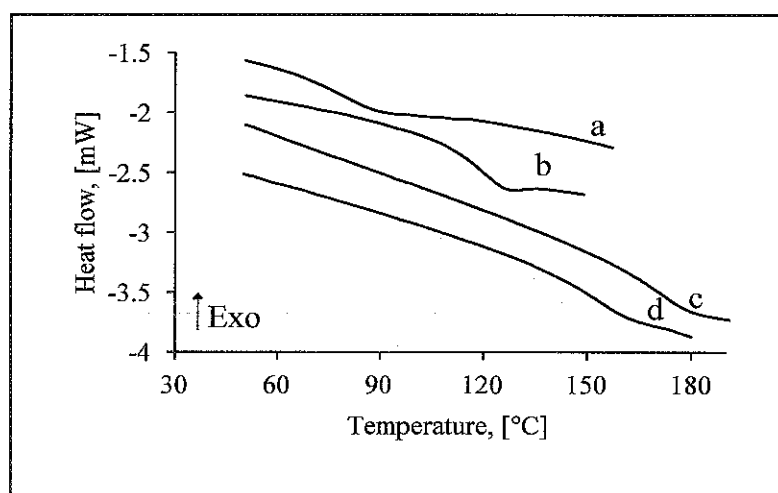


Fig. 5.9: DSC curves for pILs with different backbones : (a), p[METMA][Cl] (b) p[METMA][NO₃], (c) p[VBTMA][NO₃], (d) p[VBTMA][Cl]

5.2.3 Chloride content

The values of measured chloride content for the non-halogenated pILs are listed in Table 5.3. There are found to contain < 10 ppm residual halide showing the high purity of synthesized pILs. This concentration of chloride is sufficiently low for applications and should not have any effect on the physical properties of these poly ionic liquids.

Table 5.3: Chloride content for non-halogenated pILs.

Polymer	Chloride content [ppm]	Polymer	Chloride content [ppm]
p[VBTEA][NO ₃]	4.99	p[VBTEA][NO ₃]	4.23
p[VBTEA][CH ₃ COO]	4.56	p[METMA][NO ₃]	7.96
p[VBTEA][CH ₃ O ₄ S]	4.20	p[bDMADMVBP][NO ₃]	2.39

5.2.4 Density

The densities of some pILs and their corresponding monomers are measured to check the effect of polymerization on density. As shown in Fig. 5.10 by polymerizing the monomer a reduction in density occurs showing that the structure of monomers changes from a crystalline structure to an amorphous structure when polymerized leading to an increment in the surface area.

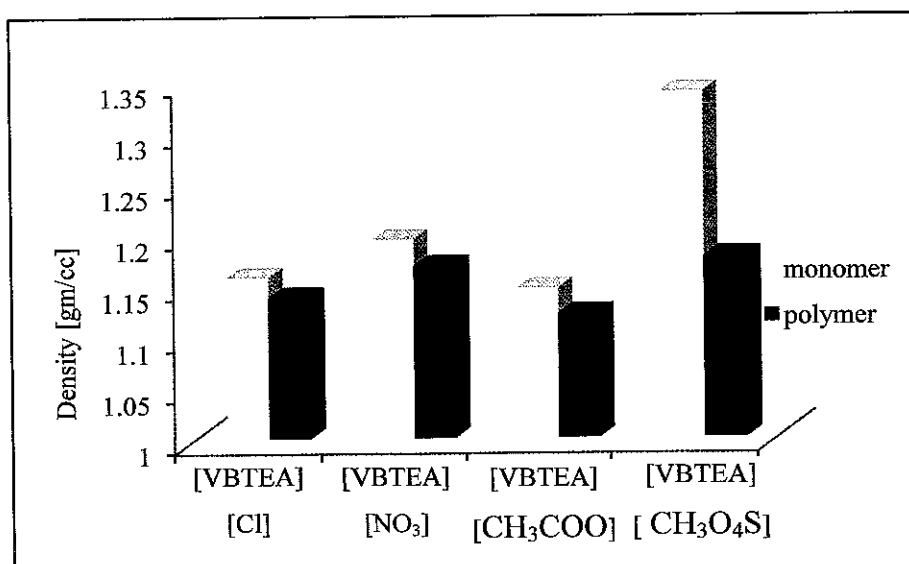


Fig. 5.10: Densities of pILs and their corresponding monomers

The densities of synthesized pILs are listed in Table 5.4.

Table 5.4: Densities of synthesized pILs.

Polymer	Density [gm/cc]	Polymer	Density [gm/cc]
p[VBTEA][Cl]	1.1375±0.0005	p[VBTMA][F ₃ C-SO ₃]	1.4062 ± 0.0019
p[VBTEA][NO ₃]	1.1681±0.0003	p[METMA][Cl]	1.2133±0.0006
p[VBTEA] [CH ₃ COO]	1.1214±0.0003	p[METMA][NO ₃]	1.2335±0.0004
p[VBTEA] [CH ₃ O ₄ S]	1.1766±0.0013	p[bDMADMVBP][Cl]	1.2094±0.0005
p[VBTMA][Cl]	1.1057±0.0002	p[bDMADMVBP][NO ₃]	1.2629±0.0010
p[VBTMA][NO ₃]	1.1805±0.0005	p[tDMAVBP][Cl]	1.4677±0.0008

5.2.5 Thermal Stability

In order to evaluate the effect of structure of pILs on their thermal stability, TGA curves for pILs with fixed cation ([VBTEA]) and different anions ([Cl], [NO₃], [CH₃COO], and [CH₃O₄S]) and with fixed anions ([Cl] and [NO₃]) and different cations (in term of backbone and alkyl chain length) are generated.

Looking at the effect of cation type on thermal stability of pILs showed the following order for 10% decomposition [VBTEA] < [METMA] < [VBTMA] < [tDMAVBP] < [bDMADMVBP] as seen in Fig. 5.11 and Fig. 5.12.

The [VBTMA] cation is more thermally stable than [VBTEA] as the ethyl substituent is more likely to leave than the methyl chain in [VBTEA] due to its movement

flexibility when subjected to heat. Thermal decomposition temperature of pILs decreases when the length of alkyl chain attached to the cation increases.

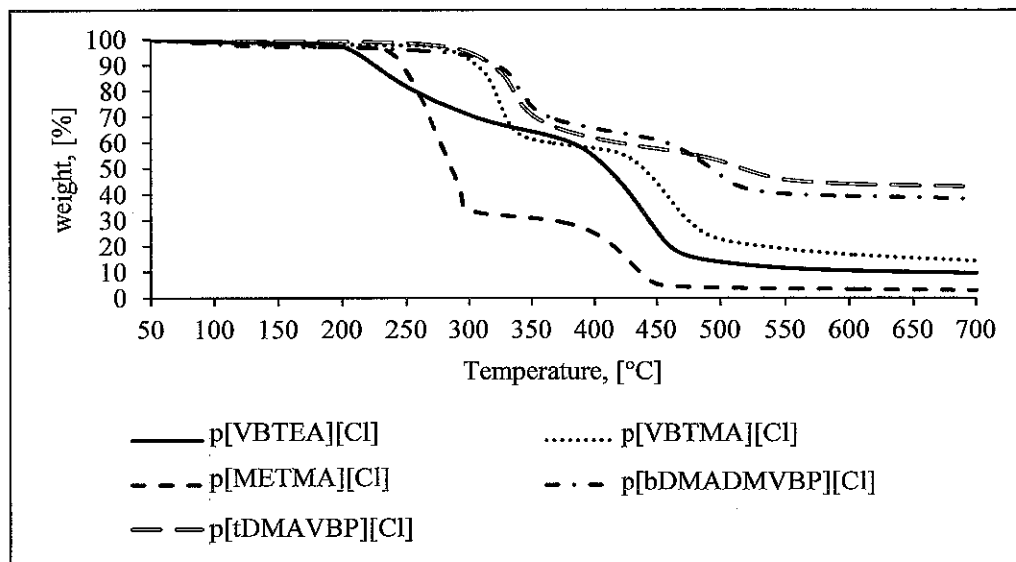


Fig. 5.11: Plot of thermal decomposition for pILs with different cations and fixed [Cl] anion

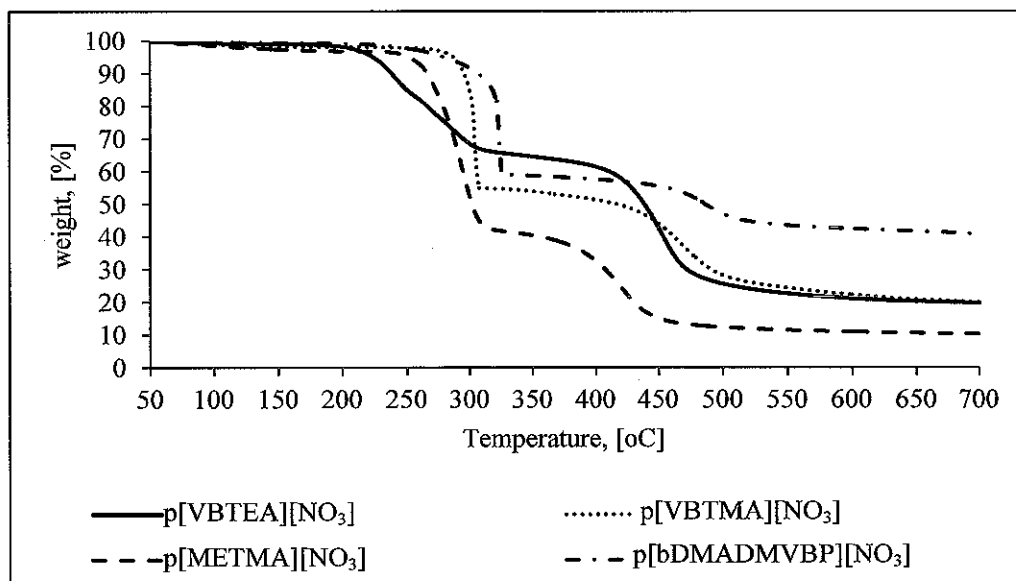


Fig. 5.12: Plot of thermal decomposition for pILs with different cations and fixed [NO₃] anion

Poly ionic liquids with polystyrene backbones have higher thermal stability temperatures compared to those with methacryloyloxy ethyl backbones as the polystyrene backbone is more rigid than the methacryloyloxy ethyl backbone.

As shown in Fig. 5.13, the anion type also affects the thermal decomposition temperature. The order of anions for 10% decomposition for [VBTEA] based pILs is as follows: $[\text{CH}_3\text{COO}] < [\text{Cl}] < [\text{NO}_3] < [\text{CH}_3\text{O}_4\text{S}]$. It can be observed that the acetate anion provide more stability to the polymer because it is relatively a strong ligand in coordination chemistry. For other anions it can be realized that the anion size affects the stability of the polymer as the longer the anion size the more tendency it has towards decomposition. Therefore, the thermal decomposition temperature of pILs is affected by cation type, length of substituent, backbone type, and anion. For comparison purposes, the temperature of 10% decomposition is also listed in Table 5.5.

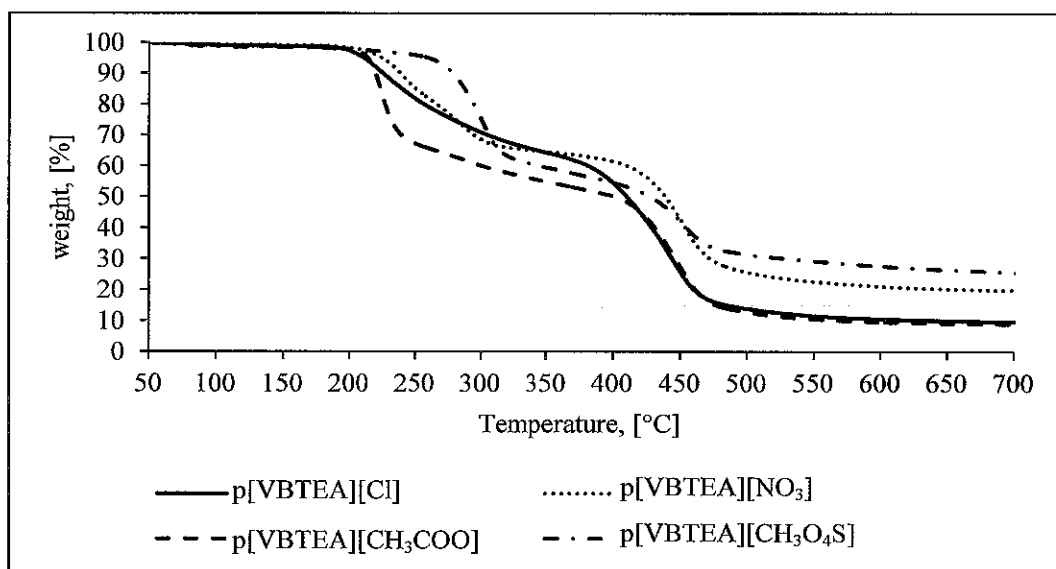


Fig. 5.13: Plot of thermal decomposition for pILs with fixed [VBTEA] cation and different anions

Table 5.5: Temperature of 10% thermal decomposition for different pILs.

Polymer	T, [°C]	Polymer	T, [°C]
p[VBTEA][Cl]	225	p[METMA][Cl]	242
p[VBTEA][NO ₃]	238	p[METMA][NO ₃]	265
p[VBTEA][CH ₃ COO]	219	p[bDMADMVBP][Cl]	321
p[VBTEA][CH ₃ O ₄ S]	278	p[bDMADMVBP][NO ₃]	305
p[VBTMA][Cl]	306	p[tDMAVBP][Cl]	318
p[VBTMA][NO ₃]	295		

5.3 Sorption of Carbon Dioxide

Carbon dioxide sorption of the poly ionic liquids is measured with standard methods, based on the following effects: polymerization, cation, anion, temperature, density reduction and water content. The selectivity and molecular interaction of different gases with the pILs, and the recyclability of pILs are also studied. Experimental results are recorded and will be described in details herein below. Tables of all the sorption data can be found in Appendix C.

5.3.1 Effect of Polymerization

Sorption of CO₂ by [VBTMA][Cl] monomer and its polymer p[VBTMA][Cl] are measured at 10 bar and 25°C using the Magnetic Suspension Balance. The experimental results are as plotted in Fig. 5.14. Now referring to Fig. 5.14, it can be concluded that the polymerization increases sorption capacity by 207%, while the amount of time required reaching the equilibrium remains almost the same (around

only 15 minutes). This is understandable due to the difference in their nature as the polymer is an amorphous material, whereas the monomer is in a crystalline form.

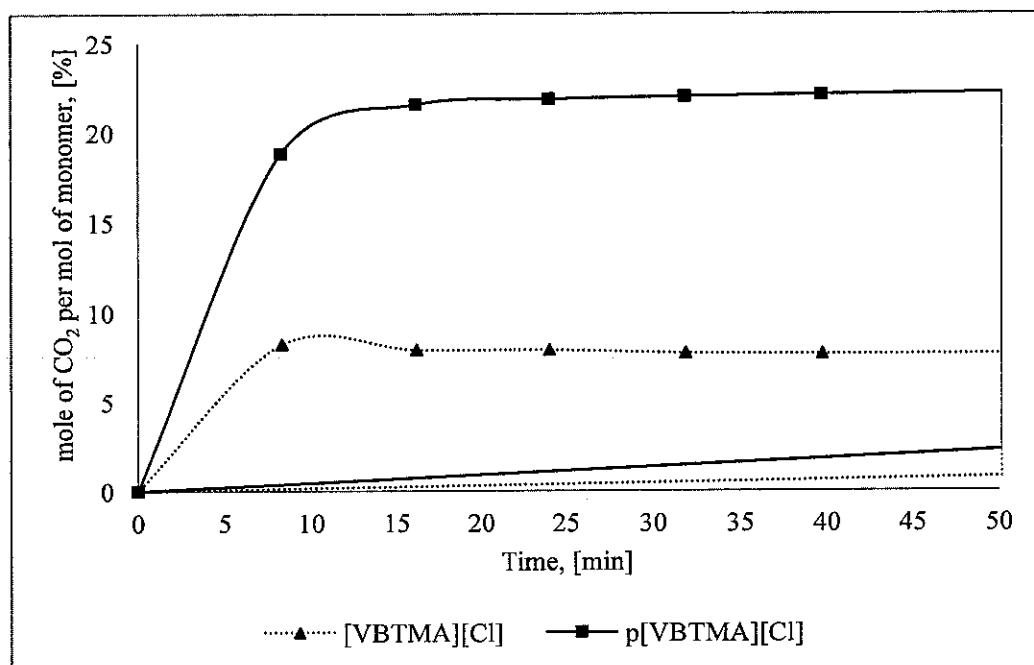


Fig. 5.14: CO₂ sorption rate for p[VBTMA][Cl] and its monomer at 10 bar and 25°C

The polymerization procedure for p[VBTEA][NO₃] is carried out at two different polymerization times, 6 and 12 hours resulting in two different molecular weight 11,518 and 21,531, respectively.

The sorption of CO₂ for p[VBTEA][Cl] Mw = 11,518, and p[VBTEA][Cl] Mw = 21,531, is measured at 10 bar and 25°C using the Magnetic Suspension Balance as shown in Fig. 5.15.

Nevertheless, it is observed that even though the molecular weight is close to doubled, the sorption capacity and rate remained the same.

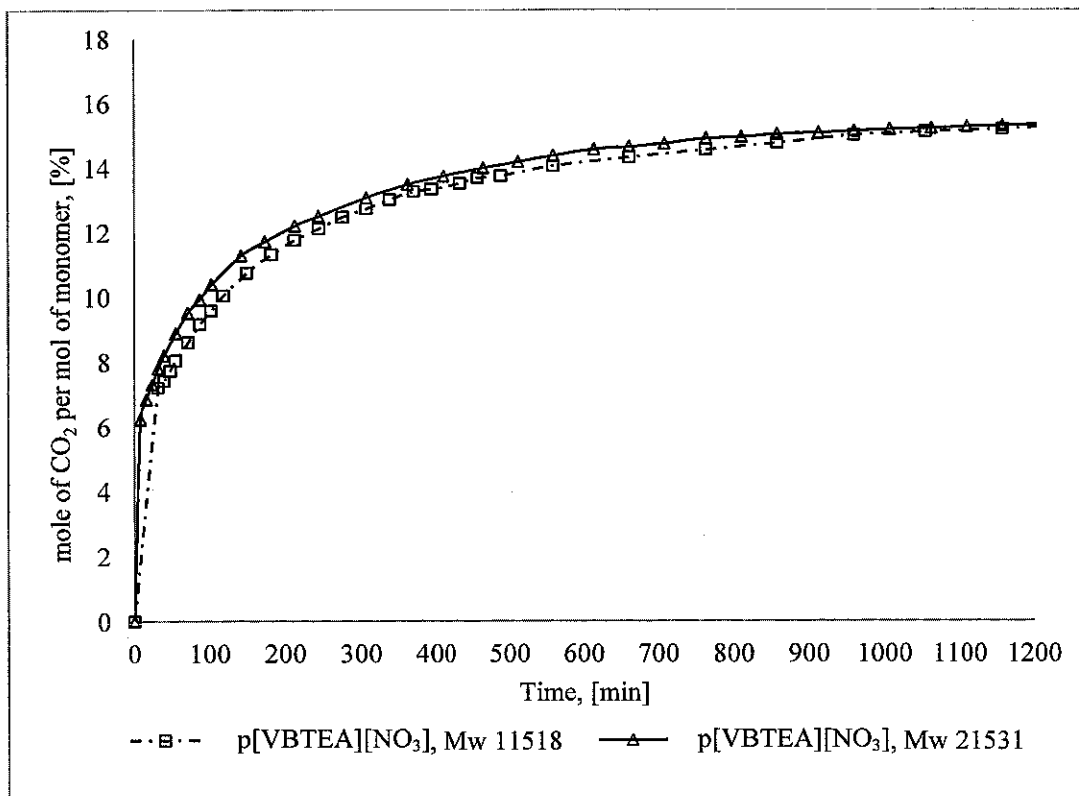


Fig. 5.15: Effect of molecular weight on CO₂ sorption rate and capacity at 10 bar and 25°C.

5.3.2 Effect of Cation

To study the effect of cation on CO₂ sorption rate and capacity, the sorption of pILs with fixed anions (*i.e.* [Cl] and [NO₃]) and different cations type in term of cation, backbone, and length of alkyl chain attached to the cation is measured at 10 bar and 25°C. The cations are [VBTEA], [VBTMA], [METMA], [bDMADMVBP] and [tDMAVBP]. The results are shown in Fig. 5.16 and Fig. 5.17.

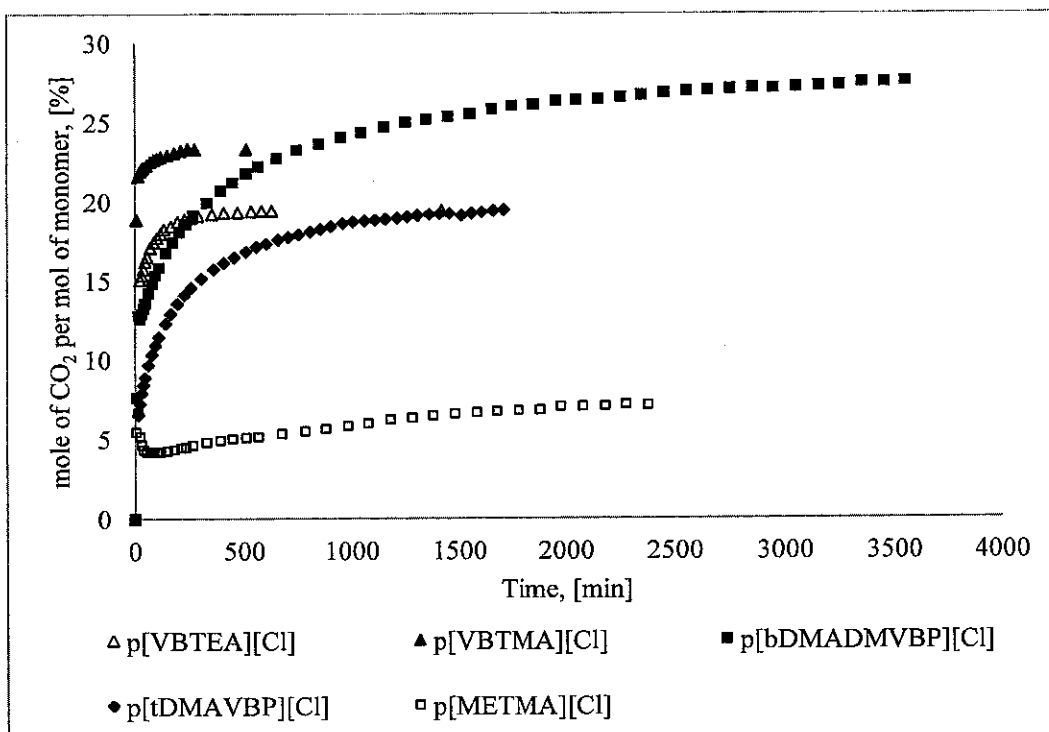


Fig. 5.16: CO₂ sorption rate for different cations with [Cl] anion at 10 bar and 25°C

At equilibrium, p[METMA][Cl] took up 7.1 mole% < p[tDMAVBP][Cl] 19.2 mole% < p[VBTEA][Cl] 19.4 mole% < p[VBTMA][Cl] 23.27 mole% < p[bDMADMVBP][Cl] 27.54 mole% in terms of their monomer units. It can be realized that the time required to reach equilibrium is faster for p[VBTMA][Cl], p[VBTEA][Cl], and p[METMA][Cl] compared to p[tDMAVBP][Cl], and p[bDMADMVBP][Cl] and this can be explained by the fact that the structure of the later polymers is more complex around the central cation Nitrogen atom (see Table 4.2-Table 4.5) leading to hard accessibility to the cation charge site than the earlier polymers.

For pILs with [NO₃] anion, cation type shows a significant effect on sorption rate and capacity as well. The order is found to be p[VBTMA][NO₃] 21.5 mole% > p[VBTEA][NO₃] 15.4 mole% > p[bDMADMVBP][NO₃] 12.9 mole% > p[METMA][NO₃] 7 mole% .

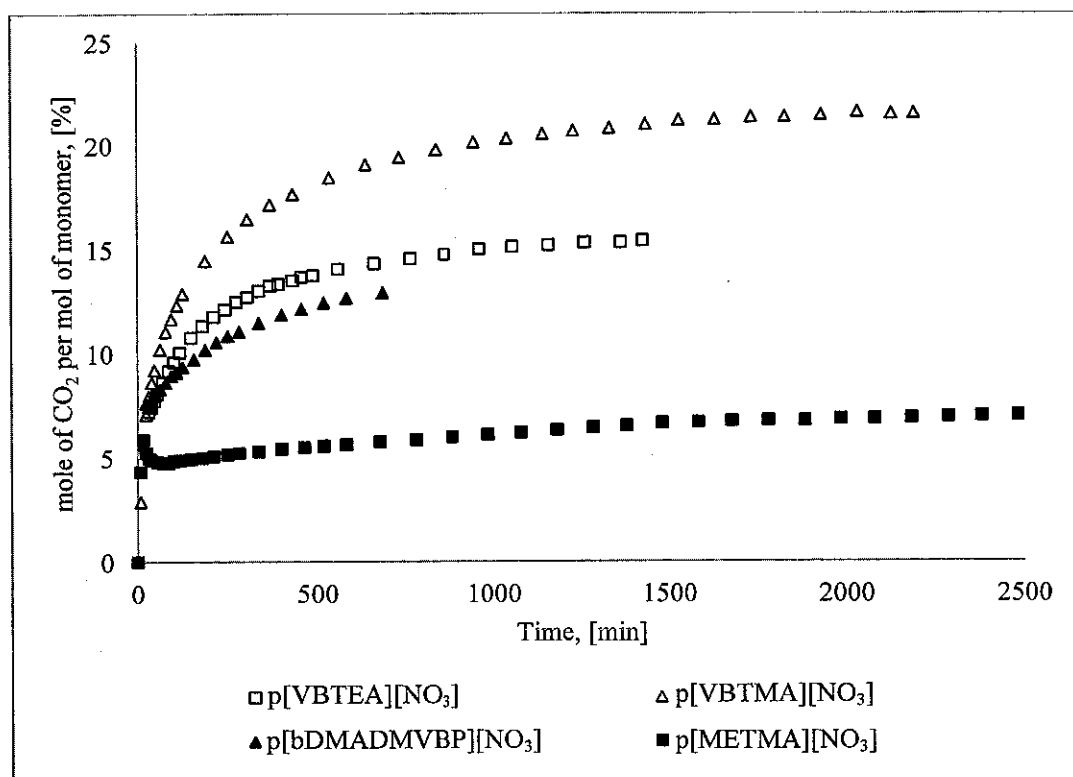


Fig. 5.17: CO₂ sorption rate for different cations with [NO₃] anion at 10 bar and 25°C

It was found that the order for sorption rate and capacity is not the same as in pILs with [Cl] anions. p[bDMADMVBP][NO₃] showed a lower capacity than expected. It is clear that the size of the anion [NO₃] which is bigger than [Cl] affects the result by blocking the CO₂ from accessing the central charged cation atom surrounding by more complex structure of atoms. This results in reduction of cation contribution in sorption capacity. As proposed earlier in our theory to explain the CO₂ sorption mechanism, the overall ion conductivity of cation will affect the sorption capacity. For a higher cation ion conductivity a higher sorption capacity can be expected. The ion conductivity for some cations and anions is listed in Table 5.6.

Usually an ethyl substituent group will weaken the positive charge of the cation central atom more than a methyl substituent group leading to less ion conductivity as can be concluded from Table 5.6. This explains the highest sorption rate of p[VBTMA][Cl] and p[VBTMA][NO₃] over p[VBTEA][Cl] and p[VBTEA][NO₃], respectively.

p[tDMAVBVP][Cl] showed lower sorption capacity than p[bDMADMVBVP][Cl] as the central cation atom in p[bDMADMVBVP][Cl] is N atom (electronegativity = 3.04 [217]) which is more electron acceptor (for structure see Table 4.5) that produce higher ion conductivity than P atom (electronegativity = 2.19 [217]) in p[tDMAVBVP][Cl].

Table 5.6: Ion conductivity for some cations and anions at 25°C [217]

Cation	$\lambda, 10^{-4}$ [m ² S mole ⁻¹]	Anion	$\lambda, 10^{-4}$ [m ² S mole ⁻¹]
H ⁺	349.65	OH ⁻	198
Benzyltrimethylammonium ⁺	34.6	I ⁻	76.8
Isobutylammonium ⁺	48	Cl ⁻	76.3
Butyltrimethylammonium ⁺	33.6	NO ₃ ⁻	71.42
Diethylammonium ⁺	42.0	PF ₆ ⁻	56.9
Dimethylammonium ⁺	51.8	F ⁻	55.4
Tetraethylammonium ⁺	32.6	Methylsulfate ⁻	48.8
Tetramethylammonium ⁺	44.9	Acetate ⁻	40.9

p[bDMADMVBVP][Cl] reported the highest sorption capacity but it takes a longer time than p[VBTMA][Cl] to reach equilibrium. The delay in reaching equilibrium can be explained by the difficulty in accessing the cation positive charge due to the complex molecular structure surrounding the central charged atom. In p[bDMADMVBVP][Cl], the fourth group connected to the central atom is atom P (for structure see Table 4.5) while CH₃ which is a more electron donor is connected to p[VBTMA][Cl] leading to higher ion conductivity for p[bDMADMVBVP][Cl] cation.

The sorption of CO₂ for p[VBTMA][Cl], p[METMA][Cl], p[VBTMA][NO₃], p[METMA][NO₃], is measured at 10 bar and 25°C using the Magnetic Suspension

Balance as shown in Fig. 5.18. The difference between [VBTMA] and [METMA] is the structure of backbone as shown in Table 4.3 and Table 4.4. It can be concluded from Fig. 5.18 that, the poly ionic liquids with vinylbenzyl backbone enhances the sorption rate and capacity of CO₂ compared to Methacryloyloxy ethyl backbone poly ionic liquids.

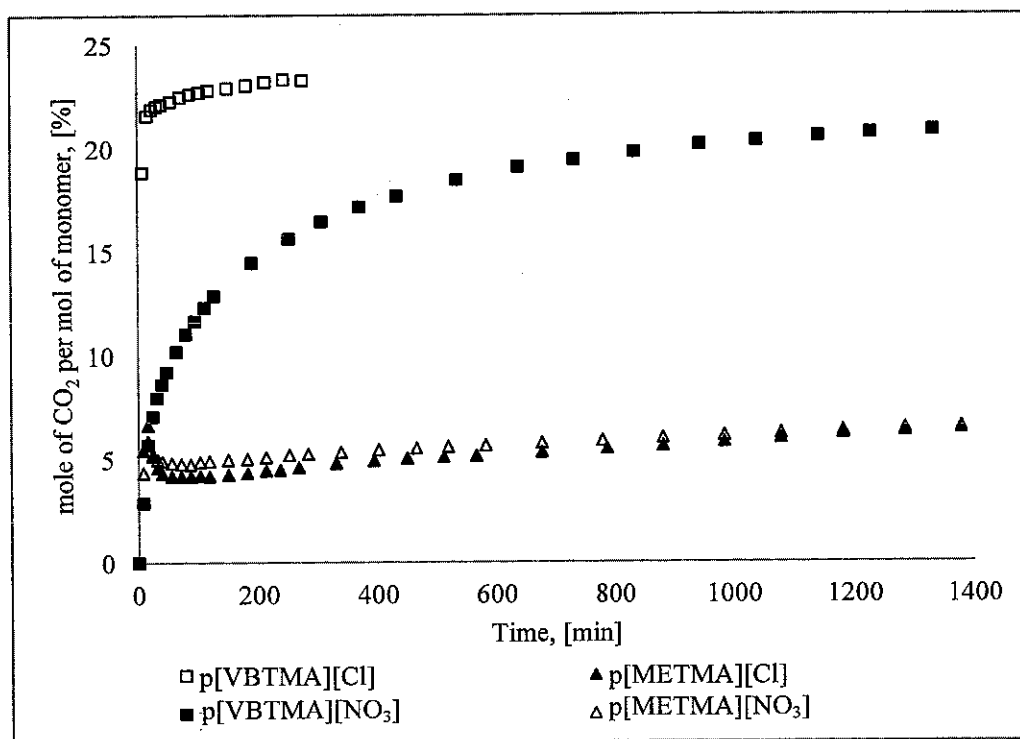


Fig. 5.18: Effect of backbone on sorption rate and capacity at 10 bar and 25°C

As the Methacryloyloxy ethyl backbone is an alkyl chain which is known to be an electron donating group than the aromatic ring in polystyrene backbone, this will reduce the positive charge of the cation producing cation with less ion conductivity and this leads to a reduction in CO₂ sorption capacity for poly ionic liquids with Methacryloyloxy ethyl backbone despite their porous structure (as reported by Tang *et al.* [147]). It can be also realized that the difference in sorption capacity between p[VBTMA][Cl] and p[VBTMA][NO₃] is significant compared to the difference between p[METMA][Cl] and p[METMA][NO₃]. This can be explained by the fact that the size of the anion will affect the sorption capacity of styrene backbone polymers more than the methacryloyloxy ethyl backbone due to the steric effect.

The CO₂ uptake for p[METMA][Cl] and p[METMA][NO₃] showed a high peak of sorption at the beginning before it equilibrated to a lower sorption value as shown in Fig. 5.19 . This can be explained by the fact that the CO₂ sorption released a heat as it is an exothermic process. This released heat results in releasing some of adsorbed CO₂ and it also lowers the low ion conductivity of [METMA] based pILs and enhancing the mobility of Methacryloyloxy ethyl electron donating group.

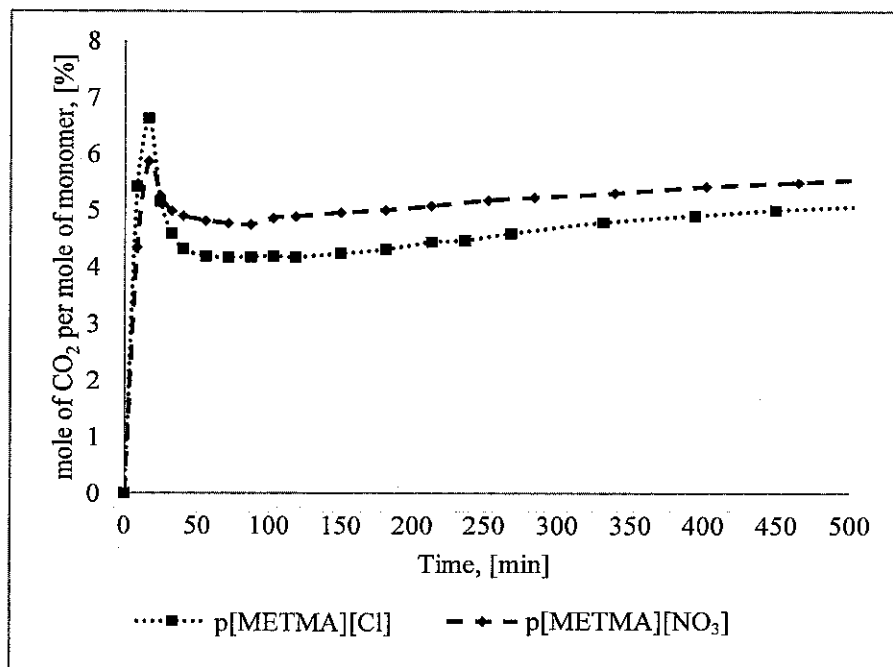


Fig. 5.19: CO₂ sorption rate for p[METMA][Cl] and p[METMA][NO₃] at 10 bar and 25°C

5.3.3 Effect of Anion

To study the effect of anion type on pILs CO₂ sorption rate and capacity, the sorption of CO₂ on p[VBTEA][Cl], p[VBTEA][NO₃], p[VBTEA][CH₃COO], and p[VBTEA][CH₃O₄S], are measured at 10 bar and 25°C using Magnetic suspension balance and the result is shown in Fig. 5.20.

Looking at the ion conductivity of these anions as tabulated in Table 5.6, the order follows: [Cl] 76.3 > [NO₃] 71.42 > [CH₃O₄S] 48.8 > [CH₃COO] 40.9. While the

sorption capacity follows the order of: p[VBTEA][Cl] 19.4 mole% > p[VBTEA][NO₃] 15.4 mole% > p[VBTEA][CH₃O₄S] 14.2 mole% > p[VBTEA][CH₃COO] 13.3 mole%. It is further observed that the pILs with chloride anions reaches equilibrium sorption capacities within a substantially reduced time period; more than 80% of their sorption capacities can be reached in around 30 minutes.

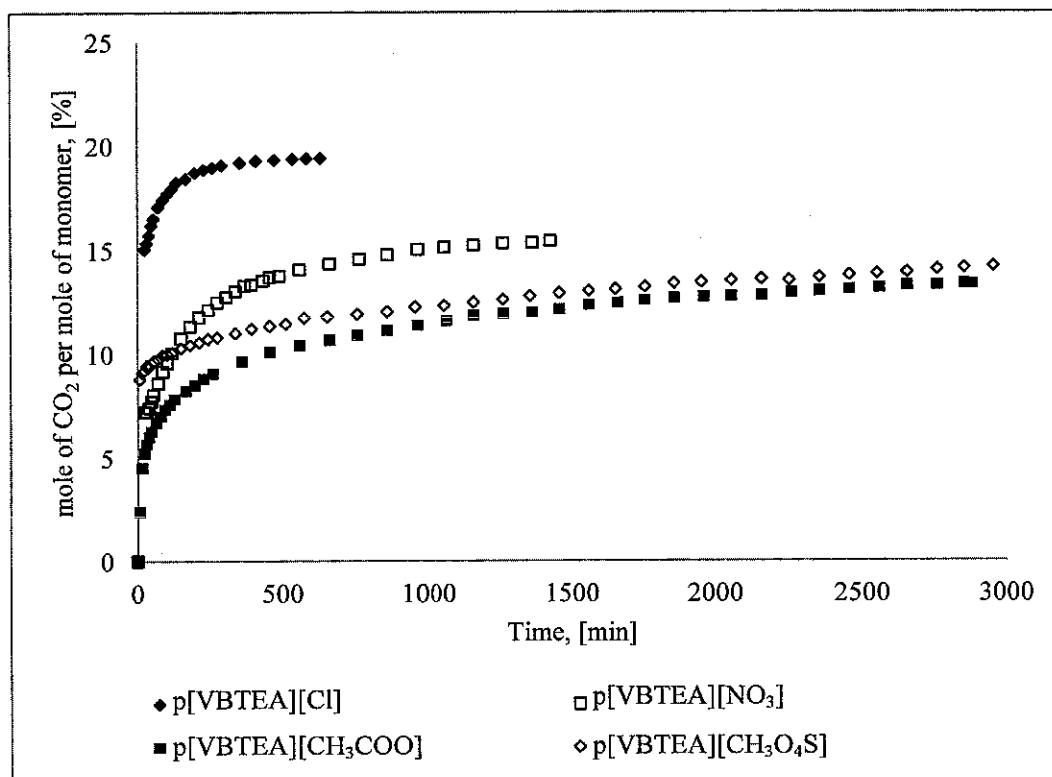


Fig. 5.20: CO₂ sorption rate for [VBTEA] cation with different anion types at 10 bar and 25°C

The sorption rate and capacity for p[VBTMA][Cl], p[VBTMA][NO₃], and p[VBTMA][F₃C-SO₃], at 10 bar and 25 °C are reported in Fig. 5.21.

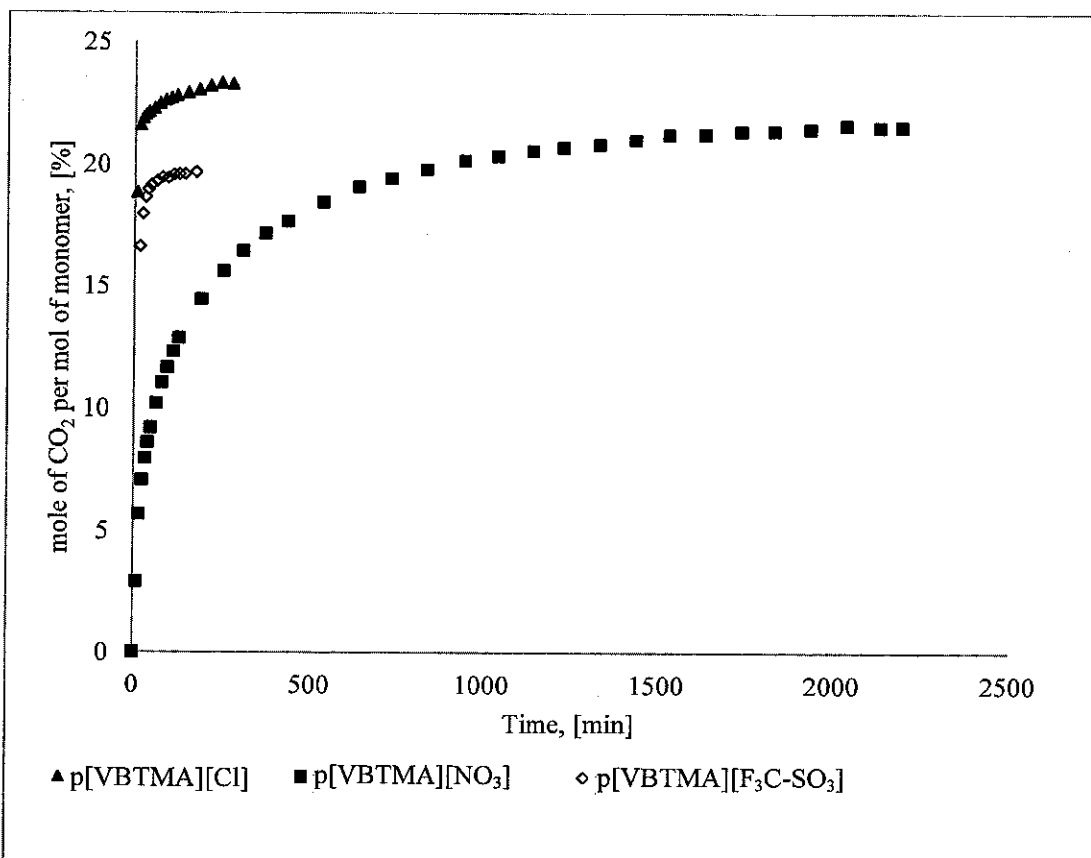


Fig. 5.21: CO₂ sorption rate for [VBTMA] cation with different anion types at 10 bar and 25°C

The sorption capacity order is as follow: p[VBTMA][Cl] 23.3 mole% > p[VBTMA][NO₃] 21.6 mole% > p[VBTMA][F₃C-SO₃] 19.7 mole%. This order follows the ion conductivity order as tabulated in Table 5.6, [Cl] > [NO₃].

It can be concluded that the anion with a smaller volume and a stronger negative charge (higher ion conductivity value) results in higher sorption capacity and faster sorption.

5.3.4 Sorption Isotherms

The sorption isotherms for p[VBTMA][NO₃] and p[VBTMA][F₃C-SO₃] are generated at different CO₂ pressures and 25 °C as shown in Fig. 5.22.

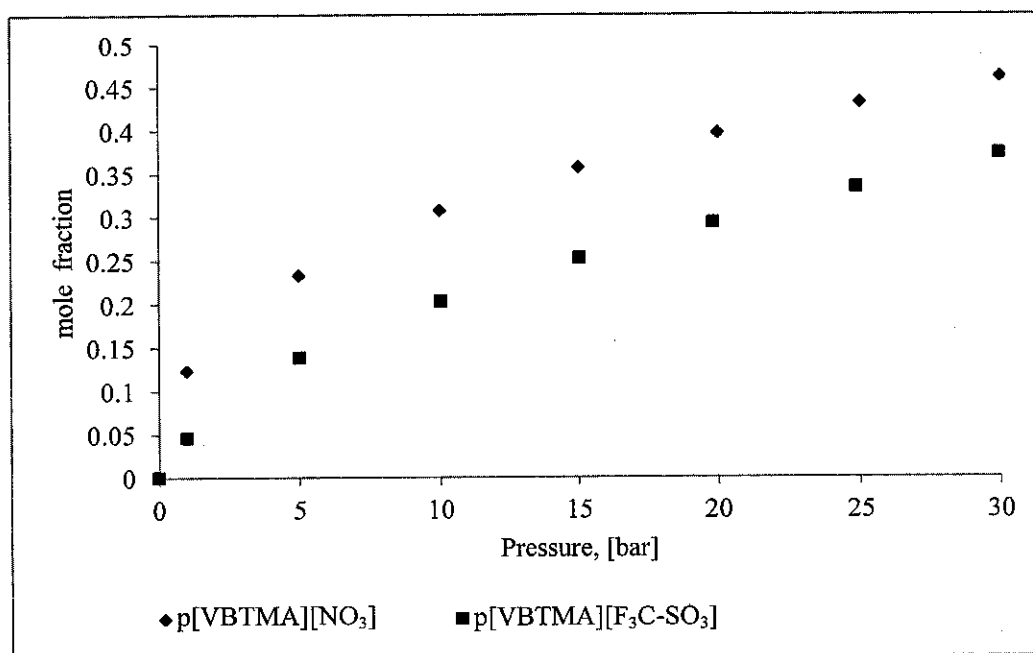


Fig. 5.22: Sorption isotherms for p[VBTMA][NO₃] and p[VBTMA][F₃C-SO₃] at 25°C

The mole fraction of CO₂ in the polymers increased with the increment of CO₂ pressure. The p[VBTMA][NO₃] showed a higher sorption isotherm compared to p[VBTMA][F₃C-SO₃], and this agreed with what previously reported on anion effect (see section 5.3.3).

To calculate the Henry's constants eq. 5.1 which defines the Henry's constant is used.

$$H = \lim_{x_i \rightarrow 0} \frac{p_i}{x_i} \quad 5.1$$

The sorption isotherms for p[VBTMA][NO₃] and p[VBTMA][F₃C-SO₃] are generated at different CO₂ low pressures and 25 °C as shown in Fig. 5.23.

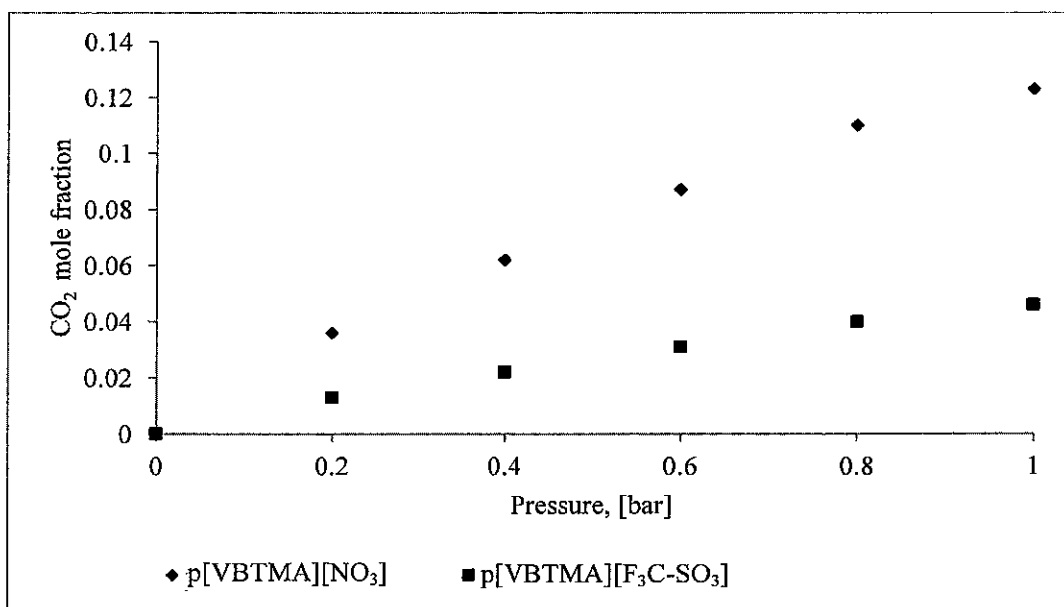


Fig. 5.23: Sorption isotherms for p[VBTMA][NO₃] and p[VBTMA][F₃C-SO₃] at different low pressures and 25°C.

Since x_i vs. p_i plot is not linear in this pressure range, Henry's constants are calculated by fitting the data and extrapolating the slope to zero CO₂ partial pressure [147].

The calculated Henry's constants for p[VBTMA][NO₃] and p[VBTMA][F₃C-SO₃] at 25 °C, are 8.9 bar and 21.6 bar respectively indicating that p[VBTMA][NO₃] is having higher CO₂ sorption capacity than p[VBTMA][F₃C-SO₃].

5.3.5 Effect of Temperature

To study the effect of temperature on sorption capacity, the sorption isotherms for p[VBTMA][NO₃] at three different temperatures (25 °C, 50 °C, and 75 °C) are generated and plotted in Fig. 5.24.

From Fig. 5.24, it can be realized that the temperature is having a great impact on CO₂ sorption capacity of pILs. By increasing the temperature, a serious reduction in CO₂ sorption capacity can be noticed.

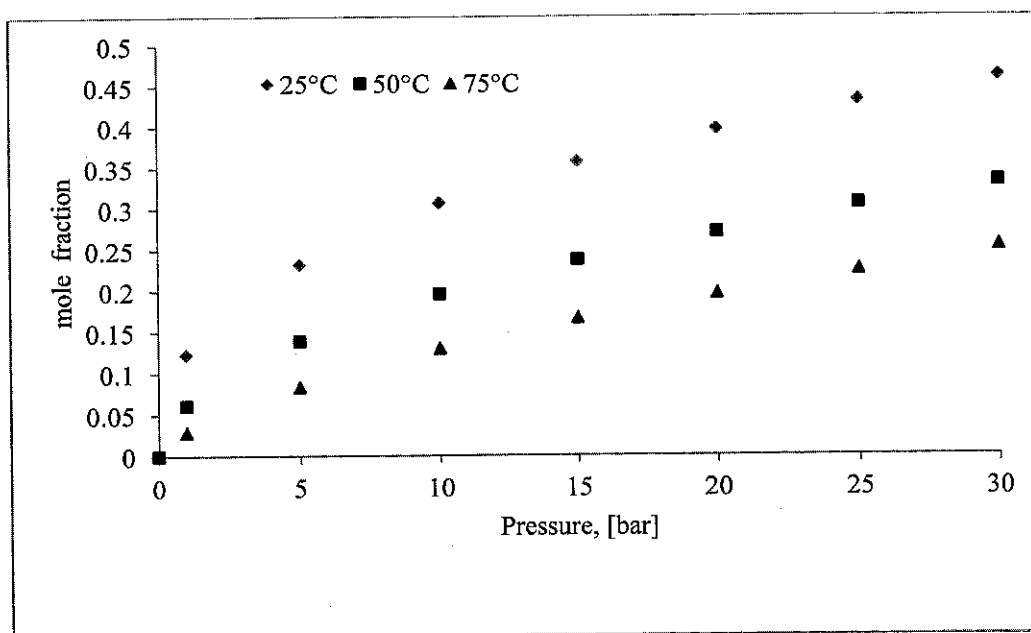


Fig. 5.24: CO₂ sorption isotherms for p[VBTMA][NO₃] at different temperatures

5.3.6 Ideal Selectivity and Molecular Interaction

Since the sorption of gases in pILs is governed by the interaction between the gas molecules and polymer molecules, it is worth to look at these gases in terms of their polarizabilities, dipole moments, and quadrupole moments. The values of these properties for each of the investigated gases are listed in Table 5.7.

Table 5.7: Polarizabilities (α), dipole moments (μ), and quadrupole moments (Q) of some gases [218, 219].

Gas	$\alpha \times 10^{24}$, [cm ³]	$\mu \times 10^{18}$, [e.s.u. × cm]	$Q \times 10^{26}$, [e.s.u. × cm ²]
CO ₂	2.64	0	-4.3
CH ₄	2.6	0	0
CO	1.95	0.112	-2.5
N ₂	1.74	0	-1.52

The negative sign associated with the quadrupole moments stands for $(- + + -)$ quadrupole structure.

The CO_2 , CH_4 , CO , and N_2 sorption rate and capacity for p[VBTMA][$\text{F}_3\text{C-SO}_3$] at 10 bar and 25 °C are shown in Fig. 5.25.

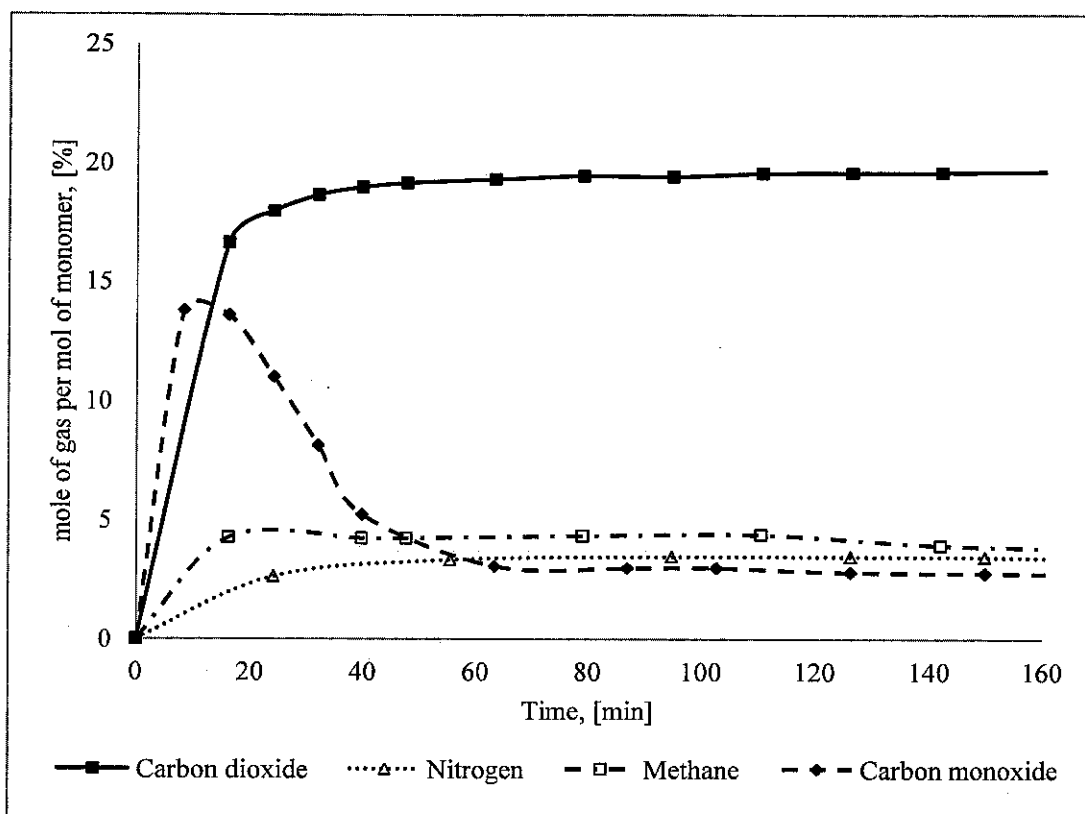


Fig. 5.25: Sorption rate and capacity for different gases on p[VBTMA][$\text{F}_3\text{C-SO}_3$] at 10 bar and 25 °C.

The gases sorption capacities correlate reasonably well with their polarizabilities (see Table 5.7) except for CO as shown in Fig. 5.25. Unexpectedly the CO capacity is lower than N_2 capacity. This might be due to the CO large dipole moment compared to N_2 as reported in Table 5.7. It can also be realized that the CO showed a high peak of sorption at the beginning before it equilibrates at low value and the reason behind this is unclear.

It can be concluded from Fig. 5.25 that pILs enhanced the selectivity towards CO_2 and the pILs selectively take up the CO_2 gas rather than CH_4 and N_2 . This makes them

applicable for separating CO₂ from natural gas and power-generation plants gas exhaust.

5.3.7 Recyclability

It is very important for economic feasibility to test the stability of sorption capacity after repeated sorption/desorption process.

Four cycles of CO₂ sorption and desorption of p[VBTMA][F₃C-SO₃] are generated and showed in Fig. 5.26.

Sorption and desorption are fast and complete, showing that the sorption/desorption is reversible. After four cycles of sorption/desorption, no change in sorption/desorption rate and capacity is observed.

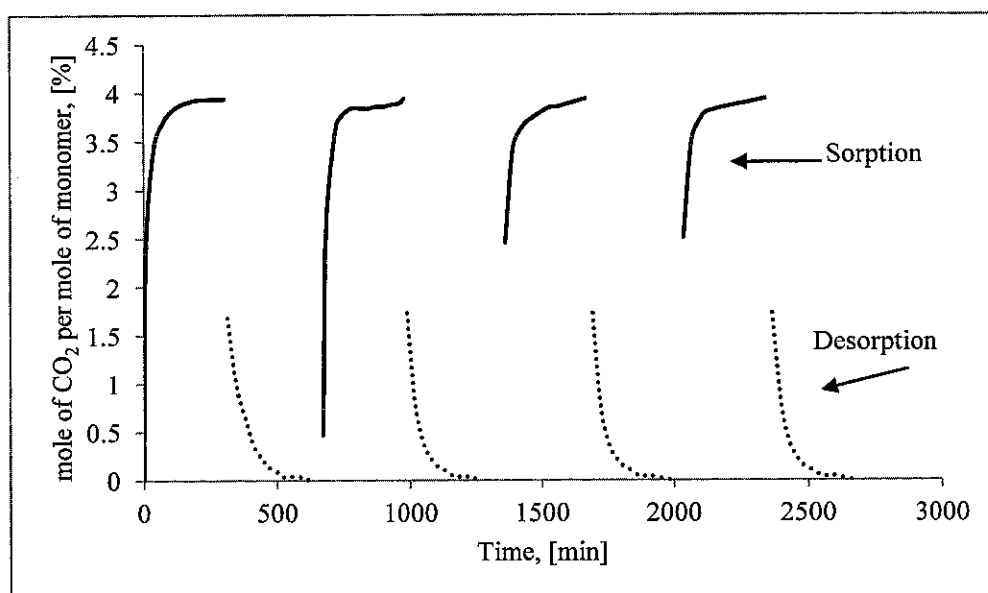


Fig. 5.26: Cycles of CO₂ sorption rate at 1 bar and 25 °C and desorption at 0.02 bar absolute pressure and 25 °C for p[VBTMA][F₃C-SO₃]

The desorption took almost the same time for the sorption to reach equilibrium as shown in Fig. 5.27.

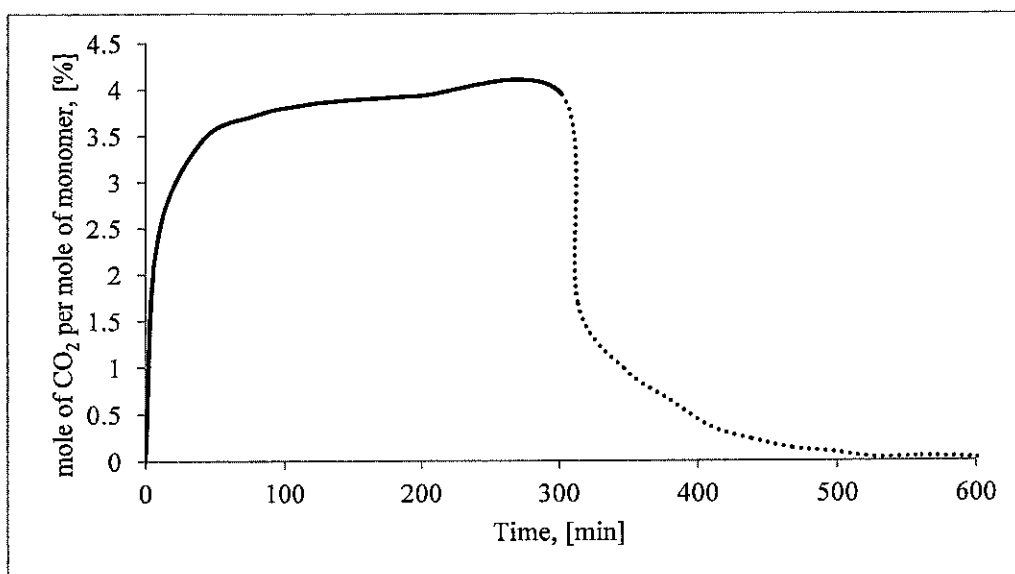


Fig. 5.27: Sorption rate at 1 bar and 25 °C and desorption by vacuuming p[VBtMA]
[F₃C-SO₃]

5.3.8 Effect of Water

It is observed that in the presence of water, the pILs start to swell. To study this phenomenon, the effect of pressure, gas type, gas flow-rate, and water content are studied. Additional study was conducted to test whether the swelling behavior is systematic or not.

5.3.8.1 Swelling Behavior

Two samples of poly vinylbenzyl trimethylammonium chloride (p[VBtMA][Cl]) containing 20% w/w of water with initial volume of 0.25 ml are independently exposed to a 100ml/min flow rate of helium at 1 bar and 10 bar. The dynamic volume is measured using MSB as illustrated in Fig. 5.28.

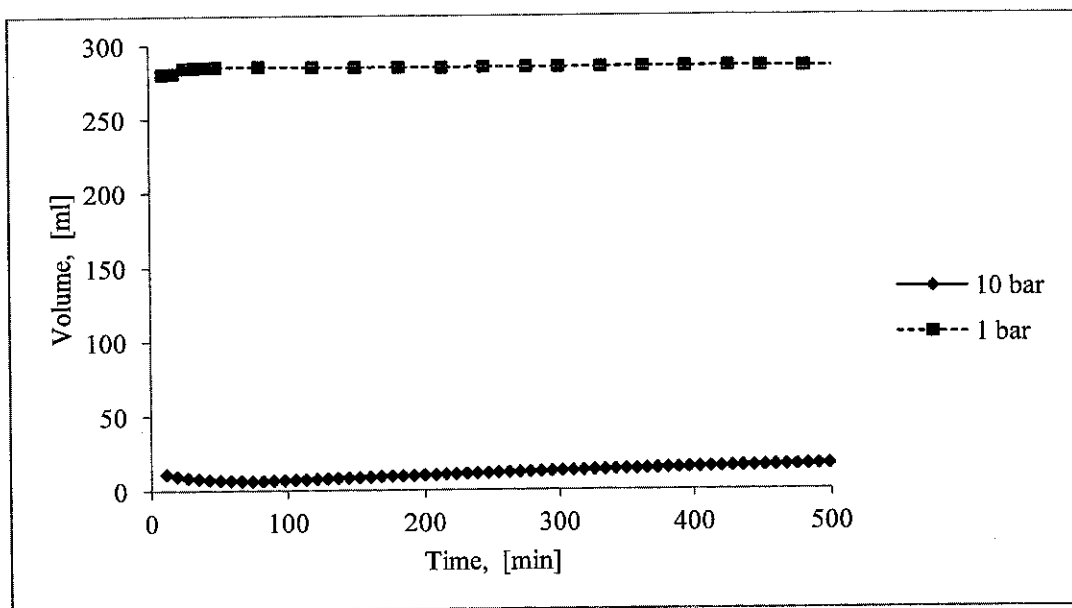


Fig. 5.28: Effect of pressure on volume of p[VBtMA][Cl] containing 20% wt water.

As shown in the figure, when p[VBtMA][Cl] containing 20% w/w water, is exposed to a 100 ml/min of Helium at 1 bar its volume increases from 0.25 ml to 285 ml within the period of 30 minutes, whereas at 10 bar for the same period, the increment in volume only reached 8 ml; and it requires 3000 minutes to reach 30 ml. This indicates that the pressure dramatically affects the dynamic swelling behavior of the poly ionic liquids containing water.

Two fresh samples of poly vinylbenzyl trimethylammonium chloride (p[VBtMA][Cl]) containing 20% w/w of water with initial volume of 0.25 ml are then independently exposed to a 100ml/min flow rate of helium at 10 bar and 100ml/min flow rate of Argon at 10 bar and the change in the dynamic volume is again measured using MSB illustrated in Fig. 5.29.

From the figure, the sample which is exposed to argon reaches a constant volume of 5.6 ml in only 18 min, while the volume of the other sample that is exposed to helium continue to increase up to 23 ml in 1000 min. It can be realized that the density of the gas will affect the dynamic swelling behavior of poly ionic liquids containing water.

We can conclude that the lighter the gas sample exposed to, the higher the increment in volume can be achieved.

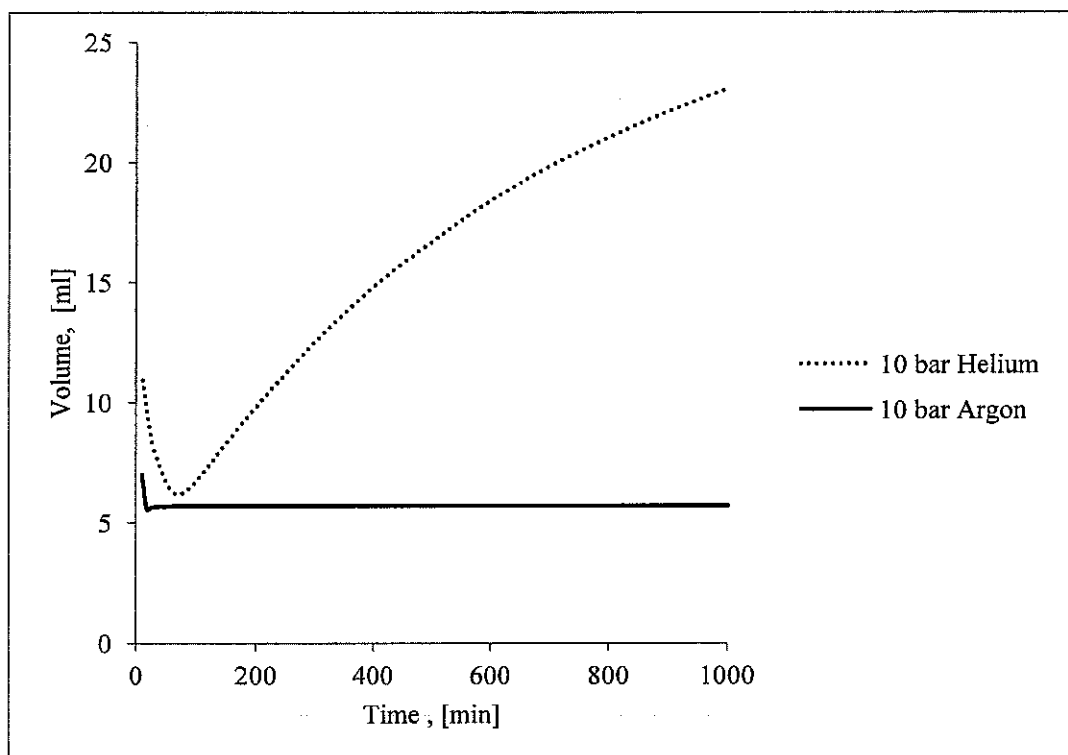


Fig. 5.29: Effect of gas type on volume of p[VBtMA][Cl] containing 20% wt water

A sample of p[VBtMA][Cl] containing 23% w/w of water with initial volume of 0.246 ml is exposed to a 200 ml/min flow rate of argon for 1080 minutes. Then the argon flow rate is stopped for sufficient time to recognize any change in the volume (1040) minutes. Again the flow rate is resumed for sufficient time (500) minutes. During this measurement the pressure is altered, whereby the alterations or adjustments are as shown in Table 5.8.

The dynamic volume is measured using MSB as shown in Fig. 5.30. From the figure it can be seen that the volume will be affected by altering the pressure, Nevertheless, it is further observed that under the 1 bar pressure, the flow of gas stopped, so as the increment of volume. When the flow rate resumed at minute 2120, the volume of the sample start to increase again.

Table 5.8: Pressure Adjustments based on time period

Period	Pressure
First 600 minutes	10 bar
From 600 to 1340 minutes	1 bar
From 1340 to 1810 minutes	1.2 bar
From 1810 to 2410 minutes	1 bar
From 2410 to 3020 minutes	10 bar
From 3020 to 3620 minutes	1 bar

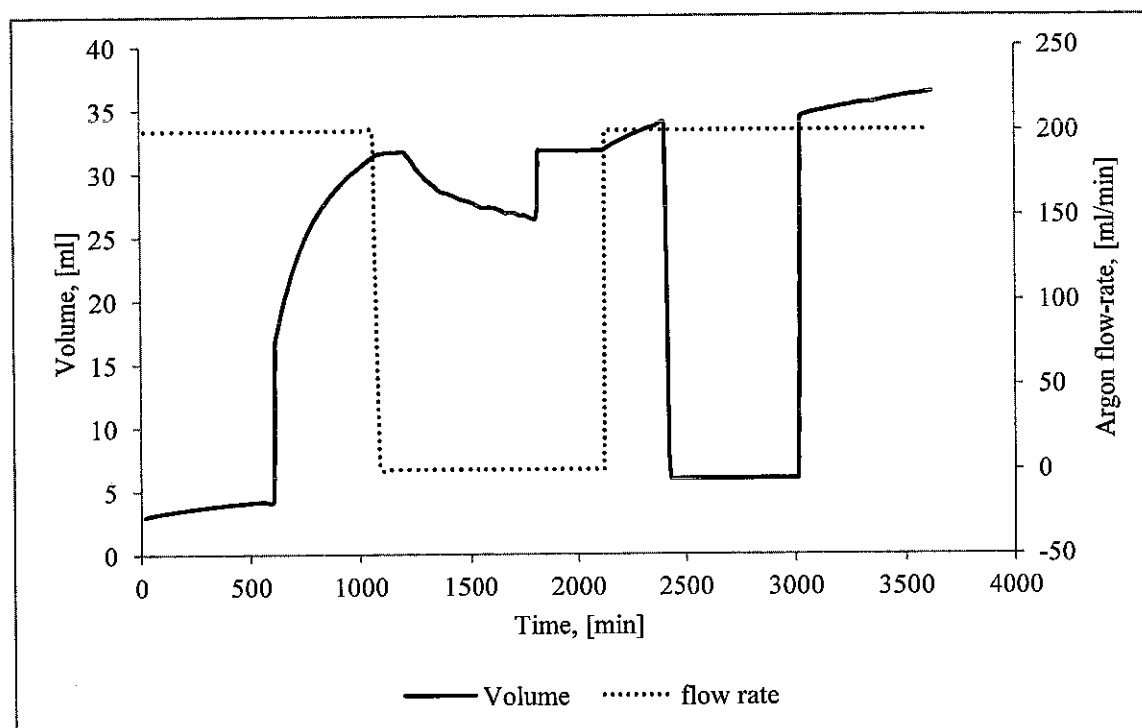


Fig. 5.30: Elasticity and effect of gas flow-rate on volume of p[VBTMA][Cl] containing 23% wt water.

Elasticity behavior is observed as the sample is exposed to different pressure values, and the volume of the sample behavior is subjected to the pressure effect.

It can be concluded that unless the volume of the sample reaches its maximum value as in the previous run using 10 bar pressure, the flow rate will affect its value. Reduction in pressure would lead to an increment in volume despite the absence of gas flow.

Water content effect is then tested. Two samples are prepared, these are poly p[VBtMA][Cl] containing 26% and 95.4% wt of water with initial volume of 0.252 and 0.76 ml respectively. Both samples are independently exposed to a 200ml/min flow rate of argon at 1 bar. The dynamic volume is measured using MSB and the result is shown in Fig. 5.31. From the figure, it can be realized that the sample with higher water content showed a higher increment in volume.

As evident in Fig. 5.31, water content affects the dynamic swelling behavior of pILs.

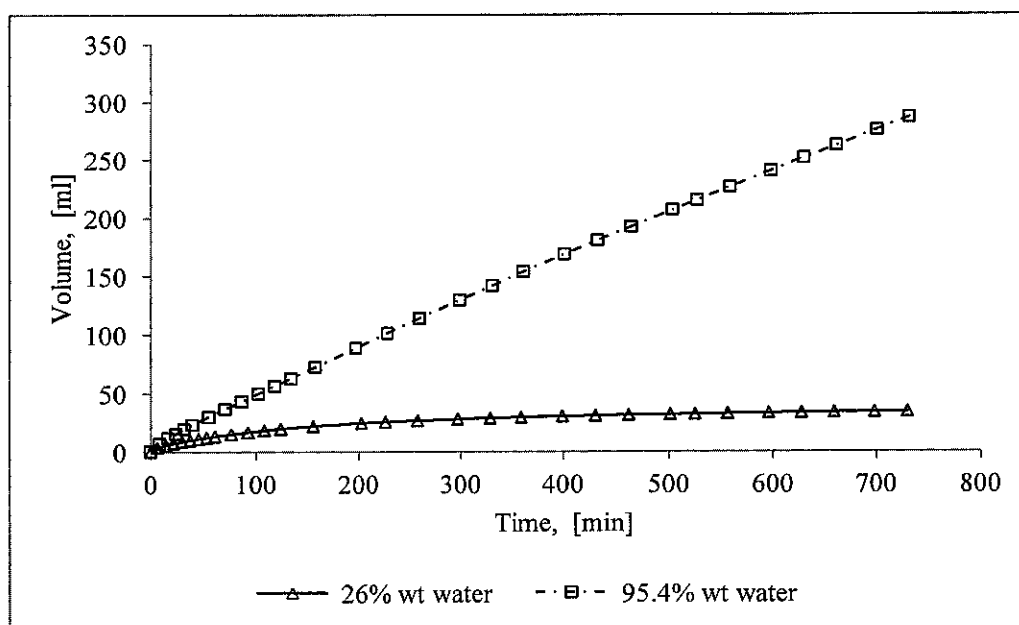


Fig. 5.31: Effect of water content on volume of p[VBtMA][Cl], exposed to a 200ml/min flow rate of argon at 1 bar.

Two samples of p[VBtMA][Cl] containing 95.4% wt of water with initial volume of 0.76 ml respectively, are independently exposed to a 200ml/min flow rate of argon at 1 bar. The dynamic volume is measured using MSB and the result is shown in Fig. 5.32.

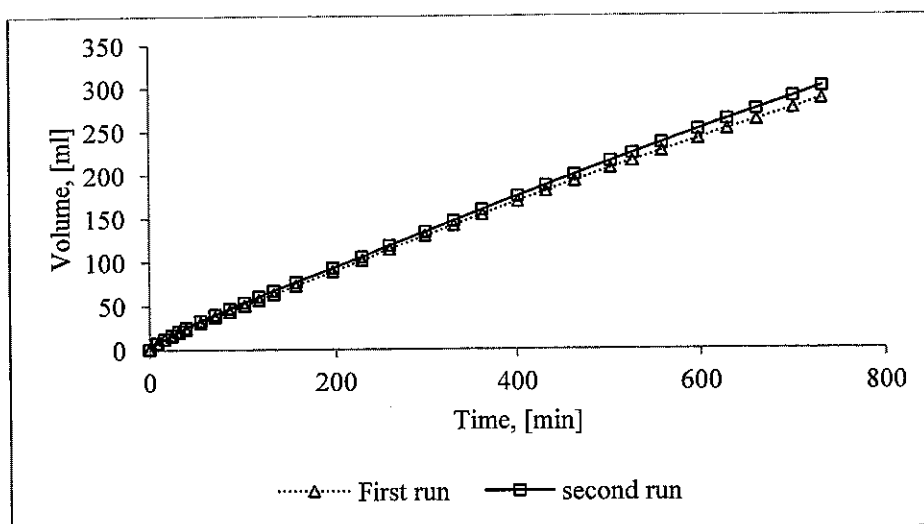


Fig. 5.32: Systematic swelling behavior of p[VBTMA][Cl] containing 95.4% wt of water exposed to 200ml/min flow rate of argon at 1 bar.

From the figure, it can be seen that the dynamic volume increment of the two samples has similar patterns indicating a systematic swelling behavior for pILs when exposed to similar conditions.

To explain this swelling phenomenon, the author suggested that as the water consist of H^+ and OH^- , the H^+ will be attracted to the anion of the pILs, whereas the OH^- will be attracted to the cation. This attraction will lead the pILs to swell and as a result of this attraction and swelling the distance between OH^- , the H^+ will increase, reducing the interaction between them, guiding them to behave as standalone parts.

5.3.8.2 Sorption in The Presence of Water

At 1 bar and 25°C, the sorption capacity and rate of p[VBTMA][Cl] dry, p[VBTMA][Cl] 26 wt% water, and p[VBTMA][Cl] 95.4 wt% water is measured using Magnetic suspension balance as shown in Fig. 5.33 and Fig. 5.34.

In contrast to that with water content, the dry p[VBTMA][Cl] showed 6.34 mole% (1.32 wt%) sorption capacity. p[VBTMA][Cl] containing 26 wt% water exhibited

sorption capacity of 22 mole% (4 wt%). p[VBTMA][Cl] containing 95.4 wt% water result in sorption capacity of 1630 mole% (340.7 wt%) at 1000 min timing. This is considered to be as highly appropriate for industrial application.

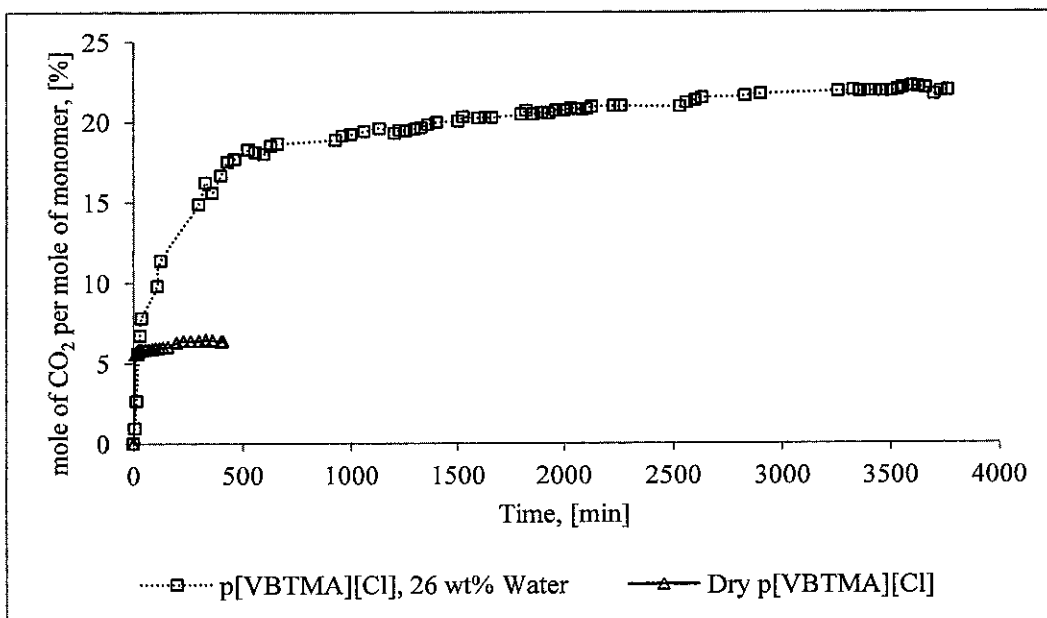


Fig. 5.33: Effect of water on CO₂ sorption capacity and rate at 1 bar and 25°C

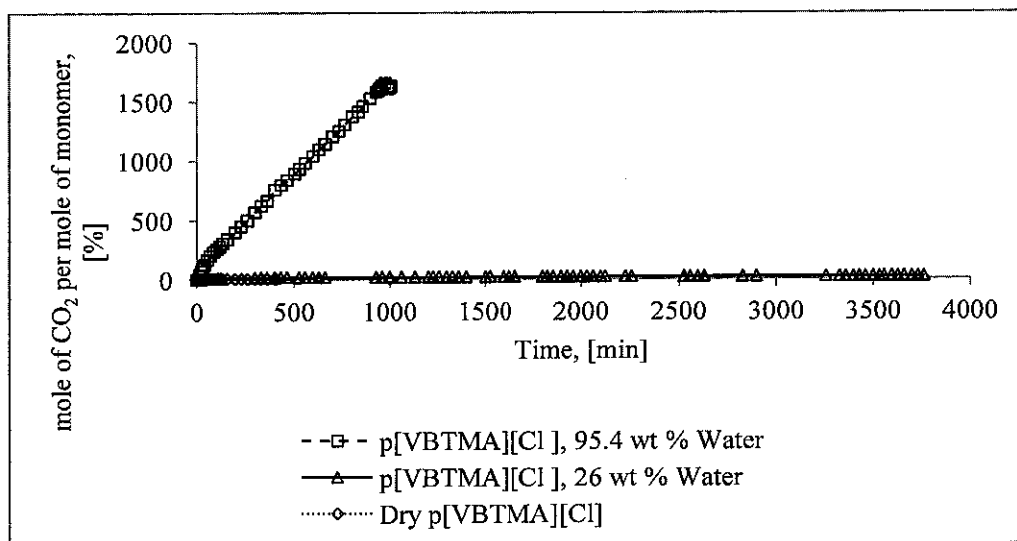


Fig. 5.34: Effect of water on CO₂ sorption capacity and rate at 1 bar and 25°C

From the experiment, significant increment in sorption capacity of pILs can be achieved with the addition of water.

Nevertheless it is worth mentioning that at 25 °C, the solubility of CO₂ in water is 0.035 mole/L [220]. Such low solubility could not explain the significant increment in sorption capacity as a result of water addition.

To explain this significant increment of CO₂ sorption capacity of wet pILs two reasons are suggested by the author. Firstly it is apparent that water content plays a major role in increasing the surface area of the material due to significant swelling behavior. The swelling behavior will offer a great surface area for CO₂ to be hosted. Secondly, as the water consists of H⁺ cation and OH⁻ anion and both of them have a high ion conductivity value (see Table 5.6) they may act as standalone cation and anion enhancing CO₂ sorption.

5.3.9 *Effect of Density Reduction*

Using ultracycrometer 1000 V2.2; the density of p[VBTMA][TFMS] is found to be 1.4062 ± 0.0019 gm/cc . The sample is soaked overnight in methanol then filtered and dried under vacuum at 100°C for three days. It is found that a reduction of 10% in the density of the new treated sample is achieved without chemical structure modification when checked with NMR Analysis.

The sorption capacity and rate are measured for both treated and non treated sample at 10 bar and 25°C using Magnetic suspension balance as suitably shown in Fig. 5.35.

It can be seen based on Fig. 5.35 that there is 10% reduction in density, thus providing a 14.3% sorption capacity increased.

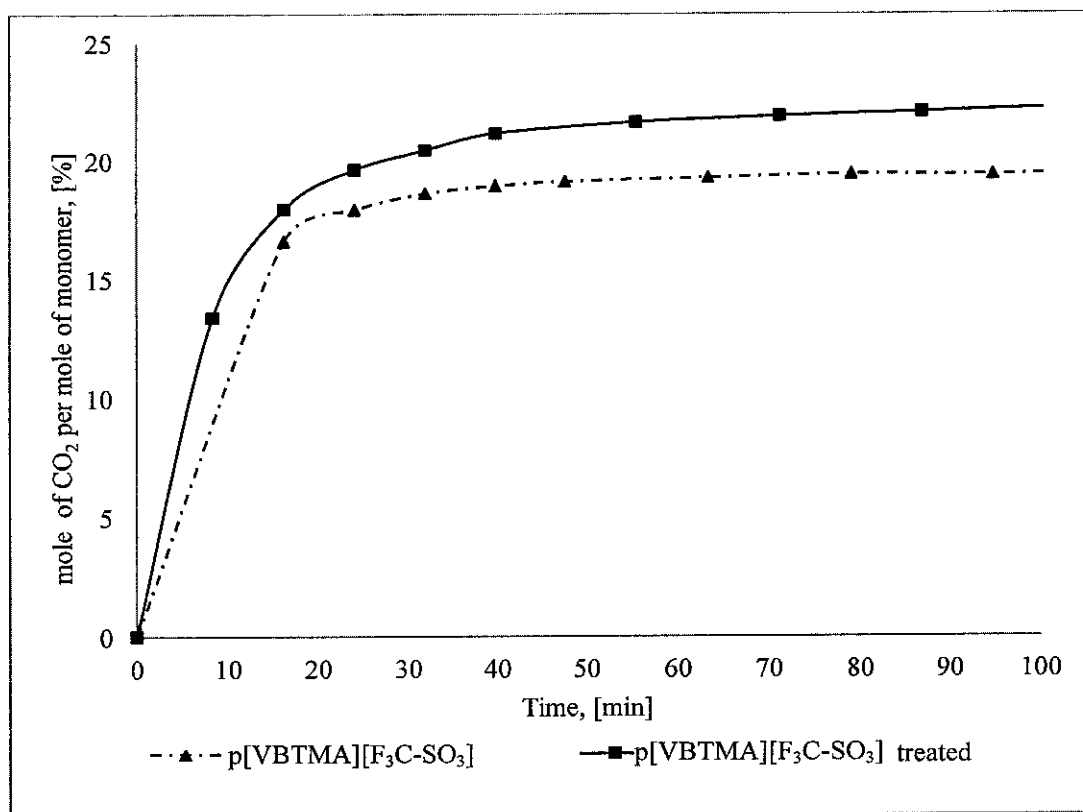


Fig. 5.35: Density reduction effect on CO₂ sorption capacity and rate at 10 bar and 25°C

5.4 Summary

Monte Carlo molecular dynamic sorption simulation results showed that the CO₂ molecules are localized around both cation and anion of pILs. This suggests both cation and anion will affect the sorption capacity of CO₂ on pILs.

Twelve new pILs differ in their cations, backbones, length of substituents, and anions are synthesized, characterized, and their sorption rates and capacities are measured and studied using MSB.

Ion conductivities of cation and anion are the key factors that influence the sorption rate and capacity of CO₂ of pILs. The larger ion conductivities of cation and anion, the higher CO₂ sorption capacity achieved.

It is found that by soaking the pILs in methanol and further drying it; a reduction in density of pILs can be achieved leading to enhancement of CO₂ sorption capacity if the ion conductivity is large enough to sustain the CO₂ and pILs interactions.

Water presence in pILs is found to lead to systematic swelling of pILs depending on pressure, gas flow, type of gas, and water content.

Significant increment in sorption capacity of poly ionic liquids is achieved with the addition of water. In addition to the swelling caused by water, water provides cations and anions enhancing CO₂ sorption capacity.

CHAPTER 6

CONCLUSIONS AND RECOMMENDATIONS

6.1 Conclusions

Twelve new pILs are synthesized, characterized, and their sorption rates for CO₂ and capacities are reported at 10 bar and 25°C. The synthesis is governed by the assumptions that the pILs consist of standalone cation and anion, and sorption capacity and rate depends mainly on ion conductivity of the cations and anions as long as there is enough space to host CO₂. The Monte Carlo molecular dynamics sorption simulation results agreed with the assumptions and showed a localization of CO₂ molecules around both cation and anion.

The twelve new pILs are designed in a way that makes it possible to study the effect of the cation type, backbone, substituent alkyl chain length, and anion. By polymerization the ionic liquids, pILs showed an increase in surface area as the structure moves from crystalline to amorphous; however, the molecular weight of the polymer doesn't really affect the CO₂ sorption rate and capacity. The backbone type and alkyl chain length affect the ion conductivity of the cation. The CO₂ sorption rate and capacity follow the cation's ion conductivity pattern. The ion conductivity of anion governs the CO₂ sorption rate and capacity as well; an increase in the ion conductivity of the anion implies increment in CO₂ sorption capacity. However, the size of the anion may affect the CO₂ sorption rate and capacity by blocking the CO₂ from accessing the cation (steric effect) resulting in a reduction of cation's share in CO₂ sorption.

Water addition to pILs is found to lead to systematic swelling of pILs depending on pressure, gas flow, type of gas, and water content as long as they are exposed to the same conditions.

A remarkable increment in the CO₂ sorption capacity of poly ionic liquids is achieved with the addition of water. In addition to the swelling caused by water, water will act as a cation and anion enhancing CO₂ sorption capacity.

6.2 Recommendations

To design the best pILs for CO₂ capture, a poly ionic liquid with a higher cation ion conductivity and smaller size and higher ion conductivity anion can be synthesized and evaluated.

Swelling behavior of pILs in the presence of water should be studied in depth accounting for all parameters that could influence the swelling (*i.e.* polymer type, pressure, temperature, gas flow etc.).

CO₂ sorption rate and capacity of dry and wet pILs at high pressure should be investigated as there are two contradictory swelling behaviors. The elevated pressure reduced the swelling caused by water presence, while the glassy polymers swelled at elevated pressure.

A pilot plant should be designed and the performance of wet pILs bed needs to be fully studied, addressing all design aspects for scaling-up to industrial level purposes.

REFERENCES

- [1] A. J. Moluijn, *Chemical Process Technology*: Wiley, 2001.
- [2] I. E. Administration, "2001 Insight. Assessing today's supplies to fuel tomorrow's growth," *International Energy Outlook 2001*.
- [3] B. D. Bhide and S. A. and Stern, "Membrane Processes for the Removal of Acid Gases from Natural Gas. II. Effects of Operating Conditions, Economic Parameters and Membrane Properties," *J. Membr. Sci.*, vol. 81, pp. 209-237, 1993.
- [4] F. J. C. Fournie and J. P. and Agostini, "Permeation Membranes Can Efficiently Replace Conventional Gas Treatment Processes," *J. Petr. Tech*, pp. 707-712, 1987.
- [5] R. W. Spillman, "Economics of gas separation membranes," *Chemical Engineering Progress*, pp. 41-62, 1989.
- [6] R. W. Spillman and a. T. E. Cooley, "Membrane gas treating," in *Proceedings of the sixty-eighth Gas Processors Association Annual Convention*, 1989.
- [7] S. Kumar, *Gas Production Engineering*: Gulf Publishing Company, 1987.
- [8] J. L. Martin, F. D. Otto, and A. E. Mather, "Solubility of hydrogen sulfide and carbon dioxide in a diglycolamine solution," *J. Chem. Eng. Data*, vol. 23 pp. 163-164, 1978.
- [9] R. Bottoms, "The Girdler Process for gas Purification," *Am. Gas Assoc. Proc.*, pp. 1071-1082, 1931.
- [10] R. R. Bottoms. vol. US Patent(1,783,901) USA, 1930.

- [11] P. Holub and M. Sheilan, " Fundamentals of Gas Treating," in *LRGCC*, 2003.
- [12] A. Kohl and R. Nielsen, *Gas Purification*, 5th Edition ed.: Gulf Publishing CO, 1997.
- [13] J. McMurry, *Organic Chemistry*: Brooks/Cole, 2000.
- [14] M. A. Al-juaied, "Carbon Dioxide Removal from Natural Gas by Membranes in the Presence of Heavy Hydrocarbons and Aqueous Diglycolamine®/Morpholine." vol. Ph.D. Dissertation Austin: University of Texas, 2004.
- [15] K. Li. and W. Teo, "Use of Permeation and Absorption Methods for CO₂ removal in Hollow Fiber Membrane Modules," *Separation and Purification Technology*, vol. 13, pp. 79-88, 1998.
- [16] H. Matsuyama, K. Hirai, and T. M., "Selective Permeation of Carbon Dioxide through Plasma Polymerized membrane from Diisopropylamine," *Journal of Membrane Science*, vol. 92, pp. 257-265, 1994.
- [17] S. Newman, *Acid and Sour Gas Treating Processes*: Gulf publishing, 1985.
- [18] R. Bartoo, "Removing Acid Gas by the Benfield Process," *Chem. Eng. Prog.*, vol. 80, pp. 35-39, 1984.
- [19] R. Zevenhoven, E. S., and S. Teir, "Chemical fixation of CO₂ in carbonates: Routes to valuable products and long-term storage," *Catal. Today*, vol. 115, pp. 73-79, 2006.
- [20] A. Behr, "Carbon Dioxide Activation by Metal Complexes," *Angew. Chem. Int. Ed. Engl.*, vol. 27, 1988.
- [21] T. Sakakura, C. J., and Y. H., "Transformation of Carbon Dioxide," *Chem. Rev.*, vol. 107, pp. 2365-2387, 2007.

- [22] Chemical, Industry, and Vision, "Technical Summaries on Ionic Liquids in Chemical Processing," in <http://www.chemicalvision2020.org>.
- [23] K. Seddon, "Ionic Liquids: A taste of the future," *Nature materials*, vol. 2, pp. 363-365, 2003.
- [24] "Super Solvents Technology," in <http://quill.qub.ac.uk>.
- [25] S. Lall-Ramnarine, "Synthesis and Characterization of new types of ionic liquids-LIPs and PILS." vol. Ph.D. Dissertation: City University of New York, 2003.
- [26] P. Wasserscheid and W. Keim, "Ionic Liquids-New "Solutions" for Transition Metal Catalysis," *Angew. Chem. Int. Ed. Engl.*, vol. 39, pp. 3772-3789, 2000.
- [27] P. Wasserscheid and W. T., *Ionic Liquids in Synthesis*. Weinheim Germany Wiley-VCH, 2003.
- [28] M. Erbedinger, M. A.J., and R. A.J., "Enzymatic catalysis of formation of Z-aspartame in ionic liquid - An alternative to enzymatic catalysis in organic solvents," *Biotechnol. Prog.*, vol. 16, pp. 1129-1131, 2000.
- [29] J. S. Wilkes, "A short history of ionic liquids-from molten salts to neoteric solvents," *Green Chemistry*, vol. 4, pp. 73-80, 2004.
- [30] C. Hardacre, S. K., and J. McGrath, "Room Temperature Ionic Liquids," Queen University Belfast 2001.
- [31] P. Walden "Molecular Weights and Electrical Conductivity of Several Fused Salts," *Bull. Acad. Sci. (St. Petersburg)* pp. 405-422, 1914.
- [32] K. R. Seddon, A. Stark, and M. j. Tores, "Influence of Chloride, Water, and Organic Solvents on the Physical Properties of Ionic Liquids," *Pure App. Chem.* , vol. 72, pp. 2275-2287, 2000.

- [33] R. A. Carpio, L. A. King, R. E. Lindstrom, J. C. Nardi, and C. L. Hussey, *J. Electrochem. Soc.*, vol. 126, pp. 1644-1650, 1979.
- [34] J. Robinson and R. Osteryoung, "An electrochemical and spectroscopic study of some aromatic hydrocarbons in the room temperature molten salt system aluminum chloride-n-butylpyridinium chloride," *J. Am. Chem. Soc.*, vol. 101, pp. 323-327, 1979.
- [35] T. M. Laher and C. L. Hussey, "Electrochemical studies of chloro complex formation in low-temperature chloroaluminate melts. 1. Iron(II), iron(III), and nickel(II)," *Inorganic chem.*, vol. 21, pp. 4079-4083, 1982.
- [36] E. M. Arnett and J. F. Wolf, "An Electrochemical Scrutiny of Organometallic Iron Complexes and Hexamethylbenzene in a Room Temperature Molten Salt " *J. Am. Chem. Soc.*, vol. Communications to the Editor pp. 3264-3265, 1975.
- [37] V. R. Koch, L. L. Miller, and R. A. Osteryoung, "Electroinitiated Friedel-Crafts transalkylation in a room-temperature molten-salt medium," *J. Am. Chem. Soc.*, vol. 98, pp. 5277-5284, 1976.
- [38] V. Chowdhry and F. H. Westheimer, "Photochemistry of Iron(II) Diimine Complexes in a Room Temperature Molten Salt " *J. Am. Chem. Soc.*, pp. 310-312 1978.
- [39] P. Singh, K. Rajeshwar, J. DuBow, and R. Job, "Photoelectrochemical behavior of n-gallium arsenide electrodes in ambient-temperature molten-salt electrolytes," *J. Am. Chem. Soc.*, vol. 102, pp. 4676-4681, 1980.
- [40] J. Robison and R. A. Osteryoung, "An investigation into the electrochemical oxidation of some aromatic amines in the room-temperature molten salt system aluminum chloride-butylpyridinium chloride," *J. Am. Chem. Soc.*, vol. 102, pp. 4415-4420, 1980.
- [41] H. A. Oye and L. A. King, *Inorg. Nucl. Letters*, vol. 16, pp. 547-550, 1980.

- [42] R. J. Gale, P. Singh, and R. Job, *J. Organometal Chem.*, vol. 199, pp. C44-C46, 1980.
- [43] C. L. Hussey and T. M. Laher, "Electrochemical and spectroscopic studies of cobalt(II) in molten aluminum chloride-n-butylpyridinium chloride," *Inorg. Chem.*, vol. 20, pp. 4201-4206, 1981.
- [44] C. Ye, W. Liu, Y. Chen, and L. Yu, "Room-Temperature Ionic Liquids: A Novel Versatile Lubricant," *Chem. Commun.*, pp. 2244-2245, 2001.
- [45] W. T. Ford, R. J. Hauri, and D. J. Hart, "Synthesis and properties of molten tetraalkylammonium tetraalkylborides," *J. Org. Chem.*, vol. 38, pp. 3916-3918, 1973.
- [46] J. E. Gordon, "Fused Organic Salts. III.1a Chemical Stability of Molten Tetra-n-alkylammonium Salts. Medium Effects on Thermal $R_4N^+X^-$ Decomposition. $RBr + I^- = RI + Br^-$ Equilibrium Constant in Fused Salt Medium," *J. Am. Chem. Soc.*, vol. 30, pp. 2760-2763, 1965.
- [47] J. E. Gordon, J. E. Selwyn, and R. L. Thorne, "Molten Quaternary Ammonium Salts as Stationary Liquid Phases for Gas—Liquid Partition Chromatography," *J. Am. Chem. Soc.*, pp. 1925-1930, 1966,.
- [48] C. M. Starks, "Phase-transfer catalysis. I. Heterogeneous reactions involving anion transfer by quaternary ammonium and phosphonium salts," *J. Am. Chem. Soc.*, vol. 93, pp. 195-199, 1971.
- [49] J. E. Gordon and G. N. SubbaRao, "Fused organic salts. 8. Properties of molten straight-chain isomers of tetra-n-pentylammonium salts," *J. Am. Chem. Soc.*, vol. 100, pp. 7445-7454, 1978.
- [50] J. S. Wilkes, J. A. Levisky, R. A. Wilson, and C. L. Hussey, "Dialkylimidazolium Chloroaluminate Melts: A new Class of Room-

- Temperature Ionic liquids for Electrochemistry, Spectroscopy and Synthesis," *Inorg. Chem.*, vol. 21, pp. 1263-1264, 1982.
- [51] J. A. Boon, J. A. Levisky, J. L. Pflug, and J. S. Wilkes, "Friedel-Crafts Reactions in Ambient-Temperature Molten Salts," *J. Org. Chem.*, vol. 51, pp. 480-483, 1986.
- [52] C. L. Hussey, "Room-temperature Haloaluminate Ionic Liquids - Novel Solvents for Transition-Metal Solution Chemistry," *Pure & Appl. Chem.*, vol. 60, pp. 1763-1772, 1988.
- [53] J. R. Sanders, E. H. Ward, and C. L. Hussey, "Aluminum Bromide-1-methyl-3-ethylimidazolium Bromide Ionic Liquids," *J. Electrochem.Soc.*, vol. 133, pp. 325-330, 1986.
- [54] B. Das, R. Carlin, and R.A. Osteryoung "The Ferro/Ferricyanide Couple in an Aluminium Chloride-1-Methyl-3-Ethylimidazolium Chloride Ambient-Temperature Molten Salt," *Inorg. Chem.*, vol. 28, pp. 421-426, 1989.
- [55] T. A. Zawodzinski, R. Kurland, and R. A. Osteryoung, "Relaxation time measurements in N-(1-butyl)pyridinium-aluminum chloride ambient temperature ionic liquids," *J. Phys. Chem.*, vol. 91, pp. 962-966, 1987.
- [56] J. S. Wilkes and M. J. Zaworotko, "Air and Water Stable 1-Ethyl-3-methylimidazolium based ionic liquids," *J. Chem. Soc. Chem. Commun.*, pp. 965-967, 1992.
- [57] H. Carmichael, *Chemistry in Britain*, vol. January, pp. 36-38, 2000.
- [58] M. Freemantle, "Eyes on Ionic Liquids," *Chem. Eng. News*, vol. 78, pp. 37-50, 2000.
- [59] M. Freemantle, "New horizons for ionic liquids," *Chem. Eng. News*, vol. 79, pp. 21-25, 2001.

- [60] J. D. Holbery and K. R. Seddon, "Ionic Liquids," *Clean Products & Processes*, vol. 1, pp. 223-236 1999.
- [61] K. R. Seddon, "Room-temperature Ionic Liquids: Neoteric Solvents for Clean Catalysis," *Kinet. Catal.*, vol. 37, pp. 693-697, 1996.
- [62] M. J. Earle, J. M. S. S. Esperanca, M. A. Gilea, J. N. C. Lopez, L. P. N. Rebelo, J. W. Magee, K. R. Seddon, and J. A. Widegren, "The Distillation and Volatility of Ionic Liquids," *Nature*, vol. 439, pp. 831-834, 2006.
- [63] M. C. Buzzeo, R. G. Evans, and R. G. Compton, "Non-Haloaluminate Room Temperature Ionic Liquids in Electrochemistry - A Review," *Chem. Phys. Chem.*, vol. 5, pp. 1106-1120 2004.
- [64] H. Olivier-Bourbigou and L. Magna, "Ionic Liquids: Perspectives for Organic and Catalytic Reactions," *J. Mol. Catal.*, vol. 182/183, pp. 419-437.
- [65] T. Welton, "Ionic Liquids in Catalysis," *Coord. Chem. Rev.*, vol. 248, pp. 2459- 2477, 2004.
- [66] P. Bonhote, A. P. Dias, N. Papageorgiou, K. Kalyanasundaram, and M. Gratzel, "Hydrophobic, Highly Conductive Ambient-temperature Molten Salts," *Inorg. Chem.*, vol. 35, pp. 1168-1178, 1996.
- [67] K. Seddon, S. A., and Torres, "Influence of chloride, water, and organic solvents on the physical properties of ionic liquids," *Pure Appl. Chem.*, pp. 2275-2287, 2000.
- [68] J. L. Anthony, E. J. Maginn, and J. F. Brennecke, "Solution Thermodynamics of Imidazolium-based Ionic Liquids and Water," *J. Phys. Chem. B*, vol. 105, pp. 10942-10949, 2001.
- [69] J. L. Anthony, E. J. Maginn, and J. F. Brennecke, "Solubilities and Thermodynamics Properties of Gases in the Ionic Liquid 1-n-butyl-3-

- methylimidazolium hexafluorophosphate," *J. Phys. Chem. B*, vol. 106, pp. 7315-7320, 2002.
- [70] J. L. Anthony, J. M. Crosthwaite, D. G. Hert, S. N. V. K. Aki, E. J. Maginn, and J. F. Brennecke, "Phase Equilibria of Gases and Liquids with 1-n-butyl-3-methylimidazolium tetrafluoroborate," *ACS Symposium Series 856*, vol. Ionic Liquids as Green Solvents, pp. 110-120, 2003.
- [71] P. T. Anastas and J. C. Warner, *Green Chemistry: Theory and Practice*. Oxford, UK: Oxford University Press, 1998.
- [72] R. Renner, "Ionic Liquids: An Industrial Cleanup Solution," *Environmental Science and Technology*, vol. 35, pp. 410A-413A, 2001.
- [73] J. D. Holbrey, W. M. Reichert, R. P. Swatloski, G. A. Broker, W. R. Pitner, K. R. Seddon, and R. D. Rogers, "Efficient, Halide Free Synthesis of New, Low Cost Ionic Liquids: 1,3-Dialkylimidazolium Salts Containing Methyl- and Ethyl Sulfate Anion," *Green Chemistry*, vol. 4, pp. 407-413, 2002.
- [74] M. T. Garcia, N. Gathergood, and P. J. Scammells, "Biodegradable Ionic Liquids. Part II. Effect of the anion and Toxicity," *Green Chemistry*, vol. 7, pp. 9-14, 2005.
- [75] V. V. Namboodiri and S. R. Varma, "Microwave-Assisted Preparation of Dialkylimidazolium Tetrachloroaluminates and Their Use as Catalysts in the Solvent-free Tetrahydropyranylation of Alcohols and Phenols," *Chemical communications*, pp. 342-343, 2002.
- [76] V. V. Namboodiri and R. S. Varma, "Solvent-Free Sonochemical Preparation of Ionic Liquids," *Organic Letters*, vol. 4, pp. 3161-3163, 2002.
- [77] G. P. Pez, R. T. Carlin, D. V. Laciak, and J. C. Sorensen, "Method for gas separation." vol. 4,761,164 U.S. Patent, 1988.

- [78] S. Zhang, Y. Chen, F. Li, X. Lu, W. Dai, and R. Mori, "Fixation and conversion of CO₂ using ionic liquids " *Catal. Today*, vol. 115, pp. 61-69, 2006.
- [79] L. A. Blanchard, Z. Y. GU, and J. F. Brennecke, "High-pressure phase behavior of ionic liquid/CO₂ systems," *J. Phys. Chem. B*, vol. 105, pp. 2437-2444, 2001.
- [80] L. A. Blanchard, D. Hancu, E. J. Beckman, and J. F. Brennecke, "Green processing using ionic liquids and CO₂ " *Nature*, vol. 399, pp. 28-29, 1999.
- [81] L. A. Blanchard and J. F. Brennecke, "Recovery of organic products from ionic liquids using supercritical carbon dioxide," *Ind. Eng. Chem. Res.*, vol. 40, pp. 287-292, 2001.
- [82] L. A. Blanchard and J. F. Brennecke, "Recovery of organic products from ionic liquids using supercritical carbon dioxide (erratum)," *Ind. Eng. Chem. Res.*, vol. 40, p. 2550, 2001.
- [83] J. L. Anthony, "Gas Solubilities in Ionic Liquids: Experimental Measurement and Applications," in *Chemical and Biomolecular Engineering*. vol. P.hD. Notre Dame: University of Notre Dame, 2004.
- [84] B. H. Lim, W. H. Choe, J. J. Shim, C. S. Ra, D. Tuma, H. Lee, and C. S. Lee, "High-pressure solubility of carbon dioxide in imidazolium-based ionic liquids with anions [PF₆] and [BF₄]," *Korean Journal of Chemical Engineering*, vol. 26, pp. 1130-1136, 2009.
- [85] M. Hasib-ur-Rahmana, M. Siaj, and F. Larachia, "Ionic liquids for CO₂ capture—Development and progress," *Chemical Engineering and Processing* vol. 49, pp. 313-322, 2010.

- [86] Y. Hou and R. E. Baltus, "Experimental measurement of the solubility and diffusivity of CO₂ in room-temperature ionic liquids using a transient thin-liquid-film method," *Ind. Eng. Chem. Res.*, vol. 46, pp. 8166-8175, 2007.
- [87] M. B. Shiflett and A. Yokozeki, "Solubilities and diffusivities of carbon dioxide in ionic liquids: [bmim][PF₆] and [bmim][BF₄]," *Ind. Eng. Chem. Res.*, vol. 44, pp. 4453-4464, 2005.
- [88] C. Cadena, J. L. Anthony, J. K. Shah, T. I. Morrow, J. F. Brennecke, and E. J. Maginn, "Why Is CO₂ So Soluble in Imidazolium-Based Ionic Liquids?," *J. Am. Chem. Soc.*, vol. 126, pp. 5300-5308, 2004.
- [89] A. Shariati and C. J. Peters, "High-pressure phase behavior of systems with ionic liquids Part III. The binary system carbon dioxide + 1-hethyl-3-methylimidazolium hexafluorophosphate," *J. Supercrit. Fluids*, vol. ASAP article, 2003.
- [90] P. Scovazzo, J. Kieft, D. A. Finan, C. Koval, D. DuBois, and R. Noble, "Gas separations using non-hexafluorophosphate [PF₆]⁻ anion supported ionic liquid membranes," *Journal of Membrane Science*, vol. 238 pp. 57-63, July 2004.
- [91] D. Camper, J. Bara, C. Koval, and R. Noble, "Bulk-Fluid Solubility and Membrane Feasibility of Rmim-Based Room-Temperature Ionic Liquids," *Ind. Eng. Chem. Res.*, vol. 45, pp. 6279-6283, 2006.
- [92] J. F. Brennecke and E. J. Maginn. vol. US20036579343 US Patent, 2003.
- [93] J. F. Brennecke and E. J. Maginn. vol. US20020189444 US Patent, 2002.
- [94] T. Yu, R. G. Weiss, T. Yamada, and M. George. vol. WO2008094846A1, W. I. P. Organization, Ed. US, 2008.
- [95] D. Chinn, D. Q. Vu, M. S. Driver, and L. C. Boudreau. vol. US20060251558A1 US Patent, 2006.

- [96] D. Camper, J. E. Bara, D. L. Gin, and R. D. Noble, "Room-temperature ionic liquid-amine solutions: tunable solvents for efficient and reversible capture of CO₂," *Ind. Eng. Chem. Res.*, vol. 47, pp. 8496-8498, 2008.
- [97] M. F. Arenas and R. G. Reddy, "Corrosion of steel in ionic liquids," *J. Min. Metall. Sect. B.*, vol. 39, pp. 81-91, 2003.
- [98] I. Perissi, U. Bardi, S. Caporali, and A. Lavacchi, "High temperature corrosion properties of ionic liquids," *Corros. Sci.*, vol. 48, pp. 2349-2362, 2006.
- [99] A. Veawab and P. Tontiwachwuthikul, "Investigation of low-toxic organic corrosion inhibitors for CO₂ separation process using aqueous MEA solvent," *Ind. Eng. Chem. Res.*, vol. 40, pp. 4771-4777, 2001.
- [100] I. R. Soosaiprakasham and A. Veawab, "Corrosion and polarization behavior of carbon steel in MEA-based CO₂ capture process," *Int. J. Greenhouse Gas Control*, vol. 2, pp. 553-562, 2008.
- [101] L. M. G. Sánchez, G. W. Meindersma, and A. B. d. Haan, "Solvent properties of functionalized ionic liquids for CO₂ absorption," *Chem. Eng. Res. Des.*, vol. 85, pp. 31-39, 2007.
- [102] S. P. M. Ventura, J. Pauly, J. L. Daridon, J. A. L. d. Silva, I. M. Marrucho, A. M. A. Dias, and J. A. P. Coutinho, "High pressure solubility data of carbon dioxide in (tri-isobutyl(methyl)phosphonium tosylate +water) systems," *J. Chem. Thermodyn.*, vol. 40, pp. 1187-1192, 2008.
- [103] R. E. Baltus, B. H. Culbertson, S. Dai, H. Luo, and D. W. DePaoli, "Low-pressure solubility of carbon dioxide in room-temperature ionic liquids measured with a quartz crystal microbalance," *J. Phys. Chem. B*, vol. 108, pp. 721-727, 2004.

- [104] A. E. Visser, J. D. Holbrey, and R. D. Rogers, "Hydrophobic ionic liquids incorporating N-alkylisoquinolinium cations and their utilization in liquid-liquid separations," *Chem. Commun.*, pp. 2484-2485, 2001.
- [105] A. E. Visser, R. P. Swatloski, W. M. Reichert, R. Mayton, S. Sheff, A. Wierzbicki, J. H. J. Davis, and R. D. Rogers, "Task-specific ionic liquids incorporating novel cations for the coordination and extraction of Hg^{2+} and Cd^{2+} : synthesis, characterization, and extraction studies.," *Environ. Sci. Technol.*, vol. 1, pp. 2523-9, 2002.
- [106] A. E. Visser, R. P. Swatloski, W. M. Reichert, R. Mayton, S. Sheff, A. Wierzbicki, J. J. H.mDavis, and R. D. Rogers, "Task-Specific Ionic Liquids for the Extraction of Metal Ions from Aqueous Solutions," *Chem. Commun.* , pp. 135-136, 2001.
- [107] D. E. Bates, R. D. Mayton, o. Ntai, and H. J. J. Davis, "CO₂ Capture by a Task-Specific Ionic Liquid," *J. Am. Chem. Soc.*, vol. 124, pp. 926-927, 2002.
- [108] J. Zhang, S. Zhang, K. Dong, Y. Zhang, Y. Shen, and X. Lv, "Supported Absorption of CO₂ by Tetrabutylphosphonium Amino Acid Ionic Liquids," *Chemistry - A European Journal*, vol. 12, pp. 4021-4026, 2006.
- [109] J. E. Bara, C. J. Gabriel, S. Lessmann, T. K. Carlisle, A. Finotello, D. L. Gin, and R. D. Noble, "Enhanced CO₂ Separation Selectivity in Oligo(ethylene glycol) Functionalized Room-Temperature Ionic Liquids," *Ind. Eng. Chem. Res.*, vol. 46, pp. 5380-5386, 2007.
- [110] K.-P. Shen and M.-H. Li, "Solubility of carbon dioxide in aqueous mixtures of monoethanolamine with methyldiethanolamine," *J. Chem. Eng. Data*, vol. 37, pp. 96-100, 1992.
- [111] J. H. Davis. vol. US20040035293A1 US Patent, 2004.

- [112] S. Zhang, X. Yuan, Y. Chen, and X. Zhang, "Solubilities of CO₂ in 1-Butyl-3-methylimidazolium Hexafluorophosphate and 1,1,3,3-Tetramethylguanidium Lactate at Elevated Pressures," *J. Chem. Eng. Data*, vol. 50, pp. 1582-1585, 2005
- [113] G. Yu, S. Zhang, X. Yao, J. Zhang, K. Dong, W. Dai, and R. Mori, "Design of Task-Specific Ionic Liquids for Capturing CO₂: A Molecular Orbital Study," *Ind. Eng. Chem. Res.*, vol. 45, pp. 2875-2880, 2006
- [114] K. E. Gutowski and E. J. Maginn, "Amine-functionalized task-specific ionic liquids: a mechanistic explanation for the dramatic increase in viscosity upon complexation with CO₂ from molecular simulation," *J. Am. Chem. Soc.*, vol. 130 pp. 14690-14704, 2008.
- [115] H. Chen, J.-H. Choi, D. S.-d. I. Cruz, K. I. Winey, and Y. A. Elabd, "Polymerized Ionic Liquids: The Effect of Random Copolymer Composition on Ion Conduction," *Macromolecules*, vol. 42, pp. 4809-4816, 2009.
- [116] N. Winterton, "Solubilization of polymers by ionic liquids," *J. Mater. Chem.*, vol. 16, pp. 4281-4293, 2006.
- [117] J. Korkisch, *Handbook of Ion Exchange Resins and their Applications*. Boca Raton FL: CRC Press, 1988.
- [118] K. A. Mauritz and R. B. Moore, "State of Understanding of Nafion," *Chem. Rev.*, vol. 104, pp. 4535-4585, 2004, .
- [119] R. Marcilla, F. Alcaide, H. Sardon, J. A. Pomposo, C. Pozo-Gonzalo, and D. Mecerreyes, "Tailor-made polymer electrolytes based upon ionic liquids and their application in all-plastic electrochromic devices " *Electrochemistry Communications*, vol. 8, pp. 482-488, 2006.

- [120] N. Ogata, K. Sanui, M. Rikukawa, S. Yamada, and M. Watanabe, "Super ion conducting polymers for solid polymer electrolytes " *Synthetic Metals*, vol. 69, pp. 521-524, 1995
- [121] M. Watanabe, S.-i. Yamada, and N. Ogata, "Ionic conductivity of polymer electrolytes containing room temperature molten salts based on pyridinium halide and aluminium chloride " *Electrochimica Acta*, vol. 40, pp. 2285-2288 1995
- [122] M. Watanabe, S.-I. Yamada, K. Sanui, and N. Ogata, "High ionic conductivity of new polymer electrolytes consisting of polypyridinium, pyridinium and aluminium chloride," *Chem. Commun.*, pp. 929 - 931, 1993.
- [123] J. Fuller, A. C. Breda, and R. T. Carlin, "Ionic Liquid-Polymer Gel Electrolytes," *J. Electrochem. Soc.*, vol. 144, pp. L67-L70, 1997.
- [124] J. Fuller, A. C. Breda, and R. T. Carlin, "Ionic liquid–polymer gel electrolytes from hydrophilic and hydrophobic ionic liquids," *J. Electroanal. Chem.*, vol. 459, pp. 29-34 1998.
- [125] M. Doyle, S. K. Choi, and G. Proulx, "High-Temperature Proton Conducting Membranes Based on Perfluorinated Ionomer Membrane-Ionic Liquid Composites," *J. Electrochem. Soc.* , vol. 147, pp. 34-37, 2000.
- [126] M. Bennett and D. Leo, "Ionic liquids as solvents for ionic polymer transducers " *Sens. Actuators A: Phys.*, vol. 115, pp. 79-90, 2004.
- [127] A. Noda and M. Watanabe, "Highly conductive polymer electrolytes prepared by in situ polymerization of vinyl monomers in room temperature molten salts " *Electrochimica Acta* vol. 45, pp. 1265-1270, 2000.
- [128] M. A. B. H. Susan, T. Kaneko, A. Noda, and M. Watanabe, "Ion Gels Prepared by in Situ Radical Polymerization of Vinyl Monomers in an Ionic

- Liquid and Their Characterization as Polymer Electrolytes," *J. Am. Chem. Soc.*, vol. 127, pp. 4976-4983, 2005.
- [129] H. Shobukawa, H. Tokuda, M. A. B. H. Susan, and M. Watanabe, "Ion transport properties of lithium ionic liquids and their ion gels " *Electrochimica Acta*, vol. 50, pp. 3872-3877 2005.
- [130] J.-H. Shin, W. A. Henderson, and S. Passerini, "Ionic liquids to the rescue? Overcoming the ionic conductivity limitations of polymer electrolytes " *Electrochem. Commun.*, vol. 5, pp. 1016-1020, 2003.
- [131] J.-H. Shin, W. A. Henderson, and S. Passerini, "PEO-Based Polymer Electrolytes with Ionic Liquids and Their Use in Lithium Metal-Polymer Electrolyte Batteries," *J. Electrochem. Soc.*, vol. 152, pp. A978-A983, 2005.
- [132] D. Zhou, G. M. Spinks, G. G. Wallace, C. Tiyapiboonchaiya, D. R. MacFarlane, M. Forsyth, and J. Sun, "Solid state actuators based on polypyrrole and polymer-in-ionic liquid electrolytes " *Electrochimica Acta*, vol. 48, pp. 2355-2359, 2003.
- [133] F. Vidal, C. Plesse, D. Teyssié, and C. Chevrot, "Long-life air working conducting semi-IPN/ionic liquid based actuator," *Synthetic Metals*, vol. 142, pp. 287-291, 2004.
- [134] P. Wang, S. M. Zakeeruddin, I. Exnar, M. Grätzel, and "High efficiency dye-sensitized nanocrystalline solar cells based on ionic liquid polymer gel electrolyte," *Chem. Commun.* , p. 2972-2973, 2002.
- [135] K. Suzuki, M. Yamaguchi, S. Hotta, N. Tanabe, and S. Yanagida, "A new alkyl-imidazole polymer prepared as an inonic polymer electrolyte by in situ polymerization of dye sensitized solar cells " *J. Photochem. Photobiol. A: Chem.*, vol. 164, p. 81, 2004.

- [136] M. Yoshizawa, W. Ogihyra, and H. Ohno, "Novel polymer electrolytes prepared by copolymerization of ionic liquid monomers," *Polym. Adv. Technol.*, vol. 13, pp. 589 - 594, 2002.
- [137] H. Ohno and a. K. Ito, "Room-Temperature Molten Salt Polymers as a Matrix for Fast Ion Conduction," *Chemistry Letters*, vol. 27, p. 751 1998.
- [138] K. Ito, N. Nishina, and H. Ohno, "Enhanced ion conduction in imidazolium-type molten salts," *Electrochim. Acta*, vol. 45, pp. 1295-1298, 2000.
- [139] M. Yoshizawa and H. Ohno, "Synthesis of molten salt-type polymer brush and effect of brush structure on the ionic conductivity " *Electrochim. Acta* vol. 46 pp. 1723-1728 2001.
- [140] H. Ohno, "Molten salt type polymer electrolytes," *Electrochim. Acta*, vol. 46 pp. 1407-1411 2001.
- [141] H. Ohno, M. Yoshizawa, and W. Ogiyara, "Development of new class of ion conductive polymers based on ionic liquids " *Electrochim. Acta*, vol. 50, pp. 255-261 2004.
- [142] H. Ohno, "Functional Design of Ionic Liquids," *Bull. Chem. Soc. Jpn*, vol. 79, pp. 1665-1680, 2006.
- [143] R. Marcilla, J. A. Blazquez, J. Rodríguez, J. A. Pomposo, and D. Mecerreyes, "Tuning the solubility of polymerized ionic liquids by simple anion-exchange reactions," *J. Polym. Sci. Part A: Polym. Chem.*, vol. 42, pp. 208 - 212, 2004.
- [144] R. Marcilla, J. A. Blazquez, R. Fernandez, H. Grande, J. A. Pomposo, and D. Mecerreyes, "Synthesis of Novel Polycations Using the Chemistry of Ionic Liquids," *Macromol. Chem. & Phys.*, vol. 206, pp. 299 - 304, 2005.
- [145] J. Tang, W. Sun, H. Tang, M. Radosz, and Y. Shen, "Enhanced CO₂ Absorption of Poly(ionic liquids)," *Macromolecules*, vol. 38, pp. 2037-2039, 2005.

- [146] J. Tang, H. Tang, W. Sun, H. Plancher, M. Radosz, and Y. Shen, "Poly(ionic liquid)s: a new material with enhanced and fast CO₂ absorption," *Chem. Commun.*, pp. 3325 - 3327, 2005.
- [147] J. Tang, H. Tang, W. Sun, M. Radosz, and Y. Shen, "Low-pressure CO₂ sorption in ammonium-based poly(ionic liquid)s " *Polymer*, vol. 46, pp. 12460-12467 2005.
- [148] J. Tang, H. Tang, W. Sun, M. Radosz, and Y. J. Shen, "Poly(ionic liquid)s as new materials for CO₂ absorption," *Polym. Sci. Part A: Polym. Chem.*, vol. 43, pp. 5477 - 5489, 2005.
- [149] H. Tang, J. Tang, S. Ding, M. Radosz, and Y. Shen, "Atom Transfer Radical Polymerization of Styrenic Ionic Liquid Monomers and Carbon Dioxide Absorption of the Polymerized Ionic Liquids," *Journal of Polymer Science: Part A: Polymer Chemistry*, vol. 43, pp. 1432-1443, 2005.
- [150] P. Snedden, A. I. Cooper, K. Scott, and N. Winterton, "Cross-Linked Polymer-Ionic Liquid Composite Materials," *Macromolecules*, vol. 36, pp. 4549-4556, 2003.
- [151] M. J. Muldoon and C. M. Gordon, "Synthesis of gel-type polymer beads from ionic liquid monomers," *Journal of Polymer Science Part A: Polymer Chemistry*, vol. 42, pp. 3865 - 3869, 2004.
- [152] O. Green, S. Grubjesic, S. Lee, and M. A. Firestone, "The Design of Polymeric Ionic Liquids for the Preparation of Functional Materials," *J. Macromolecular Science, Part C: Polymer Reviews*, vol. 49, pp. 339-360, 2009.
- [153] S. Ding, H. Tang, M. Radosz, and Y. Shen, "Atom Transfer Radical Polymerization of Ionic Liquid 2-(1- Butylimidazolium-3-yl)ethyl Methacrylate Tetrafluoroborate," *Journal of Polymer Science: Part A: Polymer Chemistry*, vol. 42, pp. 5794-5801, 2004.

- [154] Y. Shen and M. Radosz, "Novel Ionic Liquids and Poly(Ionic Liquid)s as New Materials for Gas Separation and Other Applications," W. I. P. O. I. Bureau, Ed. US 2006.
- [155] S. Kato, Y. Tsujita, H. Yoshimizu, T. Kinoshita, and J. S. Higgins, "Characterization and CO₂ sorption behaviour of polystyrene/polycarbonate blend system " *Polymer*, vol. 38, pp. 2807-2811 1997.
- [156] Z. Mogri and D. R. Paul, "Gas sorption and transport in poly(alkyl (meth)acrylate)s. II. Sorption and diffusion properties " *Polymer*, vol. 42, pp. 7781-7789, 2001.
- [157] J. L. Budzien, J. D. McCoy, D. H. Weinkauff, R. A. LaViolette, and E. S. Peterson, "Solubility of Gases in Amorphous Polyethylene," *Macromolecules* vol. 31, pp. 3368-3371, 1998.
- [158] A. Blasig, J. Tang, X. Hu, S. P. Tan, Y. Shen, and M. Radosz, "Carbon Dioxide Solubility in Polymerized Ionic Liquids Containing Ammonium and Imidazolium Cations from Magnetic Suspension Balance: P[VBTMA][BF₄] and P[VBMI][BF₄]," *Ind. Eng. Chem. Res.*, vol. 46 pp. 5542-5547, 2007.
- [159] J. Tang, Y. Shen, M. Radosz, and W. Sun, "Isothermal Carbon Dioxide Sorption in Poly(ionic liquid)s," *Ind. Eng. Chem. Res.*, vol. 48, pp. 9113-9118, 2009.
- [160] J. E. Bara, D. E. Camper, D. L. Gin, and R. D. Noble, "Room-Temperature Ionic Liquids and Composite Materials: Platform Technologies for CO₂ Capture," *Acc. Chem. Res.*, vol. 43, pp. 152-159, 2010.
- [161] X. Hu, J. Tang, A. Blasig, Y. Shen, and M. Radosz, "CO₂ permeability, diffusivity and solubility in polyethylene glycol-grafted polyionic membranes and their CO₂ selectivity relative to methane and nitrogen," *Journal of Membrane Science* vol. 281, pp. 130-138, 2006.

- [162] J. E. Bara, S. Lessmann, C. J. Gabriel, E. S. Hatakeyama, R. D. Noble, and D. L. Gin, "Synthesis and Performance of Polymerizable Room-Temperature Ionic Liquids as Gas Separation Membranes," *Ind. Eng. Chem. Res.*, vol. 46, pp. 5397-5404, 2007.
- [163] J. E. Bara, E. S. Hatakeyama, C. J. Gabriel, X. Zeng, S. Lessmann, D. L. Gin, and R. D. Noble, "Synthesis and light gas separations in cross-linked gemini room temperature ionic liquid polymer membranes " *Journal of Membrane Science*, vol. 316, pp. 186-191, 2008.
- [164] J. E. Bara, C. J. Gabriel, E. S. Hatakeyama, T. K. Carlisle, S. Lessmann, R. D. Noble, and D. L. Gin, "Improving CO₂ selectivity in polymerized room-temperature ionic liquid gas separation membranes through incorporation of polar substituents," *Journal of Membrane Science* vol. 321, 2008.
- [165] J. E. Bara, D. L. Gin, and R. D. Noble, "Effect of Anion on Gas Separation Performance of Polymer–Room-Temperature Ionic Liquid Composite Membranes," *Ind. Eng. Chem. Res.*, vol. 47, pp. 9919-9924, 2008.
- [166] J. E. Bara, R. D. Noble, and D. L. Gin, "Effect of “Free” Cation Substituent on Gas Separation Performance of Polymer–Room-Temperature Ionic Liquid Composite Membranes," *Ind. Eng. Chem. Res.* , vol. 48, pp. 4607-4610, 2009.
- [167] M. Yoshizawa and H. Ohno, "Molecular brush having molten salt domain for fast ion conduction," *Chem. Lett.*, vol. 28, pp. 889-890, 1999.
- [168] M. Yoshizawa, M. Hirao, K. Ito-Akita, and H. Ohno, "Ion conduction in zwitterionic-type molten salts and their polymers," *J. Mater. Chem.*, vol. 11, pp. 1057 - 1062, 2001.
- [169] H. L. Ricks-Laskoski and A. W. Snow, "Synthesis and Electric Field Actuation of an Ionic Liquid Polymer," *J. Am. Chem. Soc.* , vol. 128, pp. 12402-12403, 2006.

- [170] M. Morita, T. Shirai, N. Yoshimoto, and M. Ishikawa, "Ionic conductance behavior of polymeric gel electrolyte containing ionic liquid mixed with magnesium salt " *Journal of Power Sources*, vol. 139, pp. 351-355, 2005.
- [171] S. Seki, M. A. B. H. SUSAN, T. Kaneko, H. Tokuda, A. Noda, and M. Watanabe, "Distinct difference in ionic transport behavior in polymer electrolytes depending on the matrix polymers and incorporated salts," *J. phys. Chem. B*, vol. 109, pp. 3886-3892, 2005.
- [172] K.-S. Kim, S.-Y. Park, S. Choi, and H. Lee, "Ionic liquid–polymer gel electrolytes based on morpholinium salt and PVdF(HFP) copolymer " *Journal of Power Sources*, vol. 155, pp. 385-390, 2006.
- [173] B. Singh and S. S. Sekhon, "Polymer Electrolytes Based on Room Temperature Ionic Liquid: 2,3-Dimethyl-1-octylimidazolium Triflate," *J. Phys. Chem. B*, vol. 109, pp. 16539-16543, 2005.
- [174] J. J. Xu, H. Ye, and J. Huang, "Novel zinc ion conducting polymer gel electrolytes based on ionic liquids " *Electrochemistry Communications*, vol. 7, pp. 1309-1317 2005.
- [175] W. Ogihara, S. Washiro, H. Nakajima, and H. Ohno, "Effect of cation structure on the electrochemical and thermal properties of ion conductive polymers obtained from polymerizable ionic liquids " *Electrochimica Acta*, vol. 51, pp. 2614-2619, 2006.
- [176] H. JIANG and S. FANG, "New composite polymer electrolytes based on room temperature ionic liquids and polyether," *Polymers for advanced technologies* vol. 17, pp. 494-499, 2006.
- [177] Z. Li, Y. Liu, H. Liu, P. He, Q. Zhang, and J. Li, "Synthesis and ionic conductivity of polymeric ion gel containing room temperature ionic liquid and phosphotungstic acid " *Solid State Ionics* vol. 177, pp. 1281-1286, 2006.

- [178] L. T. Costa, R. L. Lavall, R. S. Borges, J. Rieumont, G. G. Silva, and M. C. C. Ribeiro, "Polymer electrolytes based on poly(ethylene glycol) dimethyl ether and the ionic liquid 1-butyl-3-methylimidazolium hexafluorophosphate: Preparation, physico-chemical characterization, and theoretical study," *Electrochimica Acta* vol. 53, pp. 1568-1574, 2007.
- [179] J.-W. Choi, G. Cheruvally, Y.-H. Kim, J.-K. Kim, J. Manuel, P. Raghavan, J.-H. Ahn, K.-W. Kim, H.-J. Ahn, D. S. Choi, and C. E. Song, "Poly(ethylene oxide)-based polymer electrolyte incorporating room-temperature ionic liquid for lithium batteries " *Solid State Ionics*, vol. 178, pp. 1235-1241, 2007.
- [180] W. Chen, H. Tang, Z. Ou, H. Wang, and Y. Yang, "Electrochemical behavior of ionically crosslinked polyampholytic gel electrolytes," *Electrochimica Acta* vol. 53, pp. 2065-2070, 2007.
- [181] C. Chauvin, F. Alloin, P. Judeinstein, D. Foscallo, and J.-Y. Sanchez, "Electrochemical and NMR characterizations of mixed polymer electrolytes based on oligoether sulfate and imide salts," *Electrochimica Acta* vol. 52, pp. 1240-1246, 2006.
- [182] J. Reiter, J. Vondr'ak, J. Mich'alek, and Z. Mi'cka, "Ternary polymer electrolytes with 1-methylimidazole ionic liquids and aprotic solvents," *Electrochimica Acta* vol. 52, pp. 1398-1408, 2006.
- [183] N. Matsumi, K. Sugai, M. Miyake, and H. Ohno, "Polymerized Ionic Liquids via Hydroboration Polymerization as Single Ion Conductive Polymer Electrolytes," *Macromolecules*, vol. 39, pp. 6924-6927, 2006.
- [184] B. Singh, M. S. Hundal, G.-G. Park, J.-S. Park, W.-Y. Lee, C.-S. Kim, K. Yamada, and S. S. Sekhon, "Non-aqueous polymer electrolytes containing room temperature ionic liquid: 2,3-dimethyl-1-octylimidazolium tetrafluoroborate " *Solid State Ionics*, vol. 178, pp. 1404-1410 2007.

- [185] F. Li, C. Shan, X. Bu, Y. Shen, G. Yang, and L. Niu, "Fabrication and electrochemical characterization of electrostatic assembly of polyelectrolyte-functionalized ionic liquid and Prussian blue ultrathin films " *Journal of Electroanalytical Chemistry* vol. 616, pp. 1-6, 2008.
- [186] H. Ohno, "Design of Ion Conductive Polymers Based on Ionic Liquids," *Macromolecular Symposia*, vol. 249-250, pp. 551 - 556, 2007.
- [187] H. Chen and Y. A. Elabd, "Polymerized Ionic Liquids: Solution Properties and Electrospinning," *Macromolecules*, vol. 42, pp. 3368-3373, 2009.
- [188] D. An, L. Wu, B.-G. Li, and S. Zhu, "Synthesis and SO₂ Absorption/Desorption Properties of Poly(1,1,3,3-tetramethylguanidine acrylate)," *Macromolecules*, vol. 40, pp. 3388-3393, 2007.
- [189] D. Chen, Q. Zhang, G. Wang, H. Zhang, and J. Li, "A novel composite polymer electrolyte containing room-temperature ionic liquids and heteropolyacids for dye-sensitized solar cells " *Electrochemistry Communications*, vol. 9, pp. 2755-2759, 2007.
- [190] B. Yu, F. Zhou, H. Hu, C. Wang, and W. Liu, "Synthesis and properties of polymer brushes bearing ionic liquid moieties," *Electrochimica Acta* vol. 53, pp. 487-494, 2007.
- [191] M. Cho, H. Seo, J. Nam, H. Choi, J. Koo, and Y. Lee, "High ionic conductivity and mechanical strength of solid polymer electrolytes based on NBR/ionic liquid and its application to an electrochemical actuator " *Sensors and Actuators B: Chemical*, vol. 128, pp. 70-74, 2007.
- [192] M. S.-P. López, D. Mecerreyes, E. López-Cabarcos, and B. López-Ruiz, "Amperometric glucose biosensor based on polymerized ionic liquid microparticles," *Biosensors and Bioelectronics*, vol. 21, pp. 2320-2328, 2006.

- [193] R. Marcilla, M. Sanchez-Paniagua, B. Lopez-Ruiz, E. Lopez-Cabarcos, E. Ochoteco, H. Grande, and D. Mecerreyes, "Synthesis and characterization of new polymeric ionic liquid microgels," *Journal of Polymer Science Part B: Polymer Physics*, vol. 44 pp. 3958 - 3965, 2006.
- [194] M. Radosz, Y. Shen, and H. Tang, "Polymers and copolymers of ionic liquids as radio frequency absorbing materials ". vol. WO2006053083, W. I. P. O., Ed. U.S.A, 2006.
- [195] S. M. Mwongela, A. Numan, N. L. Gill, R. A. Agbaria, and I. M. Warner, "Separation of Achiral and Chiral Analytes Using Polymeric Surfactants with Ionic Liquids as Modifiers in Micellar Electrokinetic Chromatography," *Anal. Chem.*, vol. 75, pp. 6089-6096, 2003.
- [196] S. A. A. Rizvi and S. A. Shamsi, "Synthesis, Characterization, and Application of Chiral Ionic Liquids and Their Polymers in Micellar Electrokinetic Chromatography," *Anal. Chem.*, vol. 78, pp. 7061-7069, 2006.
- [197] P. Cardiano, P. G. Mineo, F. Neri, S. L. Schiavo, and P. Piraino, "A new application of ionic liquids: hydrophobic properties of tetraalkylammonium-based poly(ionic liquid)s," *J. Mater. Chem.*, vol. 18, pp. 1253 - 1260, 2008.
- [198] in *Encyclopedia of Chemistry* vol. 4th Ed., D. M. Considine and G. D. Considine, Eds.: Van Nostrand Reinhold publisher, 1994.
- [199] J. McMurry and R. C. Fay, *Chemistry*: Prentice Hall, 2008.
- [200] J. Bicerano, *Prediction of polymer properties*, Third ed. New York: Marcel Dekker Inc., 2002.
- [201] N. Metropolis, A. W. Rosenbluth, M. N. Teller, and A. H. Teller, "Equation of state calculations for fast computing machines," *J. Chem. Phys*, vol. 21, pp. 1087-1092, 1953.

- [202] J. I. Siepmann and D. Frenkel, "Configurational bias Monte Carlo: a new sampling scheme for flexible chains," *Mol. Phys.*, vol. 75, pp. 59-70, 1992.
- [203] G. T. Hefter and R. P. T. Tomkins, *The experimental determination of solubilities.*: Wiley, 2003.
- [204] H. L. Clever and R. Battino, "The solubility of gases in liquids," *Techniques of Chemistry* vol. VIII: Solutions and Solubilities - Part 1, pp. 380- 441, 1975.
- [205] W. Ostwald, *Manual of Physico-chemical Measurements*. London: Macmillan, 1894.
- [206] P. Husson-Borg, V. Majer, and M. F. C. Gomes, "Solubilities of oxygen and carbon dioxide in butyl methyl imidazolium tetrafluoroborate as a function of temperature and at pressures close to atmospheric pressure," *Chem. Eng. Data*, vol. 48, pp. 480-485, 2003.
- [207] A. P. S. Kamps, D. Tuma, J. Z. Xia, and G. Maurer, "Solubility of CO₂ in the ionic liquid [bmim][PF₆]." *Chem. Eng. Data*, vol. 48, pp. 746-749, 2003.
- [208] A. Heintz, D. V. Kulikov, and S. P. Verevkin, "Thermodynamic properties of mixtures containing ionic liquids. Activity coefficients at infinite dilution of polar solutes in 4-methyl-N-butyl-pyridinium tetrafluoroborate using gas-liquid chromatography," *J. Chem. Thermodynamics*, vol. 34, pp. 1341-1347, 2002.
- [209] A. Heintz, J. K. Lehmann, and C. Wertz, "Thermodynamic properties of mixtures containing ionic liquids. 3. Liquid-liquid equilibria of binary mixtures of 1-ethyl-3-methylimidazolium bis(trifluoromethylsulfonyl)imide with propan-1-ol, butan-1-ol, and pentan-1-ol," *Chem. Eng. Data*, vol. 48, pp. 472-474, 2003.
- [210] A. Heintz, D. V. Kulikov, and S. P. Verevkin, "Thermodynamic properties of mixtures containing ionic liquids. 2. Activity coefficients at infinite dilution of

- hydrocarbons and polar solutes in 1-methyl-3-ethyl-imidazolium bis(trifluoromethyl-sulfonyl) amide and in 1,2-dimethyl-3-ethyl-imidazolium bis(trifluoromethyl-sulfonyl) amide using gas-liquid chromatography," *J. Chem. Eng. Data*, vol. 47 pp. 894-899, 2002.
- [211] A. Heintz, D. V. Kulikov, and S. P. Verevkin, "Thermodynamic properties of mixtures containing ionic liquids. 1. Activity coefficients at infinite dilution of alkanes, alkenes, and alkylbenzenes in 4-methyl-n-butylpyridinium tetrafluoroborate using gas-liquid chromatography.," *J. Chem. Eng. Data*, vol. 46, pp. 1526-1529, 2001.
- [212] W. David, T. M. Letcher, D. Ramjugernath, and J. D. Raal, "Activity coefficients of hydrocarbon solutes at infinite dilution in the ionic liquid, 1-methyl-3-octyl-imidazolium chloride from gas-liquid chromatography," *J. Chem. Thermodynamics* vol. 35, pp. 1335-1341, 2003.
- [213] T. M. Letcher, B. Soko, D. Ramjugernath, N. Deenadayalu, A. Nevines, and P. K. Naicker, " Activity coefficients at infinite dilution of organic solutes in 1-hexyl-3-methylimidazolium hexafluorophosphate from gas-liquid chromatography," *J. Chem. Eng. Data*, vol. 48, pp. 708-711, 2003.
- [214] "[http://www. Rubotherm.com.de](http://www.Rubotherm.com.de)."
- [215] N. M. Yunus, M. I. A. Mutalib, Z. Man, M. A. Bustam, and T. Murugesan, "Thermophysical properties of 1-alkylpyridinium bis(trifluoromethylsulfonyl)imide ionic liquid," *J. Chem. Thermodynamics*, vol. 42, pp. 491-495, 2010.
- [216] K. D. Pradhan, R. N. P. Choudhary, B. K. Samantaray, N. K. Karan, and R. S. Katiyar, "Effect of Plasticizer on Structural and Electrical Properties of Polymer Nanocomposite Electrolytes," *Int. J. Electrochem. Sci.*, vol. 2, pp. 861 - 871, 2007.

- [217] D. R. Lide, *CRC Handbook of Chemistry and Physics*, Internet version 2005, www.hcbnethbase.com ed. Boca Raton: CRC Press 2005.
- [218] J. M. Prausnitz, R. N. Lichtenthaler, and E. G. Azevedo, *Thermodynamics of Fluid-Phase Equilibria*, 3rd ed. Upper Saddle River: NJ: Prentice Hall, 1999.
- [219] D. E. Stogryn and A. P. Stogryn, "Molecular multiple moments," *Mol. Phys.*, vol. 11, pp. 371-393, 1966.
- [220] I. Dolamica and T. Bürgi, "Photocatalysis of dicarboxylic acids over TiO₂: An in situ ATR-IR study," *Journal of Catalysis*, vol. Volume 248, pp. 268-276, 10 June 2007.

PUBLICATIONS

- [1] C. D. Wilfred, M. I. A. Mutalib, and M. O. H. Ahmed, "polymerised Ionic Liquids with Improved Properties and Methods for Enhanced Sorption of Carbon Dioxide." vol. PI 2011001246, U. T. PETRONAS, Ed. Malaysia, 2011.

APPENDIX A

NMR SPECTRUM FOR PILS AND THEIR MONOMERS

This appendix includes the NMR spectrums for the synthesized pILs and some of their corresponding monomers.

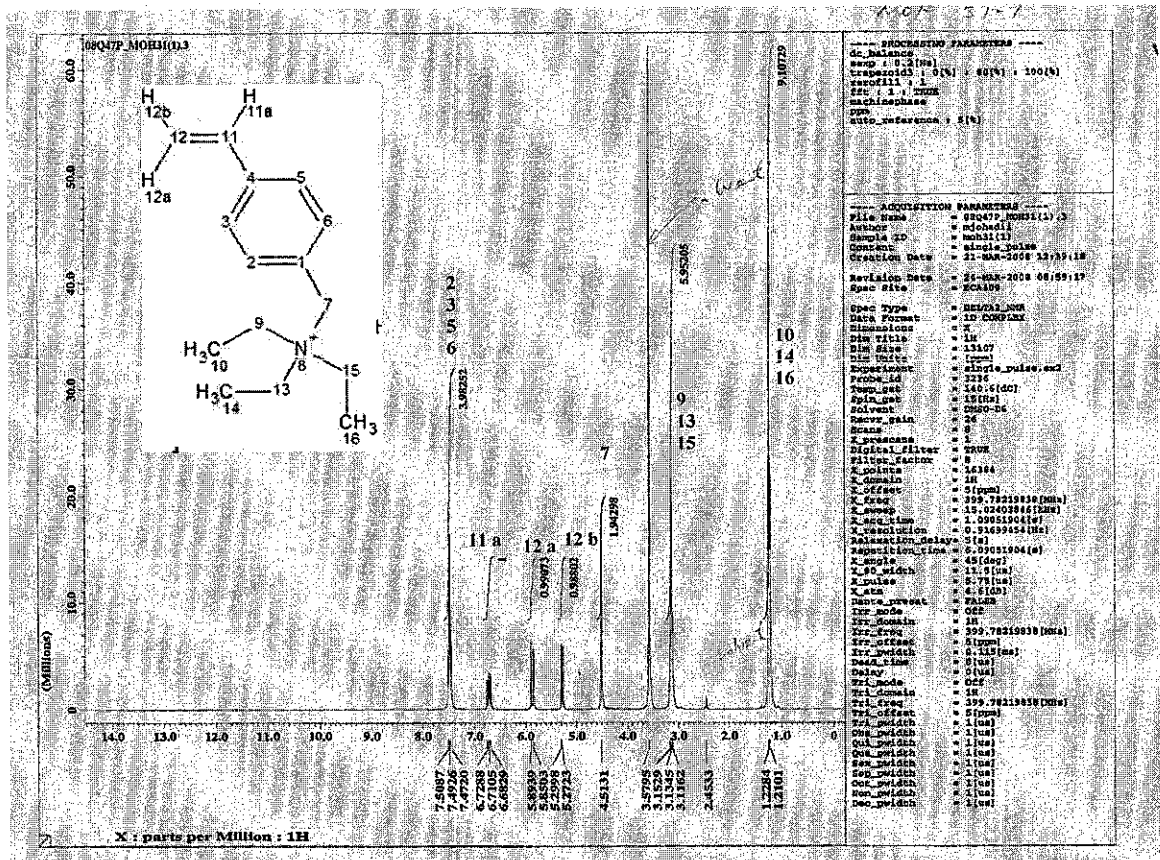


Fig. A- 1: ¹H NMR for [VBTEA] [Cl] Monomer

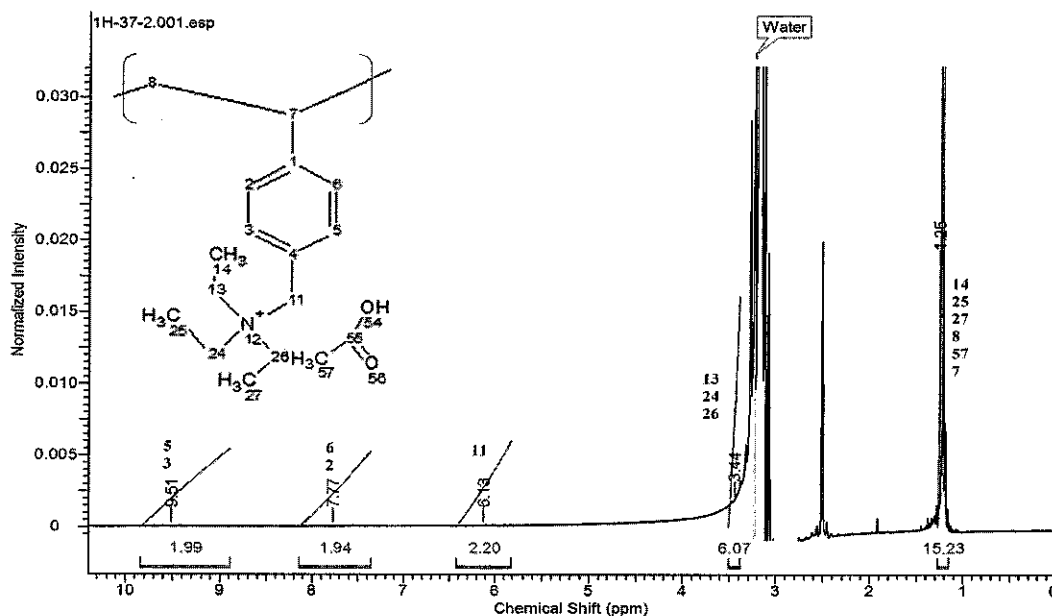


Fig. A- 6: ¹HNMR for p[VBTEA][CH₃COO]

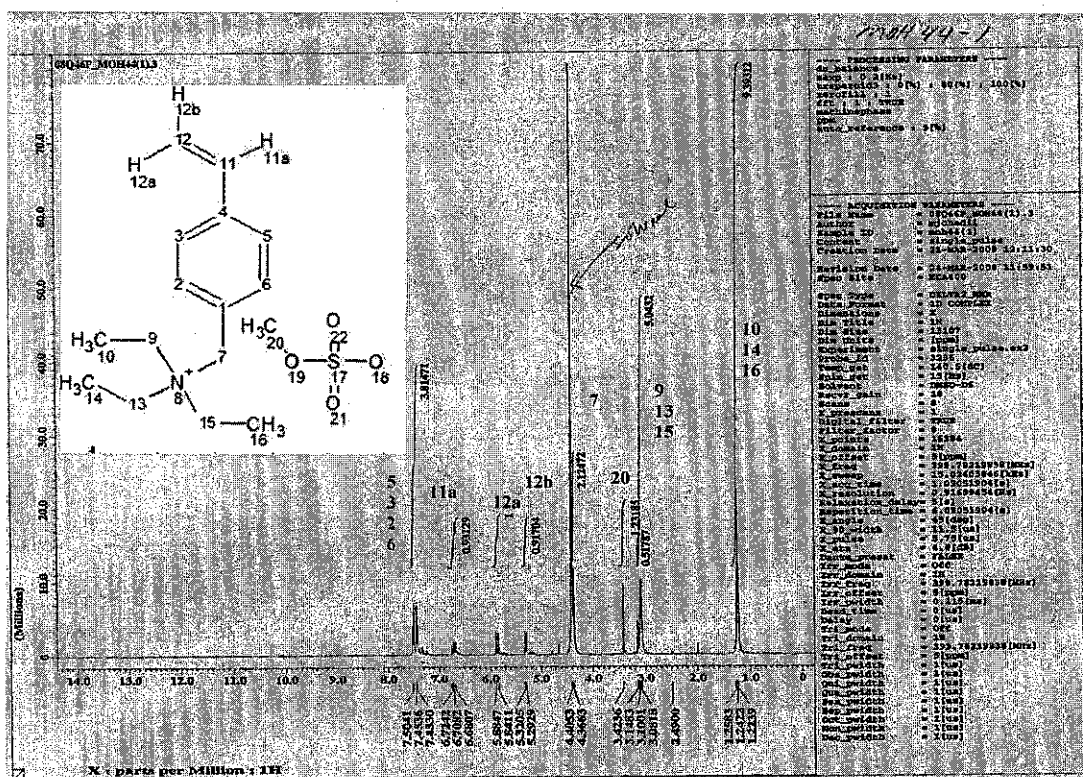


Fig. A- 7: ¹HNMR for [VBTEA][CH₃O₄S] Monomer

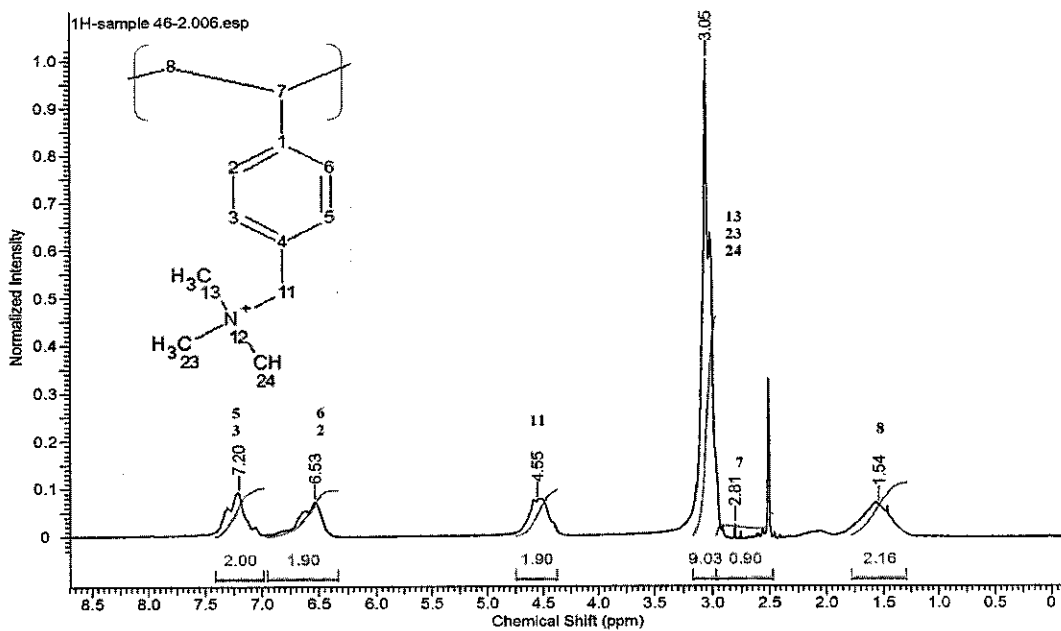


Fig. A- 12: ¹HNMR for p[VBTMA][NO₃]

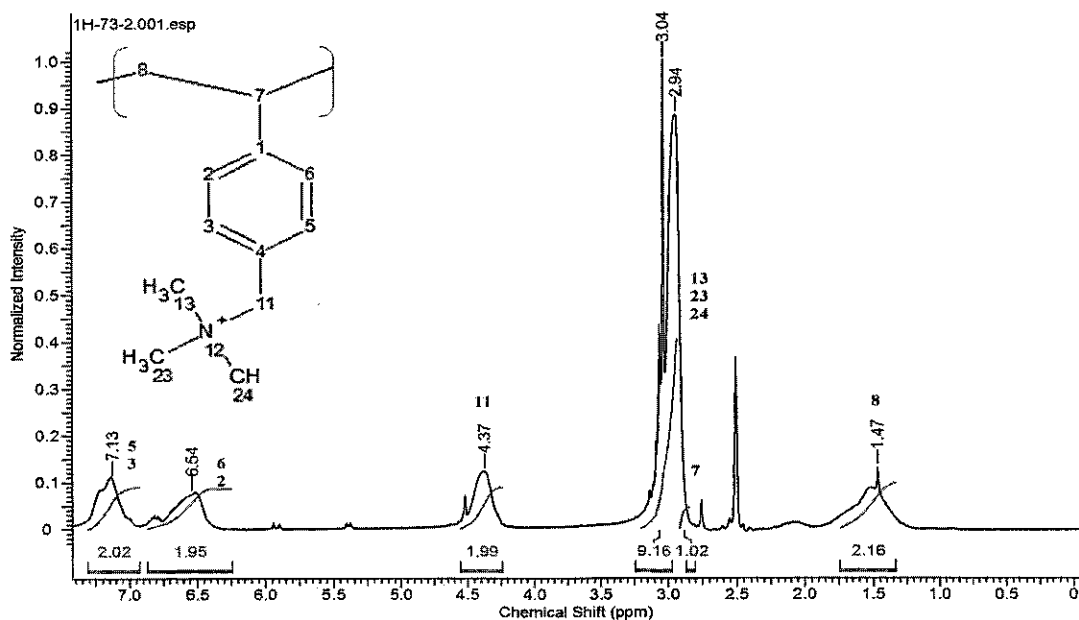


Fig. A- 13: ¹HNMR for p[VBTMA][F₃C-SO₃] (TFMS)

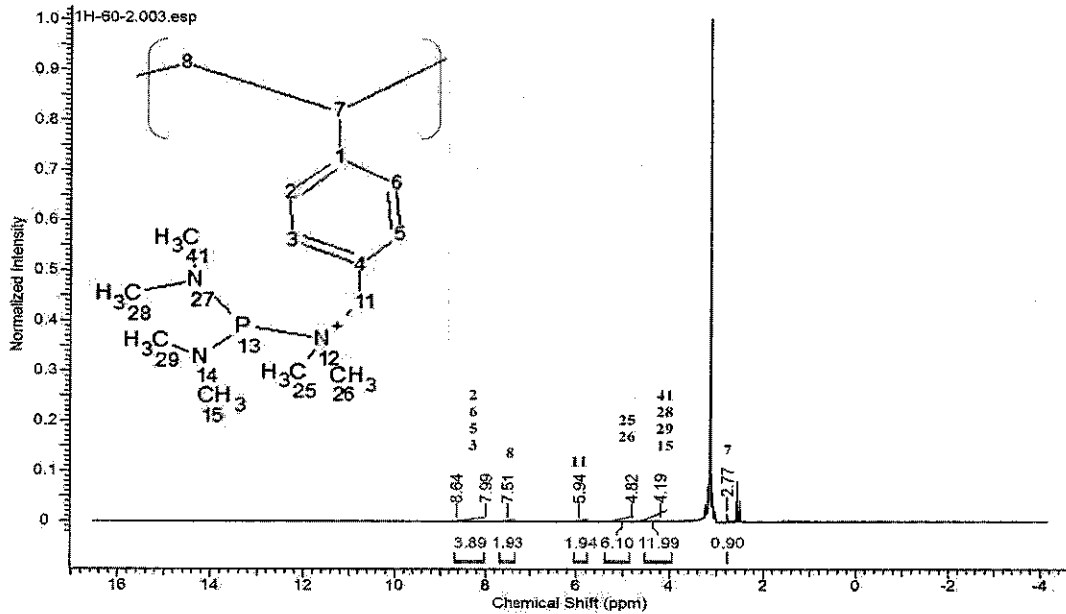


Fig. A- 18: ^1H NMR for p[bDMADMVBP][Cl]

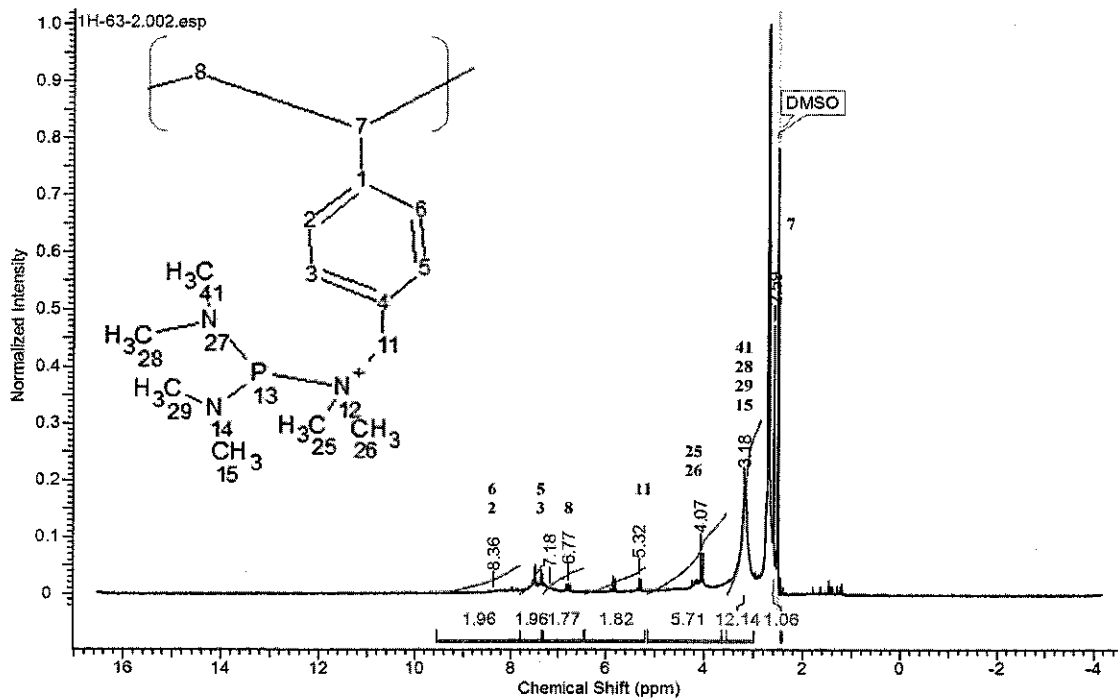


Fig. A- 19: ^1H NMR for p[bDMADMVBP][NO₃]

APPENDIX B

SEM MICROGRAPHS OF PILS

This appendix includes the SEM micrographs for the synthesized pILs.

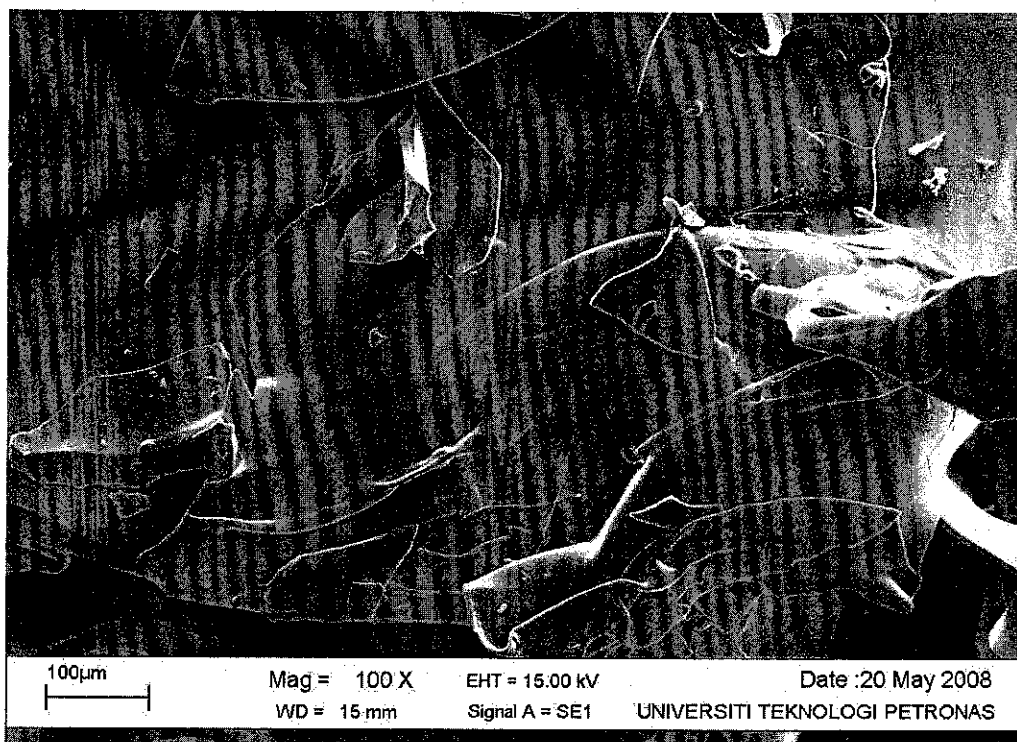


Fig. B- 1: SEM micrograph of p[VBTEA][Cl]

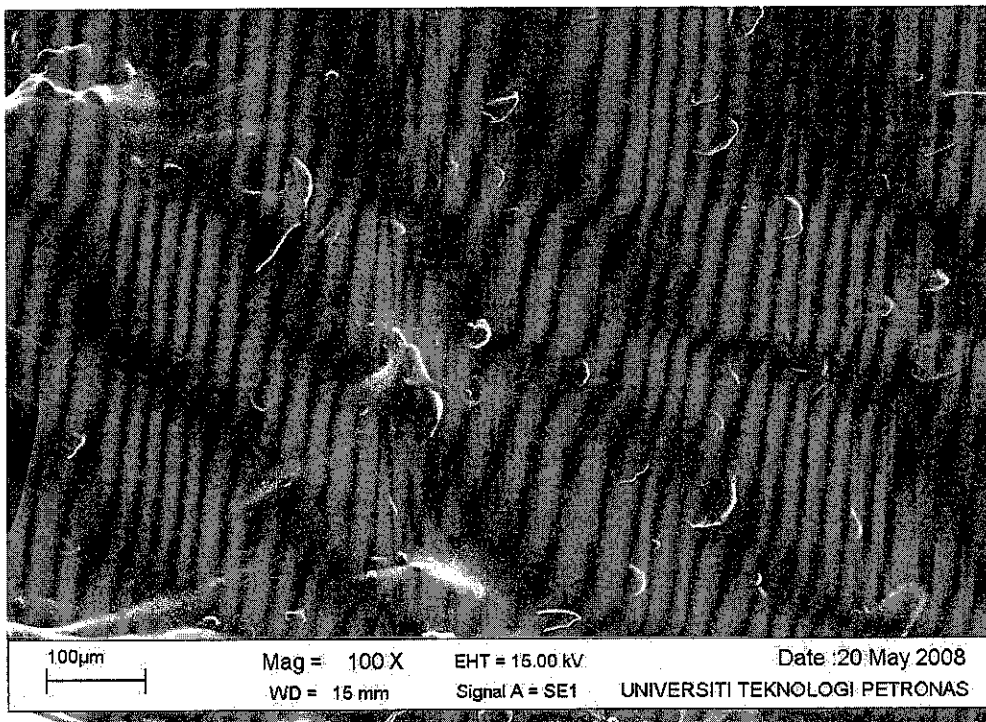


Fig. B- 2: SEM micrograph of p[VBTEA][NO₃]

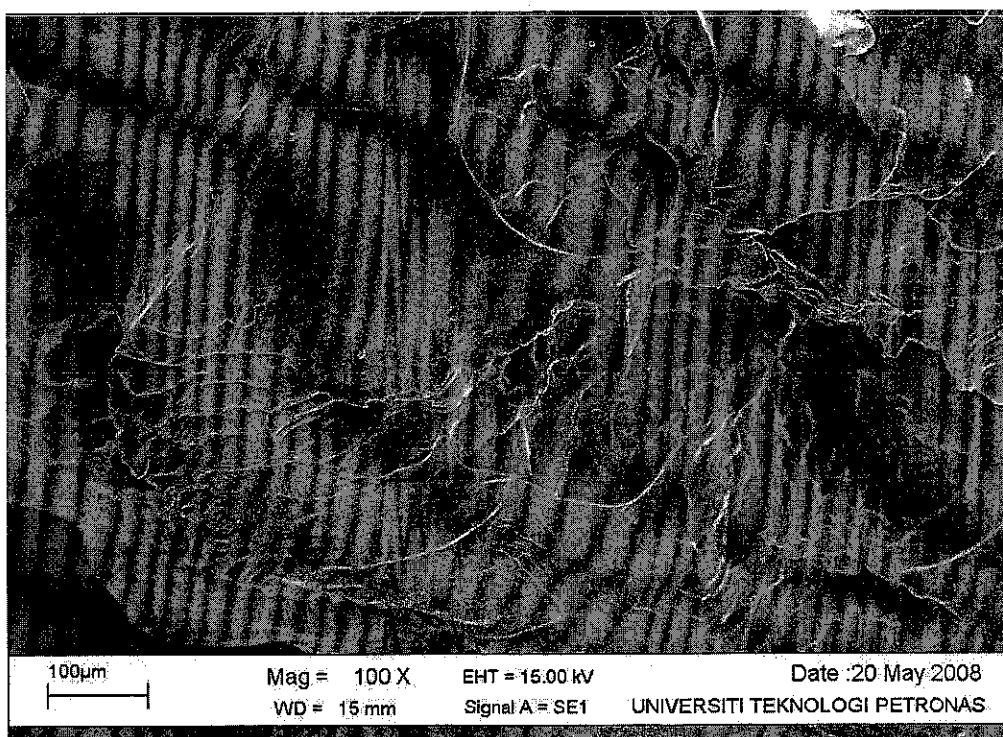


Fig. B- 3: SEM micrograph of p[VBTEA][CH₃COO]

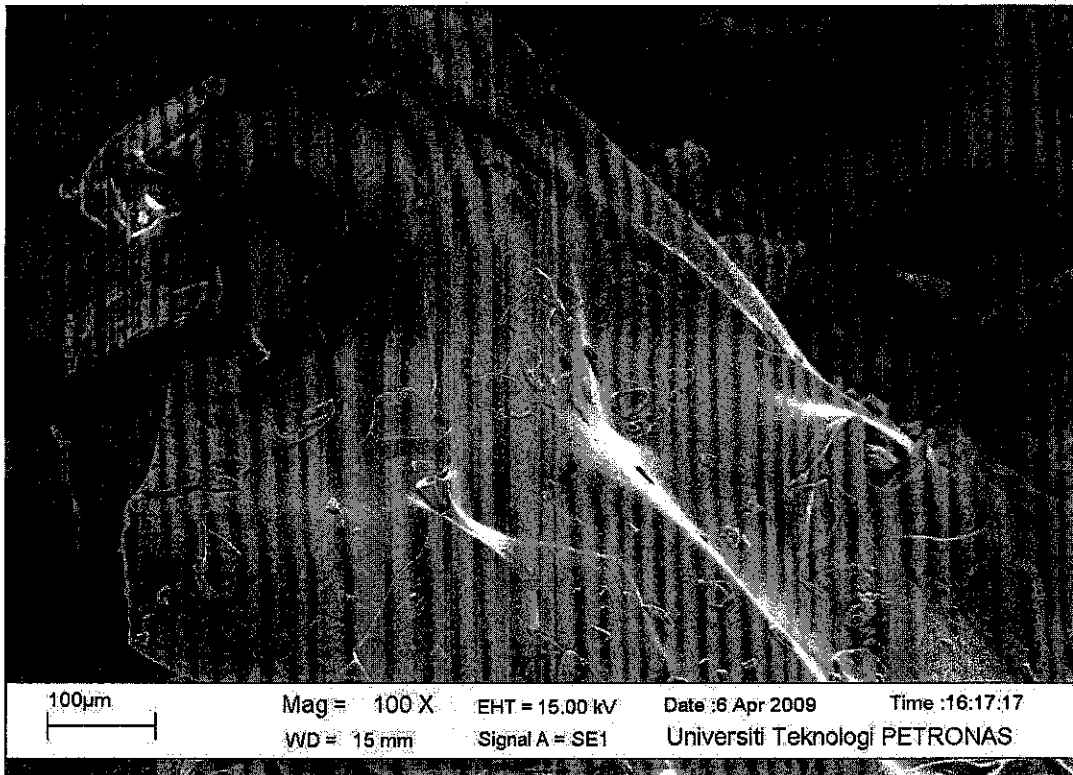


Fig. B- 4: SEM micrograph of p[VBTEA][CH₃O₄S]

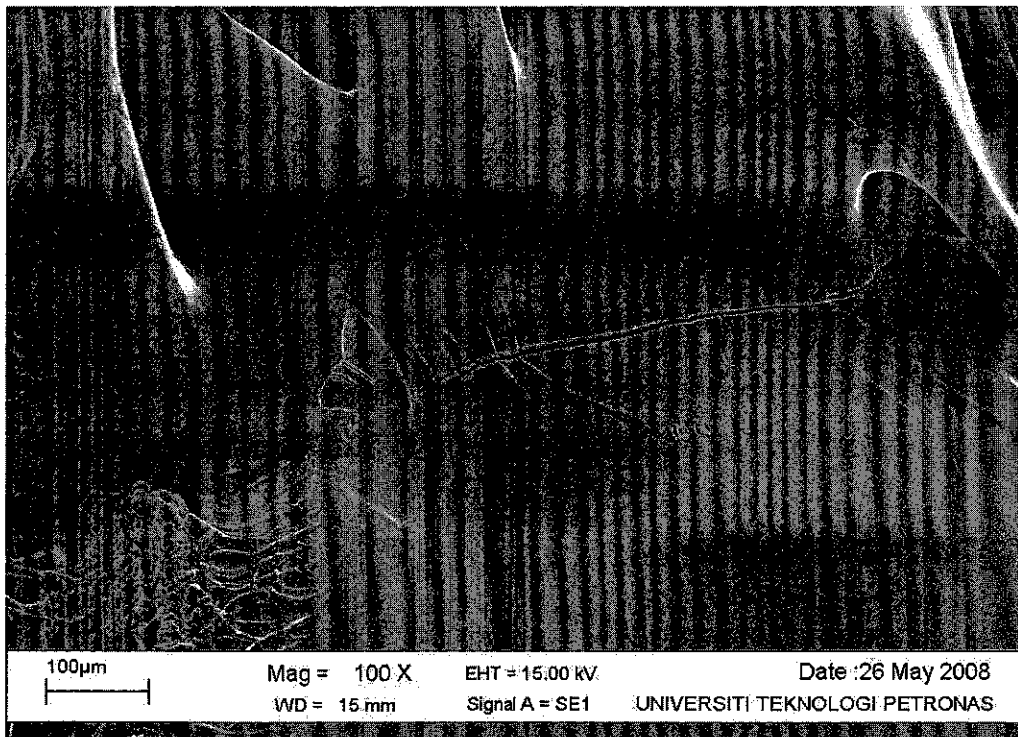


Fig. B- 5: SEM micrograph of p[VBTMA][Cl]

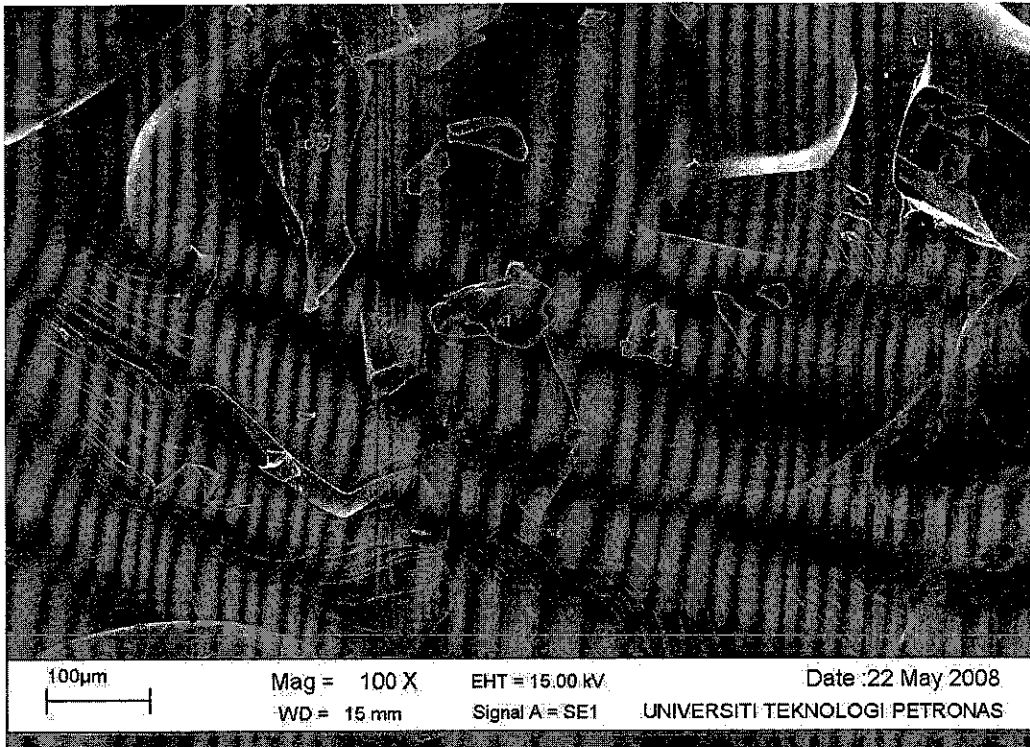


Fig. B- 6: SEM micrograph of p[VBTMA][NO₃]

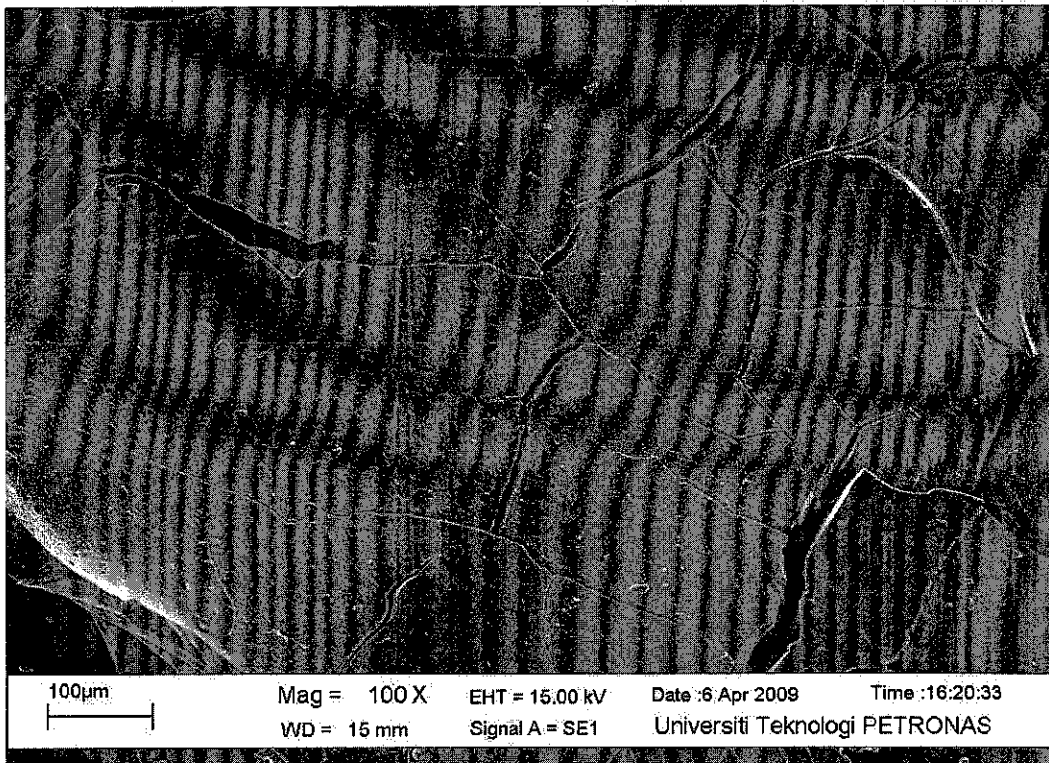


Fig. B- 7: SEM micrograph of p[METMA][Cl]

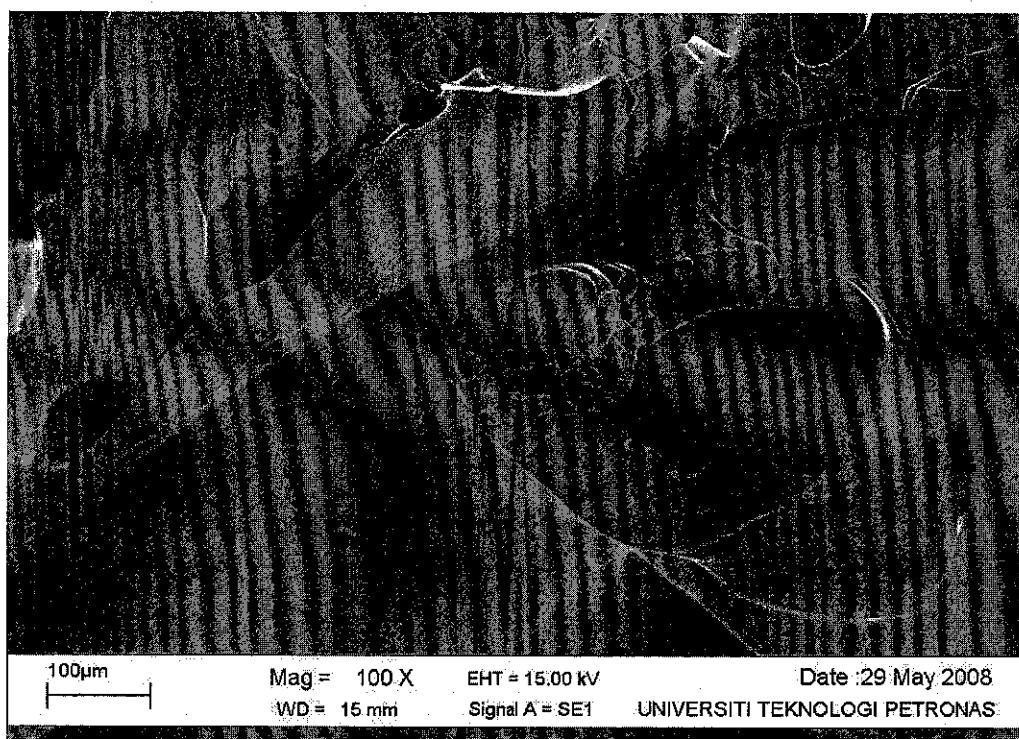


Fig. B- 8: SEM micrograph of p[METMA][NO₃]

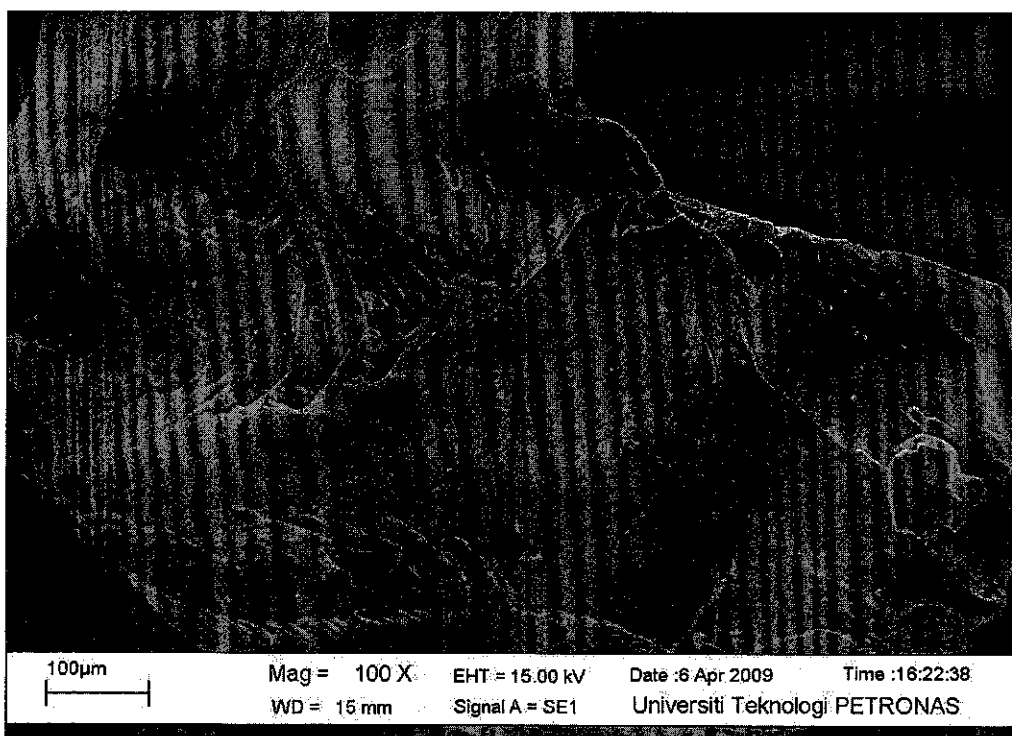


Fig. B- 9: SEM micrograph of p[bDMADMVBP][Cl]

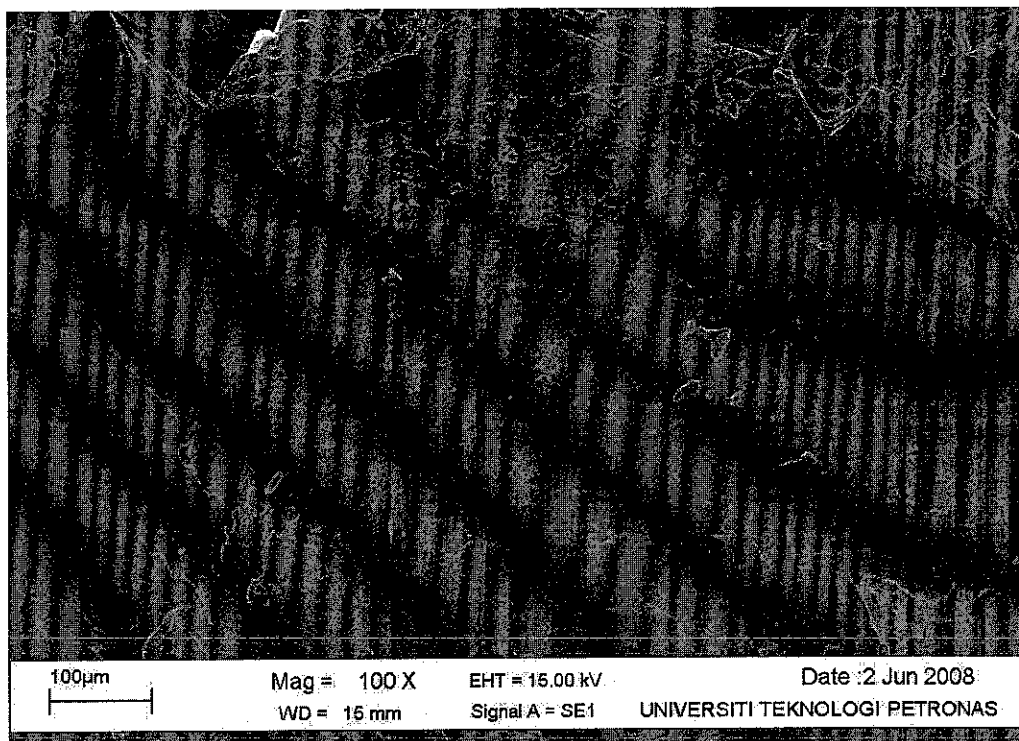


Fig. B- 10: SEM micrograph of p[bDMADMVBP][NO₃]

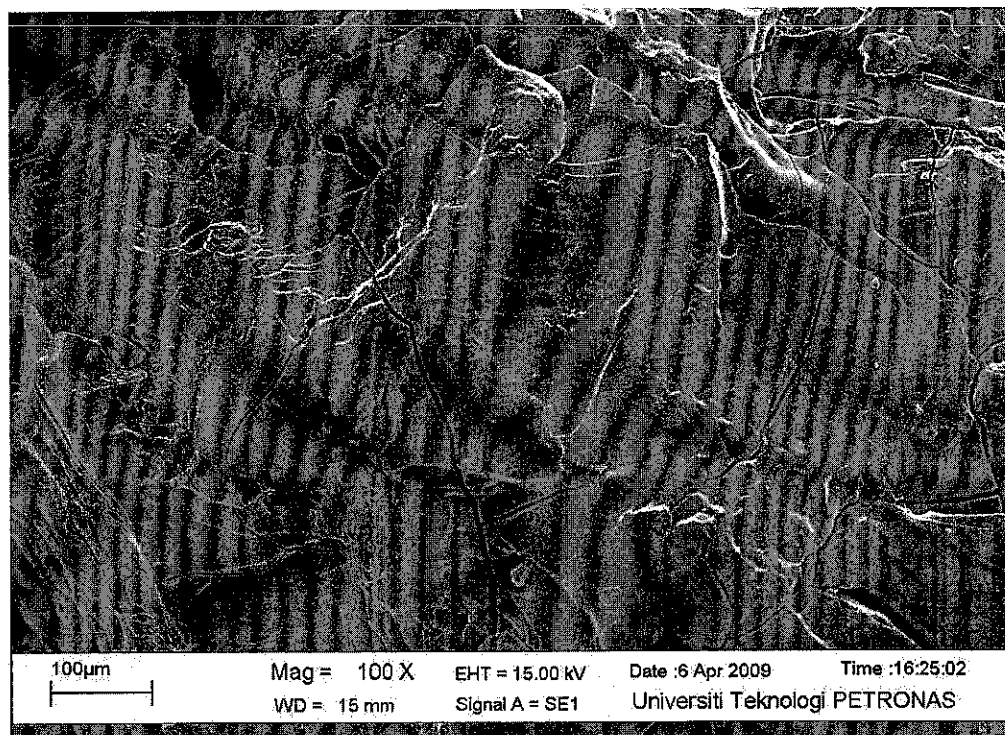


Fig. B- 11: SEM micrograph of p[tDMAVBP][Cl]

APPENDIX C

DATA FOR SORPTION MEASUREMENT

Table C- 1: CO₂ sorption data for [VBTMA][Cl] monomer at 10 bar and 25°C

Real Time, [min]	CO ₂ weight, [gm]	CO ₂ weight for 1 gm, [gm]	CO ₂ weight for one monomer, [gm]	No of CO ₂ moles, [mole]	Mole%
0	0	0	0	0	0
8.32	0.01332	0.01705	3.61504	0.08216	8.22
16.18	0.01280	0.01639	3.47533	0.07898	7.90
24.03	0.01280	0.01639	3.47499	0.07898	7.90
31.88	0.01251	0.01602	3.39632	0.07719	7.72
39.75	0.01242	0.01590	3.37103	0.07661	7.66
55.48	0.01237	0.01583	3.35667	0.07629	7.63
71.21	0.01232	0.01577	3.34387	0.07600	7.60
86.9	0.01229	0.01573	3.33524	0.07580	7.58
102.63	0.01229	0.01573	3.33461	0.07579	7.58
134.1	0.01227	0.01571	3.32999	0.07568	7.57
157.7	0.01228	0.01573	3.33381	0.07577	7.58

Table C- 2: CO₂ sorption data for p[VBTMA][Cl] at 10 bar and 25°C

Real Time, [min]	CO ₂ weight, [gm]	CO ₂ weight for 1 gm, [gm]	CO ₂ weight for one monomer, [gm]	No of CO ₂ moles, [mole]	Mole%
0	0	0	0	0	0
8.3	0.01865	0.03908	8.28558	0.18831	18.8
16.2	0.02137	0.04479	9.49490	0.21579	21.6
24.0	0.02166	0.04540	9.62536	0.21876	21.9
31.9	0.02180	0.04569	9.68596	0.22014	22.0
39.7	0.02190	0.04591	9.73233	0.22119	22.1
55.4	0.02205	0.04621	9.79548	0.22262	22.3
71.2	0.02226	0.04665	9.88881	0.22475	22.5
86.9	0.02238	0.04691	9.94549	0.22603	22.6
102.6	0.02247	0.04709	9.98353	0.22690	22.7
118.3	0.02257	0.04729	10.02651	0.22788	22.8
149.8	0.02267	0.04752	10.07428	0.22896	22.9
181.3	0.02281	0.04780	10.13376	0.23031	23.0
212.7	0.02296	0.04813	10.20257	0.23188	23.2
244.2	0.02309	0.04839	10.25806	0.23314	23.3
275.7	0.02304	0.04829	10.23712	0.23266	23.3
511.7	0.02305	0.04830	10.24061	0.23274	23.3

Table C- 3: CO₂ sorption data for p[VBTEA][NO₃] Mw 11518, at 10 bar and 25°C

Real Time, [min]	CO ₂ weight, [gm]	CO ₂ weight for 1 gm, [gm]	CO ₂ weight for one monomer, [gm]	No of CO ₂ moles, [mole]	Mole%
0	0	0	0	0	0
24.4	0.00686	0.01126	3.17844	0.07224	7.22
31.9	0.00685	0.01123	3.17182	0.07209	7.21
39.8	0.00704	0.01154	3.25861	0.07406	7.41
48.0	0.00734	0.01204	3.40062	0.07729	7.73
55.1	0.00764	0.01253	3.53716	0.08039	8.04
71.5	0.00818	0.01340	3.78524	0.08603	8.60
87.3	0.00871	0.01428	4.03133	0.09162	9.16
102.3	0.00910	0.01492	4.21459	0.09579	9.58
118.4	0.00955	0.01566	4.42166	0.10049	10.05
149.5	0.01022	0.01676	4.73171	0.10754	10.75
181.7	0.01075	0.01763	4.97863	0.11315	11.32
212.5	0.01118	0.01833	5.17493	0.11761	11.76
244.6	0.01151	0.01887	5.32773	0.12108	12.11
276.1	0.01185	0.01943	5.48693	0.12470	12.47
307.2	0.01209	0.01982	5.59839	0.12724	12.72
338.3	0.01236	0.02026	5.72209	0.13005	13.00
370.1	0.01260	0.02066	5.83557	0.13263	13.26
393.4	0.01267	0.02077	5.86486	0.13329	13.33
433.1	0.01284	0.02105	5.94461	0.13510	13.51
457.0	0.01300	0.02131	6.01758	0.13676	13.68
488.5	0.01305	0.02140	6.04415	0.13737	13.74
558.9	0.01335	0.02189	6.18181	0.14050	14.05
661.2	0.01361	0.02231	6.29976	0.14318	14.32
763.6	0.01383	0.02267	6.40169	0.14549	14.55
858.2	0.01402	0.02299	6.49303	0.14757	14.76
960.7	0.01426	0.02339	6.60463	0.15011	15.01
1055.2	0.01436	0.02355	6.65101	0.15116	15.12
1157.6	0.01444	0.02368	6.68632	0.15196	15.20
1260.0	0.01455	0.02386	6.73735	0.15312	15.31
1362.5	0.01456	0.02387	6.74206	0.15323	15.32
1425.5	0.01465	0.02401	6.78123	0.15412	15.41

Table C- 4: CO₂ sorption data for p[VBTEA][NO₃] Mw 2153, at 10 bar and 25°C

Real Time, [min]	CO ₂ weight, [gm]	CO ₂ weight for 1 gm, [gm]	CO ₂ weight for one monomer, [gm]	No of CO ₂ moles, [mole]	Mole%
0	0	0	0	0	0
8.3	0.00516	0.00969	2.73669	0.06220	6.22
16.2	0.00567	0.01065	3.00686	0.06834	6.83
24.0	0.00606	0.01138	3.21264	0.07301	7.30
31.9	0.00647	0.01215	3.43207	0.07800	7.80
39.8	0.00680	0.01277	3.60695	0.08198	8.20
55.5	0.00737	0.01384	3.90767	0.08881	8.88
71.2	0.00789	0.01482	4.18548	0.09512	9.51
86.9	0.00823	0.01546	4.36713	0.09925	9.93
102.6	0.00862	0.01619	4.57251	0.10392	10.39
142.0	0.00936	0.01758	4.96474	0.11283	11.28
173.4	0.00971	0.01824	5.14974	0.11704	11.70
212.8	0.01011	0.01900	5.36577	0.12195	12.19
244.2	0.01035	0.01945	5.49198	0.12482	12.48
307.1	0.01083	0.02034	5.74485	0.13056	13.06
362.2	0.01117	0.02099	5.92643	0.13469	13.47
409.4	0.01139	0.02139	6.04048	0.13728	13.73
464.5	0.01159	0.02178	6.14923	0.13976	13.98
511.7	0.01176	0.02209	6.23795	0.14177	14.18
558.9	0.01191	0.02238	6.32013	0.14364	14.36
614.0	0.01207	0.02268	6.40549	0.14558	14.56
661.2	0.01214	0.02281	6.44123	0.14639	14.64
708.4	0.01222	0.02295	6.48237	0.14733	14.73
763.6	0.01235	0.02320	6.55255	0.14892	14.89
810.9	0.01239	0.02328	6.57385	0.14941	14.94
858.2	0.01246	0.02341	6.61087	0.15025	15.02
913.4	0.01250	0.02349	6.63220	0.15073	15.07
960.6	0.01254	0.02357	6.65489	0.15125	15.12
1007.9	0.01259	0.02365	6.67995	0.15182	15.18
1063.0	0.01262	0.02371	6.69468	0.15215	15.22
1110.3	0.01266	0.02379	6.71708	0.15266	15.27
1157.5	0.01268	0.02382	6.72650	0.15288	15.29
1212.7	0.01272	0.02390	6.74891	0.15338	15.34
1236.3	0.01275	0.02395	6.76217	0.15369	15.37

Table C- 5: CO₂ sorption data for p[VBTEA][Cl] at 10 bar and 25°C

Real Time, [min]	CO ₂ weight, [gm]	CO ₂ weight for 1 gm, [gm]	CO ₂ weight for one monomer, [gm]	No of CO ₂ moles, [mole]	Mole%
0	0	0	0	0	0
24.7	0.01012	0.02605	6.61687	0.15038	15.0
32.6	0.01031	0.02655	6.74402	0.15327	15.3
40.5	0.01056	0.02719	6.90753	0.15699	15.7
48.3	0.01089	0.02804	7.12118	0.16185	16.2
56.2	0.01110	0.02857	7.25707	0.16493	16.5
71.9	0.01148	0.02955	7.50668	0.17061	17.1
87.6	0.01171	0.03015	7.65784	0.17404	17.4
103.4	0.01190	0.03065	7.78412	0.17691	17.7
119.1	0.01207	0.03108	7.89549	0.17944	17.9
134.8	0.01227	0.03159	8.02260	0.18233	18.2
166.3	0.01239	0.03191	8.10534	0.18421	18.4
197.7	0.01259	0.03241	8.23252	0.18710	18.7
229.2	0.01268	0.03266	8.29446	0.18851	18.9
260.7	0.01274	0.03281	8.33389	0.18941	18.9
292.1	0.01282	0.03302	8.38673	0.19061	19.1
355.0	0.01290	0.03322	8.43811	0.19178	19.2
410.1	0.01296	0.03337	8.47483	0.19261	19.3
473.0	0.01298	0.03343	8.49029	0.19296	19.3
536.0	0.01302	0.03354	8.51809	0.19359	19.4
583.3	0.01304	0.03357	8.52682	0.19379	19.4
630.5	0.01305	0.03361	8.53645	0.19401	19.4

Table C- 6 CO₂ sorption data for p[bDMADMVBP][Cl] at 10 bar and 25°C

Real Time, [min]	CO ₂ weight, [gm]	CO ₂ weight for 1 gm, [gm]	CO ₂ weight for one monomer, [gm]	No of CO ₂ moles, [mole]	Mole%
0	0	0	0	0	0
8.3	0.00702	0.01058	3.34230	0.07596	8.3
16.2	0.01181	0.01778	5.62004	0.12773	16.2
24.0	0.01163	0.01751	5.53345	0.12576	24.0
31.9	0.01192	0.01795	5.67337	0.12894	31.9
39.7	0.01224	0.01844	5.82597	0.13241	39.7
47.6	0.01254	0.01890	5.97117	0.13571	47.6
63.3	0.01315	0.01981	6.25840	0.14224	63.3
79.0	0.01369	0.02061	6.51401	0.14805	79.0
94.7	0.01417	0.02134	6.74395	0.15327	94.7
110.4	0.01464	0.02205	6.96927	0.15839	110.4
141.9	0.01548	0.02332	7.36794	0.16745	141.9
173.4	0.01611	0.02426	7.66637	0.17424	173.4
204.8	0.01667	0.02512	7.93652	0.18038	204.8
236.3	0.01717	0.02586	8.17190	0.18572	236.3
267.8	0.01766	0.02660	8.40651	0.19106	267.8
330.7	0.01841	0.02773	8.76212	0.19914	330.7
393.6	0.01914	0.02883	9.11053	0.20706	393.6
448.6	0.01960	0.02952	9.32828	0.21201	448.6
511.6	0.02012	0.03031	9.57909	0.21771	511.6
566.8	0.02053	0.03093	9.77239	0.22210	566.8
653.3	0.02101	0.03164	9.99916	0.22725	653.3
747.9	0.02149	0.03237	10.23047	0.23251	747.9
850.3	0.02185	0.03291	10.39877	0.23634	850.3
952.8	0.02221	0.03346	10.57250	0.24028	952.8
1047.3	0.02250	0.03390	10.71126	0.24344	1047.3
1149.8	0.02284	0.03440	10.86977	0.24704	1149.8
1252.2	0.02311	0.03480	10.99805	0.24996	1252.2
1346.8	0.02327	0.03505	11.07541	0.25171	1346.8
1449.2	0.02344	0.03531	11.15847	0.25360	1449.2
1551.8	0.02360	0.03554	11.23105	0.25525	1551.8
1654.3	0.02385	0.03593	11.35334	0.25803	1654.3
1748.8	0.02403	0.03620	11.43807	0.25996	1748.8
1851.4	0.02411	0.03631	11.47404	0.26077	1851.4
1953.8	0.02431	0.03662	11.57161	0.26299	1953.8
2048.4	0.02439	0.03674	11.60876	0.26384	2048.4
2150.9	0.02443	0.03680	11.62990	0.26432	2150.9
2253.4	0.02453	0.03695	11.67511	0.26534	2253.4
2348.1	0.02465	0.03714	11.73535	0.26671	2348.1

2450.8	0.02478	0.03733	11.79603	0.26809	2450.8
2553.4	0.02488	0.03747	11.84170	0.26913	2553.4
2648.2	0.02492	0.03754	11.86365	0.26963	2648.2
2750.8	0.02501	0.03767	11.90289	0.27052	2750.8
2853.5	0.02507	0.03776	11.93192	0.27118	2853.5
2948.3	0.02506	0.03774	11.92599	0.27105	2948.3
3051.1	0.02512	0.03784	11.95714	0.27175	3051.1
3153.8	0.02519	0.03795	11.99193	0.27254	3153.8
3248.7	0.02524	0.03802	12.01335	0.27303	3248.7
3351.5	0.02541	0.03827	12.09352	0.27485	3351.5
3454.3	0.02541	0.03828	12.09590	0.27491	3454.3
3549.4	0.02546	0.03835	12.11992	0.27545	3549.4

Table C- 7: CO₂ sorption data for p[tDMAVBP][Cl] at 10 bar and 25°C

Real Time, [min]	CO ₂ weight, [gm]	CO ₂ weight for 1 gm, [gm]	CO ₂ weight for one monomer, [gm]	No of CO ₂ moles, [mole]	Mole%
0	0	0	0	0	0
16.2	0.00711	0.00903	2.85477	0.06488	6.5
24.0	0.00787	0.01001	3.16220	0.07187	7.2
31.9	0.00862	0.01096	3.46237	0.07869	7.9
39.8	0.00920	0.01169	3.69433	0.08396	8.4
47.6	0.00969	0.01232	3.89390	0.08850	8.8
63.3	0.01056	0.01343	4.24363	0.09645	9.6
79.0	0.01128	0.01434	4.53281	0.10302	10.3
94.8	0.01191	0.01514	4.78555	0.10876	10.9
110.5	0.01250	0.01589	5.02223	0.11414	11.4
142.0	0.01345	0.01710	5.40387	0.12282	12.3
165.6	0.01413	0.01796	5.67560	0.12899	12.9
197.0	0.01483	0.01885	5.95651	0.13538	13.5
228.5	0.01542	0.01961	6.19556	0.14081	14.1
260.0	0.01593	0.02025	6.39971	0.14545	14.5
307.1	0.01657	0.02106	6.65540	0.15126	15.1
362.2	0.01720	0.02187	6.91132	0.15708	15.7
409.4	0.01765	0.02244	7.09212	0.16118	16.1
456.6	0.01802	0.02291	7.23941	0.16453	16.5
511.7	0.01842	0.02342	7.40021	0.16819	16.8
558.9	0.01875	0.02384	7.53365	0.17122	17.1
606.1	0.01896	0.02411	7.61806	0.17314	17.3
661.2	0.01924	0.02447	7.73158	0.17572	17.6
708.4	0.01943	0.02470	7.80544	0.17740	17.7
755.7	0.01959	0.02491	7.87210	0.17891	17.9

810.9	0.01980	0.02517	7.95484	0.18079	18.1
858.1	0.01997	0.02539	8.02305	0.18234	18.2
905.4	0.02017	0.02564	8.10183	0.18413	18.4
960.6	0.02037	0.02590	8.18508	0.18602	18.6
1007.9	0.02047	0.02603	8.22510	0.18693	18.7
1063.0	0.02054	0.02611	8.25113	0.18753	18.8
1110.3	0.02059	0.02618	8.27215	0.18800	18.8
1157.6	0.02066	0.02627	8.30219	0.18869	18.9
1212.7	0.02074	0.02637	8.33241	0.18937	18.9
1260.0	0.02081	0.02646	8.36054	0.19001	19.0
1307.3	0.02090	0.02658	8.39848	0.19087	19.1
1362.4	0.02098	0.02668	8.42991	0.19159	19.2
1409.7	0.02102	0.02672	8.44491	0.19193	19.2
1457.1	0.02105	0.02676	8.45536	0.19217	19.2
1512.3	0.02091	0.02659	8.40227	0.19096	19.1
1559.6	0.02106	0.02677	8.45985	0.19227	19.2
1606.9	0.02113	0.02687	8.48934	0.19294	19.3
1662.0	0.02123	0.02699	8.52896	0.19384	19.4
1709.3	0.02129	0.02707	8.55307	0.19439	19.4

Table C- 8: CO₂ sorption data for p[VBTMA][NO₃] at 10 bar and 25°C

Real Time, [min]	CO ₂ weight, [gm]	CO ₂ weight for 1 gm, [gm]	CO ₂ weight for one monomer, [gm]	No of CO ₂ moles, [mole]	Mole%
0	0	0	0	0	0
8.3	0.00319	0.00532	1.27220	0.02891	2.9
16.2	0.00625	0.01044	2.49480	0.05670	5.7
24.0	0.00778	0.01300	3.10641	0.07060	7.1
31.9	0.00876	0.01464	3.49816	0.07950	8.0
39.7	0.00949	0.01585	3.78869	0.08611	8.6
47.6	0.01014	0.01694	4.04823	0.09201	9.2
63.3	0.01123	0.01876	4.48248	0.10187	10.2
79.1	0.01216	0.02031	4.85477	0.11034	11.0
94.8	0.01283	0.02144	5.12359	0.11645	11.6
110.5	0.01356	0.02265	5.41423	0.12305	12.3
126.3	0.01417	0.02367	5.65773	0.12858	12.9
189.2	0.01592	0.02660	6.35858	0.14451	14.5
252.2	0.01720	0.02873	6.86679	0.15606	15.6
307.2	0.01812	0.03028	7.23686	0.16447	16.4
370.2	0.01889	0.03157	7.54438	0.17146	17.1
433.1	0.01945	0.03249	7.76616	0.17650	17.7
535.4	0.02032	0.03395	8.11440	0.18442	18.4
637.8	0.02101	0.03511	8.39118	0.19071	19.1
732.2	0.02139	0.03574	8.54189	0.19413	19.4
834.6	0.02180	0.03642	8.70355	0.19781	19.8
945.0	0.02220	0.03709	8.86519	0.20148	20.1
1039.6	0.02240	0.03743	8.94536	0.20330	20.3
1142.0	0.02264	0.03783	9.04218	0.20550	20.6
1228.7	0.02280	0.03810	9.10594	0.20695	20.7
1331.1	0.02293	0.03832	9.15788	0.20813	20.8
1433.6	0.02315	0.03868	9.24460	0.21010	21.0
1528.3	0.02337	0.03905	9.33285	0.21211	21.2
1630.7	0.02340	0.03910	9.34382	0.21236	21.2
1733.2	0.02354	0.03933	9.39959	0.21363	21.4
1827.8	0.02355	0.03935	9.40580	0.21377	21.4
1930.3	0.02364	0.03949	9.43865	0.21451	21.5
2032.8	0.02381	0.03977	9.50598	0.21605	21.6
2127.4	0.02372	0.03963	9.47163	0.21526	21.5
2190.4	0.02374	0.03967	9.48128	0.21548	21.5

Table C- 9: CO₂ sorption data for p[bDMADMVBP][NO₃] at 10 bar and 25°C

Real Time, [min]	CO ₂ weight, [gm]	CO ₂ weight for 1 gm, [gm]	CO ₂ weight for one monomer, [gm]	No of CO ₂ moles, [mole]	Mole%
0	0	0	0	0	0
16.2	0.00667	0.01108	3.50144	0.07958	7.96
24.0	0.00637	0.01059	3.34661	0.07606	7.61
31.9	0.00630	0.01046	3.30599	0.07514	7.51
39.8	0.00652	0.01083	3.42371	0.07781	7.78
47.6	0.00666	0.01106	3.49579	0.07945	7.94
63.3	0.00695	0.01154	3.64679	0.08288	8.29
79.1	0.00720	0.01196	3.77925	0.08589	8.59
94.8	0.00748	0.01242	3.92504	0.08921	8.92
110.5	0.00761	0.01264	3.99445	0.09078	9.08
126.2	0.00782	0.01300	4.10733	0.09335	9.33
157.7	0.00814	0.01352	4.27145	0.09708	9.71
189.1	0.00852	0.01416	4.47320	0.10166	10.17
220.6	0.00882	0.01465	4.62955	0.10522	10.52
252.1	0.00908	0.01509	4.76869	0.10838	10.84
283.6	0.00925	0.01536	4.85505	0.11034	11.03
338.6	0.00961	0.01596	5.04288	0.11461	11.46
401.6	0.00992	0.01648	5.20825	0.11837	11.84
456.6	0.01016	0.01687	5.33164	0.12117	12.12
519.6	0.01041	0.01729	5.46459	0.12420	12.42
582.6	0.01060	0.01761	5.56408	0.12646	12.65
684.8	0.01081	0.01796	5.67397	0.12895	12.90

Table C- 10: CO₂ sorption data for p[METMA][NO₃] at 10 bar and 25°C

Real Time, [min]	CO ₂ weight, [gm]	CO ₂ weight for 1 gm, [gm]	CO ₂ weight for one monomer, [gm]	No of CO ₂ moles, [mole]	Mole %
0	0	0	0	0	0
8.3	0.00574	0.00811	1.90650	0.04333	4.3
16.1	0.00776	0.01096	2.57649	0.05856	5.9
24.0	0.00695	0.00982	2.30713	0.05243	5.2
31.9	0.00659	0.00931	2.18837	0.04974	5.0
39.8	0.00648	0.00915	2.15141	0.04890	4.9
55.5	0.00637	0.00899	2.11376	0.04804	4.8
71.2	0.00631	0.00891	2.09467	0.04761	4.8
86.9	0.00628	0.00887	2.08429	0.04737	4.7
102.6	0.00644	0.00909	2.13636	0.04855	4.9
118.3	0.00647	0.00914	2.14779	0.04881	4.9
149.8	0.00656	0.00927	2.17834	0.04951	5.0
181.3	0.00662	0.00935	2.19817	0.04996	5.0
212.7	0.00672	0.00949	2.22971	0.05068	5.1
252.1	0.00686	0.00969	2.27631	0.05173	5.2
283.5	0.00692	0.00977	2.29707	0.05221	5.2
338.6	0.00702	0.00992	2.33105	0.05298	5.3
401.5	0.00718	0.01014	2.38289	0.05416	5.4
464.5	0.00727	0.01027	2.41362	0.05485	5.5
519.5	0.00737	0.01041	2.44579	0.05559	5.6
582.5	0.00745	0.01052	2.47225	0.05619	5.6
677.0	0.00761	0.01075	2.52713	0.05743	5.7
779.4	0.00776	0.01096	2.57484	0.05852	5.9
881.9	0.00793	0.01121	2.63328	0.05985	6.0
984.3	0.00807	0.01140	2.67983	0.06091	6.1
1078.9	0.00821	0.01159	2.72465	0.06192	6.2
1181.4	0.00838	0.01183	2.78030	0.06319	6.3
1283.8	0.00852	0.01204	2.82859	0.06429	6.4
1378.4	0.00863	0.01219	2.86513	0.06512	6.5
1480.9	0.00881	0.01245	2.92460	0.06647	6.6
1583.4	0.00885	0.01250	2.93806	0.06677	6.7
1678.0	0.00896	0.01266	2.97407	0.06759	6.8
1780.4	0.00898	0.01269	2.98173	0.06777	6.8
1882.9	0.00896	0.01265	2.97366	0.06758	6.8
1985.4	0.00906	0.01280	3.00808	0.06837	6.8
2079.9	0.00908	0.01282	3.01346	0.06849	6.8
2182.5	0.00914	0.01292	3.03503	0.06898	6.9
2285.0	0.00920	0.01300	3.05495	0.06943	6.9
2379.7	0.00926	0.01308	3.07403	0.06986	7.0
2482.4	0.00931	0.01316	3.09157	0.07026	7.0
2569.3	0.00936	0.01323	3.10878	0.07065	7.1

Table C- 11: CO₂ sorption data for p[METMA][Cl] at 10 bar and 25°C

Real Time, [min]	CO ₂ weight, [gm]	CO ₂ weight for 1 gm, [gm]	CO ₂ weight for one monomer, [gm]	No of CO ₂ moles, [mole]	Mole%
0	0	0	0	0	0
8.3	0.00406	0.01144	2.37993	0.05409	5.4
16.2	0.00497	0.01400	2.91183	0.06618	6.6
24.0	0.00386	0.01088	2.26262	0.05142	5.1
31.9	0.00344	0.00970	2.01705	0.04584	4.6
39.8	0.00324	0.00912	1.89680	0.04311	4.3
55.5	0.00314	0.00884	1.83930	0.04180	4.2
71.2	0.00313	0.00880	1.83110	0.04162	4.2
87.0	0.00313	0.00881	1.83351	0.04167	4.2
102.7	0.00314	0.00885	1.83997	0.04182	4.2
118.4	0.00313	0.00881	1.83205	0.04164	4.2
149.9	0.00318	0.00895	1.86177	0.04231	4.2
181.4	0.00323	0.00910	1.89381	0.04304	4.3
212.8	0.00333	0.00937	1.94945	0.04431	4.4
236.5	0.00335	0.00944	1.96315	0.04462	4.5
267.9	0.00345	0.00970	2.01810	0.04587	4.6
330.8	0.00359	0.01012	2.10394	0.04782	4.8
393.8	0.00368	0.01037	2.15725	0.04903	4.9
448.8	0.00375	0.01057	2.19895	0.04998	5.0
511.8	0.00381	0.01072	2.23021	0.05069	5.1
566.9	0.00385	0.01083	2.25347	0.05122	5.1
677.0	0.00399	0.01122	2.33426	0.05305	5.3
787.3	0.00411	0.01158	2.40782	0.05472	5.5
881.9	0.00421	0.01186	2.46769	0.05608	5.6
984.3	0.00435	0.01226	2.55063	0.05797	5.8
1078.8	0.00448	0.01262	2.62470	0.05965	6.0
1181.2	0.00466	0.01312	2.72833	0.06201	6.2
1283.6	0.00474	0.01334	2.77501	0.06307	6.3
1378.2	0.00484	0.01364	2.83677	0.06447	6.4
1480.6	0.00493	0.01390	2.89034	0.06569	6.6
1583.2	0.00499	0.01406	2.92360	0.06645	6.6
1677.8	0.00503	0.01416	2.94479	0.06693	6.7
1780.3	0.00507	0.01429	2.97140	0.06753	6.8
1882.7	0.00512	0.01441	2.99629	0.06810	6.8
1977.3	0.00528	0.01487	3.09203	0.07027	7.0
2079.7	0.00527	0.01485	3.08833	0.07019	7.0
2182.2	0.00530	0.01491	3.10167	0.07049	7.0
2276.9	0.00536	0.01510	3.14069	0.07138	7.1
2379.4	0.00534	0.01503	3.12549	0.07103	7.1

Table C- 12: CO₂ sorption data for p[VBTEA][acetate] at 10 bar and 25°C

Real Time, [min]	CO ₂ weight, [gm]	CO ₂ weight for 1 gm, [gm]	CO ₂ weight for one monomer, [gm]	No of CO ₂ moles, [mole]	Mole%
0	0	0	0	0	0
8.3	0.00303	0.00381	1.05634	0.02401	2.4
16.2	0.00571	0.00719	1.99078	0.04524	4.5
24.0	0.00660	0.00831	2.30229	0.05232	5.2
31.9	0.00716	0.00901	2.49502	0.05670	5.7
39.7	0.00760	0.00956	2.64939	0.06021	6.0
47.6	0.00794	0.00999	2.76737	0.06289	6.3
63.3	0.00849	0.01069	2.96029	0.06728	6.7
79.0	0.00888	0.01118	3.09585	0.07036	7.0
94.7	0.00928	0.01168	3.23605	0.07355	7.4
110.5	0.00957	0.01205	3.33778	0.07586	7.6
126.2	0.00990	0.01246	3.45227	0.07846	7.8
165.5	0.01041	0.01310	3.62868	0.08247	8.2
197.0	0.01076	0.01354	3.75030	0.08523	8.5
228.5	0.01112	0.01400	3.87841	0.08815	8.8
259.9	0.01144	0.01440	3.98974	0.09068	9.1
362.2	0.01219	0.01534	4.24972	0.09658	9.7
456.6	0.01275	0.01605	4.44580	0.10104	10.1
558.9	0.01315	0.01655	4.58507	0.10421	10.4
661.3	0.01346	0.01695	4.69440	0.10669	10.7
755.7	0.01376	0.01732	4.79645	0.10901	10.9
858.2	0.01406	0.01770	4.90253	0.11142	11.1
960.6	0.01435	0.01807	5.00474	0.11374	11.4
1063.0	0.01463	0.01841	5.09980	0.11590	11.6
1157.6	0.01493	0.01880	5.20739	0.11835	11.8
1260.0	0.01505	0.01894	5.24720	0.11925	11.9
1362.5	0.01513	0.01904	5.27501	0.11989	12.0
1457.1	0.01531	0.01927	5.33705	0.12130	12.1
1559.6	0.01558	0.01961	5.43135	0.12344	12.3
1662.1	0.01570	0.01976	5.47310	0.12439	12.4
1756.6	0.01585	0.01995	5.52548	0.12558	12.6
1859.2	0.01598	0.02012	5.57382	0.12668	12.7
1961.6	0.01604	0.02020	5.59403	0.12714	12.7
2056.2	0.01611	0.02027	5.61609	0.12764	12.8
2158.6	0.01614	0.02032	5.62789	0.12791	12.8
2261.1	0.01633	0.02056	5.69471	0.12943	12.9
2355.7	0.01641	0.02065	5.72117	0.13003	13.0
2458.3	0.01651	0.02078	5.75702	0.13084	13.1
2561.0	0.01661	0.02091	5.79181	0.13163	13.2
2655.8	0.01676	0.02110	5.84416	0.13282	13.3
2758.4	0.01678	0.02112	5.84944	0.13294	13.3
2853.1	0.01685	0.02121	5.87405	0.13350	13.4
2881.1	0.01682	0.02118	5.86601	0.13332	13.3

Table C- 13: CO₂ sorption data for p[VBTEA][methylsulfate] at 10 bar and 25°C

Real Time, [min]	CO ₂ weight, [gm]	CO ₂ weight for 1 gm, [gm]	CO ₂ weight for one monomer, [gm]	No of CO ₂ moles, [mole]	Mole%
0	0	0	0	0	0
8.3	0.00825	0.01173	3.87245	0.08801	8.8
16.2	0.00853	0.01214	4.00522	0.09103	9.1
24.0	0.00864	0.01229	4.05465	0.09215	9.2
31.9	0.00885	0.01259	4.15430	0.09442	9.4
39.8	0.00881	0.01254	4.13733	0.09403	9.4
55.5	0.00905	0.01288	4.25042	0.09660	9.7
71.2	0.00915	0.01302	4.29737	0.09767	9.8
86.9	0.00932	0.01326	4.37612	0.09946	9.9
102.6	0.00936	0.01332	4.39565	0.09990	10.0
118.3	0.00943	0.01342	4.42874	0.10065	10.1
149.8	0.00964	0.01371	4.52590	0.10286	10.3
181.3	0.00977	0.01390	4.58658	0.10424	10.4
212.7	0.00990	0.01408	4.64695	0.10561	10.6
244.2	0.01005	0.01430	4.71816	0.10723	10.7
275.6	0.01011	0.01439	4.74740	0.10790	10.8
338.6	0.01030	0.01465	4.83584	0.10991	11.0
393.6	0.01050	0.01493	4.92849	0.11201	11.2
456.6	0.01062	0.01510	4.98372	0.11327	11.3
511.7	0.01071	0.01524	5.02890	0.11429	11.4
574.6	0.01098	0.01562	5.15469	0.11715	11.7
653.3	0.01103	0.01569	5.17879	0.11770	11.8
755.6	0.01114	0.01585	5.23088	0.11888	11.9
858.0	0.01126	0.01601	5.28389	0.12009	12.0
952.6	0.01147	0.01632	5.38513	0.12239	12.2
1055.1	0.01153	0.01640	5.41321	0.12303	12.3

1157.6	0.01167	0.01661	5.48080	0.12456	12.5
1260.0	0.01180	0.01679	5.54086	0.12593	12.6
1354.6	0.01196	0.01701	5.61283	0.12756	12.8
1457.0	0.01210	0.01721	5.67837	0.12905	12.9
1559.6	0.01219	0.01735	5.72430	0.13010	13.0
1654.2	0.01227	0.01745	5.75960	0.13090	13.1
1756.7	0.01237	0.01760	5.80832	0.13201	13.2
1859.2	0.01252	0.01782	5.87940	0.13362	13.4
1953.7	0.01259	0.01790	5.90850	0.13428	13.4
2056.3	0.01266	0.01801	5.94349	0.13508	13.5
2158.8	0.01272	0.01810	5.97312	0.13575	13.6
2253.3	0.01266	0.01801	5.94380	0.13509	13.5
2355.9	0.01281	0.01822	6.01158	0.13663	13.7
2458.5	0.01290	0.01835	6.05494	0.13761	13.8
2553.3	0.01296	0.01844	6.08546	0.13831	13.8
2655.9	0.01302	0.01853	6.11329	0.13894	13.9
2758.6	0.01316	0.01872	6.17619	0.14037	14.0
2853.3	0.01322	0.01881	6.20661	0.14106	14.1
2956.1	0.01328	0.01889	6.23522	0.14171	14.2
3153.7	0.01332	0.01895	6.25267	0.14211	14.2
3256.6	0.01336	0.01900	6.27154	0.14254	14.3
3359.4	0.01333	0.01896	6.25737	0.14221	14.2

Table C- 14: CO₂ sorption data for p[VBTMA][BF₄] at 10 bar and 25°C

Real Time, [min]	CO ₂ weight, [gm]	CO ₂ weight for 1 gm, [gm]	CO ₂ weight for one monomer, [gm]	No of CO ₂ moles, [mole]	Mole%
0	0	0	0	0	0
8.3	0.00482	0.01146	3.03837	0.06905	6.9
16.2	0.00851	0.02022	5.35914	0.12180	12.2
24.0	0.00966	0.02295	6.08288	0.13825	13.8
31.9	0.01054	0.02505	6.63972	0.15090	15.1
39.7	0.01122	0.02666	7.06803	0.16064	16.1
55.5	0.01219	0.02896	7.67639	0.17446	17.4
71.2	0.01301	0.03090	8.19081	0.18615	18.6
86.9	0.01365	0.03242	8.59504	0.19534	19.5
102.6	0.01410	0.03350	8.88081	0.20184	20.2
118.3	0.01458	0.03462	9.17829	0.20860	20.9
181.3	0.01579	0.03750	9.94093	0.22593	22.6
244.2	0.01643	0.03903	10.34747	0.23517	23.5
299.3	0.01703	0.04046	10.72611	0.24378	24.4
362.3	0.01736	0.04125	10.93407	0.24850	24.9
425.2	0.01758	0.04175	11.06790	0.25154	25.2
480.3	0.01777	0.04221	11.19054	0.25433	25.4
543.2	0.01782	0.04234	11.22339	0.25508	25.5
598.3	0.01785	0.04240	11.23988	0.25545	25.5
661.3	0.01801	0.04277	11.33950	0.25772	25.8
724.2	0.01809	0.04298	11.39317	0.25894	25.9
779.4	0.01818	0.04319	11.44940	0.26021	26.0
818.8	0.01819	0.04321	11.45426	0.26032	26.0
881.9	0.01827	0.04340	11.50561	0.26149	26.1
944.9	0.01833	0.04354	11.54168	0.26231	26.2
1000.1	0.01837	0.04363	11.56536	0.26285	26.3
1063.1	0.01832	0.04352	11.53779	0.26222	26.2
1118.3	0.01839	0.04367	11.57795	0.26314	26.3
1181.3	0.01836	0.04362	11.56283	0.26279	26.3
1244.4	0.01838	0.04367	11.57564	0.26308	26.3
1299.5	0.01836	0.04361	11.56020	0.26273	26.3
1362.6	0.01838	0.04366	11.57550	0.26308	26.3
1417.8	0.01849	0.04392	11.64331	0.26462	26.5
1512.5	0.01853	0.04402	11.66973	0.26522	26.5

Table C- 15: CO₂ sorption data for p[VBTMA][PF₆] at 10 bar and 25°C

Real Time, [min]	CO ₂ weight, [gm]	CO ₂ weight for 1 gm, [gm]	CO ₂ weight for one monomer, [gm]	No of CO ₂ moles, [mole]	Mole%
0	0	0	0	0	0
16.2	0.00454	0.01490	4.81752	0.10949	10.9
24.0	0.00535	0.01759	5.68754	0.12926	12.9
31.9	0.00599	0.01969	6.36476	0.14465	14.5
39.8	0.00644	0.02116	6.84087	0.15547	15.5
47.6	0.00682	0.02240	7.24187	0.16459	16.5
63.4	0.00736	0.02419	7.81802	0.17768	17.8
79.1	0.00770	0.02531	8.18313	0.18598	18.6
94.8	0.00796	0.02615	8.45269	0.19211	19.2
110.5	0.00813	0.02671	8.63353	0.19622	19.6
126.3	0.00825	0.02710	8.76141	0.19912	19.9
157.7	0.00848	0.02786	9.00737	0.20471	20.5
189.2	0.00868	0.02851	9.21553	0.20944	20.9
220.6	0.00882	0.02898	9.36783	0.21291	21.3
252.1	0.00882	0.02898	9.36897	0.21293	21.3
291.5	0.00893	0.02933	9.48177	0.21549	21.5
322.9	0.00891	0.02926	9.45873	0.21497	21.5
354.4	0.00895	0.02941	9.50657	0.21606	21.6
393.7	0.00901	0.02961	9.57265	0.21756	21.8
425.2	0.00906	0.02976	9.62049	0.21865	21.9
456.6	0.00909	0.02987	9.65629	0.21946	21.9
488.1	0.00911	0.02993	9.67407	0.21987	22.0
519.6	0.00913	0.03001	9.70020	0.22046	22.0
558.9	0.00911	0.02993	9.67530	0.21989	22.0
590.4	0.00910	0.02991	9.66724	0.21971	22.0
621.9	0.00902	0.02964	9.58032	0.21773	21.8
661.3	0.00903	0.02968	9.59540	0.21808	21.8
692.7	0.00908	0.02982	9.63898	0.21907	21.9
724.3	0.00909	0.02987	9.65624	0.21946	21.9

Table C- 16: CO₂ sorption data for p[VBTMA][F₃-CSO₃] at 10 bar and 25°C

Real Time, [min]	CO ₂ weight, [gm]	CO ₂ weight for 1 gm, [gm]	CO ₂ weight for one monomer, [gm]	No of CO ₂ moles, [mole]	Mole%
0	0	0	0	0	0
16.2	0.01359	0.02233	7.30907	0.16612	16.6
24.0	0.01468	0.02412	7.89566	0.17945	17.9
31.9	0.01524	0.02504	8.19735	0.18630	18.6
39.8	0.01550	0.02546	8.33623	0.18946	18.9
47.6	0.01565	0.02571	8.41661	0.19129	19.1
63.3	0.01578	0.02592	8.48570	0.19286	19.3
79.1	0.01591	0.02613	8.55366	0.19440	19.4
94.8	0.01589	0.02609	8.54241	0.19415	19.4
110.5	0.01600	0.02629	8.60509	0.19557	19.6
126.2	0.01601	0.02631	8.61193	0.19573	19.6
142.0	0.01602	0.02632	8.61599	0.19582	19.6
173.4	0.01608	0.02642	8.64950	0.19658	19.7